Modelling of Equatorial Wave Motions in the Middle Atmosphere

Euain F. Drysdale

A thesis submitted for the degree of Doctor of Philosophy

in the University of Oxford

Atmospheric, Oceanic and Planetary Physics

Department of Physics

Oxford University

Trinity Term, 1998

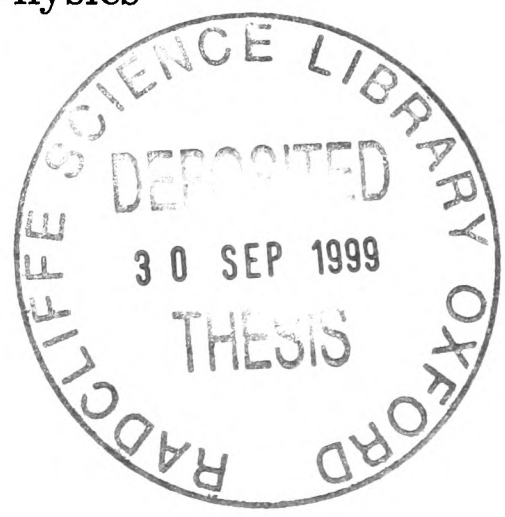

Modelling of Equatorial Wave Motions in the Middle Atmosphere

Euain Fraser Drysdale
Trinity College, Oxford

A thesis submitted for the degree of Doctor of Philosophy in the University of Oxford

Trinity Term, 1998

A three-dimensional mechanistic model of the middle atmosphere is used to model various classes of equatorial wave motions that are observed in the atmosphere. These waves are thought to be largely responsible for the forcing of the quasi-biennial oscillation (QBO) in the tropical lower stratosphere. By generating a combination of different classes of equatorial waves in the model, an oscillation which has many similarities to the observed QBO is produced in the model.

The numerical model used is run in a variety of configurations, including running it at different vertical resolutions and with two different radiation parameterisation schemes. It is found that model used in the project must be modified to allow the accurate modelling of equatorial waves. Several modelling problems are encountered while applying the modifications necessary in the model; the steps necessary to rectify these problems are detailed in this thesis.

Equatorial waves are then forced in this modified model under a range of conditions and their interaction with the mean flow is observed. Their dissipation mechanisms and the influence of changes in model conditions on these waves are investigated. The model is found to be generally very successful in modelling these equatorial waves.

Modelling of the QBO is one of the principle aims of this project and a QBO is successfully generated in a variety of model configurations. The modelled QBO is found to be sensitive to changes in the temperature structure of the model (brought about by changes in the model's radiation scheme) and several experiments are performed in order to learn what processes affect this sensitivity. A QBO is then generated in series of model runs where the state of the model is varied from very idealised (where temperatures in the model are relaxed towards an isothermal state by the radiation scheme) to a state that is far more realistic (a perpetual January run with realistic boundary information). A fairly realistic QBO is generated throughout many of the experiments. The properties of this QBO are investigated and compared to the observed QBO.

The model is then run with planetary waves forced in addition to the QBO. The interaction between the planetary waves and the QBO is investigated. It is found that the planetary waves have little effect on the QBO propagation. The QBO however has a fairly strong modulating effect on the planetary waves in certain regions.

Acknowledgements

There are many people I should thank for helping me to write this thesis. Firstly I would like to thank my supervisor, David Andrews, who has been enormously helpful (and patient) throughout this project. Bryan Lawrence has been a huge help both before leaving for New Zealand and since then by e-mail.

Within the group at Oxford, I would like to thank Warwick Norton for the useful suggestions he has given me and Alan Iwi for many things, ranging from software that he has written to the LaTeX tips he has supplied. Also Susan Rosier (for the LaTeX style files), Helen Rogers (again for LaTeX style files) and all the current members of the MAD group.

The people at Rutherford Appleton Labs have been a great help. Lesley Gray for letting me get my thesis finished and Mike Bithell for encouragement.

Huge amounts of gratitude are due to Christine Appel for the proof reading and especially for putting up with me for the last 6 months.

Euain Drysdale

Contents

Chapter 1

Introduction

The Earth's atmosphere supports a wide range of wave-like phenomena. These waves have a great influence on the circulation in the atmosphere through their ability to transport large amounts of momentum between remote regions. In this thesis, a particular group of waves, equatorial waves, will be modelled using a computer and their properties and influence on the atmospheric circulation investigated.

Equatorial waves are a class of waves that are observed only at low latitudes where the Coriolis force is very small. Their dynamics are described in section 2.3.1. They transport momentum vertically in the tropics, and are thought to play a key role in the forcing of the equatorial stratospheric quasi-biennial oscillation (QBO). The QBO, described in more detail in chapter 3, is the dominant feature of the zonal winds of the lower tropical stratosphere, consisting of descending layers of easterly and westerly winds between the altitudes of approximately 17 and 32 km, with typical peak zonal-wind velocities of around $\pm 20\,\mathrm{ms}^{-1}$.

Computer models are becoming increasingly more sophisticated and can simulate many aspects of the atmosphere very well. The QBO, and indeed equatorial waves, are however extremely poorly modelled in the current generation of atmospheric computer models. Often a realistic QBO can only be represented in a model by relaxing winds explicitly towards observed or idealised equatorial winds [Hamilton, 1998]. This represents a sizeable shortcoming in our current models as the QBO is thought to have a far reaching role in many aspects of the variability of the atmosphere. The reasons for this failing are

not completely established. Through forcing a QBO in this model, some clarification of the model conditions that are necessary to support the QBO will be sought.

One feature of equatorial waves is that, although they are global in scale in the horizontal, they typically have vertical wavelengths of only a few kilometres. It is likely that this is one of the key reasons why GCMs, which typically have vertical resolution of several kilometres in the lower stratosphere, have trouble simulating the QBO [Boville and Randel, 1992]. Through a variety of model experiments, the sensitivity of modelled equatorial waves to the model vertical resolution will be examined and the vertical resolution necessary to support them ascertained.

Through a combination of equatorial wave forcings, a fairly realistic QBO will be generated and some properties of this long timescale oscillation investigated. Through this modelling, several questions regarding the forcing and evolution of the QBO are addressed. It is still not clear what proportion of the QBO forcing is supplied by equatorial waves and it is generally accepted that gravity waves are responsible for supplying a significant portion of the driving required to generate the QBO ([Takahashi and Holton, 1991],[Dunkerton, 1996]). In this study, the ability of equatorial waves to generate a QBO is investigated and the magnitude of the equatorial waves which are required to generate this QBO is examined. A comparison is made between the amplitudes of the equatorial waves forced in the model and observed amplitudes of equatorial waves is made. Such wave amplitudes are likely to be necessary in GCMs in order to generate a QBO and the experiments performed here should provide a useful comparison for the equatorial waves seen in other models.

Further modelling is performed where the sensitivity of the modelled oscillation to changes in the model's background state are examined. It is seen that the modelled QBO greatly affected by changes in the the temperature structure, both through a mechanism whereby changes in the vertical temperature structure are affecting the propagation of the waves by changing the stratification of the atmosphere and through changes in the background circulation of the model.

Having generated a robust QBO in the model, the modelling study is extended through

the addition of a source of planetary waves in the extra-tropics. The extent of the interaction between planetary waves and the tropical QBO is not well known. It is thought that the QBO has a modulating effect on the propagation of planetary waves [Dunkerton and Baldwin, 1991], [Hamilton, 1998] whereas the effect of planetary waves on the QBO is poorly understood, but thought to be small [O'Sullivan, 1997*a*]. Such a modulation of planetary waves is very important as it is thought to play a role in generating interannual, in this case quasi-biennial, variability in the extra-tropical circulation [Holton and Tan, 1980]. This model is particularly well suited to studying such interactions as it can be integrated for long periods and experiments can be performed under very controlled conditions.

1.1 The Structure of this Thesis

The structure of this thesis is as follows:

- The relevant dynamics governing the QBO and its interactions with the atmosphere are outlined in chapter 2. In chapter 3, the properties of the QBO are described along with its forcing mechanisms. Finally, the current state of QBO modelling is described.

- The computer model used is described in chapter 4. The model used is the United Kingdom Meteorological Office Stratosphere-Mesosphere Model. The properties of this model are described and some details on the structure of the model code will be given. Significant modifications have been made to the model and these will be described in some detail. A large amount of time was spent tracing the cause of model crashes at higher vertical resolution. These problems, and the measures taken to correct them, are described in section 4.3. Some source code from the model is given in appendix B.

- In chapters 5, 6 and 7, the modelling of equatorial waves and the quasi-biennial oscillation is described. Several different model experiments are performed as described below:

- Forcing equatorial waves in isolation. In chapter 5, the model is run with a very idealised radiation scheme and equatorial waves of Kelvin and Rossby-gravity classes are forced. The effect of varying several model parameters on the propagation and dissipation of these waves is observed.
- Forcing a QBO. The QBO is generated in chapter 6 by forcing a combination of equatorial waves in the model. This QBO is generated in a variety of model configurations. Experiments in this chapter are again performed using a simplified radiation scheme (Newtonian cooling) but this scheme is used in a variety of ways to allow both highly idealised and slightly more realistic atmospheres to be simulated. Properties of the modelled QBO are found to be sensitive to the configuration of the radiation scheme and this is explored in this chapter.
- Additional modelling of the QBO. In chapter 7, the modelling is extended by adding a source of planetary waves into the modelled atmosphere. These waves are seen to interact with the modelled QBO.

The last chapter of this thesis contains a summary of the work performed during the project, in addition to conclusions drawn from this work. It also contains suggestions for future research that have been brought up during this project.

Chapter 2

Dynamics and Properties of the Middle Atmosphere

Figure 2.1 shows the largest-scale vertical structure in the atmosphere over a range of altitude from 10 to 84 km. The atmosphere can very broadly be considered to consist of a series of layers, marked in the figure, that are characterised by certain properties of the air within that layer. The troposphere is the layer of air, characterised by high water content and low static stability, that spans the ground to around 15 km. Above the tropopause, the stratosphere is a layer of air with low humidity. The stratosphere is, as the name suggests, strongly stratified due to an increase in temperature with height. This temperature increase is caused by the absorption of incoming solar radiation by the ozone layer. In the next layer, the mesosphere, the temperature of the atmosphere again decreases with height. This is a very dynamically-active region which is particularly affected by propagating gravity waves from the levels below, which drive the circulation and temperatures in this region away from their radiative equilibrium states.

For the purposes of this project, the middle atmosphere can be considered to consist of the stratosphere and mesosphere, spanning the altitudes of around 15–80 km. The quasi-biennial oscillation, the focus of the work presented in this thesis, is the dominant large scale feature of the winds in the equatorial lower stratosphere and influences many other processes in the atmosphere. In this chapter the basic atmospheric dynamics which

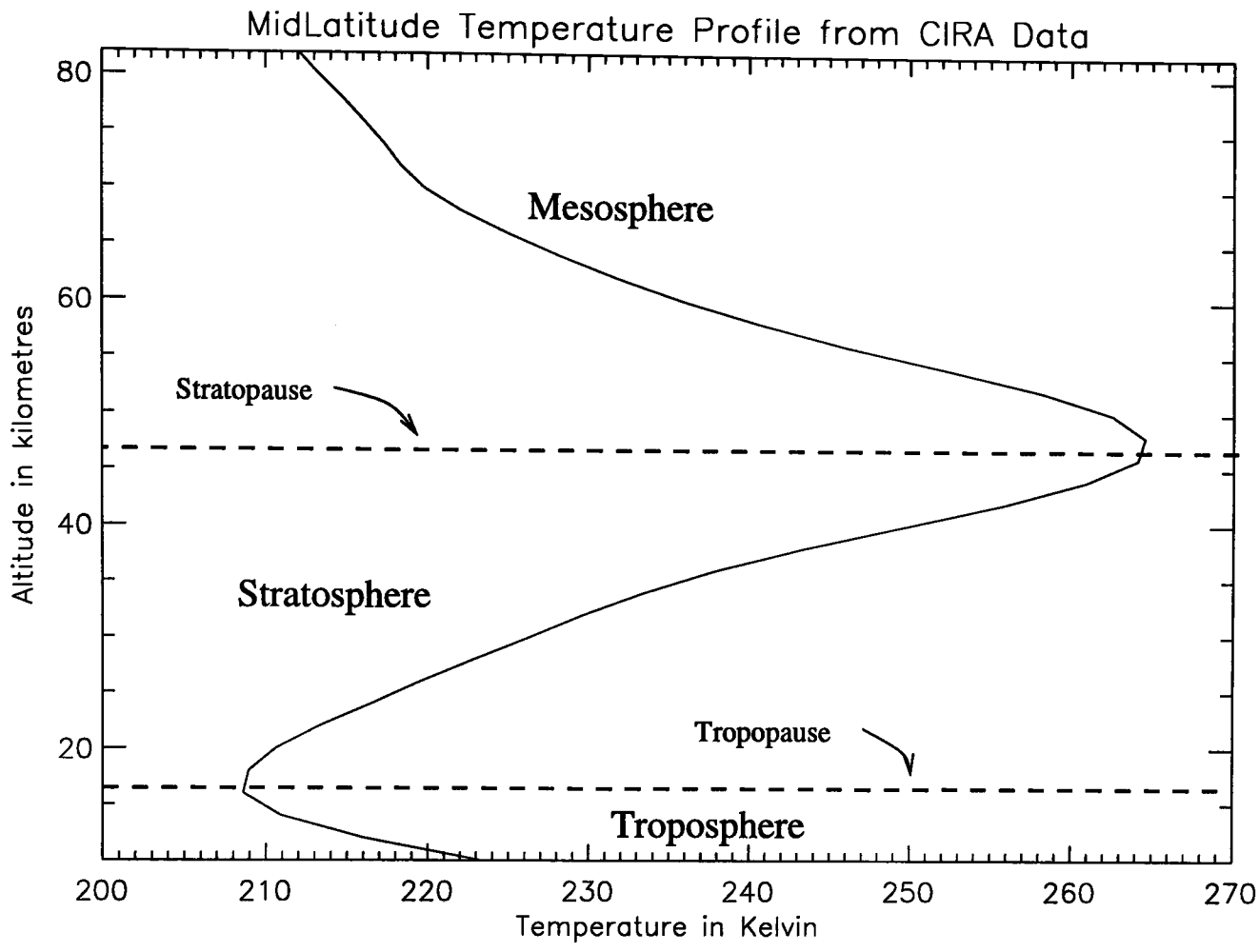

Figure 2.1: A plot of gross temperature structure of the middle atmosphere at mid-latitudes. Data is from the CIRA climatology.

are particularly relevant to the QBO, and the associated wave motions, are described. A more thorough description of the dynamics of the middle atmosphere can be found in Andrews, Holton and Leovy [1987].

2.1 The Primitive Equations

The primitive equations provide a useful starting place for an investigation into the dynamics of the atmosphere. The primitive equations can be written as follows[1]:

$$\frac{Du}{Dt} - \left(f + \frac{u\tan\phi}{a}\right)v + \frac{\Phi_\lambda}{a\cos\phi} = X, \tag{2.1}$$

$$\frac{Dv}{Dt} + \left(f + \frac{u\tan\phi}{a}\right)u + \frac{\Phi_\phi}{a} = Y, \tag{2.2}$$

$$\Phi_z - \frac{R}{H}\theta e^{-\kappa z/H} = 0, \tag{2.3}$$

[1]Notation used is standard. See appendix C for a list of symbols.

$$\frac{[u_\lambda + (v\cos\phi)_\phi]}{a\cos\phi} + \frac{(\rho_o w)_z}{\rho_o} = 0, \tag{2.4}$$

$$\frac{D\theta}{Dt} = Q. \tag{2.5}$$

The operator $\frac{D}{Dt}$ is the material time derivative, otherwise written as

$$\frac{\partial}{\partial t} + \frac{u}{a\cos\phi}\frac{\partial}{\partial\lambda} + \frac{v}{a}\frac{\partial}{\partial\phi} + w\frac{\partial}{\partial z},$$

and represents the rate of change following the flow. Equations (2.1)-(2.5) are a balance of forces in which several small terms, such as the vertical component of the Coriolis force, have been neglected. They represent the zonal momentum balance, the meridional momentum balance, hydrostatic equation, continuity and thermodynamic energy balance respectively. Terms X, Y and Q represent unspecified forcing terms in the respective equations.

In the middle atmosphere, friction can often be ignored, and in the absence of other unspecified non-conservative forcing, X and Y can be neglected. Q, in the middle atmosphere, is dominated by radiative heating or cooling. For time-scales of a few days and less, it is often useful and a fairly good approximation to neglect the Q term as the time-scales involved in radiative processes are of order tens of days. The QBO, however, has time-scales of months and such an approximation would not be good. The primitive equations will form the basis for most of the analysis considered in this chapter.

2.2 β-plane Approximation

The primitive equations prove overly cumbersome for use in certain circumstances. Simplifications of these equations, under certain assumptions, will allow a more easily manipulated set of expressions to be used. A very useful simplification of the primitive equations, known as the β-plane approximation, can be obtained if the Coriolis parameter, f, is linearised about a given latitude. This approximation is good where the region of interest is latitudinally localised. In this project, the majority of the dynamics considered is going to be on or near the equator making the β-plane approximation a good one.

The coordinates are changed from the full spherical coordinates to a set of rectangular coordinates with unit vectors in upwards, z, northwards, y and eastwards, x directions. They map to the spherical coordinates by the relations $dx = a\cos\phi(d\lambda)$ and $dy = a(d\phi)$. (Spherical coordinates will be used in later sections to describe other dynamical systems.)

The Coriolis parameter, f, is defined as $f = 2\Omega\sin\phi$. It is natural now to centre the β-plane on the equator such that the Coriolis parameter becomes:

$$f \approx f_0 + \beta y, \rightarrow f_0 = 0, \text{ giving } f \approx \beta y, \text{ where } \beta = 2\Omega a^{-1}. \tag{2.6}$$

In this new coordinate system, under the β-plane approximation, the primitive equations become:

$$\frac{Du}{Dt} - \beta y v + \Phi_x = X, \tag{2.7}$$

$$\frac{Dv}{Dt} + \beta y u + \Phi_y = Y, \tag{2.8}$$

$$\Phi_z - H^{-1}R\theta e^{-\kappa z/H} = 0, \tag{2.9}$$

$$u_x + v_y + \frac{(\rho_0 w')_z}{\rho_0} = 0, \tag{2.10}$$

$$\frac{DQ}{Dt} = Q. \tag{2.11}$$

These equations are a lot simpler to write down than the full primitive equations and are quite adequate to describe, for example, the equatorial waves that will be considered later in this chapter.

Thermal Wind Equation

A useful diagnostic result that comes quickly from the β-plane equations is the thermal wind equation. In the steady state, there exists a balance between the dominant terms in the β-plane equations such that the Coriolis force acting on an air parcel and the pressure gradient cancel. The vertical derivative of this gives the *thermal wind* balance, which can be written as:

$$u_z = -\frac{R}{H\beta y}T_y. \tag{2.12}$$

This relation is useful in understanding many atmospheric phenomena. It is of particular relevance to the QBO (as will be discussed in section 3.2.1) as it gives a description of the horizontal temperature gradients associated with the vertical shear in the QBO. These horizontal temperature gradients imply further circulations which are important in the circulation of the middle atmosphere.

2.2.1 Separation into Zonal Mean and Eddy Components

In phenomena examined in this project, it is often natural and convenient to look at the motions of the atmosphere in terms of its zonal mean component and the deviations from this zonal mean. These departures from the zonal mean are known as 'eddies' or 'waves'.[2] This separation, although a convenient way of simplifying the primitive equations, may not always be the most natural framework to describe the motions of the atmosphere. In the case of the QBO, the separation into zonal mean and eddy quantities is very useful as the QBO can be very well described in terms of smaller-scale eddy disturbances, the waves that are going to be modelled in this project, interacting with the zonal mean flow.

As a first step, the 'zonal mean' of a quantity (or more precisely, the 'Eulerian zonal mean' as it is averaged over a region defined in a frame stationary with respect to the earth), denoted by an over-bar, is defined such that

$$\overline{g}(\phi, z, t) = \frac{1}{2\pi} \int_0^{2\pi} g(\lambda, \phi, z, t) d\lambda,$$

where g is the quantity being investigated, λ is the longitude, ϕ latitude, t time and z is log-pressure height. Further, any departure from this zonal mean will be denoted as the quantity primed i.e. $g'(\lambda, \phi, z,) \equiv g - \overline{g}$.

Separation of the terms in the primitive equations into zonal mean and eddy quantities produces (in spherical coordinates),

$$\overline{u}_t + \overline{v}\left[\frac{(\overline{u}\cos\phi)_\phi}{a\cos\phi} - f\right] + \overline{w}\overline{u}_z - \overline{X}$$

[2] Although the term 'wave' implies a disturbance of sinusoidal shape.

$$= -\frac{1}{a\cos^2\phi}(\overline{v'u'}\cos^2\phi)_\phi - \frac{1}{\rho_o}(\rho_o\overline{w'u'})'_z, \tag{2.13}$$

$$\overline{v}_t + a^{-1}\overline{v}\,\overline{v}_\phi + \overline{w}\,\overline{v}_z + \overline{u}\left(f + \frac{\overline{u}\tan\phi}{a}\right) + \frac{\overline{\Phi}_\phi}{a} - \overline{Y}$$

$$= -\frac{1}{a\cos\phi}(\overline{v'^2}\cos\phi)_\phi - \frac{1}{\rho_o}(\rho_o\overline{w'v'})_z - \frac{\overline{u'^2}\tan\phi}{a}, \tag{2.14}$$

$$\overline{\Phi}_z - \frac{R\overline{\theta}}{H}e^{-\kappa z/H} = 0, \tag{2.15}$$

$$\frac{(\overline{v}\cos\phi)_\phi}{a\cos\phi} + \frac{1}{\rho_o}(\rho_o\overline{w})_z = 0, \tag{2.16}$$

$$\overline{\theta}_t + \frac{\overline{v}\,\overline{\theta}_\phi}{a} + \overline{w}\,\overline{\theta}_z - \overline{Q} = -\frac{(\overline{v'\theta'}\cos\phi)_\phi}{a\cos\phi} - \frac{1}{\rho_o}(\rho_o\overline{w'\theta'})_z. \tag{2.17}$$

This set of equations is known as the Eulerian mean equations and describes the evolution of the zonal mean state of the atmosphere as related to various eddy quantities that are present. The advantages of this formulation over the primitive equations are somewhat limited as the quantities on the right-hand side of these equations are not easily related to physical phenomena. For example, it would not be easy to see how the u-wind would respond to the addition of a propagating wave to the system without solving the system of equations.

2.2.2 The Transformed Eulerian-Mean Equations

A more useful way of describing the evolution of the zonal mean state of the atmosphere may be obtained by performing a transformation on the meridional and vertical wind variables into their 'residual mean' variables (denoted by $\overline{v}^*$ and $\overline{w}^*$).[3] The crucial transformation of the quantities v and w into their 'residual mean' coordinates can be written as $\overline{\mathbf{u}}^* = (0, \overline{v}^*, \overline{w}^*)$ such that,

$$\overline{v}^* \equiv \overline{v} - \rho_o^{-1}(\rho_o\overline{v'\theta'}/\overline{\theta}_z)_z, \tag{2.18}$$

$$\overline{w}^* \equiv \overline{w} + (a\cos\phi)^{-1}(\cos\phi\overline{v'\theta'}/\overline{\theta}_z)_\phi. \tag{2.19}$$

Substitution into the Eulerian mean equations (Equations (2.13–2.17)) gives the trans-

[3] A more detailed discussion of these equations is given Andrews et al. [1987] and references therein.

formed Eulerian mean equations. These equations may be written:

$$\overline{u}_t + \overline{v}^*[(a\cos\phi)^{-1}(\overline{u}\cos\phi)_\phi - f] + \overline{w}^*\overline{u}_z - \overline{X}$$
$$= (\rho_o a\cos\phi)^{-1}\nabla.\mathbf{F}, \tag{2.20}$$
$$\overline{u}(f + \overline{u}a^{-1}\tan\phi) + a^{-1}\overline{\Phi}_\phi = G, \tag{2.21}$$
$$\Phi_z - H^{-1}R\overline{\theta}e^{-\kappa z/H} = 0, \tag{2.22}$$
$$(a\cos\phi)^{-1}(\overline{v}^*\cos\phi)_\phi + \rho_o^{-1}(\rho_o\overline{w}^*)_z = 0, \tag{2.23}$$
$$\overline{\theta}_t + a^{-1}\overline{v}^*\overline{\theta}_\phi + \overline{w}^*\overline{\theta}_z - \overline{Q} = -\rho_o^{-1}[\rho_o(\overline{v'\theta'}\,\overline{\theta}_\phi/a\overline{\theta}_z + \overline{w'\theta'})]_z. \tag{2.24}$$

The quantity G represents terms leading to a departure from the gradient wind balance. The vector $\mathbf{F}$ is known as the Eliassen-Palm (EP) flux and can be written $\mathbf{F} = (0, F^{(\phi)}, F^{(z)})$ such that:

$$F^{(\phi)} \equiv \rho_o a\cos\phi(\overline{u}_z\,\overline{v'\theta'}/\overline{\theta}_z + \overline{v'u'}),$$
$$F^{(z)} \equiv \rho_o a\cos\phi\{[f - (a\cos\phi)^{-1}(\overline{u}\cos\phi)_\phi]\overline{v'\theta'}/\theta_z - \overline{w'u'}\}.$$

There are several advantages to this formulation over the Eulerian mean equations. The response of the zonal mean state to a prescribed eddy forcing is not trivial to calculate in the Eulerian mean equations as a set of coupled equations must be solved. In the TEM formulation, the right-hand side of equation 2.24 is often small, leaving the EP-flux divergence as the dominant wave-induced forcing term. The EP-flux divergence in model output can be used to ascertain where waves are being dissipated and the mean flow experiencing a force. The EP-flux itself is a useful diagnostic quantity as vector plots of EP-flux show the path along which wave activity is propagating and so can show the relation between remote forcing and dissipation regions.

The residual circulation is close to the 'transport circulation' that will advect material around the atmosphere. (It can be shown, under steady, linear dissipation-free conditions to be equal to the transport circulation.) This is not true for the Eulerian mean wind quantities. This makes the residual circulation a very useful diagnostic for examining the

meridional and vertical transport in the atmosphere due to the large-scale circulation. From equation (2.20) it can be seen that $\overline{v}^*$ and $\overline{w}^*$ are responsible for advecting momentum. This term is shown to be important for the modelling of the QBO in section 6.3.

2.3 Waves and Equatorial Waves

An important property of the atmosphere is that it can support a wide range of 'wave-like' disturbances. These disturbances can transfer energy and momentum between regions of the atmosphere and play a very large role in maintaining the observed atmospheric state. The atmosphere supports a huge range of waves from acoustic sound waves with frequencies of several thousand Hertz and higher to waves with periods of days to weeks. Models cannot support certain classes of waves due to restrictions in their resolution, for example small scale gravity waves, or restrictions imposed by the model equations of motion (for example, models using the hydrostatic approximation will be unable to support non-hydrostatic waves). The primitive equations (as written above and solved by the model) do not support acoustic or non-hydrostatic waves. Even some of the larger-scale waves are not adequately resolved in models being run at present. The waves modelled in this project are often limited by the vertical resolution of the model. In some cases these restrictions are unimportant, or even beneficial, acting to filter out waves which have negligible effect on the circulation but which could cause the model to be unstable if they were present. This includes acoustic sound waves which have a very high phase velocity, and so would be computationally expensive to model, and do not contribute to the driving of the atmosphere. In other cases, for example gravity waves, the missing waves play a crucial role in maintaining the atmospheric circulation and their effects must be somehow parameterised in the model.

The waves considered in the atmosphere can be thought of as having two restoring mechanisms. The vertical stratification of the atmosphere provides a restoring force to parcels that are moved vertically from their original positions (assuming that the atmosphere is in a stable state to begin with). Horizontal parcel displacements, again in a

stable atmosphere, are subject to the Rossby restoring force. This restoring mechanism is due to the northward gradient in potential vorticity that exists in the earth's atmosphere. Generally, the vertical stratification effects are dominant for waves of small scale, whereas the Rossby restoring force is dominant for larger-scale disturbances.

This separation of scales becomes somewhat blurred near the equator, where the f-parameter becomes very small. There are some classes of waves that are observed only in the tropics. These include the Kelvin and Rossby-gravity waves described in the next section.

2.3.1 Equatorial Kelvin and Rossby-gravity Waves

Kelvin and Rossby-gravity waves are thought to play an important role in driving the QBO. In this section the dynamics of these waves will be described and the way in which they can play a part in forcing the QBO investigated. These waves are confined to the equatorial region as shall be seen later. This allows the geometry of the situation to be simplified by looking at the waves on β-plane centred on the equator.

Using the primitive equations, linearised around a basic flow $\overline{u}(y,z)$, gives the following relations:

$$\overline{D}u' + (\overline{u}_y - \beta y)v' + \overline{u}_z w' + \Phi'_x = X', \tag{2.25}$$

$$\overline{D}v' + \beta y u' + \Phi'_y = Y', \tag{2.26}$$

$$\Phi'_z - H^{-1}R\theta' e^{-\kappa z/H} = 0, \tag{2.27}$$

$$u'_x + v'_y + \rho_0^{-1}(\rho_0 w')_z = 0, \tag{2.28}$$

$$\overline{D}\theta' + \overline{\theta}_y v' + \overline{\theta}_z w' = Q', \tag{2.29}$$

where the prime ($'$) represents deviation from the background state and X', Y' and Q' represent east-west frictional forces, north-south frictional forces and diabatic heating respectively. The subscripts (eg. Φ'_x) denote the derivative of the quantity with respect to the subscript. $\overline{D}$ is a reduced form of the material derivative, such that $\overline{D} = \frac{\partial}{\partial t} + \overline{u}\frac{\partial}{\partial x}$.

To a reasonably good approximation X', Y', and Q' can be neglected (meaning that

the flow is assumed to be frictionless and diabatic heating is negligible over the time-scale of the period of the oscillation). Further, as an initial simplification, $\overline{u}$ shall be set to zero. A non-zero $\overline{u}$ shall be considered later in this section.

Under these assumptions, the equations simplify to the following:

$$u'_t - \beta y v' + \Phi'_x = 0, \tag{2.30}$$

$$v'_t + \beta y u' + \Phi'_y = 0, \tag{2.31}$$

$$u'_x + v'_y + \rho_0^{-1}(\rho_0 w')_z = 0, \tag{2.32}$$

$$\Phi'_{zt} + N^2 w' = 0. \tag{2.33}$$

N is assumed constant (a reasonable approximation in the stratosphere) and wave-like solutions are sought such that:

$$(u', v', w', \Phi') = e^{\frac{z}{2H}} \Re\{[\hat{u}(y), \hat{v}(y), \hat{w}(y), \hat{\Phi}(y)] \exp i(kx + mz - \omega t)\}. \tag{2.34}$$

Substituting equation (2.34) into equations (2.30) to (2.33), we get:

$$\hat{w} = -\frac{\omega}{N^2}(m - \frac{i}{2H})\hat{\Phi}, \tag{2.35}$$

and,

$$-i\omega\hat{u} - \beta y\hat{v} + ik\hat{\Phi} = 0, \tag{2.36}$$

$$-i\omega\hat{v} + \beta y\hat{u} + \hat{\Phi}_y = 0, \tag{2.37}$$

$$ik\hat{u} + \hat{v}_y - i\omega m^2 N^{-2}\hat{\Phi} = 0. \tag{2.38}$$

Kelvin Waves

Observations in the equatorial middle atmosphere show that there exists a class of waves with a very small meridional wind component v'. These waves are a solution of equations (2.36,2.37,2.38) where $\hat{v}$ has been set to zero. Under this simplification, the equations

reduce to:

$$-\omega\hat{u} + k\hat{\Phi} = 0, \qquad \beta y\hat{u} + \hat{\Phi}_y = 0, \qquad k\hat{u} - \omega m^2 N^{-2}\hat{\Phi} = 0. \tag{2.39}$$

These equations give immediately $\omega = \pm Nk/m$, and hence vertical group velocity $c_g^{(v)} \equiv \partial\omega/\partial m = \mp Nk/m^2$. It is reasonable to assume that the realistic term in the middle atmosphere is that with a positive vertical group velocity, as this will correspond to wave propagation upwards from the troposphere. This gives a dispersion relation of:

$$\omega = -Nk/m, \tag{2.40}$$

and an expression for the vertical group velocity of:

$$c_g^{(v)} = Nk/m^2 = \omega^2/Nk. \tag{2.41}$$

It should be observed that the dispersion relation, equation (2.40), is the same as that for gravity waves with a meridional wave number, l, equal to 0.

The meridional structure of this wave is found by elimination of $\hat{u}$ from equations (2.39) to give, $\hat{\Phi}_y + k\beta\omega^{-1}y\hat{\Phi} = 0$ hence,

$$\hat{\Phi}(y) = \hat{\Phi}_0 \exp(-\beta k y^2/2\omega). \tag{2.42}$$

This wave has an eastward zonal phase velocity (i.e. $c_p^{(h)} = \omega/k > 0$) since the terms within the exponential in equation (2.42) must be negative if the wave is to be bounded far from the equator.

Allowance can be made for the background zonal wind if the frequency of the waves is replaced by a 'Doppler-shifted' or intrinsic frequency such that

$$\omega^+ \equiv \omega - k\overline{u}. \tag{2.43}$$

This assumes that the background wind is constant, an assumption that is reasonable

when it is considered that oscillations in the background such as the QBO are of time-scales of tens of months whereas the Kelvin waves are of period of order tens of days. An assumption is also made that the background wind is uniform in space. This assumption is harder to justify, but application of this Doppler shift produces realistic looking Kelvin waves and so appears to be a reasonable approximation.

If equation (2.43) for the Doppler shifted ω is put into equation (2.41) then, the vertical group velocity becomes (using the fact that $c_p^{(h)}$, horizontal phase velocity, equals ω/k),

$$c_g^{(v)} = \frac{k(c_p^{(h)} - \overline{u})^2}{N}. \tag{2.44}$$

The important result here is that the vertical group velocity tends to zero as c and $\overline{u}$ become similar.

A reasonable simplistic model for the dissipation of these waves is a relaxation towards some background state with some e-folding time-scale (i.e. $\delta\lambda = -\delta t \times \eta(\lambda - \lambda_0)$, where λ is the quantity in question, and η the time constant). Nothing is being stated about the mechanics of the dissipation at the moment. It could conceivably be through processes such as radiative cooling or friction. The decay of these waves with height can accordingly be expressed as:

$$\frac{\Delta\hat{\Phi}}{\Delta z} = -\alpha/c_g^{(v)} = \frac{-\alpha N}{k(c_p^{(h)} - \overline{u})^2}, \tag{2.45}$$

where Δ represents a small change and α is a factor that depends on the dissipation time-scales (η in the description above). The dependence of damping rate on the difference between the phase speed of the wave and the background zonal wind is important in the theories used to describe the QBO.(The Holton and Lindzen theory is described in detail in section 3.1.1.) A similar relationship between the phase speed and background wind is found in many wave-like phenomena in the atmosphere.

For the purposes of modelling these waves in this project, the shape of the geopotential perturbation of these waves is important. Combining equation (2.42) with equation (2.34),

the shape of a geopotential disturbance on a certain pressure surface is given by:

$$\Phi' = \hat{\Phi}_1 \exp\left(\frac{-\beta k y^2}{2\omega}\right) \Re\left[\exp i(kx - \omega t)\right] \tag{2.46}$$

where $\hat{\Phi}_1$ is a constant amplitude, defined for the pressure level.

Rossby-gravity Waves

If $\hat{v}$ is not set to zero in equations(2.36,2.37, 2.38), then other classes of waves, including mixed Rossby-gravity waves, can be described. Manipulation of equations(2.36,2.37, 2.38) and the elimination of $\hat{u}$ and $\hat{\Phi}$ gives,

$$\left[\frac{d^2}{dy^2} + \left(\frac{m^2\omega^2}{N^2} - k^2 - \frac{k\beta}{\omega}\right) - \frac{\beta^2 m^2}{N^2} y^2\right] \hat{v} = 0. \tag{2.47}$$

Substitution of

$$\eta \equiv \left(\frac{\beta|m|}{N}\right)^{1/2} y, \qquad M \equiv \frac{N}{\beta|m|}\left(\frac{m^2\omega^2}{N^2} - k^2 - \frac{k\beta}{\omega}\right) \tag{2.48}$$

into equation(2.47) produces

$$\left(\frac{d^2}{d\eta^2} + M - \eta^2\right) \hat{v} = 0,$$

which is familiar as the Schroedinger equation for a quantum harmonic oscillator. Solutions to this equation are worked through in detail in many quantum mechanics textbooks, see for example [Rae, 1992].

Solutions of this equation may be written as:

$$\hat{v} = \hat{v}_0 \exp(-\eta^2/2) H_n(\eta), \tag{2.49}$$

provided that $M = 2n + 1$, where n is a non-negative integer. (Actually, n=-1 produces the not particularly useful expression, $\hat{v} = 0$ and corresponds to the Kelvin wave solution.)

H_n are the Hermite Polynomials, the first three of which are given by: $H_0 = 1$, $H_1 = 2\eta$ and $H_2 = 4\eta^2 - 2$. Rossby-gravity waves are the solution to this equation when n=0. Further modes exist as equatorial Rossby waves but these are not investigated in this thesis.

Substitution of equations (2.48) into equation (2.49), and the substitution of the correct ($n = 0$) Hermite polynomial, gives solutions to equation (2.47) in $\hat{v}$ of:

$$\hat{v} = \hat{v}_0 \exp(-\beta|m|y^2/2N)[(\beta|m|N^{-1})^{1/2}y], \tag{2.50}$$

with the condition on M becoming:

$$\frac{m^2\omega^2}{N^2} - k^2 - \frac{\beta k}{m} = \frac{\beta|m|}{N}. \tag{2.51}$$

The properties of this wave are evident from these equations. The equatorial confinement is evident in equation (2.50). From equation (2.51), we get the dispersion relation for these waves:

$$|m| = \frac{N}{\omega^2}(\beta + \omega k), \tag{2.52}$$

and from this, we can show that, since $|m| > 0$ (for waves that can propagate in the vertical) then $c(= \omega/k) > -\beta/k^2$.

The vertical group velocity, as was seen in the Kelvin wave case, is an important quantity, giving us an estimate of dissipation of the wave. The vertical group velocity, $\frac{\partial\omega}{\partial m}$, is found from equation (2.52) to be:

$$c_g^{(v)} = \left(\frac{\partial m}{\partial \omega}\right)^{-1} = \frac{\mp\omega^3}{N(2\beta + \omega k)}. \tag{2.53}$$

Again, we can use the concept of a 'Doppler-shift' to allow for a background zonal wind. This provides expressions for the vertical wavenumber of:

$$|m| = N\left[\frac{\beta}{k^2(c-\overline{u})^2} + \frac{1}{(c-\overline{u})}\right] \tag{2.54}$$

and for the vertical group velocity:

$$c_g^{(v)} = \frac{-[\omega - k\overline{u}]^3}{N(2\beta + [\omega - k\overline{u}]k)}. \tag{2.55}$$

Using the same argument as used in deriving equation (2.45), we can get a simple expression for the decay of this wave with height. In this case, the propagation of the waves is described by:

$$\frac{\Delta\Phi}{\Delta z} = \frac{-\alpha}{c_g^{(v)}} = \frac{-\alpha N}{k(\overline{u} - c)^2}\left(\frac{\beta}{k^2(\overline{u} - c)} - 1\right). \tag{2.56}$$

Again, it is seen that the waves are strongly dissipated when passing through background winds of the same sense as the wave's phase velocity. A singularity occurs when $\overline{u} = c$ in the equations. This is the 'critical level' through which the wave cannot propagate. In nature, and in the model, the wave will dissipate before reaching this level through various processes described later.

Wave-Mean Flow Interactions

The dissipation of the waves has been considered in essentially a one-dimensional system, with the waves being dissipated through unspecified mechanisms as they propagate vertically. It might be reasonable to assume that the momentum deposited as the waves propagate will be centred on the equator, with a latitudinal profile akin to the latitudinal profile of the wave amplitudes (equations 2.42 and 2.50). A more complete treatment of the wave–mean-flow interactions as equatorial waves propagate in the stratosphere was performed in Andrews and McIntyre [1976*a*] and Andrews and McIntyre [1976*b*]. It is found that, particularly in the case of Rossby-gravity waves, the meridional structure of the acceleration produced is strongly affected by the dissipating mechanism. In the extreme case, where dissipation is purely by radiative mechanisms, it is found that the resulting accelerations in the mean flow are off the equator, with no acceleration seen at the equator. Such a jet structure would be quite different to the jets seen in the QBO. Theory predicts that only a small amount of mechanical dissipation is needed to centre

the jet on the equator and it may well be that the mechanical dissipation in the model will be adequate to cause the jet to be centred on the equator. Runs are performed in section 5.3.3 with Rossby-gravity waves forced in a model with varying levels of radiative and mechanical damping applied and it is found that in all cases an easterly jet is formed over the equator.

2.3.2 Rossby and Planetary Waves

Another class of waves that are very common in the atmosphere is Rossby or planetary waves.[4] The restoring force in the Rossby wave oscillation is the northward potential vorticity gradient. These waves are generated by a variety of mechanisms, including instabilities in the atmosphere and air flow over large-scale topography, generally in the troposphere. They are of global scale and are generally well resolved in models. Rossby waves are known to propagate through the tropics [O'Sullivan, 1997*a*] and to be influenced by the QBO [Dunkerton and Baldwin, 1991]. Their interactions in the tropics are however not well known. Their observation is complicated as the temperature signature of Rossby waves in the tropics becomes small with the decreasing f.

As with Kelvin and Rossby-gravity waves, the propagation of Rossby waves is strongly affected by the background zonal wind. In particular, Rossby waves are able to propagate vertically only in a 'window' of background zonal flows, which can be given as:

$$0 < \overline{u} < \overline{u}_c \quad \text{where} \quad \overline{u}_c = \frac{\beta}{k^2 + l^2 + \frac{f^2}{4N(z)^2 H^2}} \tag{2.57}$$

The implications of equation (2.57) are that Rossby waves can only propagate when the winds are westerly, but below a certain critical limit. It also suggests that long wavelength (lower k and l) planetary waves will be able to propagate more easily than shorter wavelength waves. Accordingly, observations show that planetary waves are only seen to any large degree in the the winter hemisphere middle atmosphere (as the winds here are

[4]The term planetary waves is normally used to refer to the largest-scale waves which are stationary or nearly stationary with respect to the earth's surface. The discussion here will concentrate mainly on planetary waves.

normally westerly). Here, they are responsible for the large deviations from zonal symmetry seen in many meteorological fields, especially in the northern winter stratosphere. The large inter-annual variability observed in the stratosphere, again especially true of the northern winter, is thought to be largely due to planetary waves propagating upwards form the troposphere.

Planetary Rossby waves propagate upwards and generally equator-ward from the tropospheric regions in which they are forced. Most of these Rossby waves are absorbed in the winter hemisphere sub-tropics. Here wave breaking acts to create a well mixed 'surf' zone. The QBO, with its associated changes in the tropical zonal wind, is thought to have a large effect on the propagation of these planetary waves. The 'zero wind line', the iso-surface of u=0, is normally located in the tropical region with westerly winds seen in the winter hemisphere and easterly winds to the summer-hemisphere side of the line. This surface represents a barrier to the propagation of Rossby waves. This 'zero wind line' position is strongly modulated in the lower stratosphere by the QBO, and this modulation in turn has a strong influence on the path that planetary waves may take. The influence of the QBO on the propagation of Rossby waves is described further in section 3.2.2 and experiments are performed in chapter 7 to investigate these effects.

Chapter 3

The Quasi-Biennial Oscillation

The modelling of the equatorial Quasi-Biennial Oscillation (QBO) in the zonal wind is one of the main aims of this project. In this chapter the QBO itself, its effect on the atmosphere and the current state of modelling the QBO are discussed.

From a dynamical point of view, the QBO is one of the best examples of wave-mean flow interaction observed in the atmosphere. It is also one of the few processes in the atmosphere with timescales greater than a year which makes it interesting as a source of interannual variability. From a modelling point of view, the QBO is an interesting challenge as it is generally not observed in GCMs and other complex three-dimensional models. This failure may be due to a number of reasons such as the limited vertical resolution of many GCMs in the stratosphere or the failure of GCMs to generate adequate waves to force the QBO. This is a significant failing of the models as the QBO (as will be described later in this chapter) has a far reaching influence throughout the atmosphere.

The phenomenon itself consists of a reversal in the tropical zonal mean winds, between the altitudes of around 17-32 km, with a period not far from 24 months. A time-series of the equatorial zonal mean zonal winds (figure 3.1) shows the oscillation. It is characterised by descending zones of easterly and westerly winds. These regions descend at an average rate of around 1 km per month so that at any altitude, there appears to be an oscillation. The maximum amplitude of the QBO winds is around $20\,\mathrm{ms}^{-1}$ at an altitude of around 24 km. The QBO has a very variable period, with an observed range of between 22 to 35 months and an average value of around 27 months.

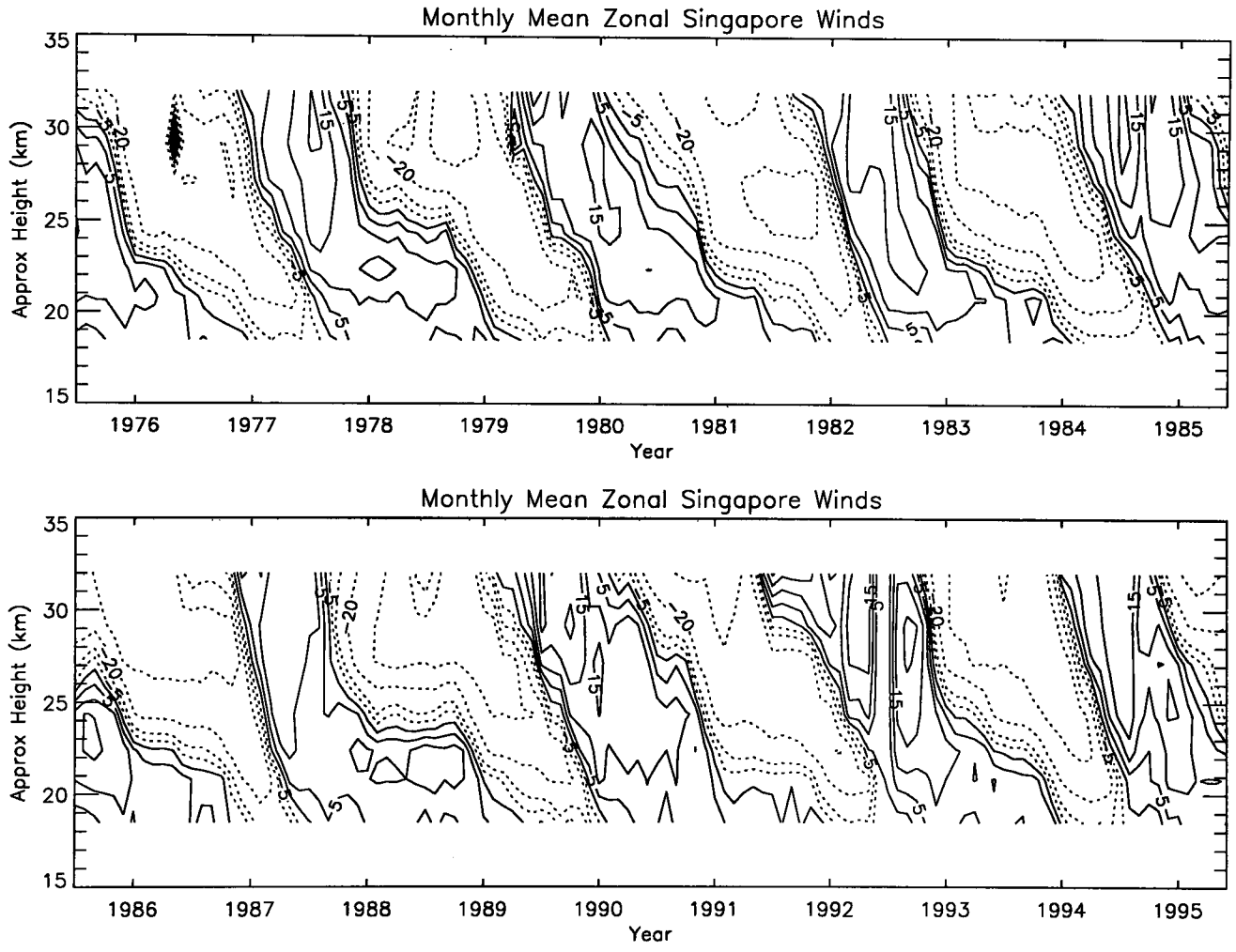

Figure 3.1: A plot showing equatorial zonal wind, in ms^{-1}, over several decades. The descending regions of easterly and westerly wind are clearly seen. Other features of this figure are described in the text. This data is taken from the Singapore wind data set, supplied by Barbera Naujokat.

Several key features of the QBO are evident in figure 3.1. The descending shear zones are immediately obvious. This plot shows the raw u-winds over the station and there has been no subtraction of any long term average or cleaning of the signal. It is clear that over this height range, the QBO is the dominant feature in the zonal wind field. The variability in the period of the QBO is also evident in this plot. The easterly shear zone especially can be seen to 'stall' on occasion (this can be seen in the figure in 1978/79 and 1988/89), contributing to the large variability of the period of the QBO. Finer details of the QBO are apparent such as the observation that the shear associated with the descending westerly jet is consistently stronger than that of an easterly jet.

Although the phase of the QBO is uncorrelated with the annual cycle, there appears to be a relation between the rate of phase progression of the QBO and the season [Wallace, Panetta and Estberg, 1993], [Kinnersley and Pawson, 1996]. A representation of the QBO in EOF phase space allows the rate of phase propagation of the QBO to be well defined. Wallace et al. [1993] found that the rate of phase propagation of the QBO could be related to both the phase of the QBO and the season. They show that the phase progression of the QBO is more rapid when a westerly jet is descending than when an easterly jet is descending. (This can be explained in terms of the enhanced vertical motion associated with the vertical shears in the wind, see section 3.2.1.) They find that the rate of change of the QBO phase has a maximum in April/May and a minimum in December/January (rates of phase progression averaging at 0.05 cycles per month in Apr/May as opposed to 0.03 cycles per month in Dec/Jan). This seasonal influence on the progression of the QBO is not entirely understood, but may be related to variations in the wave forcing of the QBO and the seasonal cycle in the background winds that will advect the QBO winds.

3.1 Driving the QBO

Although the full details of the mechanism that forces the QBO are not known, it is widely accepted to be driven by vertically-propagating waves. These waves accelerate the mean flow as they are dissipated in such a way as to generate the QBO. The Holton-Lindzen [Holton and Lindzen, 1972] model of the QBO forms a good basis for a consideration of

the forcing of the QBO. In this theory, the vertically propagating waves thought to drive the QBO are a Kelvin wave and a Rossby-gravity wave. It is now widely recognised that the forcing mechanism is more complicated, with especially gravity waves thought to have a large role in the forcing of the QBO.

3.1.1 Holton-Lindzen Theory of the QBO

In 1968 Lindzen and Holton produced a paper [Lindzen and Holton, 1968] that described the forcing of the QBO in terms of vertically propagating gravity waves that accelerate the mean flow as they are dissipated. According to linear theory, which is described in section 2.3, the vertical group velocity of the waves varies with the difference between the wave's phase velocity and the background wind velocity. The vertical group velocity of the waves, c_{gz}, decreases as the background wind velocity, $\overline{u}$, becomes closer to the wave's horizontal phase velocity, c, and as $\overline{u} \rightarrow c$, $c_{gz} \rightarrow 0$ and vertical propagation is impossible. The Lindzen-Holton theory of the QBO describes the forcing in terms of a spectrum of waves that propagate upwards until they reach such 'critical levels', where they are dissipated and the background wind is accelerated in the direction of the wave's phase velocity.

A revised theory of the QBO was produced in 1972 [Holton and Lindzen, 1972] by the same authors. Observational evidence suggested that the lower stratosphere does not have such a large, continuous spectrum of waves present, but only several classes of waves present at large amplitudes. The revised Holton-Lindzen theory of the QBO cites two waves, a westward propagating Rossby-gravity wave and an eastward propagating Kelvin wave. These waves are dissipated continuously as they propagate, with the dissipation being strongly dependent on the difference between the phase velocity and the background wind speed (as described in section 2.3). The dissipation is stronger when the wave's phase velocity is near the wind's background speed. In both theories, the generation of the oscillation is dependent on the following properties of the waves:

- Dissipation of the waves is stronger as the wind speed and the wave's phase velocity become closer.

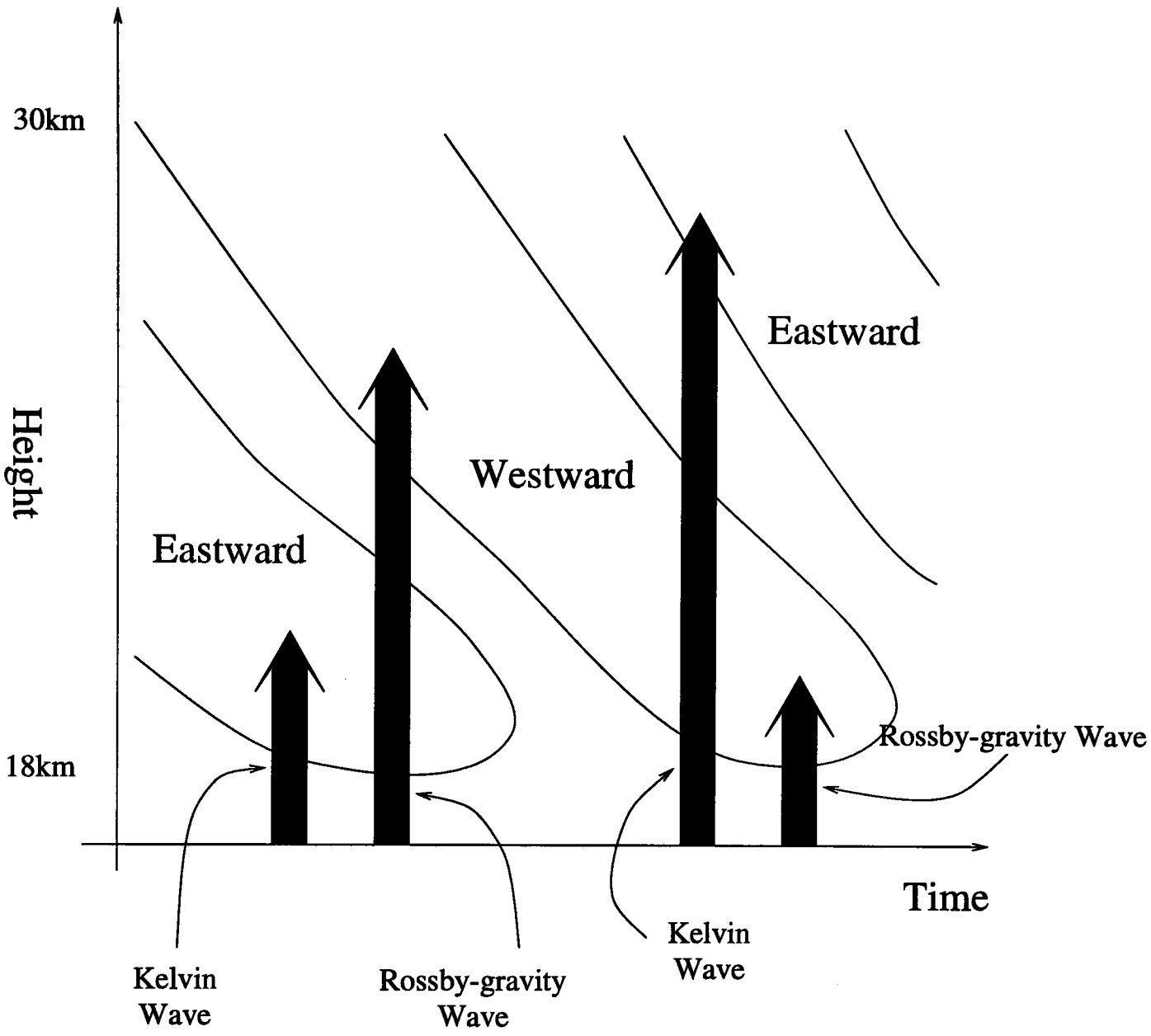

Figure 3.2: A diagram showing the principles of the Holton-Lindzen theory of the QBO. The contours represent zonal mean u-winds in the sense shown. The Kelvin waves are preferentially absorbed in the eastward jet, where they act to further enhance this jet. Rossby-gravity waves pass easily through this jet, and are dissipated above, where a westward jet is accelerated.

- As the waves are dissipated, the background wind is accelerated in the direction of the wave's phase velocity.

Figure 3.2 demonstrates how the dissipating waves generate an oscillation. In this diagram, the waves are labelled as Kelvin and Rossby-gravity waves although they could also include gravity and other classes of waves.

The one-dimensional model of the QBO was proposed by Holton and Lindzen [1972] and has been modelled on a computer by the author. In this model, the atmosphere is modelled by a parameterised wave forcing driving the mean wind away from a state that

is determined by a diffusion type profile. The equations governing $\overline{u}$ may be written:

$$\frac{\partial \overline{u}}{\partial t} = K\frac{\partial^2 \overline{u}}{\partial z^2} + G. \tag{3.1}$$

G is the wave forcing and may be written:

$$G = \frac{1}{\rho_o(z)}\left(\frac{\partial F}{\partial z}\right) \tag{3.2}$$

where

$$F(z,t) = F_1(0)\exp\left\{-\int_{z_1}^{z} g_1(z)dz\right\} + F_2(0)\exp\left\{-\int_{z_1}^{z} g_2(z)dz\right\}. \tag{3.3}$$

z_1 is the bottom boundary height of the model, nominally set to 17 km. The quantities g_1 and g_2 are the amounts that the waves are dissipated in the increment dz as the waves propagate upwards. They can be written as

$$g_1(z) = \frac{\alpha N}{k_1(u-c_1)^2}$$

for the Kelvin waves and

$$g_2 = \frac{\alpha N}{k_2(u-c_2)^2}\left\{\frac{\beta}{k_2^2(u-c_2)} - 1\right\}$$

for the Rossby-gravity waves (these expressions are derived in section 2.3). The model is integrated with a vertical grid spacing of 250m and a time-step of a day. This model is very cheap to run, as would be expected with such a simple and small system, requiring only a few seconds of computer time to do several years of model run. Using these expressions and supplying suitable values for $F_1(0)$ and $F_2(0)$, an oscillation can be produced. Such an oscillation is shown in figure 3.3. In this case, constants are set at $F_1 = -F_2 = 4 \times 10^{-3}\,\mathrm{m^2 s^{-2}}$. The oscillation in this extremely idealised model certainly shows the descending zones that characterise the QBO and demonstrate that an oscillation may be produced in a way consistent with the Holton–Lindzen model.

By varying the parameters of momentum flux, wave phase speed and diffusion coeffi-

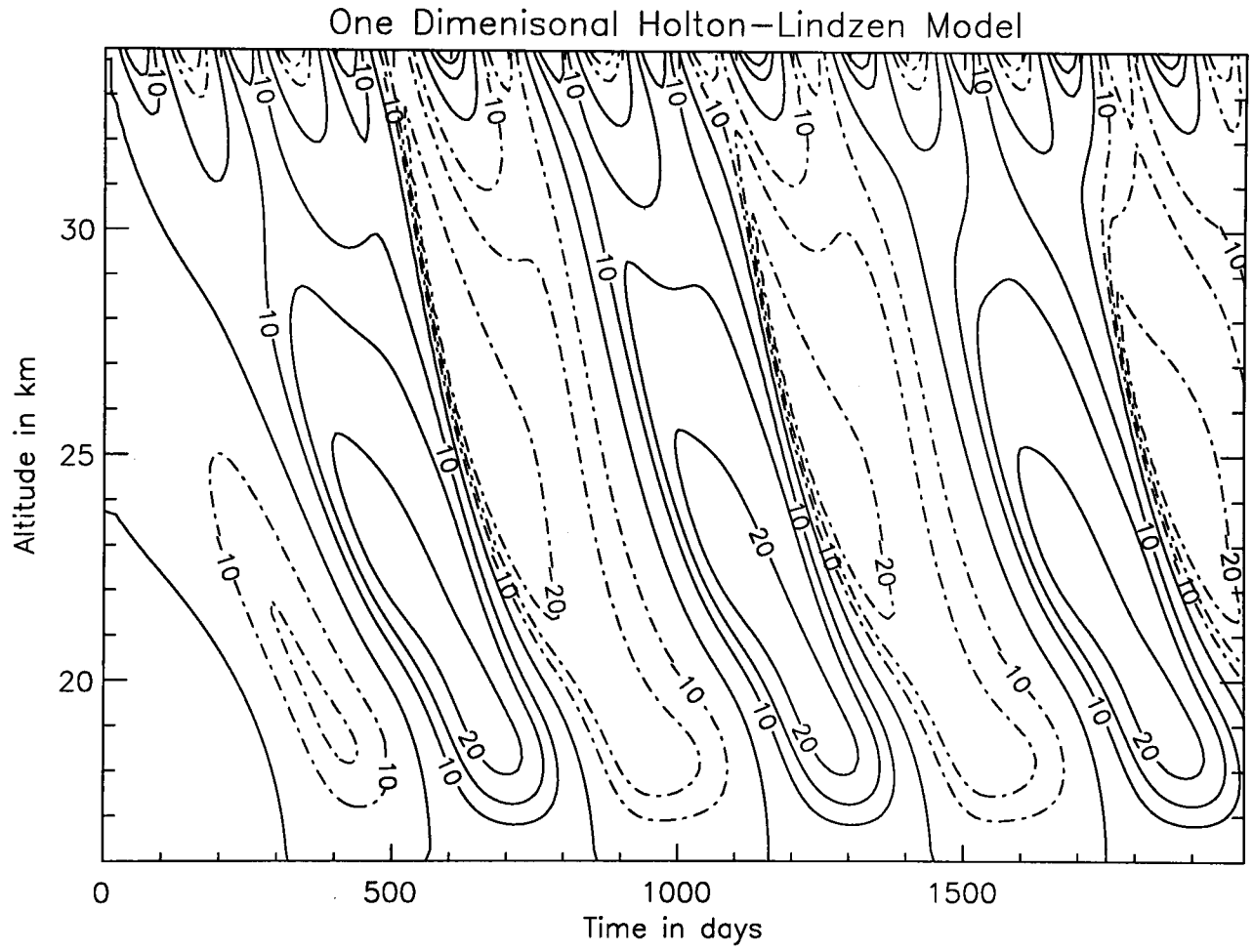

Figure 3.3: The $\overline{u}$ wind produced in a one-dimensional model of the QBO as described in the text. The contours are in metres per second. Many of the gross features of the QBO are produced in this very simple model.

cient, the properties of the oscillation can be investigated to find the physical mechanisms that are controlling the oscillation. Altering the diffusion coefficient has a very strong effect on the period of the oscillation (a higher diffusion coefficient results in a shorter period oscillation), with minimal effect on the amplitude of the oscillation. Changing the phase speed of the waves at the bottom of the model domain has a direct effect on the amplitude of the oscillation (perhaps as expected as the waves cannot induce a jet speed greater than their phase speed). Altering the momentum flux has a principle effect on the period of the oscillation, higher momentum fluxes resulting in a shorter period oscillation. This is due to more rapid accelerations in the runs with greater momentum flux, seen as sharper shear zones, resulting in a faster propagation of the oscillation.

Plumb and McEwan [1978] produced a QBO-like oscillation in a laboratory experiment. In this experiment, standing waves were forced on the bottom of a cylindrical tank containing a stratified salt solution. This produced internal gravity waves with phase speeds in opposite directions. As they were dissipated, an oscillation of much longer timescales than the forcing waves was produced, demonstrating wave mean flow interactions acting to produce an oscillation in a laboratory experiment.

3.1.2 Gravity Waves and other Forcing Mechanisms

As mentioned above, the forcing of the QBO is thought to be considerably more complicated than described by the Holton-Lindzen theory. When model and theoretical values of the momentum fluxes necessary to drive the QBO are compared to those of observed waves, it becomes apparent that the observed Kelvin and Rossby-gravity waves have insufficient momentum flux to drive the QBO. This is especially true in the case of Rossby-gravity waves, which are observed to have only between a quarter and a half of the necessary momentum flux to drive the easterly phase of the QBO. It is found in this project that the required amplitudes of forcing waves are indeed larger than those observed in nature. A detailed discussion of the wave amplitudes used in this model is given in section 6.1.1.

Gravity waves are an obvious candidate to provide the necessary additional momen-

tum flux. Gravity waves are particularly challenging to model as they are typically too small in scale to explicitly represent in any reasonably complex and/or global scale model and must therefore be parameterised. The parameterisation of gravity waves in models is a very active area of research at the moment. Dunkerton [1996] describes the role that gravity waves are thought to play in the QBO, and performs several model runs that simulate the QBO. He finds that gravity waves are likely to supply some of the momentum for the easterly phase of the QBO, but are unlikely to provide all of it. Gravity wave parameterisation in models is a developing field and improved parameterisation schemes are likely to aid the modelling of the QBO. It is interesting that many gravity wave parameterisation schemes tend to produce descending wind zones in the tropics. These wind zones can be 'tuned' by altering different constants in the gravity wave parameterisation schemes to give, in some cases, a quite realistic QBO.

As well as the gravity wave contribution to the QBO, other waves may provide additional sources of momentum. Haynes [1996] describes how the latitudinal extent of the QBO is not governed by the extent of the forcing waves but is restricted by the changing response of the atmosphere to a zonal force as the Coriolis parameter changes with latitude. This means that the forcing of the QBO need not be limited to equatorially confined waves. A potential source of additional wave forcing is the lateral propagation and dissipation of Rossby waves. Dunkerton [1983] and Takahashi and Holton [1991] describe the possible role of these waves in the forcing of the QBO but conclude that they are unlikely to supply much of the 'missing' easterly momentum. In section 7.2, planetary waves are introduced to the model through the addition of some 'topography' to the bottom boundary and their interaction with the QBO observed. No great changes are observed in the generated QBO, although there are some changes to the descending shear zones.

3.2 Some Properties of the QBO

The circulation of a large part of the atmosphere is affected by the presence of the QBO. In this section, some of the direct effects of the QBO will be described. In section 3.3,

some of the more far reaching effects of the QBO on the atmosphere system will be described. There are many 'quasi-biennial' signals observed in the atmosphere and it is often not easy to separate those that are directly attributable to the influence of the QBO and those that have, of their own accord, periods of nearly two years. Often, the period over which measurements have been made of these phenomena is inadequate to separate signals which although unrelated, have similar periods.

3.2.1 The QBO in the sub-tropical meridional and vertical winds

As well as the zonal wind oscillation associated with the QBO, there is also an oscillation in the meridional and vertical winds. This circulation is very much weaker than the zonal wind oscillation and is in fact a perturbation on the stronger meridional and vertical winds that exist in the middle atmosphere. The tropical and sub-tropical oscillation can be described in terms of the adjustments in the circulation necessary to maintain thermal wind balance with the vertical shear of the QBO jets. The thermal wind relation is given in section 2.2. The vertical shear of the $\overline{u}$ wind is related to the latitudinal variation of the temperature on a β-plane by the equation (2.12):

$$\overline{u}_z = -\frac{R}{H\beta y}\overline{T}_y.$$

Rearranged, this gives the temperature perturbation associated with the shear in the QBO as:

$$\overline{T}_y = -\frac{H\beta y}{R}\overline{u}_z. \tag{3.4}$$

In the case of a positive vertical shear in $\overline{u}$ (winds becoming more westerly with height), this leads to a negative value of $\overline{T}_y$ in the northern hemisphere (temperatures getting warmer as latitude decreases), and conversely a positive value of $\overline{T}_y$ in the southern hemisphere. This implies that a warm temperature perturbation must exist for thermal balance to be met. Conversely, the shear produced by easterly winds over westerly produces a cold perturbation. This temperature perturbation must be sustained through vertical motion of air parcels, with a warm perturbation maintained by an enhanced de-

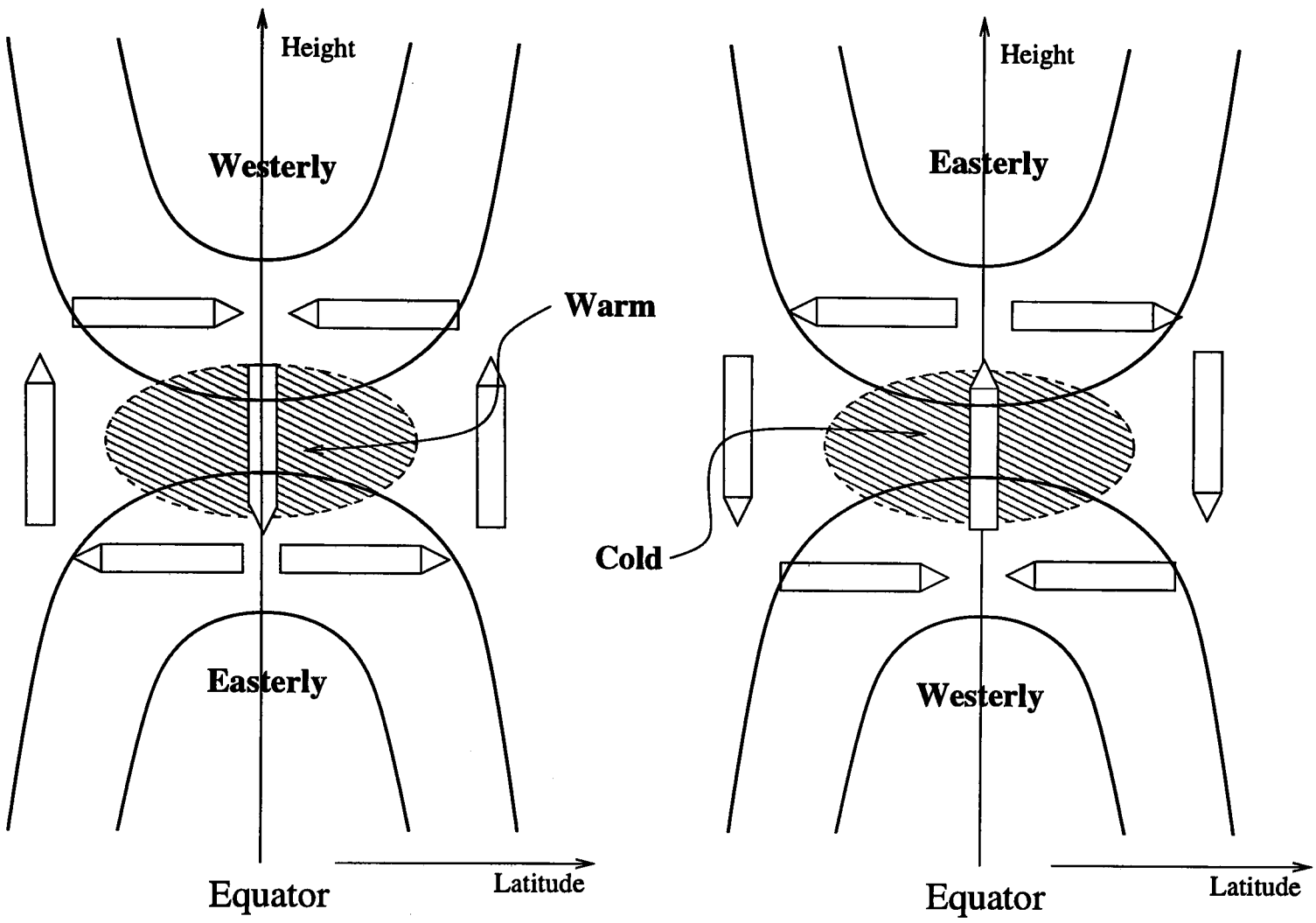

Figure 3.4: A schematic diagram showing the temperature perturbations and associated meridional and vertical motion necessary to maintain the thermal wind balance of the wind shear in the QBO.

scent over the equator (and cold temperatures corresponding to enhanced ascent). The resulting meridional and vertical motions are shown schematically in figure 3.4. These motions are the generation of cells where enhanced descent (ascent) over the equator is matched by an enhanced ascent (descent) in the sub-tropics, with meridional winds completing the cells. These cells can be seen in the model runs performed in chapter 6. These motions are superimposed on the winds present at the equator, which in general is an ascent driven by diabatic heating.

An estimate of the approximate amplitude of the temperature perturbation may be obtained by estimating the quantities in equation (3.4). A rough estimate gives the shear associated with the QBO to be around $5\,\mathrm{ms}^{-1}/\mathrm{km}$, and the extent of the QBO to be of order 10° from the equator. Integration of equation (3.4) gives a value of $\overline{T}$ of order 2–3 K. The associated vertical motions are of the order several millimetres per second, or several kilometres per month, which is the same order as the descent rate of the QBO shear

zones. This circulation, as well as its effect on other atmospheric phenomena, affects the the propagation of the QBO. The asymmetry between the easterly and westerly phases of the QBO may be partially explained by the difference in vertical winds associated with their shears.

3.2.2 The Effect of the QBO on the Zero Wind Line and Planetary Wave propagation

The QBO has many effects on properties of the atmosphere outside the tropics. The meridional circulation of the atmosphere is not strong enough to transfer QBO information from the tropics to the higher latitude directly. Another process must be found for this transfer of information. Such a process may exist in the modulation and channelling of planetary waves by the QBO.

The propagation and ultimate dissipation of waves in the atmosphere can have a huge effect on the circulation. In turn, the zonal-mean state of the atmosphere strongly affects the propagation of waves. Planetary waves generated in the mid-latitudes are thought to have a huge effect on the circulation. As described in chapter 2, they have a key role in many processes seen in the stratosphere, for example stratospheric sudden warmings, and their influence is visible in tracer distributions through their contribution to the mixing of atmospheric constituents. It should be remembered that planetary waves are able only to propagate in a westerly background wind that is not too strong. Such conditions typically exist in the winter mid-latitude stratosphere. In the summer hemisphere, easterly winds dominate the circulation throughout the stratosphere. The 'zero-wind line', the zero contour in the zonal mean u-wind, is normally found near the equator where the wind changes sign between the hemispheres. This zero-wind line represents an impassable barrier to the Rossby waves as they cannot propagate vertically in the easterly winds present on the summer side of this contour. The position of this line in the lower stratosphere, as can be imagined, is strongly modulated by the QBO. Figure 3.5 shows January height–latitude plots of the zonal mean u-wind for two phases of the QBO. These plots are taken from a model run where the QBO has been modelled, somewhat differently to the way it will be

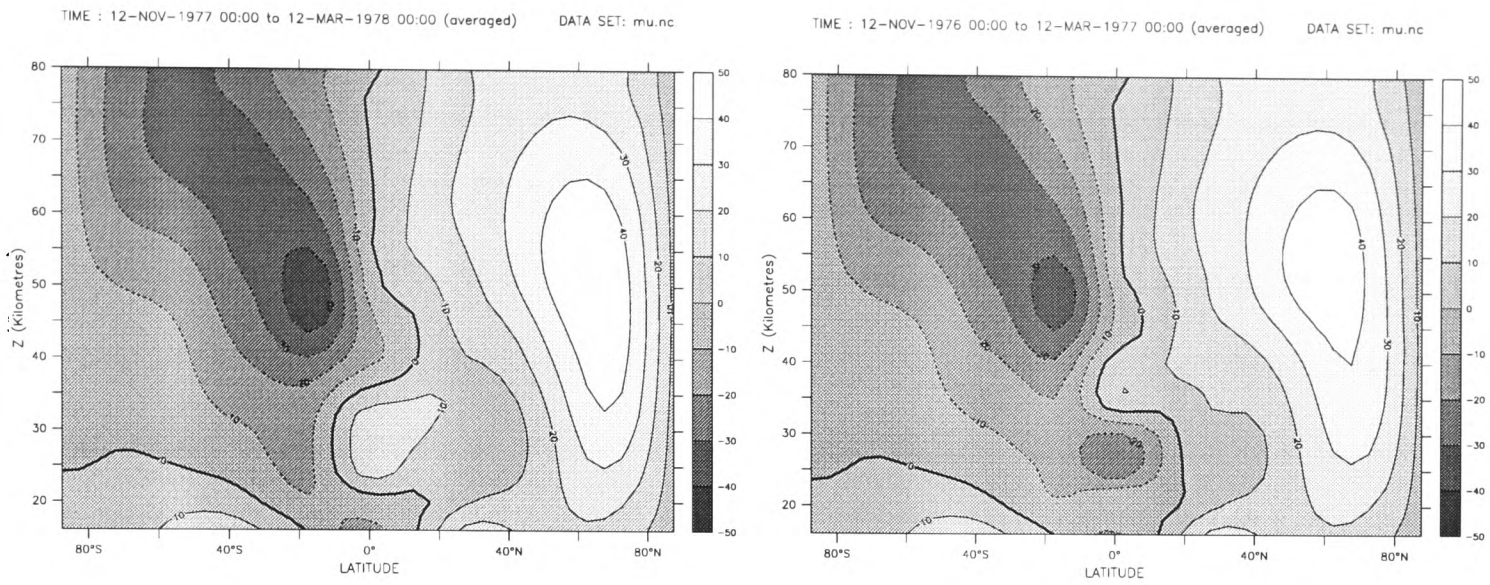

Figure 3.5: The zonal mean u-wind (in ms^{-1}) associated with two different phases of the QBO. The left hand plot shows the zonal wind in a westerly phase of the QBO. The right hand plot shows an easterly phase of the QBO. The heavy solid contour is the zero wind contour and can be seen to be significantly shifted between the two phases of the QBO.

produced in this project, by relaxing the equatorial winds towards observations over the tropical region.

3.3 Other Signatures of the QBO

The effect of the QBO is not confined to the tropical lower stratosphere. The influence of the QBO on other processes in the atmosphere is an important area of study. Through these interactions, the QBO has a wide reaching influence on many aspects of the climate system. In this section, QBO effects in column ozone, various tracer distributions and some dynamical phenomena are described. Although these mechanisms are not investigated in this project, they are described here as they illustrate the importance of the QBO in many other processes which are of interest to atmospheric scientists.

3.3.1 The QBO in Column Ozone

There is a substantial QBO signal in the column ozone over a large part of the globe. Within the tropics, this signal is closely correlated with the dynamical QBO. At higher latitudes, the signal becomes more complicated and appears to be influenced by a combination of the equatorial dynamical QBO and the annual cycle.

The symmetric tropical and sub-tropical ozone QBO can be explained largely in terms of the vertical motions induced as the atmosphere moves towards thermal wind balance with the shears in the zonal wind, [Gray and Ruth, 1993].[1] These induced motions are described in section 3.2.1. There is a large vertical gradient in ozone in the stratosphere, with ozone concentrations increasing sharply from low tropospheric levels at the tropopause to a peak in ozone mixing ratio at around 35 km. Enhanced descent will advect higher, upper stratospheric concentrations of ozone downwards. Below around 25 km, the ozone may be regarded as a passive tracer. The ozone in the upper stratosphere will not be significantly depleted as it will be replenished quickly through fast photo-chemical reactions, resulting in a high column ozone anomaly. Conversely, ascending motion will restrict the advection of the higher ozone air downwards and lead to a relative deficit in the column ozone.

The more complicated QBO signal in the extra tropics is the result of a combination of factors. Here, the ozone variation shows significant dependence on the season as well the phase of the QBO which makes a description of the relationship complicated. The lack of a fixed phase relationship between the QBO and the seasonal cycle means that if the QBO was regular at 28 months, the same phase of QBO/seasonal position would happen only once every seven years, and studies of the extra-tropical ozone phenomenon must be made over long timescales. The gross features of the structure observed in the extra-tropical QBO may be described in terms of the symmetrical QBO interacting with the asymmetrical annual cycle to produce an asymmetrical signal [Gray and Ruth, 1993],[Gray and Pyle, 1989],[Gray and Dunkerton, 1990].

The model does not have an interactive ozone scheme[2] and so is of limited use in investigating ozone effects and the QBO in ozone is not investigated in this project. There is nothing in principle that would prevent an interactive ozone scheme being implemented in the SMM at some point in the future. This is planned as future work with this model in a variety of scenarios (see chapter 8).

[1]The situation is actually more complicated as the radiative feedback effects of the ozone perturbation are significant and must be considered if the correct phase relation is to be found between the dynamical and ozone QBOs [Hasebe, 1994].

[2]Ozone is not explicitly specified in the Newtonian cooling radiative scheme and the `MIDRAD` scheme uses climatological ozone fields.

3.3.2 Polar Vortex and the Ozone Hole

There appears to be a QBO signature in the temperature of the polar vortices in both the northern and southern hemispheres. It is observed that in years where the westerly phase of the QBO is dominant, the polar vortex is less disturbed and colder than in years when there are easterly winds over the equator. In the Northern hemisphere, this signal manifests itself in a tendency for more sudden warmings in years with an easterly QBO [Labitzke, 1982]. In the southern hemisphere the signature is easily seen in the temperature within the polar vortex [Baldwin and Dunkerton, 1998]. Importantly, a colder winter vortex can result in conditions that are favourable for increased ozone depletion. Especially relevant in the southern hemisphere is the formation of polar stratospheric clouds at low temperatures (they can be formed when $T \leq 195$K) which can provide a site for heterogeneous reactions which can very rapidly deplete ozone levels. These reactions are thought to be very important in the generation of the ozone hole found in the Antarctic spring stratosphere.

The mechanism by which the equatorial stratospheric signal is transported to the polar latitudes is not well established. Planetary waves are thought to play a large role in the dissemination of this signal. These waves are described in section 2.3.2. The interannual variation in the polar vortices depends on many more factors than the QBO. There is mounting evidence that solar activity may have a significant effect on the polar temperatures [Labitzke, 1987],[Naito and Hirota, 1997] and that considering the QBO in isolation is not enough to predict the state of the polar vortex.

Another mechanism by which the tropical atmosphere is thought to influence the extra-tropical atmosphere is described in Rosier [1996]. In this thesis, an interesting dependence of the evolution of a stratospheric sudden warming on tropical conditions is observed. The most robust feature which differs between model runs which capture a strong warming and those which fail to capture the warming is the amount of inertial instability that is present in the equatorial upper stratosphere.[3] Although the QBO is the dominant feature

[3]Inertial instability is a condition, in some ways analogous to static instability which acts to remove potential temperature gradients which decrease with height, which is present if the condition $(f - \overline{u}_y) \leq 0$ is met. Inertial instability manifests itself in very flat 'rolls' where air moves meridionally to eliminate the instability. Inertial instability is normally limited to near the equator, where f is small.

in the zonal winds only in the lower stratosphere, a significant QBO signal can be seen in the semi-annual oscillation in the upper stratosphere. Such an effect may be significant in the QBO signal seen in the polar regions.

3.3.3 The QBO in the Troposphere

Often research in the stratosphere is prompted by a need to understand the atmospheric phenomena that affect us directly. These phenomena are, with only a few exceptions, found the troposphere. Observations reveal many signatures in the troposphere that have periods around 24 months and statistical methods often link these signatures with the equatorial stratospheric QBO. Such quantities include tropical rainfall (a link is proposed between the temperature perturbations associated with the QBO shear zones and the deep convection in the troposphere [Collimore, Hitchman and Martin, 1998]), rainfall and hurricane frequency.

GCM studies [Hamilton, 1998] have generally been unsuccessful in reproducing such relations between the stratospheric QBO and these tropospheric phenomena. It is still not clear whether this is a failing in the models or an indication that the links do not exist. Alternative descriptions of the tropospheric QBO in terms of an interaction between other signals present in the troposphere have been formulated. Goswami [1995] find that the tropical tropospheric QBO may be modelled using an interaction between the annual cycle, the El Niño-Southern oscillation and a high frequency synoptic signal and is independent of the stratospheric QBO. The source of the tropospheric QBO is far from established, and may be a combination of stratospheric influence as well as tropospheric processes.

To be able to identify and model any stratospheric QBO–troposphere links would be very desirable as it would allow some degree of long range prediction in tropospheric quantities. Although an investigation of such effects is well outside the bounds of this project (the model used does not model the troposphere), an improvement in the modelling of the QBO in current GCMs would lead to a greater understanding of the interaction between the QBO and the rest of the atmosphere.

3.4 Past and Present Modelling of the QBO

Modelling of the QBO stretches from the Holton–Lindzen one-dimensional model described in section 3.1.1 to its appearance in three-dimensional primitive equation models. The QBO has proven extremely hard to model in general circulation models. This is thought to be due to several factors including the inability of GCMs to generate adequate forcing waves and limitations in the resolution available in GCMs. Model results in this thesis will show that both these factors are likely to result in an inability to generate a QBO in a model.

One-dimensional models are still employed to investigate properties of the QBO. They have the advantage that they are very cheap to run and large variations in model parameters may be investigated rapidly. Such experiments may be impractical with a three-dimensional model which may take several weeks of model time to provide a model run that could be performed in several seconds in a one-dimensional model. One such investigation is performed by Cordero and Nathan [1998] where the effect of ozone feedbacks in the dissipation of equatorial waves is investigated. A series of decadal runs using a one-dimensional model are used to examine the effects on the QBO.

A lot of valuable work has been performed with two-dimensional models. These models represent the zonal mean state of the atmosphere, with axes in the vertical and meridional directions. Waves cannot be explicitly modelled in such models but a QBO may be introduced either through parameterising the effect of the driving waves [Gray and Pyle, 1989], in a manner similar to that used in the one-dimensional model, or by relaxing the model state to observed equatorial winds and investigating the associated circulation, for example as used by Gray and Ruth [1993]. Two-dimensional models lend themselves well to modelling of tracer transport and chemistry.

Three-dimensional models with an assortment of complexities have been used to model the QBO. Again the QBO may be modelled by a variety of means. Some recent GCMs appear to be able to generate a QBO spontaneously [Takahashi, 1996]. The QBO may be forced by adding the necessary waves explicitly. This is the method used in this project. The QBO can also be introduced to the model by performing a relaxation of the

model winds towards observations (or indeed a prescribed idealised QBO). This method can be used to generate a realistic QBO in a complex model. Several such studies have been published recently. Hamilton [1998] relaxes the zonal winds in a GCM towards an idealised QBO and investigates many effects on the circulation. His study includes a (largely unsuccessful) search for tropospheric effects of the QBO and a (more successful) investigation of the effect of the QBO on planetary waves and the northern polar winter.

The SMM (the same model as used in this study) was used in a similar mode to investigate the effects on tracer transport by the QBO [Kennaugh, Ruth and Gray, 1997]. In this case, model zonal winds were relaxed towards observed QBO winds and the resulting tracer fields were compared to observed tracer fields. The model was very successful in reproducing the QBO modulation in tracer fields seen in the satellite data.

Perhaps some of the most exciting developments in modelling the QBO is the appearance of a QBO in some general circulation models. Such spontaneous QBOs are described in Takahashi [1996] and Nagashima and Takahashi [1998]. Nagashima and Takahashi [1998] add an interactive ozone scheme to their GCM and manage to get a remarkably good simulation of the observed QBO in both the wind and ozone fields. The model used in both these studies has very a fine vertical resolution, with the lower stratosphere represented at about 500m resolution. This is very unusual for a general circulation models, which are typically geared towards modelling the troposphere accurately and only devote a few model layers to the lower stratosphere. A spontaneous QBO is also seen in the European Centre for Medium Range Weather Forecasting (ECMWF) GCM and is shown in figure 3.6. There is some uncertainty as to how robust this QBO will be in the model and it can be seen that there seems to be a trend towards more westerly winds as the run progresses.

The modelling performed in this project will provide a greater understanding of the QBO in several areas. The modelling of equatorial waves and the QBO in chapters 5 and 6 will provide a greater understanding of the problems that modern models have when trying to reproduce the QBO. Work is currently being performed with several models, for example the UKMO Unified Model, with the aim of producing a realistic QBO. The

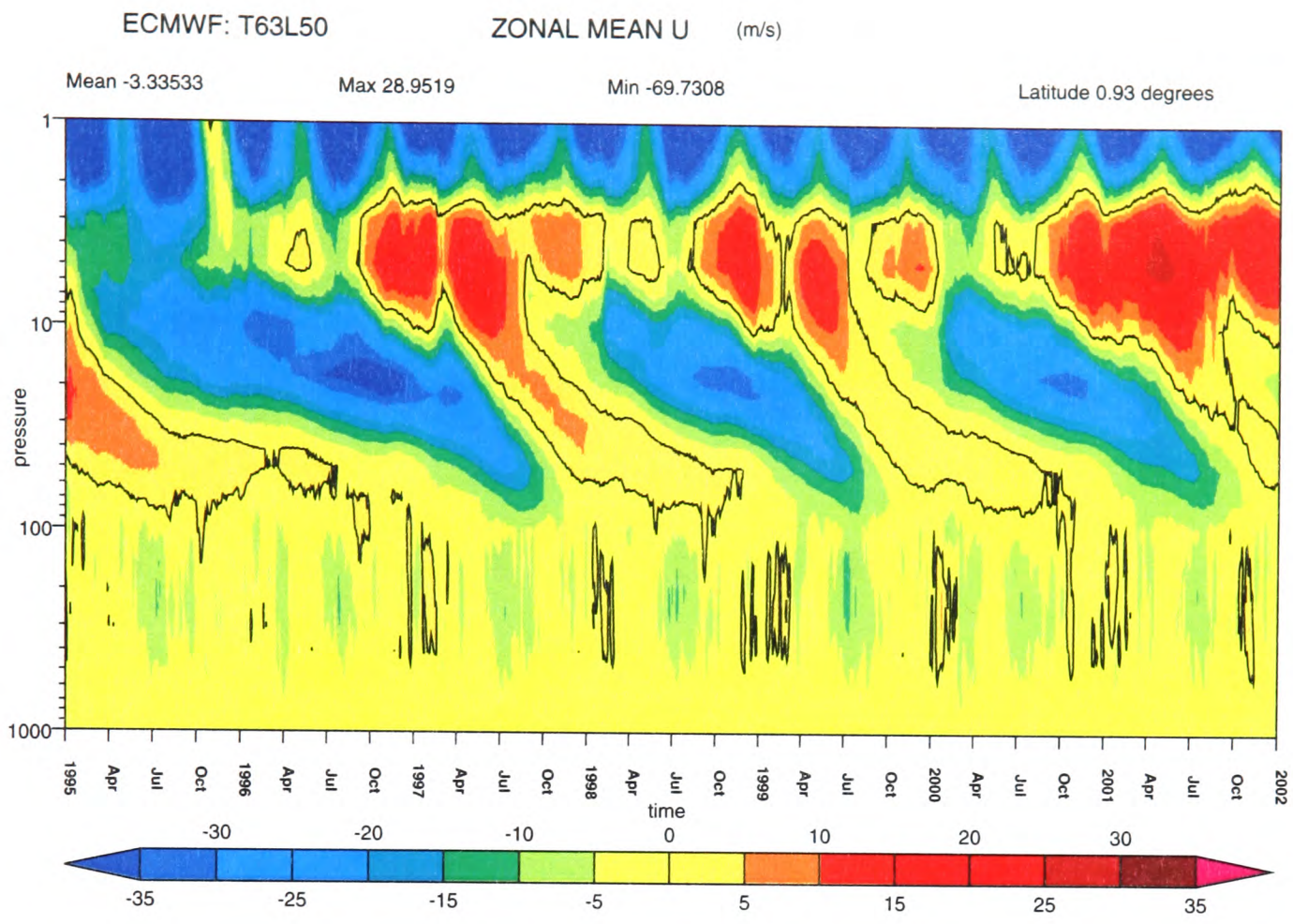

Figure 3.6: A plot showing the equatorial zonal mean u-winds (in ms^{-1}) against time and height for part of a run in the ECMWF GCM. A very realistic QBO is seen in these winds. This plot was supplied by Agathe Untch at the ECMWF.

modelling of a QBO in the SMM will allow a set of necessary conditions for the successful modelling of the QBO to be established. Further modelling performed in these chapters demonstrate the sensitivity of the modelled QBO to other factors of the in the simulated middle atmosphere.

Interactions between the equatorial QBO and the extra-tropics are one source of the large interannual variability seen in the stratosphere. This two-way interaction between the QBO and planetary waves is thought to be one mechanism by which the QBO is communicated to the extra-topics [Holton and Tan, 1980]. This interaction has been modelled to some extent in recent studies, for example O'Sullivan [1997*b*], but is still poorly understood. The modelling performed in this project (and described in chapter 7) will allow the full two-way interaction between the QBO and planetary waves to be observed and analysed under controlled circumstances.

Chapter 4

Model and Methods Used

4.1 The UKMO Stratosphere-Mesosphere Model

The model used throughout this project is the UKMO Stratosphere-Mesosphere model.[1] This is a global, mechanistic, primitive equation grid-point model of the middle atmosphere. The model was originally formulated by Murgatroyd in 1971 and completely rewritten in the then new `FORTRAN77` language by Mike Fisher in approximately 1983. It has been largely rewritten by Bryan Lawrence and parts of it extensively modified by the author. The model is described in a UKMO technical note [Fisher, 1987] which, although slightly out of date, is still largely applicable to the model used. In its present standard configuration, the model is a fairly complex middle atmosphere model with a sophisticated radiation scheme, `MIDRAD` [Shine, 1987], and parameterisations for gravity wave drag[2], vertical diffusion (added by the author in the course of this thesis project) and dry convection. Through the course of the project, the model has been run in many configurations, for example, with a simplified radiation scheme, increased vertical resolution and in a perpetual January mode.

In this chapter, the model, including the dynamics represented by its equations, the physics parameterised, the logical structure of the model and some aspects of the code will be described. Many of the features of the standard model are well described in

[1] Referred to as the SMM from this point on.

[2] In this study, Rayleigh friction is the gravity wave parameterisation, although a Hines [Hines, 1996] scheme is being implemented in the model by Bryan Lawrence

[Rosier, 1996] and only those with significant bearing on this project will be repeated here. New and modified subroutines are described in this chapter. Some of the model code (from some of the more relevant subroutines used in this project) is given in appendix B.

4.1.1 General Features of the Model

The model domain is of global extent in the horizontal and occupies a height range of 100 hPa to 0.01 hPa (approximately 16–80 km) in the vertical. This domain is represented by a finite difference grid, with default resolutions of 5° by 5° in the horizontal and 2 km (in log-pressure height) in the vertical. This vertical resolution is modified (resolutions used are 1 km and 500m) through the course of the project. The horizontal resolution is not altered in this project but it has been used at different horizontal resolutions by other researchers [Iwi, 1997].

The troposphere is not modelled, but instead a lower boundary condition is specified on the 100hPa pressure level. There are several options available for the lower boundary forcing. In the standard configuration, a bottom boundary of the geopotential height of the 100hPa pressure level is specified. The next level of bottom boundary specification adds a temperature field into the boundary data. This forcing has been used for some of the runs and is described in section 5.4.1. In addition to these forcing terms, the bottom boundary may also be forced with temperature, geopotential and the zonal and meridional components of the wind field at the lower level. This was never done in this project. In the absence of explicit T, u or v bottom boundary forcing, these prognostic model variables are linearly extrapolated onto a level below the lowest full model level when they are needed. This under-specification of the model bottom boundary produces some problems, especially at higher vertical resolutions, which are described in section 4.3. The boundary is typically taken from satellite data (or observational data that has been assimilated into another model) and is read into the model as daily data fields from file. The need for a supplied bottom boundary prevents this model being used for forecasting, but allows the middle atmosphere to be studied under very controlled conditions. Idealised waves and

perturbations are introduced into the model by manipulating the lower boundary. This is achieved in the model subroutine `GEOPER` (described in section 4.2.1) which is one of the key modifications performed on the model and allows a wide range of wave-like and stationary perturbations to be added to the bottom boundary.

At the upper limit of the model, there is a boundary condition imposed of no vertical motion through a level half a grid box above the upper model level. This is a fairly standard upper boundary condition in atmospheric models. In order to prevent spurious reflections of waves off the top of the model, a *sponge layer* is created in the higher model levels where strong Rayleigh damping of the horizontal winds (towards a state of rest) acts to damp out any disturbances that would otherwise reach the top level of the model. The Rayleigh friction also provides some degree of gravity wave parameterisation in the model and is described in section 4.1.2.

The model has been significantly modified during the course of the project and now differs from distributed code in a number of ways. These modifications include additional or modified subroutines, described in section 4.2, as well as changes to the model resolution. The more fundamental changes include:

- The model vertical resolution has been modified. Through most of this project, the model is run at a vertical resolution of 1 km, although some runs are performed at the standard 2 km resolution as well as at 500 m.

- The model radiation scheme has been simplified greatly, with the sophisticated `MIDRAD` scheme of Shine [1987] being replaced with a simple Newtonian cooling scheme for many runs.

- The bottom boundary code has been modified such that a temperature value may be specified along with the geopotential height information. This temperature forcing extends into the `GEOPER` routine, allowing wave-like perturbations in temperature to be forced in parallel with perturbations in the geopotential height.

4.1.2 The Model Physics

The model, as mentioned above, is a mechanistic middle atmosphere model. Although not a complete GCM in that the model domain is limited in vertical extent from 100 to 0.01 hPa, it treats the physics of the middle atmosphere in a fairly complete manner, with a degree of complexity similar to that used in many current GCMs. During the course of this project, many physical parameterisations in the model will be simplified for various reasons. The model equations describing the dynamics of the stratosphere were not altered.

The Basic Model Equations

The model solves the non-linear, hydrostatic, primitive equations[3], discretised on a 'box' type finite grid. This grid, as mentioned previously, has grid spacing of 5° by 5° in the horizontal. Vertical discretisation is performed on an isobaric vertical grid with equal spacing in log-pressure. The model equations solved are given by:[4]

$$\delta_t \overline{u}^t + D(u) - (f + \frac{u}{a}\tan\phi)v + \frac{1}{a\cos\phi}\left(\frac{4}{3}\delta_\lambda \overline{\Phi}^\lambda - \frac{1}{3}\delta_{2\lambda}\overline{\Phi}^{2\lambda}\right) = F_\lambda, \tag{4.1}$$

$$\delta_t \overline{v}^t + D(v) + (f + \frac{u}{a}\tan\phi)u + \frac{1}{a\cos\phi} \times \left(\frac{4}{3}[\delta_\phi(\overline{\Phi}^\phi \cos\phi) - \Phi\delta_\phi(\cos\phi)] - \frac{1}{3}[\delta_{2\phi}(\overline{\Phi}^{2\phi}\cos\phi) - \Phi\delta_{2\phi}(\cos\phi)]\right) = F_\phi, \tag{4.2}$$

$$\delta_t \overline{T}^t + D(T) - \frac{\kappa(\overline{p\dot{s}}^s)T}{p} = Q/C_p, \tag{4.3}$$

$$D(1) = 0 \quad \text{and} \tag{4.4}$$

$$\delta_s \Phi + R\overline{T}^s = 0. \tag{4.5}$$

The model equations shown above are fourth order accurate in the horizontal directions and second order accurate in the vertical. Time integration is performed using a second

[3]Described in section 2

[4]Notation is given in appendix C

order accurate leapfrog time-stepping scheme, such that:

$$\mathbf{X}(t+1) = \mathbf{X}(t-1) + 2\Delta t \times f(\mathbf{X}(t)),$$

where $\mathbf{X}$ is the state vector of the model and $f(\mathbf{X})$ is an operator describing the evolution of the model's state vector with time.

As with any numerical scheme, there are certain issues that must be addressed with the numerics of the model. This time-stepping scheme is an explicit scheme and will only be conditionally stable. The condition for stability in such a model depends on the relation between the grid spacing and the time-step. Stability is ensured if $c\frac{\Delta t}{\Delta x} \leq 1$, where c is the phase speed of any waves (or the wind speed) and Δx and t are the increment sizes in space and time. This condition on the stability is known as the Courant-Freiderich-Levy (CFL) criterion. The quantity $c\frac{\Delta t}{\Delta x}$ is known as the Courant number.

The model is run with a short time-step of 240 seconds throughout this project, ensuring that the Courant number is always much less than one. Near the poles, even such a short time-step may be insufficient to ensure stability and the effective resolution must be degraded by Fourier truncating the model fields in the zonal direction. Throughout this project, the parameters used for this zonal filtering are:

Latitude at which filtering starts	$\pm 72.5°$
Zonal truncation limit	12 @ 72.5° 9 @ 77.5° 6 @ 82.5° 3 @ 87.5°
c corresponding to $c\Delta t/\Delta x$=1 at 87.5°	$\sim 1400\,\mathrm{ms}^{-1}$

These parameters were previously established in the model and no changes were made to them. This decrease in resolution guarantees that the model will satisfy the CFL stability criterion for any realistic (and any reasonable imposed) atmospheric situation at all latitudes.

In addition, the leapfrog time-stepping scheme has an undesirable property in that odd and even time-steps can separate and the results can become very noisy, with large

oscillations of period two time-steps. This is prevented by performing forward time-steps when model fields are written to disk[5] and also by the application of a mild (Asselin) time filter, as described in Fisher [1987]. Nonlinear instability, the aliasing of high wavenumber waves onto lower wavenumber modes through the restrictions of the finite difference scheme, is controlled by the application of a Shapiro filter in both the meridional and zonal directions. This filter removes small wavelength waves from the increment fields and has a response curve such that waves with wavelength greater than 3 grid boxes are unaffected, but for wavelengths of 2 grid boxes or less, the waves are completely filtered out. This filtering is described in detail in Fisher [1987].

Parameterisations in the Model

The model represents unresolveable processes by a series of 'physics' parameterisation subroutines called from the **SUBSCALE** routine. The model setup used in the project has parameterisations for:

Dry Convection The dry convection code was added to the model by Bryan Lawrence as a result of instability problems caused by the introduction of several experimental gravity wave schemes. The dry convection is switched on if a temperature profile is steeper than the adiabatic lapse rate and effectively mixes the potential temperature of the air in the vertical vicinity of the instability until a just stable situation is obtained. The dry convection scheme has a minimal effect when the model is running under normal conditions.

Rayleigh Friction In the model, Rayleigh friction is used as both a simple gravity wave parameterisation and to prevent wave reflections off the model ceiling. This Rayleigh friction consists of a relaxation towards some prescribed background state, in this case zero wind. The contribution to a wind field is given by:

$$\frac{\partial(u,v)}{\partial t} + ... = -\alpha(u,v).$$

[5]Which also means that when the model is restarted from a dump, where a forward time-step is forced as there is only the current model state in memory, the model integration is identical to a continuous run over the dump time.

The Rayleigh friction coefficient α is dependent on height. The relaxation time-scale is shown in figure 4.1. Thermal relaxation is very slow up to around 50 km (around 115 days relaxation time) and decreases quickly to around 11 days above 50 km. This increased friction doubles as a *sponge layer* at the top of the model and prevents waves reaching and reflecting from the top of the model.

Rayleigh friction is also used at some points in the project to apply a force to the zonal mean u-wind (for example see section 5.3.2). When this force is to be applied, a term is added to the model increment fields according to the expression

$$\frac{\partial u}{\partial t} + ... = -\alpha_{zm}[\overline{u} - \overline{u}_0(\phi, z)].$$

The use of this friction term is described in section 7.1.

Vertical Diffusion A vertical diffusion scheme based on that in the NCAR Community Climate Model [Hack, Boville et al., 1993] was added to the model in response to stability problems as the model resolution was increased as detailed in section 4.3. The model stability problem was traced to erroneous vertical diffusion through the bottom boundary of the model, rendering the vertical diffusion unnecessary in this case. As the code is proving to be useful to others using the model, it has been left in place, and will be described in this thesis.

Radiation The model as distributed used the `MIDRAD` radiation scheme (described in Shine [1987]). For many of the integrations performed in the course of this project, the `MIDRAD` scheme has been replaced with a much simpler Newtonian cooling scheme, where the model temperature field is relaxed towards a predefined reference profile such that

$$\frac{\Delta T}{\Delta t} = -\alpha(z)[T - T_0(\phi, z)],$$

where ΔT is the change in temperature over a time-step (Δt). $T_0(\phi, z)$ is a predefined temperature profile. Several different T_0 profiles are used in the project. The Newtonian cooling is described in some detail in section 4.2.2

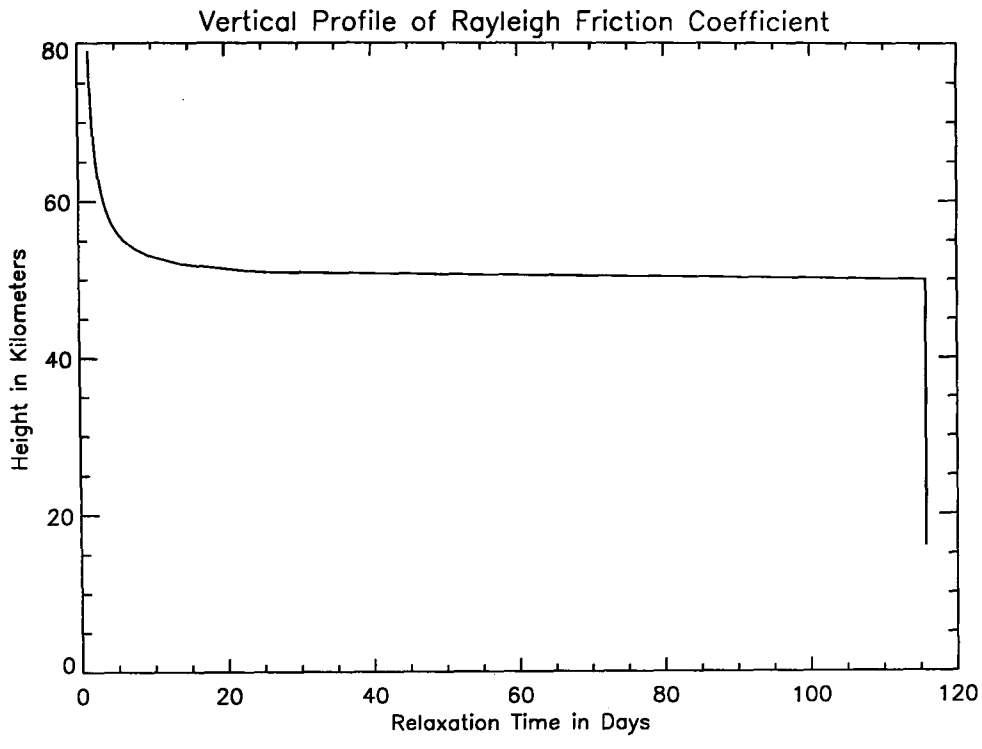

Figure 4.1: The vertical profile of the Rayleigh friction relaxation e-folding time (in days) used in the model. The friction timescales are very large throughout the stratosphere (very weak friction applied) and decrease sharply from 50 km to the top of the model.

4.1.3 The Structure of the Model

The model code as distributed is not written in standard FORTRAN77, but in a series of 'decks', consisting of the subroutines in a format that requires preprocessing. Modifications to the code can be written to separate 'update' decks, which the preprocessor then combines with the model source to produce compilable FORTRAN77 code, which is built to create the working model executable. This somewhat long-winded process has the advantage that the original model code remains intact so that any bugs that may be introduced to a model build should be easily traceable in the small update deck. The model was also designed with a view to allowing easy collaboration between different groups who may be using the model and the small update decks are simpler to exchange and understand than modified copies of the model source code. The model uses the FORTRAN77 programming language and is in the most part fairly portable. The input/output routines use some **DIGITAL** extensions to the FORTRAN77 standard and are possibly the largest obstacle to porting the model freely between architectures which may lack a compiler that can handle such extensions. These problems with portability would not be insurmountable if the model was required on another system.

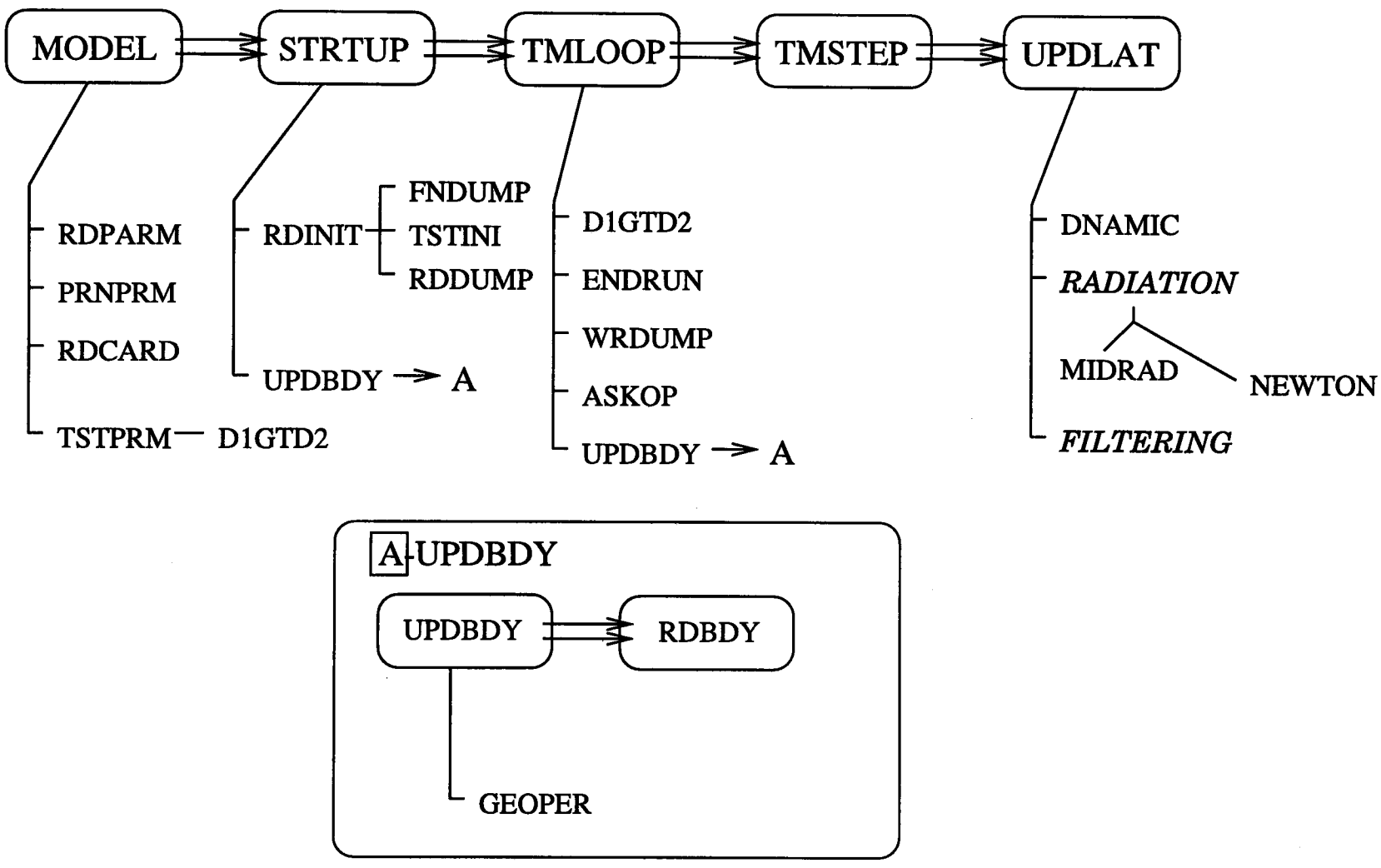

Figure 4.2: A schematic diagram of the model structure, showing the main subroutines controlling the course of a model integration.

Although this model is a later version of the model than that used by Rosier [1996], the changes to the model consist largely of coding improvements. The logical structure of the model is largely unchanged from that described in her thesis. It is however worth examining some of the gross features of the model structure for completeness and as a framework for describing the action of the new routines that have been added.

The flow of a model run is controlled through a hierarchy of small subroutines, each of which with a well defined role in the model integration. Figure 4.2 is a somewhat simplified schematic diagram of the model structure. A model run can be traced as control passes through the various subroutines in the figure.

Model integration begins in the `MODEL` subroutine. At the beginning of the run, this subroutine calls routines to initialise the model parameters, such as the acceleration due to gravity, the earth's rotation rate and the model resolution and time-step. These parameters are read, tested for sanity (for example, it is checked that the run end date is later than the start date), and then control is passed to the `STARTUP` subroutine. This subroutine is responsible for filling the model domain with the initial values of T, u and v (typically from file) and setting up the initial bottom boundary. This having been accomplished, control is passed on to the subroutine `TMLOOP`. This routine now controls the rest of the model run. It is this subroutine that checks to see whether a dump to disk must be made, the model should be stopped or if the next day's bottom boundary data should be read into the model. The subroutine `UPDBDY`, which updates the model bottom boundary conditions, is particularly significant to this project, and will be returned to in section 4.2.1. This 'housekeeping' completed, `TMLOOP` performs a time-step if necessary, by calling the subroutine `TMSTEP`. `TMSTEP` performs a single time-step and then returns control back to the `TMLOOP` subroutine. A normal time-step is performed by calling the subroutine `UPDLAT` for each latitude in the model domain. Latitudes are calculated independently of each other and can be calculated in any order. As used in this project, the model latitudes are looped over in order. This stage of the integration, which accounts for a large part of the processor time, could be very efficiently processed on a parallel machine by calculating the model latitudes independently.

4.2 New Routines in the Model

Several routines, not described in Rosier [1996], have been added to the model or extensively modified. These routines are described in this section.

4.2.1 The GEOPER Routine

The GEOPER routine is an addition to the standard model code that is used extensively throughout this project. It was originally written in 1994 by Bryan Lawrence as a means to introduce waves and disturbances into the model by modifying the model lower boundary. It has since been extensively modified by the author to expand the range of waves that can be forced and to allow the additional forcing of temperature on the lower boundary.

GEOPER's position in the model structure can be seen in figure 4.2. It is in many ways an extension and partial replacement to the UPDBDY subroutine. At each model time step, a call is made to UPDBDY. In the standard model, UPDBDY would interpolate between the daily geopotential heights provided from file to get instantaneous boundary conditions. In the model with GEOPER, the interpolation step is moved from the UPDBDY routine into GEOPER. GEOPER performs the same interpolation as UPDBDY and then adds the required wave perturbations to the boundaries.

Figure 4.3 shows the structure of the GEOPER subroutine. The subroutine stores values for the bottom boundary from the supplied data files in the z1 and z2 arrays. These data are spaced a day apart, with z2 being the future data. The operation of the subroutine is controlled by the IFLAG argument. With IFLAG set to -2, -1 or 1, the GEOPER subroutine manages these values of z1 and z2. With an IFLAG value of 0, which is the normal operating value, GEOPER interpolates between z1 and z2 to get the current state of the bottom boundaries, then cycles through the various applied waves and adds their contribution to the boundaries. When IFLAG$\neq$0, then GEOPER is to perform some housekeeping function such as updating the data it holds in the z1 and z2 arrays.

The ZNOW argument to GEOPER is an array of floating point data. In the normal operation (IFLAG=0) of the subroutine, the ZNOW field is used to pass the bottom boundary data back to the model. In the cases of IFLAG$\neq$0, ZNOW is used to pass the bottom

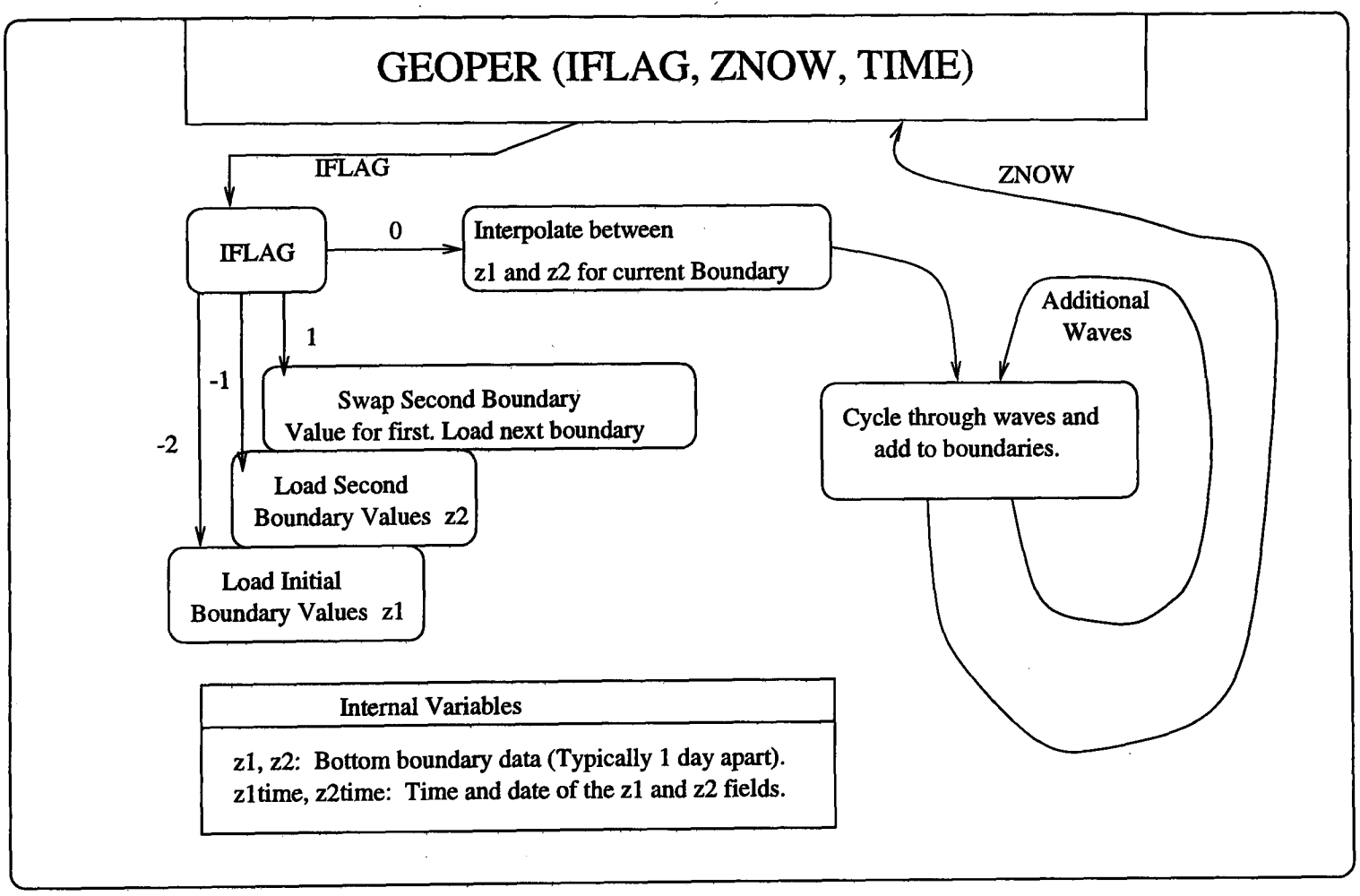

Figure 4.3: A schematic of the `GEOPER` subroutine. `GEOPER` is called with the control flag, `IFLAG`, a data field `ZNOW`, and information about the time and date. `ZNOW` can either feed information into the subroutine, for `IFLAG`$\neq$0, or return information from the subroutine in the `IFLAG`=0 case.

boundary data, read from file by another routine, into the GEOPER subroutine.

The perturbations added to the model boundary by the GEOPER subroutine are described in detail in section 2.3. The form of the waves that can be added to the bottom boundary is very flexible. As the model is normally run, traveling waves of constant amplitude are forced. Standing waves can be forced, as can any arbitrary perturbation. The GEOPER subroutine does not store any phase information at model dumps, which means that at model restarts, there can be some noise in the model fields as the waves are re-established. This restart adjustment was never enough to threaten the stability of the model and where unavoidable, is ignored in analysis.

4.2.2 Newtonian Cooling

The model as standard uses a complex radiation scheme called MIDRAD [Shine, 1987]. This is an expensive scheme numerically and unnecessarily complex for some of the modelling done in this project. For both these reasons, the MIDRAD scheme has been replaced by much simpler Newtonian cooling in many of the experiments. Newtonian cooling had been used in the model before the MIDRAD scheme was added and some of the code to implement the scheme remains in the model. The simplicity of the Newtonian cooling scheme allows a wide variety of scenarios (for example, a near isothermal atmosphere) to be very easily imposed on the model. The radiation scheme is important in this model as it is the primary source of dissipation for the waves forced on the bottom boundary. Later experiments will show the sensitive dependence of many aspects of modelled disturbances on the radiation scheme.

Newtonian cooling acts by relaxing the model temperature field towards a reference temperature field according to the relation

$$\frac{\Delta T}{\Delta t} = -\alpha(z)(T - \overline{T}_0(y,z)), \tag{4.6}$$

where $\overline{T}_0$ is the reference temperature field and α is the Newtonian relaxation timescale.

This reference field can be a climatological value or an idealised temperature field, for example an isothermal case. In this project, a zonal mean reference field is specified. In the

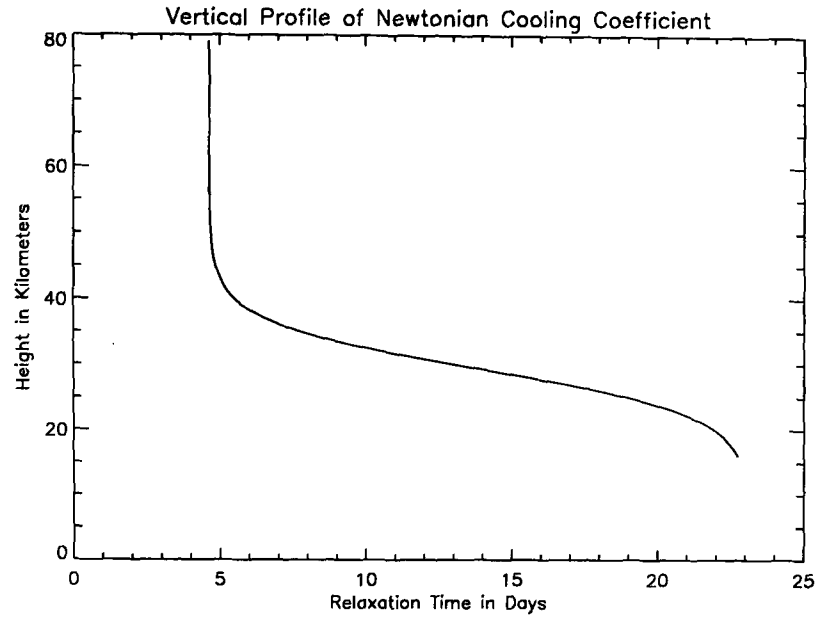

Figure 4.4: The vertical profile of Newtonian cooling timescale. The figure shows the relaxation time in days.

isothermal experiments, the reference temperature is set at 240K throughout the model domain. Other possible reference temperature fields are investigated in section 6.2.1, where the model is run in conditions close to those described in the CIRA climatology.

The relaxation time-scale in this model is a function of height only. The vertical profile for the Newtonian relaxation coefficient is set when the Newtonian cooling routine is first called. The subroutine to set the profile has survived in the model code, being ignored by the preprocessor, through the introduction of `MIDRAD`. The profile used in these runs, shown in figure 4.4, is that used in the model before the introduction of `MIDRAD`, when Newtonian cooling was the standard model radiation scheme. The relaxation time is fairly constant at around 5 days above 40km in altitude. This represents the very fast adjustment to radiative equilibrium in the upper atmosphere. The timescale increases rapidly below this height as the atmosphere becomes denser and more radiatively insulated. This implies strong damping of waves above 40km and significantly weaker damping below this level. This profile is not altered in the course of the project.

4.2.3 Vertical Diffusion

A vertical diffusion parameterisation has been written for the model. This routine can be called from the model as required. In most of the runs described, this routine is not

in fact called. The tendencies in the model fields are calculated by applying the diffusion equation,

$$\frac{\partial \Phi}{\partial t} = -\frac{\partial}{\partial z}\left[K\frac{\partial \Phi}{\partial z}\right] \tag{4.7}$$

to the model fields, T, u and v. The diffusion coefficient, given below, is dependent on the shear in the flow as well as a set parameter, the mixing length. The details of the vertical diffusion algorithm are taken from the NCAR Community Climate Model (CCM2) [Hack et al., 1993]. The tendencies of the model quantities T, u and v are given by the statements:

$$\frac{\partial u}{\partial t} + \ldots = -\frac{1}{\rho}\frac{\partial \tau_\lambda}{\partial z}, \tag{4.8}$$

$$\frac{\partial v}{\partial t} + \ldots = -\frac{1}{\rho}\frac{\partial \tau_\mu}{\partial z}, \tag{4.9}$$

$$\frac{\partial T}{\partial t} + \ldots = -\frac{1}{\rho}\frac{\partial H}{\partial z}, \tag{4.10}$$

where the quantities τ_λ, τ_μ and H are given by:

$$\tau_\lambda = -\rho K_c \frac{\partial u}{\partial z}, \tag{4.11}$$

$$\tau_\mu = -\rho K_c \frac{\partial v}{\partial z}, \tag{4.12}$$

$$\text{and } H = -\rho K_c \frac{\partial \theta}{\partial z}. \tag{4.13}$$

In this equation, θ is the potential temperature and K_c is a varying diffusion coefficient which is defined as:

$$K_c = l_c^2 S F_c(Ri). \tag{4.14}$$

The parameter l_c, the so-called the mixing length, is a tunable parameter that is initially set to 30m as in the NCAR model. The function giving F_c is conditional on the sign of the Richardson number (Ri).[6] If Ri is greater then zero, which is true if $N^2 > 0$, implying

[6]The Richardson number is defined as $\frac{N^2}{(\frac{\partial V}{\partial z})^2}$, the ratio between the buoyancy frequency squared and the vertical shear in the wind

that the atmosphere is statically stable (as is the case for much of the stratosphere), then

$$F_c = \frac{1}{1 + 10Ri(1 + 8Ri)}.$$

In the statically unstable case ($N^2 < 0,\ Ri < 0$),

$$F_c = (1 - 18Ri)^{1/2}.$$

The subroutine may be tested by feeding it with trial profiles and looking at the resulting tendencies. A constant shear is the easiest situation to calculate manually. The subroutine is run with a constant vertical shear of 1 ms^{-1} per km supplied for the wind field (Temperature is set to a constant 240 K). A manual calculation gives a height independent tendency of -8.42$\times 10^{-10}$ ms^{-1} per day. The vertical diffusion subroutine produces a tendency of -8.4$\times 10^{-10}$ ms^{-1} per day, matching this very well. The accelerations produced in this calculation are vanishingly small compared with other terms in the momentum balance of the model but it is worth noting that the Richardson number in this example is over 400, indicating a very stable state. The diffusion coefficient varies strongly with the vertical shear in the flow as shown in figure 4.5, and the vertical diffusion will act very much more strongly on structures with larger shears.

For a Richardson number of 0.25, the vertical diffusion coefficient would be 4.13 m^2s^{-1} (compared to 6.8$\times 10^{-8}$ m^2s^{-1} in the constant shear case described above). Figure 4.6 shows a Gaussian profile of vertical winds, and the corresponding tendency fields. In this profile, the maximum shear is $\sim$40 ms^{-1}/km, yielding a Richardson number of 0.25. The tendencies are indeed very much larger in this case than in the weaker shear case shown before, with accelerations of around 10 ms^{-1} per day evident. These accelerations are comparable with to the typical accelerations seen in the model runs.

Perhaps a more realistic model situation is when the subroutine is required to act upon a grid-scale (in the vertical) disturbance. Such a case is shown in figure 4.7 (it should be noted that the mixing length scale, l_c, has been raised to 200m). In this case, the wind magnitudes are not excessively large but the small vertical scale of the disturbance

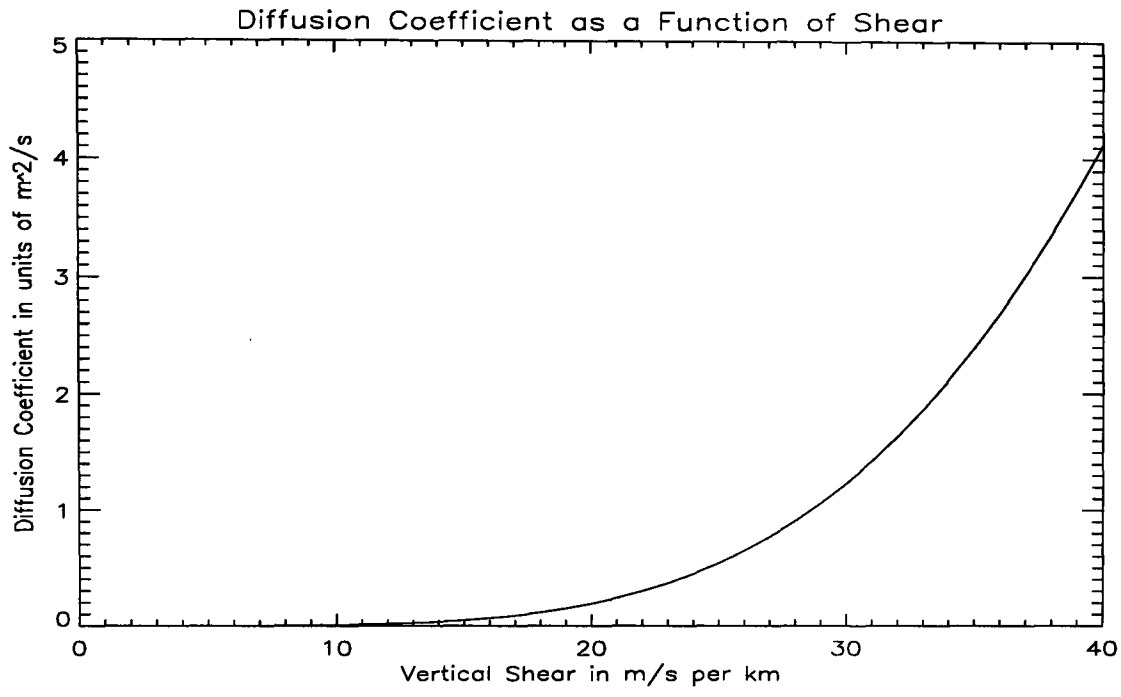

Figure 4.5: The variation of the diffusion coefficient with vertical shear in the vertical diffusion subroutine.

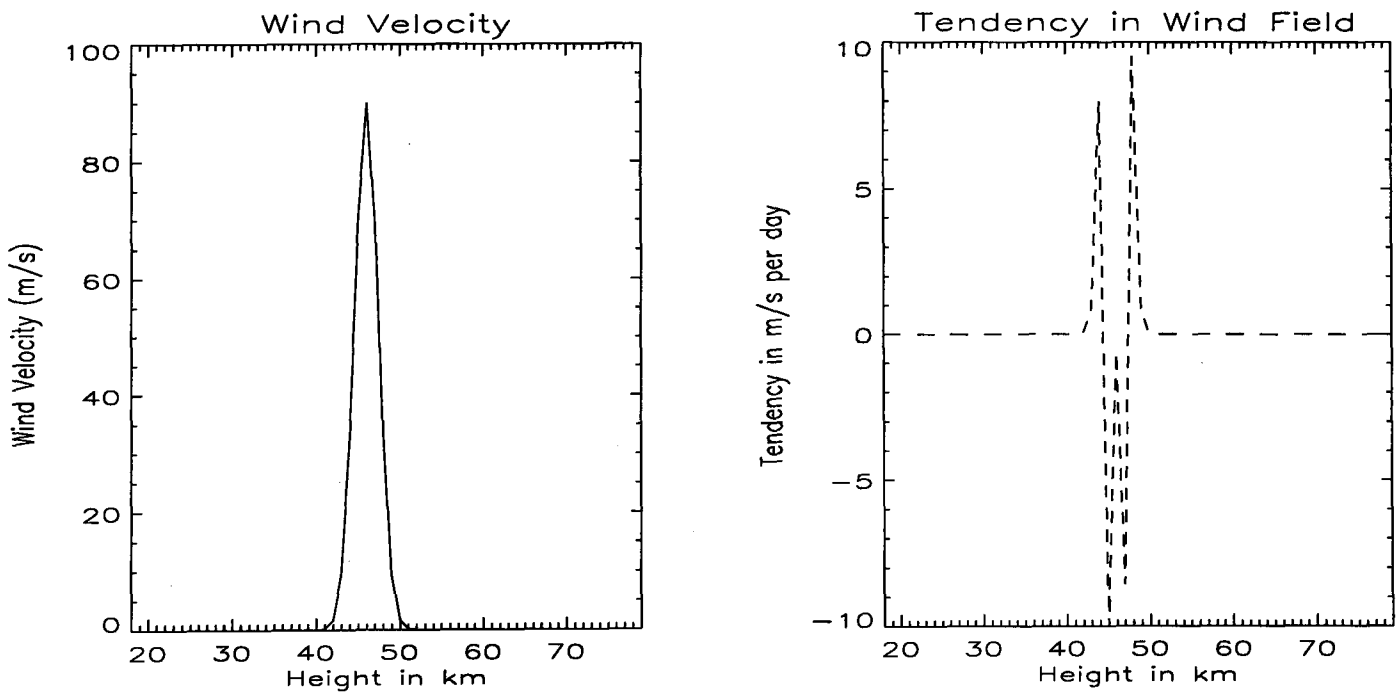

Figure 4.6: A Gaussian profile of winds is put into the vertical diffusion subroutine. The maximum shear results in a Richardson number of 0.25, and a resulting diffusion coefficient of around 4.13 m^2s^{-1}. The tendencies in this are very much larger than in the lower (constant) shear case described before, and are certainly significant compared to typical accelerations in the model.

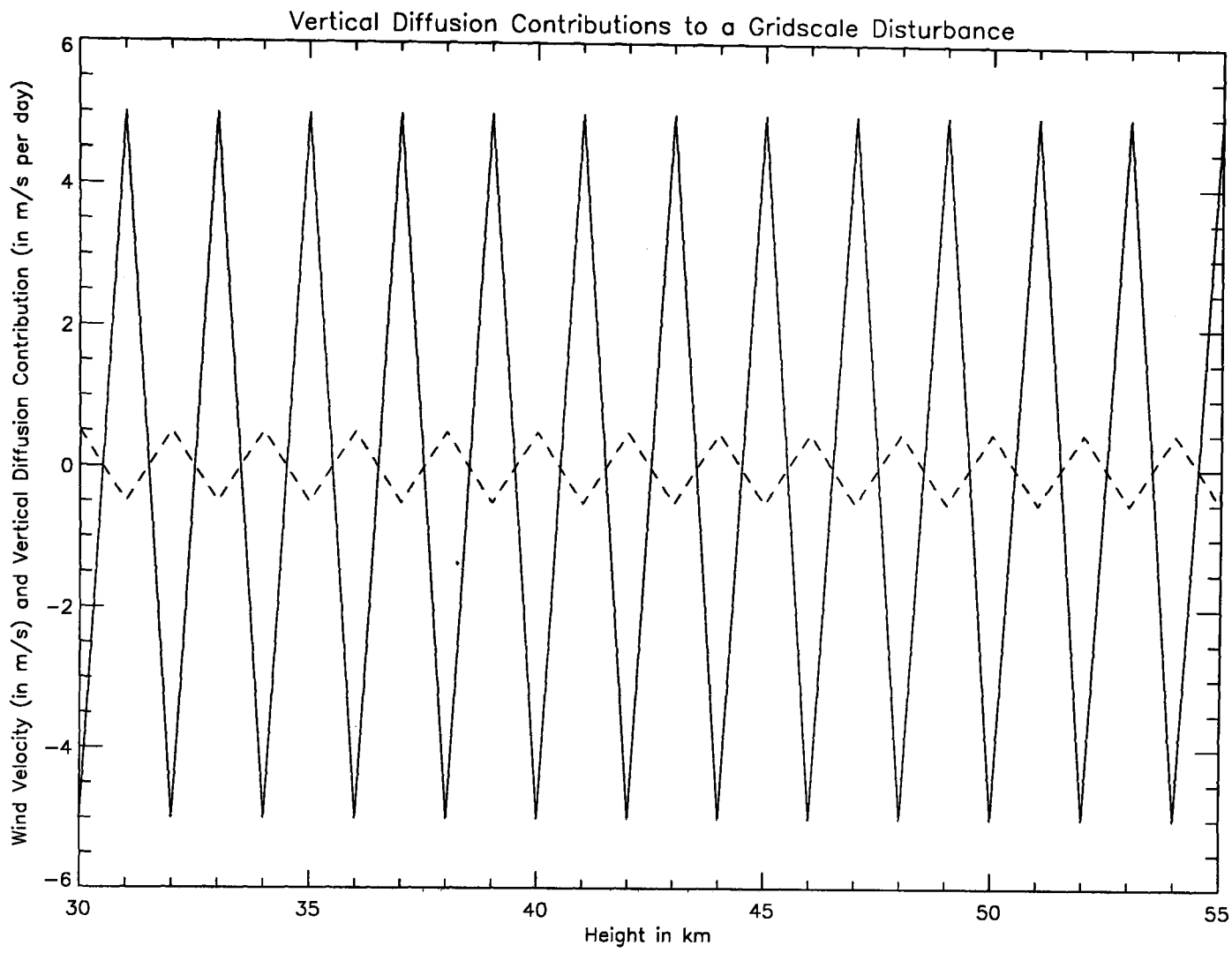

Figure 4.7: The vertical diffusion subroutine acting on a grid-scale disturbance. The wind field (solid line) is alternating between $\pm 5\,\mathrm{ms}^{-1}$ on each model level. The resulting contributions from the vertical diffusion (dashed line) are acting to eliminate this disturbance.

provides large values of shear. The vertical diffusion can be seen to be acting to eliminate the grid-scale structure fairly strongly.

4.3 Increasing the Model Resolution

Increasing the model vertical resolution from 2 km to 1 km was quickly realised to be crucial in modelling the short vertical wavelength equatorial waves thought to play a part in forcing the QBO. In theory, the change to a higher resolution should require only a change in the model parameters block, followed by compiling the model against the correct input/output libraries. In practice however, it was found that such a model was unstable, and would crash under some circumstances. After considerable investigation, the source of the instability was eventually traced to a problem in the vertical advection

at the lowest level of the model.

4.3.1 The Stability Problem

When run at 1km vertical resolution, the model was found to crash if a moderate amplitude geopotential perturbation was applied to the lower boundary (in this case, when a perturbation of 70m was applied to the equatorial geopotential height). These perturbations could be the forcing applied to produce Kelvin or Rossby-gravity waves. To illustrate the nature of the crashes, several days from a model run are shown in figure 4.8 where such a crash has occurred. Near the lower boundary, the v-winds are seen to get very large. These winds grow over several model days from normal levels of a few metres per second to large values of several hundred metres per second. Various gravity waves are also generated, and can be seen propagating from the region of the crash, as the model tries to adjust to the very high winds present.

The model time-step was reduced to ensure that the model was not violating the CFL criterion, and hence becoming numerically unstable. With the time-step halved, the model still crashed in the same way, indicating that the cause of the instability was not a time-stepping problem. The vertical diffusion subroutine, described section 4.2.3, was added at this point in an attempt to smooth the spurious winds and stabilise the model. The vertical diffusion could slightly delay the crash, but was insufficient to stop it. The vertical diffusion subroutine was retained in the model code as it will be useful for future users of the model.

Figure 4.8 shows that the anomalously high winds are appearing near the model bottom boundary as the model crashes. The vertical advection code is a possible culprit for causing the crash as it is responsible for adding increments to the model fields and has to make certain assumptions about the properties of these fields near the lower boundary. When there is vertical motion through the bottom level of the model, there must be some estimate made of the values of T, u and v below the bottom level of the model. In the standard model, the `DYNVAD` subroutine (which is the dynamics subroutine responsible for calculating the vertical advection) extrapolates model fields linearly over the bottom two

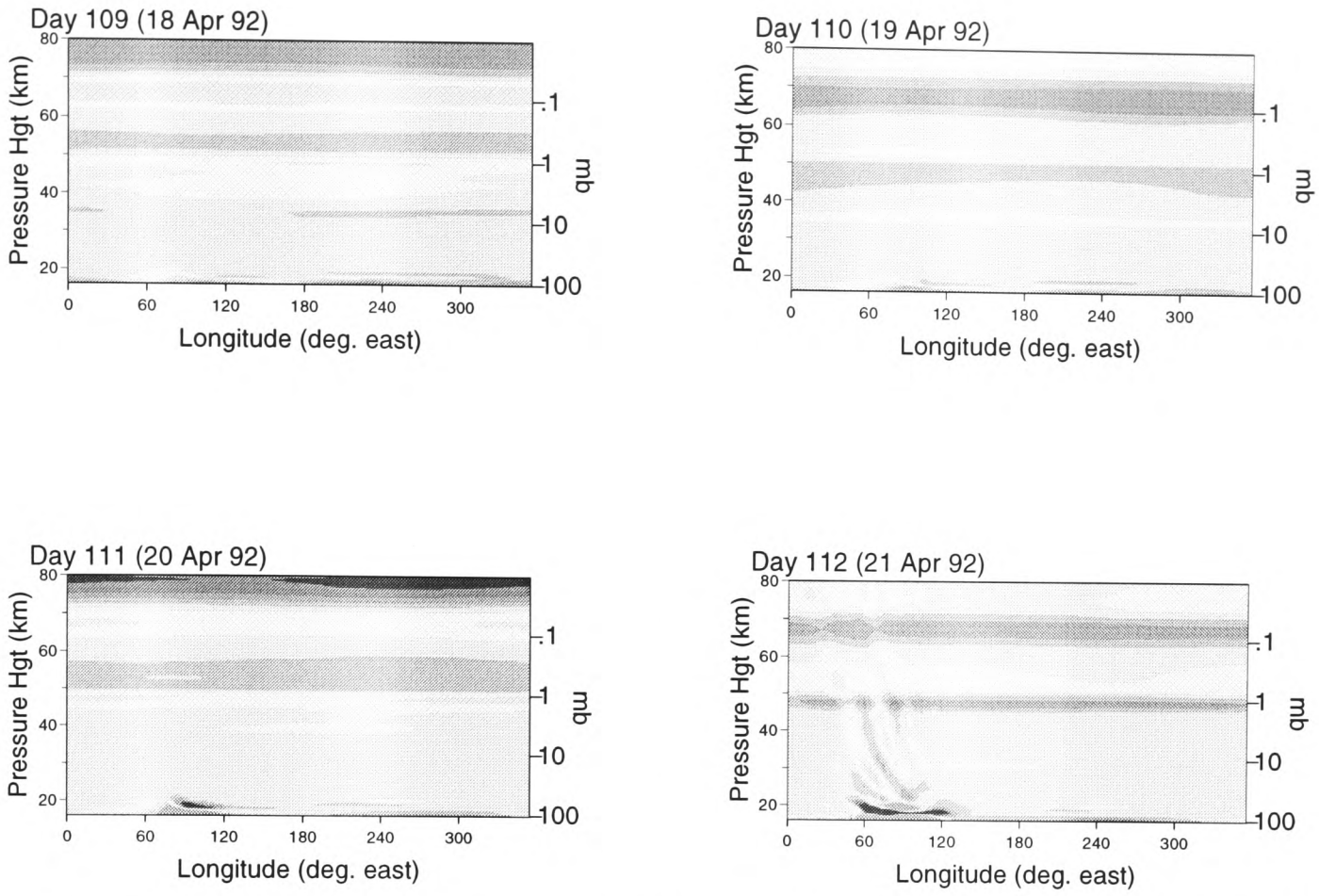

Figure 4.8: Four plots showing the evolution of the meridional wind at the equator as the model crashes. No scale is shown but the darkest colours represent a v-wind of $\sim 400\,\mathrm{ms}^{-1}$. Near the lower boundary, the v-winds rapidly accelerate over several model days. Gravity waves can be seen radiating from the region.

full levels to get a value of the field in the level below the model domain. This extrapolation can under certain circumstances lead to a positive feedback situation, resulting in the model blowing up. The problem is shown schematically in figure 4.9.

If there is upwards vertical motion, a condition likely at the equator where there is a lot of diabatic heating, then values of T, u and v from below the model will be advected into the model domain. As mentioned before, the model has no information about these values and must make some assumption about them. The model extrapolates the values at the lowest two levels downwards to get the estimated model field value that is to be advected upwards. Normally this will produce quite reasonable results. However, a problem can arise, as illustrated in figure 4.9.

The quantity plotted can be any of the model prognostic variables, T, u or v. If the quantity has some structure in the vertical which is represented by the figure, a problem can arise because the model's linear extrapolation will guess at the value shown by **A** for the quantity to be advected upwards. Another value, perhaps **B** in this case, would

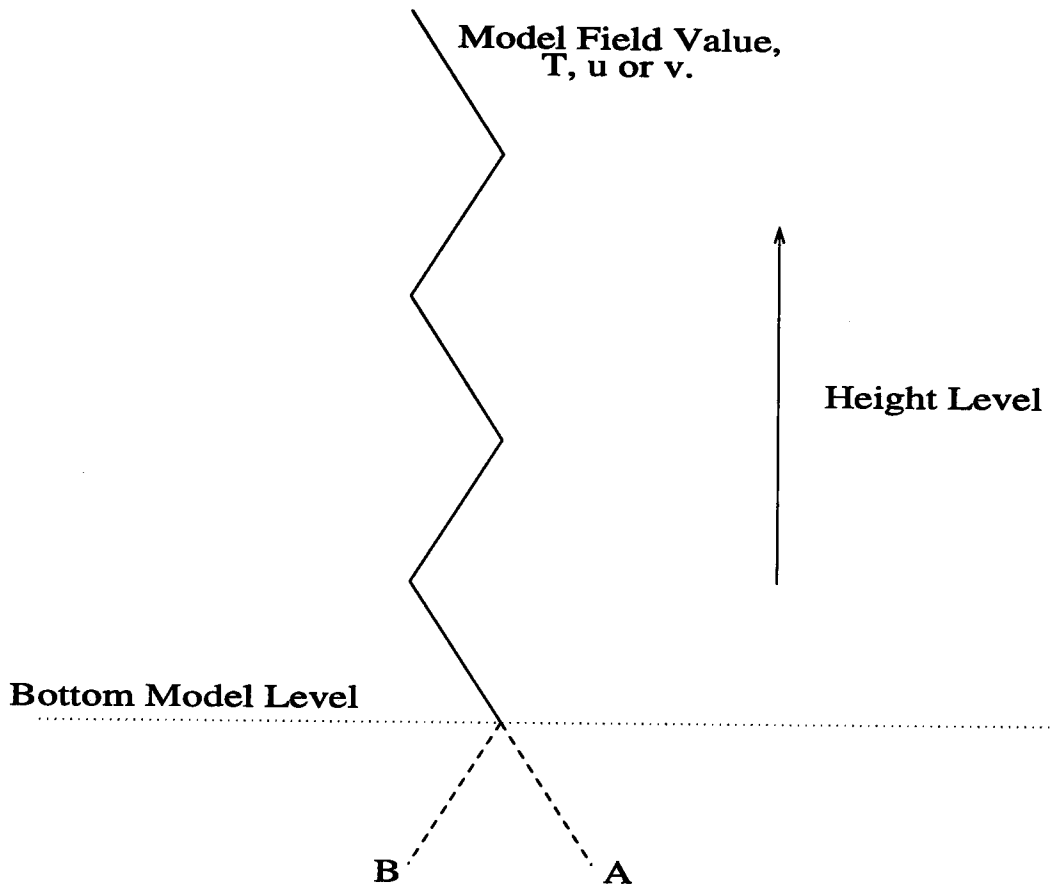

Figure 4.9: An imaginary vertical profile of a model quantity, showing how the extrapolation of values to an imaginary lower boundary may cause problems at the lower boundary. Extrapolation will yield a value represented by point A, whereas a better guess would be value B.

be a better choice. The erroneous value **A** is advected upwards which tends to move the first model level further away from zero. At the next time-step, the guessed value will be even further from the value **B** and an even worse guess. As these increasingly unrealistic values are advected upwards, it can be seen that a positive feedback mechanism is possible. Removal of this mechanism removes the instability and the model becomes stable, even for very large bottom boundary perturbations.

This instability can be considered in mathematical terms as the failure to specify a sufficient lower boundary condition to solve the equations. (The specification of only geopotential is not an adequate boundary condition of the model equations, and the boundary is under-specified.) Linear extrapolation is used to obtain the necessary values of the variables T, u and v on the boundary, which allows the equations to be solved. This solution is not necessarily realistic as these computed boundary conditions can lead to an unrealistic solution being obtained. In this case, such a failure is observed as the computed boundary values lead to the model crashing with ever increasing wind speeds near the lower boundary.

4.3.2 Elimination of the Model Instability

With the cause of the model crash clear, there are several ways that the problem can be addressed. An elegant way would be to try and get a better value for the quantity to be advected upwards. It should be remembered that any extrapolation is merely an estimate and provides no knowledge of the model fields below the bottom boundary. The model can be forced with additional bottom boundary values of T, u and v. Bottom boundary forcing in T and geopotential has been used in this project and it was found that this slowed the crashing of the model. It is possible that specification of the horizontal wind field on the bottom boundary will eliminate the problem. This was not done however as model bottom boundary fields were not available in all the model quantities.

Another option considered was to refine the extrapolation to be a quadratic or higher order scheme which would use more points to estimate what would be, hopefully, a better extrapolated value. This would give a better guess in the situation described in figure 4.9 but it is still possible to imagine profiles where the positive feedback situation could appear again.

For the purposes of this project, it was decided that a simpler solution would be used. No increment is added to the bottom model level due to vertical advection. This is equivalent in effect to setting the value of a model quantity at the extrapolated model level to the same as the value on the bottom level. This assures that no positive feedback situation exists and application of this modification has proven adequate to eliminate the instability.

Other more subtle solutions are being experimented with in the model. Bryan Lawrence has observed similar instabilities in the model at 2 km resolution.[7] He has inserted various flux limited vertical diffusion schemes [Thuburn, 1993] into the model, but has so far been unable to entirely eliminate the problem.

[7] In this case, the problem appears to have arisen as ascent through the model bottom boundary increases with the application of a realistic gravity wave drag scheme and the raising of the model lid [Lawrence, 1997].

4.4 Hardware and Software Used

The model was run almost entirely on Digital Alpha machines running Digital Unix (formerly known as OSF1). Some model runs have been performed on 'PC-compatible' machines running the Linux operating system. Depending on configuration, the model takes of order a few minutes to integrate over a model day. (Running with `MIDRAD` present and 65 levels in the vertical, it runs at a rate of about one model day every 5 minutes of CPU time on a Digital Personal Workstation 433au (which has an Alpha 21164 CPU running at 433MHz).)

Extensive use has been made of computer packages to analyse the data produced by the model. The principal packages used are the Middle Atmosphere Dynamics Package at Oxford (MADPO) and Interactive Data Language (IDL). MADPO has been developed, and is maintained, principally by Bryan Lawrence and provides both a suite of command-line driven analysis and visualisation programs, and a useful set of library subroutines which allow complex calculations to be performed on large data sets very quickly [Lawrence and Allinson, 1992]. IDL is a commercial software package that is widely used in the atmospheric physics community.

As of version 15 of the model, MADPO libraries are used to perform the model file input and output. Model output fields are dumped directly into MADPO binary format and can then be processed by the various MADPO packages as required. The MADPO binary format has been developed by Bryan Lawrence and is a self describing data format. Applications exist that allow rapid conversion of MADPO format data into various other formats, including the widely used NetCDF format.

In addition to these tools, the Ferret package has been used to create several of the plots displayed in this thesis. Ferret is a data plotting package, with some data analysis capabilities, that is available from the National Centre for Atmospheric Research in Colorado. It is freely available at *http://ferret.wrc.noaa.gov/Ferret/*.

4.5 Summary

The model used throughout the project is described in this chapter. A general description of the model is given, including details of the model domain, physical parameterisations and finite difference equations. Especially relevant in this project are details of the bottom boundary supplied to the model, the geopotential height of the 100 hPa pressure surface. This bottom boundary is particularly important to this project both as it is modified in order to generate equatorial waves to the model and it is through the specification of only geopotential on this boundary that the model is, under certain circumstances, liable to crash.

The model is modified in several ways to allow different experiments to be performed. New and modified subroutines described in this chapter include:

`GEOPER` This subroutine is used to add disturbances to the bottom boundary of the model. The original subroutine was added to the model by Bryan Lawrence. The version of `GEOPER` used in the project was significantly modified to allow a wider variety of waves to be forced (traveling Kelvin waves and Rossby-gravity waves being added) and to allow forcing to be carried out in the temperature and geopotential fields. The `GEOPER` subroutine is listed in appendix B as it is central to the modelling work performed in this thesis.

Radiation The model's complex `MIDRAD` radiation scheme is replaced for many runs by the much simpler Newtonian cooling scheme, which is described in section 4.2.2. This has several advantages for the modelling work performed, which include being able to easily simplify the background state of the model towards an 'isothermal' model (where temperatures are held at near 240 K throughout the model domain) and being computationally cheaper. `MIDRAD` is reinstated for later modelling work as a more reliable and well-tested radiation scheme.

Vertical Diffusion As part of the search for the cause of the numerical instabilities found in the model at higher resolution, a vertical diffusion scheme was written for the model. This scheme is found to be unnecessary to ensure model stability

(following modifications to the model vertical advection subroutine) but is described as it is likely to prove useful in further modelling studies.

During the course of this project, a lot of time was lost solving problems encountered with the SMM. These problems are described in section 4.3. The instability problem was due to the vertical advection subroutines needing to extrapolate the model prognostic variables through the bottom of the domain in order to get values that could be advected upwards. These instabilities were avoided by not incrementing the T, u or v values on the model's lowest level from the vertical advection subroutine. This is rather a crude fix, but it appears to work well. No problems were observed through the application of this patch although the amplitude of forcing needed to generate equatorial waves was found to increase after the fix was applied.

Chapter 5

Forcing of Equatorial Waves in the Model

In this chapter, equatorial waves, as described in chapter 2, are going to be generated in the model. It is thought that one of the main reasons why (most) GCMs fail to produce a realistic QBO is that they are unable to support the equatorial waves that are thought to supply a large part of the momentum forcing necessary to drive the QBO. Through modelling equatorial waves in this model, it will be found that the successful simulation of these waves is sensitive to the configuration of the model, especially to the model vertical resolution. Having established the model setup necessary to support these waves, which will be relevant in other models that are to simulate equatorial waves, the properties of the waves generated will be investigated. Modelling the QBO is one of the chief aims of this project and it is essential that equatorial waves are well simulated in the model if their effectiveness at generating a realistic QBO is to be investigated.

This chapter will describe the forcing of these waves in the SMM and some analysis will be performed on the disturbances produced as the waves propagate. Waves are generated through perturbations added to the model bottom boundary through the `GEOPER` subroutine which is described in section 4.2.1. It is found that the model in its standard configuration is unable to model some classes of waves properly. This is not unexpected as the standard model vertical resolution (2 km) is coarse compared to typical vertical

wavelengths of 4–16 km for the various equatorial waves to be described in this chapter. In order to represent a wave, a grid-point model such as this must have at least four grid points within a wavelength, and ideally many more if the wave's evolution is to be accurately modelled. Changes to the model vertical resolution prove necessary to successfully model the shorter wavelength Rossby-gravity waves. Details of the changes in the model necessary to increase the vertical resolution are described in section 4.3. Runs described in this chapter are a mixture of those performed with the 32 level model (for some of the Kelvin wave runs and the unsuccessful Rossby-gravity wave run) and the 64 level model (the remainder of the runs, and most of them).

5.1 Modelling Kelvin Waves

Kelvin waves, as described in section 2.3.1, are the simplest wave-like solution to the primitive equations on an equatorial β-plane. Their relatively large vertical wavelength (compared to Rossby-gravity waves) of around 12 km should make them fairly straightforward to model, even in the model with the coarser vertical resolution of 2 km. Kelvin waves were cited by Holton and Lindzen [1972] as the source for the westerly momentum necessary to drive the QBO and are still thought to play an important role in the driving of the QBO.

5.1.1 Forcing the Kelvin Waves

Kelvin waves are forced in the `GEOPER` subroutine through the addition of a perturbation in the lower boundary geopotential height. Equation (2.46) gives the shape of the expected geopotential height perturbation in a Kelvin wave type disturbance. A forcing of the form

$$\Phi' = \hat{\Phi}(y)\sin(kx - \omega t) \tag{5.1}$$

is predicted to be the geopotential signature of a Kelvin wave on a pressure level. Figure 5.1 is a schematic diagram of this forcing shape.

Early Kelvin wave experiments were done with a standing wave pattern, but this

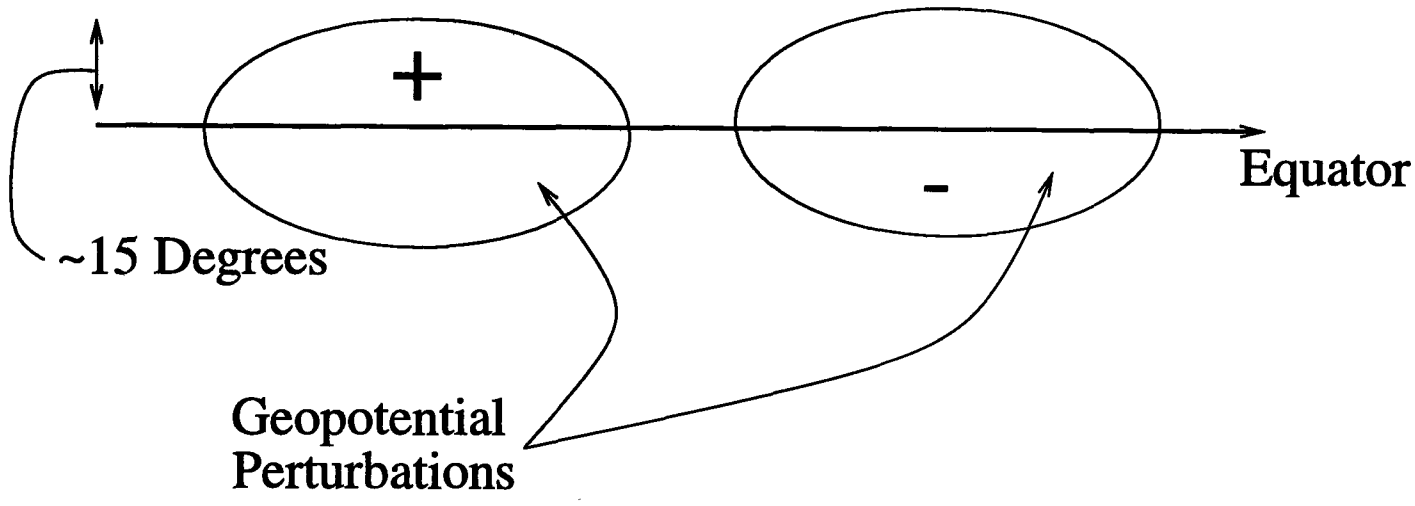

Figure 5.1: A schematic diagram of the geopotential perturbation applied to the bottom boundary of the model to generate a Kelvin wave. This disturbance propagates in in a westerly sense.

was changed to a traveling wave pattern as the GEOPER routine was modified to generate other forms of waves. The only difference noticed was that the magnitude of geopotential disturbance needed was halved. This is due to the fact that a standing wave is the superposition of 2 traveling waves of equal amplitude and opposite direction of travel. The westerly wave component of the standing wave was responsible for forcing the Kelvin waves, whereas the easterly component cannot, according to equation (2.42), excite Kelvin waves within the interior of the model.

5.1.2 Preliminary Results of the Kelvin Wave Runs

A Kelvin wave geopotential height perturbation with amplitude of 30 m, period 16 days and wavenumber 1 is forced. The values for period and wavenumber are taken to closely match those observed in the atmosphere [Andrews et al., 1987]. The amplitude is chosen by trial and error after several runs, such that the accelerations produced are similar to those seen in the QBO. The amplitude of the waves forced in model runs is discussed in section 6.1.1.

There are wave-like disturbances produced in the interior of the model as a result of the applied boundary forcing. It is necessary to verify that these are in fact Kelvin waves. There are several key properties of Kelvin waves that can be checked in the propagating waves to confirm this. Important properties of Kelvin waves include small (theoretically zero) meridional wind oscillation and equatorial confinement. Also, linear theory predicts

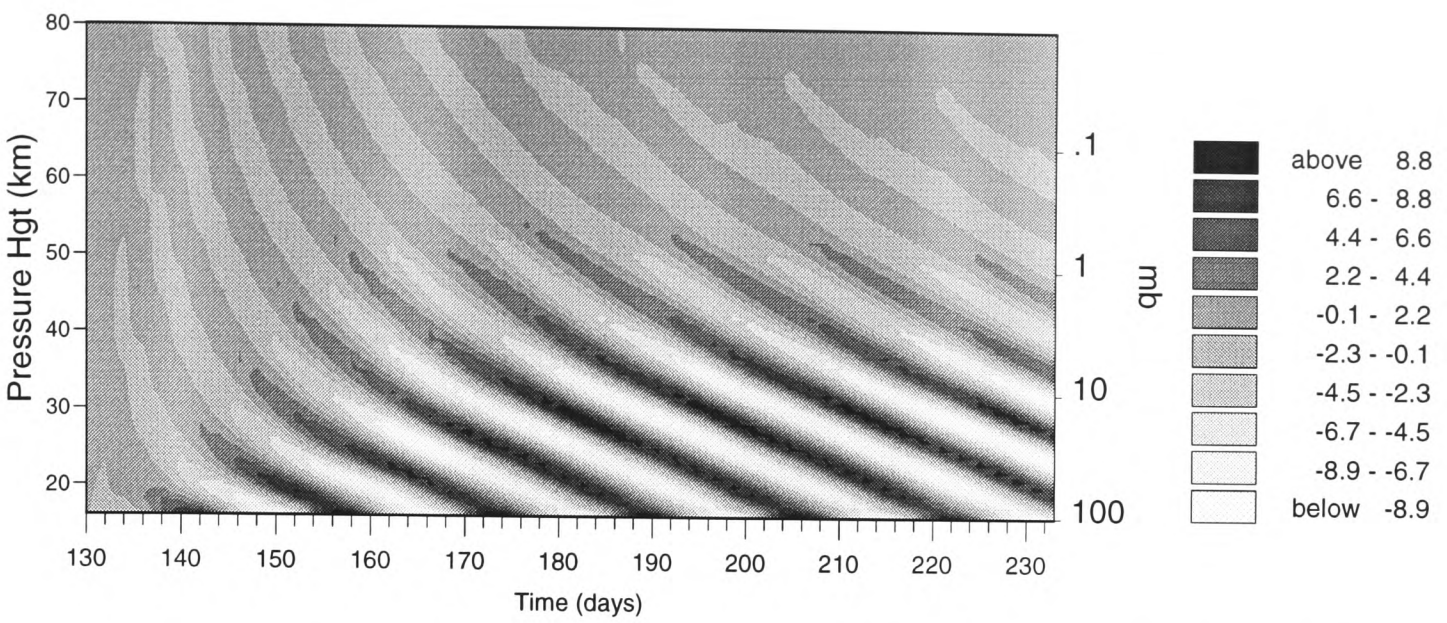

Figure 5.2: The u-wind perturbation against time for a Kelvin wave. Contour units are in ms^{-1}. The propagation of waves and the downward phase velocity of these waves is clearly visible.

the dispersion relation for Kelvin waves to be $\omega = -\frac{Nk}{m}$, which gives a predicted value for the vertical wavelength of Kelvin waves which may be compared to that obtained in the model.

Figure 5.2 shows the zonal wind perturbation associated with a Kelvin type perturbation. The vertical wavelength obtained in the Kelvin wave simulation is measured and a vertical wavelength of around 11 km is obtained. This is close to the value of 12 km arrived at through linear theory. The amplitude of the oscillation in the u and v-winds is compared in figure 5.3. This plot shows that the amplitude of wave number one in the v-wind is much smaller than in the u-wind. The plot also shows clearly that the wave is equatorially confined, with the amplitude dropping away rapidly beyond 15 degrees. This match between the modelled properties and the theoretical properties of linear Kelvin waves is convincing evidence that the waves propagating in the model are in fact Kelvin waves.

According to theory, and in order to generate a QBO, the Kelvin wave must induce a westerly jet as it is dissipated. Figure 5.4 shows the zonal mean u-wind for this run over several months and shows the generation of a strong westerly jet in the lower stratosphere. The generation of this jet and the dependence of the jet on the radiation scheme and wave properties forced are examined in section 5.3 later in this chapter.

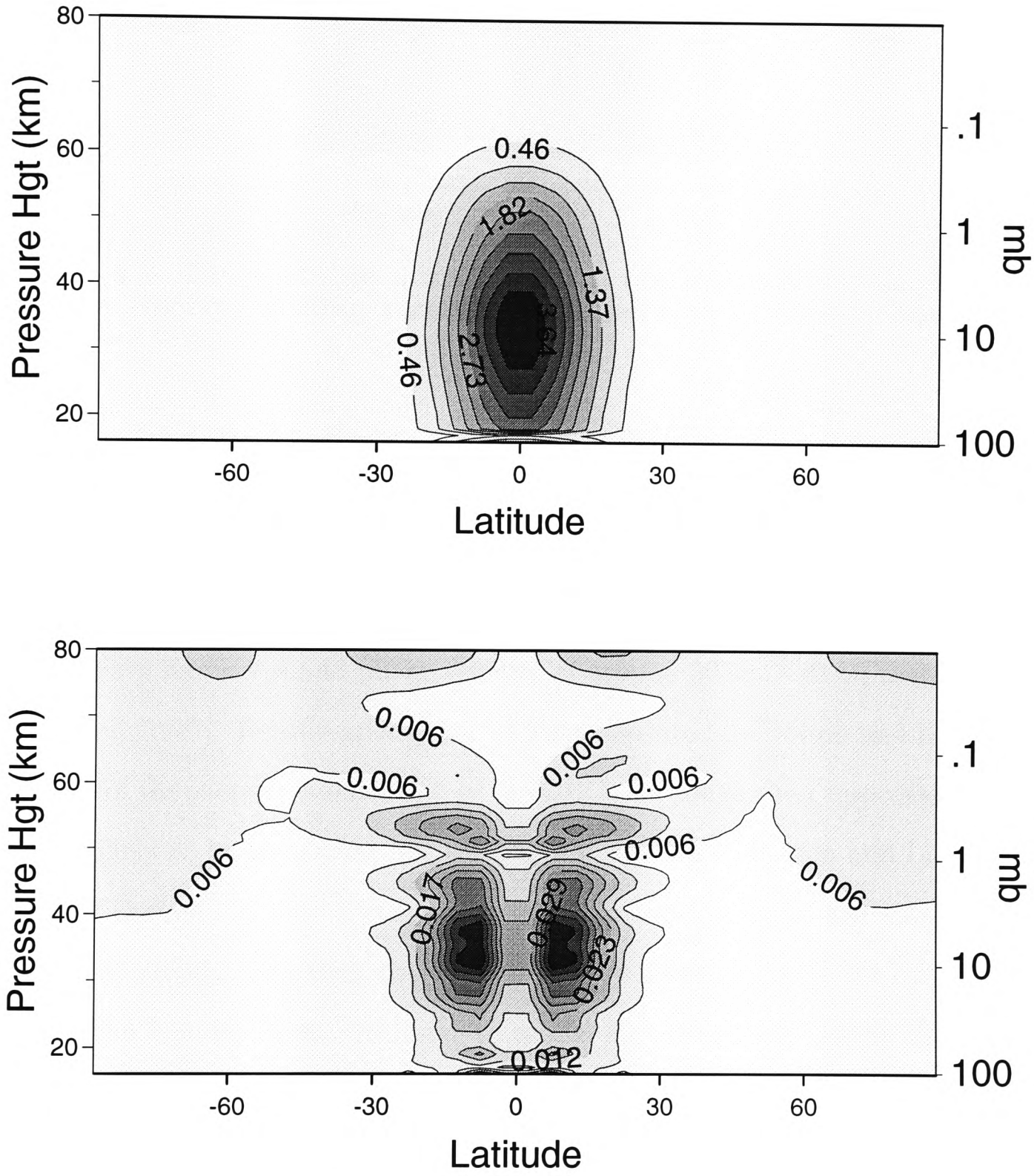

Figure 5.3: The amplitudes of the wave number 1 component, in ms^{-1}, of u (upper) and v (lower) in the equatorial winds in a Kelvin wave run. The magnitude of u is far greater than v, in line with linear theory.

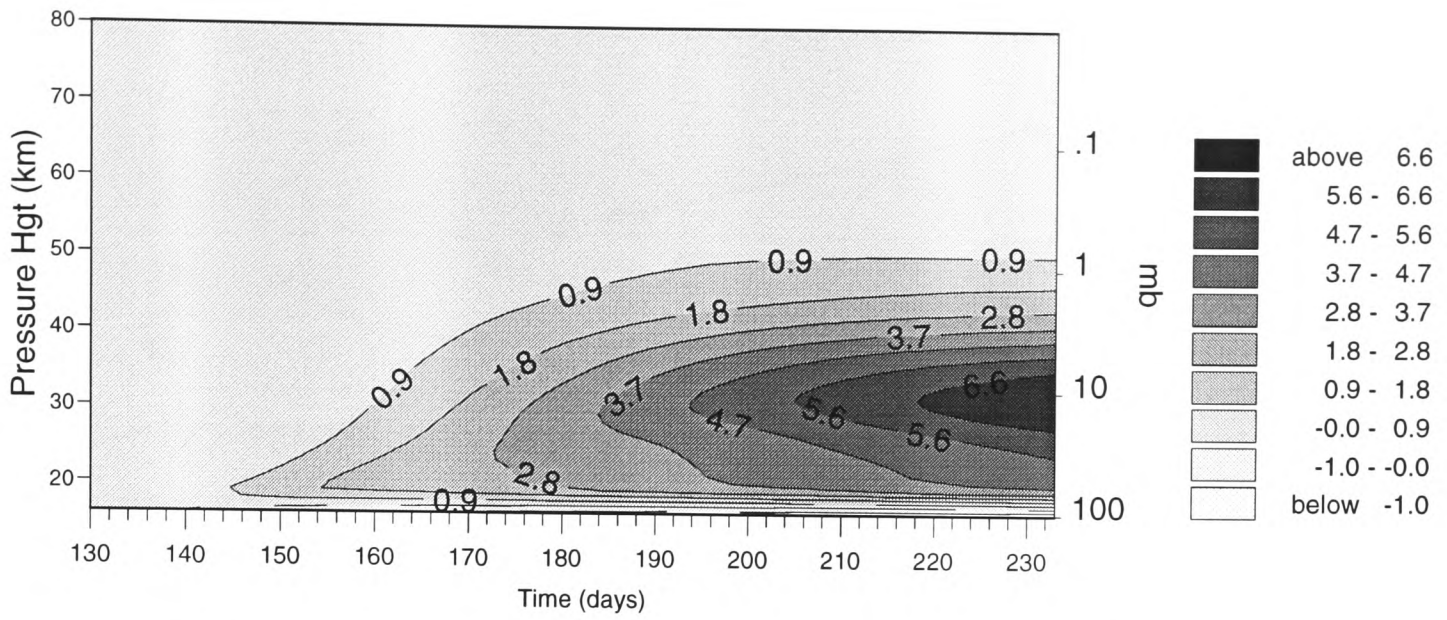

Figure 5.4: The zonal mean u-wind, in ms^{-1}, associated with the Kelvin waves in a run of several months. A westerly jet is generated as would be expected in accordance with theory.

5.2 Modelling Rossby-gravity Waves

After Kelvin waves, Rossby-gravity waves are the gravest wave-like solutions of the primitive equations on an equatorial β-plane. They are observed in nature with periods of 4–5 days, zonal wave number 4 and phase velocity of around $30\,\mathrm{ms}^{-1}$ in an easterly direction [Andrews et al., 1987]. Rossby-gravity waves were also cited by Holton and Lindzen [1972] as the source of the easterly momentum in the QBO. Although their importance in forcing the QBO is likely to be somewhat less than that described in Holton and Lindzen [1972], they are still thought to play a considerable role in the forcing of the easterly phase of the QBO.[1] As already indicated, the Rossby-gravity waves prove to be more difficult to model than the Kelvin waves. In order to model Rossby-gravity waves effectively, it is necessary to increase the model's vertical resolution. This modification in turn brings to light some shortcomings of the model's handling of vertical advection through the bottom boundary, which required attention in order to run the model at this resolution. The modelling aspects of these modifications are described in 4.3. The model modifications having been completed, Rossby-gravity waves are forced in the model.

[1] Although they are not observed to be of sufficient amplitude in the atmosphere to account completely for the easterly phase of the QBO [Takahashi, 1996].

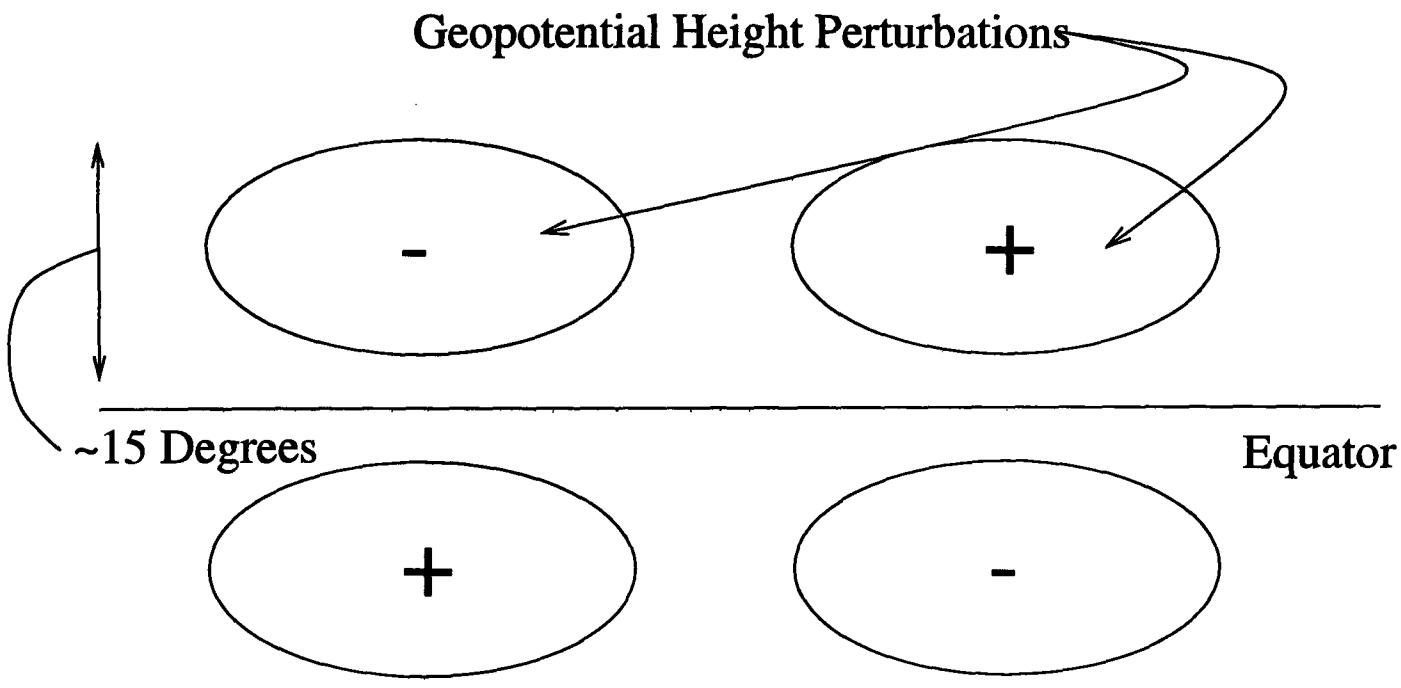

Figure 5.5: A schematic diagram of the geopotential perturbation associated with a Rossby-gravity wave. Rossby-gravity waves have an easterly horizontal phase velocity.

5.2.1 Forcing of Rossby-gravity Waves

The forcing of Rossby-gravity waves is similar in principle to the forcing of Kelvin waves. The same β-plane linear theory described in section 2.3 gives wave-like geopotential perturbation, on a pressure level, of the form:

$$\Phi' = \hat{\Phi}(y)\sin(kx + \omega t).$$

In the case of the Rossby-gravity wave, the structure of $\hat{\Phi}(y)$ is asymmetric about the equator and given by:

$$\hat{\Phi}(y) = \omega y \exp\left(\frac{-\beta|m|y^2}{2N}\right).$$

Figure 5.5 is a schematic diagram of the Rossby-gravity shaped geopotential perturbation.

In accordance with observations, the Rossby-gravity wave forcing is applied with zonal wavenumber four and period four days. This corresponds to a horizontal phase speed of -30 ms^{-1}. In an initial run, using the distribution (32 level) model, Rossby-gravity waves did not propagate. This is likely to be due to inadequate vertical resolution. These failing Rossby-gravity waves can be seen in a plot of equatorial v-winds against height and time, as shown in figure 5.6. These disturbances have very little phase change with

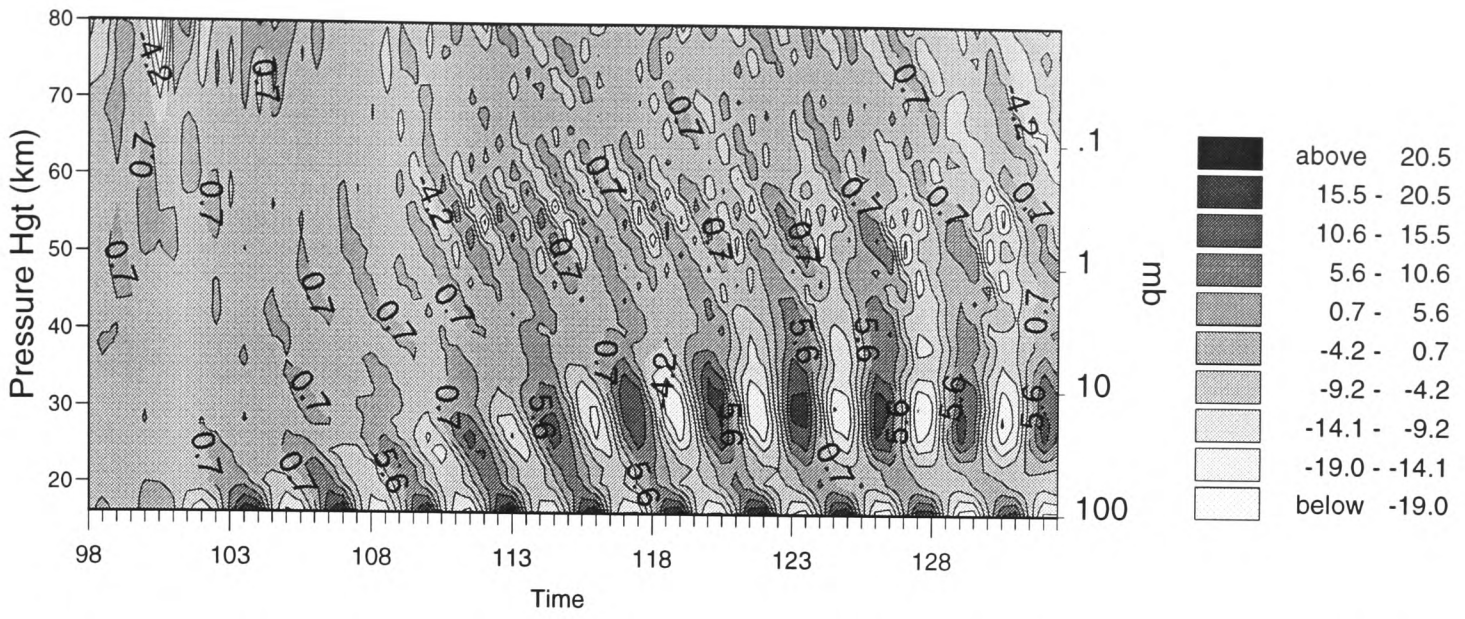

Figure 5.6: A height–time plot of the equatorial v-winds for a model run with 2 km vertical resolution and a Rossby-gravity shaped forcing on the bottom boundary. Propagating structures can be seen but these are very different from the expected Rossby-gravity waves.

height up to 40 km or so and the vertical wavelength is considerably longer than the vertical domain of the model. The 2 km vertical resolution has failed to represent the waves, which are predicted to have vertical wavelength of 4–6 km. In order to capture the Rossby-gravity waves in the model, the finer vertical resolution is implemented. Following these modifications, the model was successfully run with 64 height levels corresponding to 1 km vertical resolution in log-pressure.

The higher vertical resolution version of the model is run with the Rossby-gravity forcing in the geopotential. Figure 5.7 shows a height-time plot of propagating waves in the deviation of v-wind from the zonal mean. These propagating waves have vertical wavelength of around 8 km, close to 7 km as predicted by linear theory. The waves force a large jet in the zonal-mean u-wind, shown in figure 5.8, as they are dissipated. This again is in line with expectations.

5.2.2 Initial Examination of the Rossby-gravity Waves

As with the Kelvin waves, linear theory predicts certain properties for Rossby-gravity waves that can be tested in the modelled disturbances. Again, the waves are expected to be equatorially confined and the vertical wavelength is given by the dispersion relation. Linear theory also predicts that the v-wind disturbance will be centred over the equator,

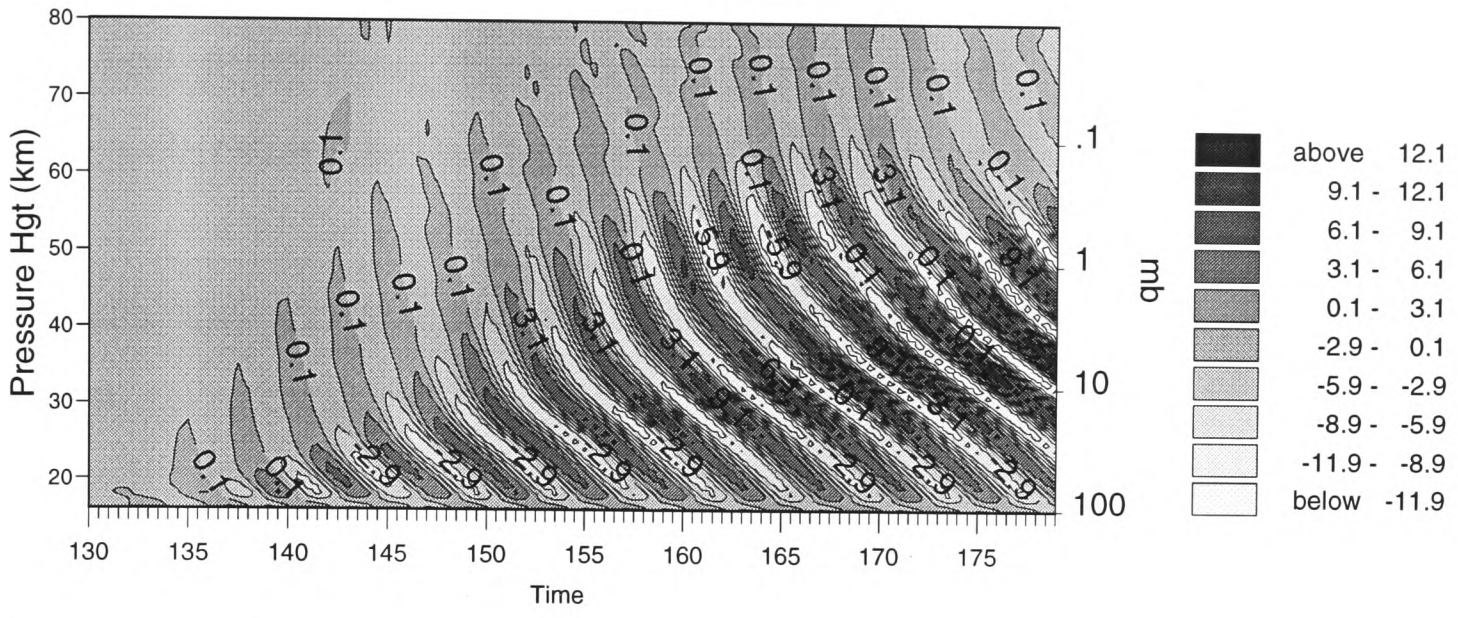

Figure 5.7: Height–time plot showing the deviations from the zonal mean of the v-wind (in ms^{-1}) in a run with Rossby-gravity waves forced on the bottom level.

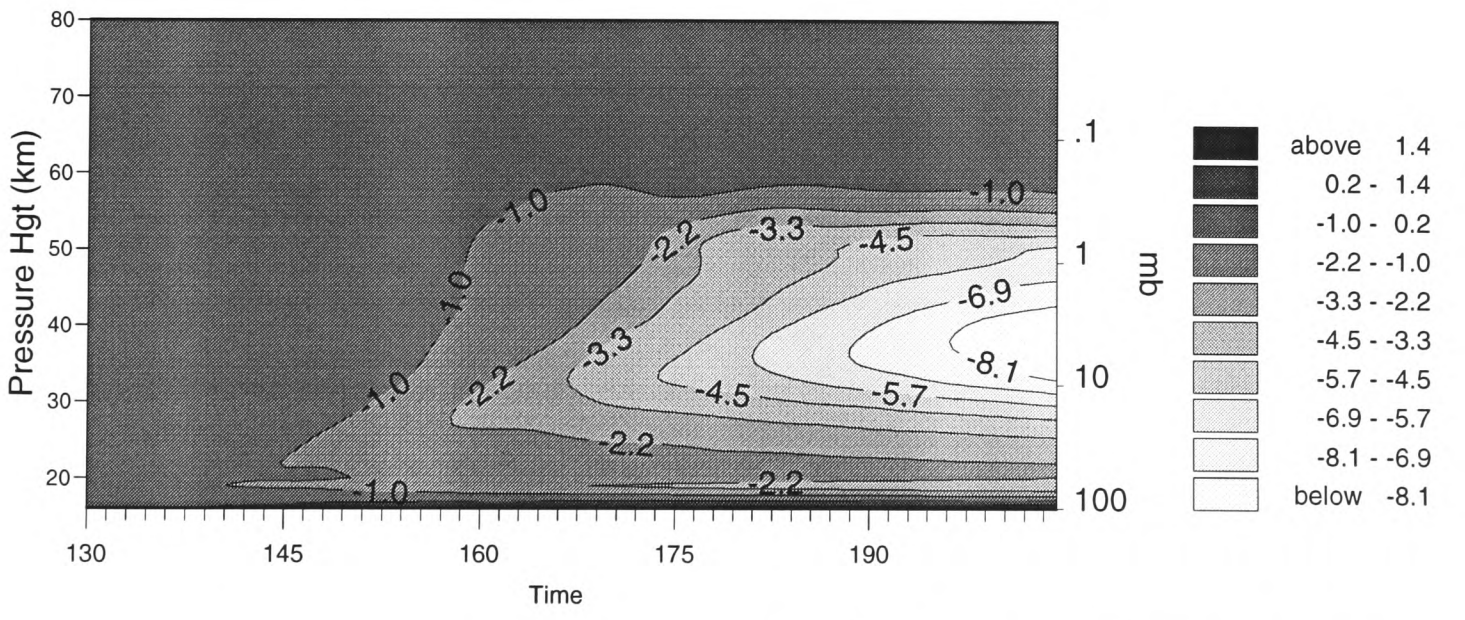

Figure 5.8: The zonal mean u-wind (in ms^{-1}) from a Rossby-gravity wave run. A large easterly jet is seen to be created as the waves are dissipated.

while the u-wind disturbance will have maxima either side of the equator and zero amplitude over the equator. To examine the latitudinal structure of the forced Rossby-gravity waves, the amplitude of the wave number 4 in u and v is plotted in figure 5.9. The upper panel in this figure shows that the v-wind perturbation is indeed centred on the equator and confined to the tropics. Similarly, the lower panel shows the amplitude of wave-number 4 in the model u-winds. In this case the waves are at a maximum either side of the equator with a minimum on the equator. They are still confined to tropical latitudes.

In addition, linear theory predicts that the meridional component of the Rossby-gravity wave disturbance should lead the zonal component by $\pi/2$ in the northern hemisphere, and the zonal component will lead the meridional component in the southern hemisphere. Figure 5.10 shows that this is indeed the case.

The vertical wavelength of the waves is easily measured from a plot such as figure 5.7. The vertical wavelength, as mentioned above, is measured to be 8 km which is very close to the theoretical value of 7 km. With the waves in the model having properties that match those predicted by linear theory so closely, we can be fairly confident that these can indeed be identified as Rossby-gravity waves.

5.3 Some Experiments with Waves in the Model

There are several prescribed parameters in the model forcing that may be altered to change the properties of the waves. Such parameters are specified in the `GEOPER` routine for each wave to be forced and consist of the wavenumber, period and amplitude of the wave. (The routine can also specify the latitude and longitude of a geopotential disturbance, although this is not relevant in this case where the waves are forced on the equator and are traveling in the zonal sense.) A series of short model runs are performed examining the variation of the waves in the model as the amplitude of the waves is changed. In addition, the effect on the waves of varying the background wind conditions and model Newtonian cooling are investigated.

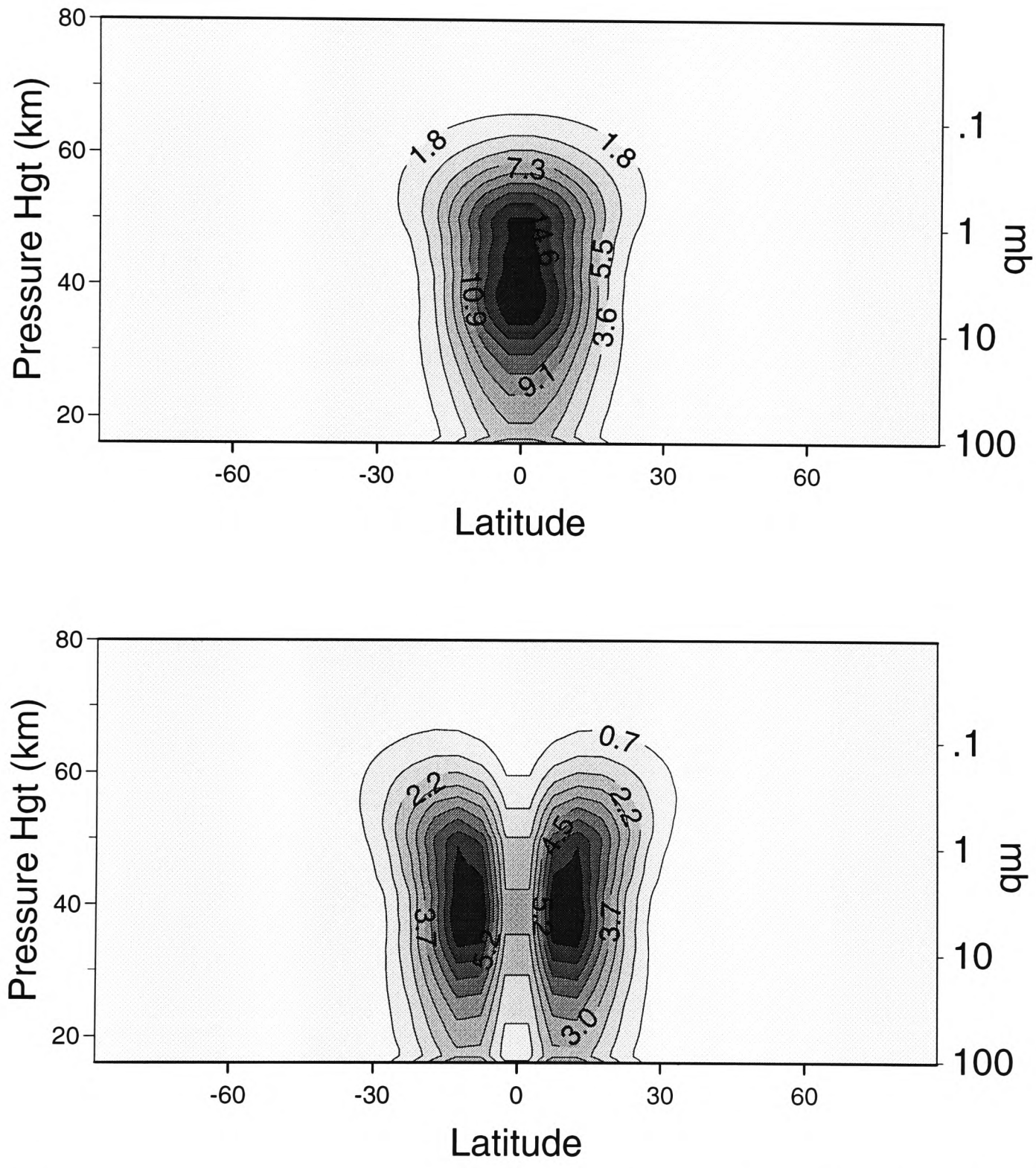

Figure 5.9: The amplitudes of wave-number 4 (in ms^{-1}) in the model fields of v (upper) and u (lower) winds. The v-wind oscillation can clearly be seen to be centred over the equator, while the u-wind oscillation has maxima either side of the equator.

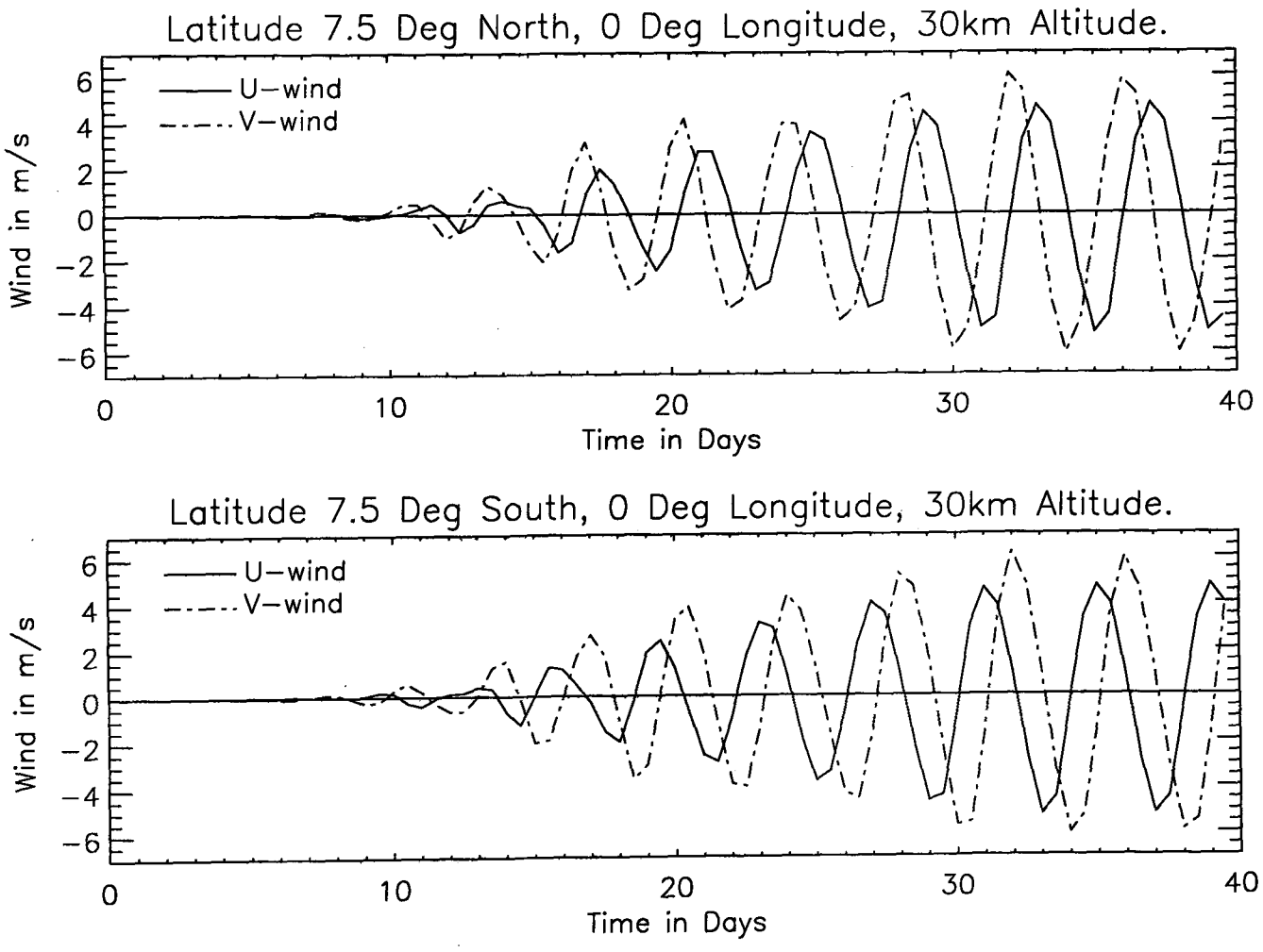

Figure 5.10: A plot showing the u and v wind at 30km altitude, 0 degrees latitude, 7.5 degrees north and south, from a run with Rossby-gravity waves forced at the lower boundary. Linear theory predicts that the v wind will lead the u wind by $\pi/2$ in the northern hemisphere, and the reverse in the southern hemisphere.

5.3.1 Varying the Forcing Amplitude

Both Kelvin and Rossby-gravity waves are forced with a variety of amplitudes ranging from very small (below the amplitude of waves observed in nature) to considerably larger than the amplitudes that will be used in the QBO modelling runs. Figure 5.11 shows the amplitude of the wave number 1 u-wind oscillation for two runs where the Kelvin waves are forced with a 10m (upper) and a 60m (lower) geopotential forcing. The wave amplitudes are shown in metres per second. It can be seen that the maximum amplitude of the waves varies very linearly with forcing amplitude (an increase in forcing amplitude from 10m to 60m - a factor of 6 - corresponds to an increase in the wave amplitude by a factor very close to 6). It would appear from this that the waves are close to behaving in a linear fashion in the model.

Although the forced waves appear to vary in a predictable way with the forcing amplitude, the resulting mean flow variations are very dissimilar. In the course of the 5 month run performed, the 10m forcing amplitude run fails to produce any discernible westerly jet. However, the 60m forcing amplitude run, as might be expected, produces a strong jet (not shown), similar to that seen in section 5.1.

5.3.2 Dissipation of Waves in a Background Zonal Flow

According to linear theory, the dissipation of waves is expected to depend strongly on the difference between the phase speed of the waves and the background zonal wind. As a preliminary experiment before attempting a QBO modelling run, and with particular relevance to the QBO, waves can be forced in a model with an existing zonal jet structure. As the vertical group velocity of the waves (see equations (2.44) and (2.53)) will depend strongly on the difference between the background zonal wind and the phase speed of the wave, it would be expected that the propagation of the waves through a jet will be strongly influenced by the jet. If a Kelvin wave is forced in an atmosphere with a strong westerly jet in the lower stratosphere, it would be expected that the Kelvin wave would be strongly dissipated as it passed through the jet. However, if an easterly jet exists in the lower stratosphere, corresponding to the easterly phase of the QBO, the Kelvin wave

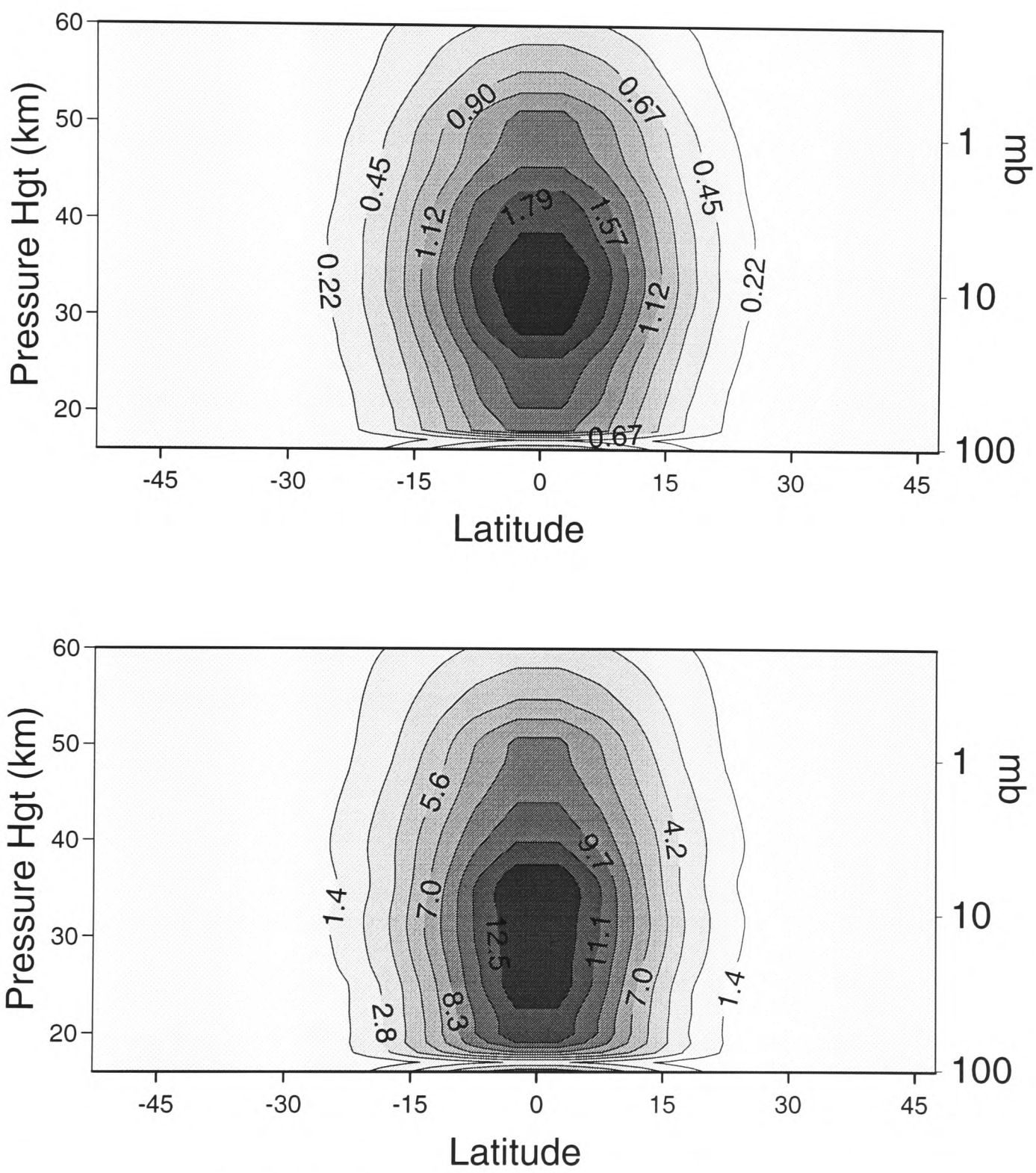

Figure 5.11: Amplitudes of wavenumber 1 wave in the u-wind for two runs with a geopotential height forcing of 10m (upper) and 60m (lower). It can be seen that the amplitude of the u-wind increases by a factor of 6 with this increase in forcing.

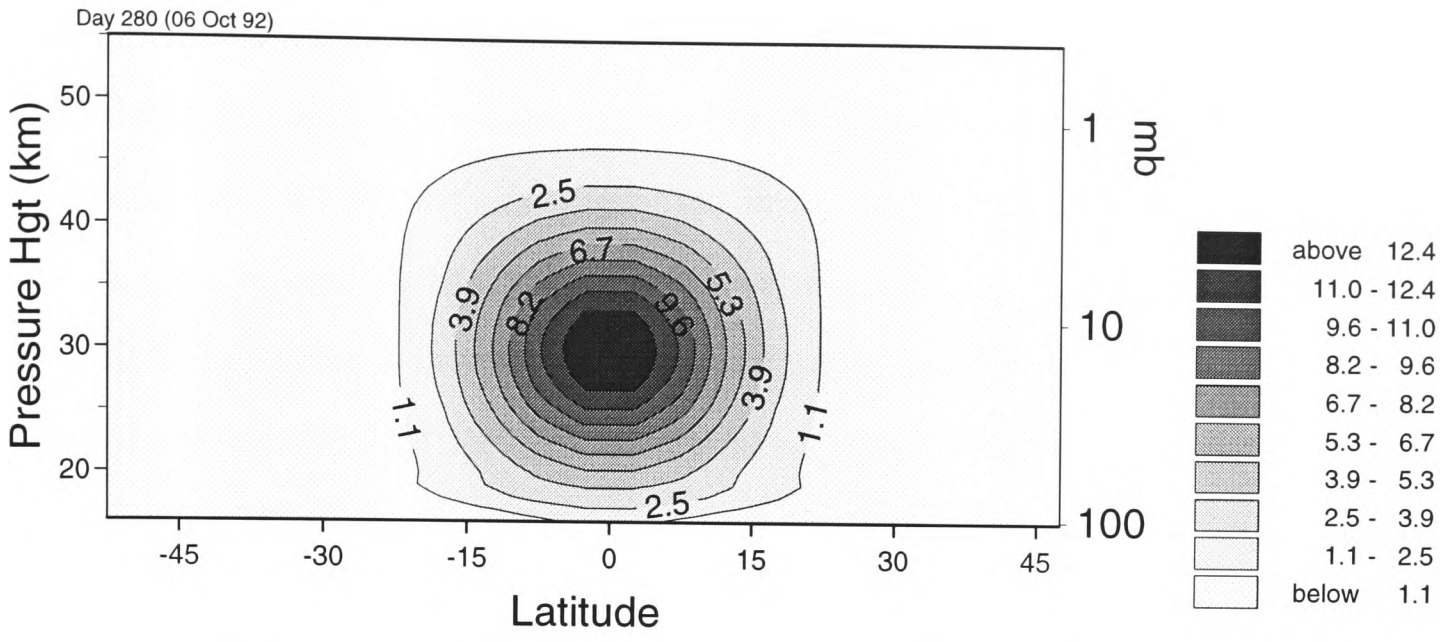

Figure 5.12: The u-wind profile $\overline{u}_0$ (in ms^{-1}). The easterly case is simply -$\overline{u}_0$.

would be expected to propagate through this region relatively unaffected, to be dissipated above. Similarly, a Rossby-gravity wave would be expected to propagate relatively easily through a westerly jet and be strongly dissipated in an easterly jet.

The model is slightly modified so that there is strong Rayleigh friction applied to the zonal mean u-wind, relaxing it towards an arbitrary zonal wind structure $\overline{u}_0$. The form of this term is a relaxation on every point given by:

$$\frac{\partial u}{\partial t} + ... = -\alpha_{zm}[\overline{u} - \overline{u}_0(\phi, z)]. \tag{5.2}$$

The profile u_0 is specified for each run. In runs done here, α_{zm} is a constant, although there is no reason α_{zm} could not be a function of height and/or latitude. In these runs, a value of α_{zm} of $1 \times 10^{-6}\ s^{-1}$ is used, equivalent to an e-folding time of 11.5 days. This will be too strong to allow any zonal jets to form as the waves are dissipated, but as the Rayleigh friction is applied only to the zonal mean u-wind, it will not directly affect the propagation of waves.

Two jet structures are used, one consisting of a westerly and the other of an easterly jet in the mean flow, as shown in figure 5.12. (The easterly jet is just the reverse of the shown westerly initial jet.) Both Kelvin and Rossby-gravity waves are forced into these jet structures and the wave properties are observed as they propagate and dissipate. Figure 5.13 shows the amplitude of the wavenumber 1 u-wind for a run with Kelvin waves forced

with westerly (upper plot) and easterly (lower plot) background winds present. As would be expected, the Kelvin waves propagate well through the easterly jet and are evident up to high altitudes but are rapidly dissipated in the westerly jet run, resulting in the waves being largely confined to the lower regions of the jet. As there is a strong zonal mean Rayleigh friction present in this run, no zonal mean flow is accelerated by the dissipating waves. However, a plot of EP-flux divergence against height and latitude in figure 5.14 shows the position where momentum is being deposited by the waves. It can be seen that in the easterly jet case, the waves are propagating with little attenuation through the atmosphere until they reach the model *sponge layer* at 50 km, where they are being strongly dissipated, resulting in a highly localised area of strong positive EP-flux divergence. In the westerly jet case, the opposite is happening as the waves are strongly dissipated in the lower stratosphere, through radiative processes, and are depositing momentum in this region. These plots are consistent with what would be predicted by the linear theory of these waves.

Figure 5.15 shows the amplitude of the wavenumber 4 v-wind oscillation in runs of Rossby-gravity waves forced into westerly (upper panel) and easterly (lower panel) background flows. It can be seen that the background wind structure has a very great effect on the propagation of these Rossby-gravity waves. In the westerly jet, the Rossby-gravity waves are able to propagate very easily and make it through the main domain of the model up to the 50km level where the Rayleigh friction becomes larger.

The effect of the background winds on the vertical wavelength can be clearly seen in figure 5.16. This plot shows the Rossby-gravity wave through the two background jet scenarios. It can be seen that in the easterly background jet case, the vertical wavelength is very much reduced as the waves propagate through the jet. Conversely, in the westerly background case, the vertical wavelength is much increased as the wave propagates through this region. In Plumb and Bell [1982] the variation of vertical wavelength with background flow of Kelvin and Rossby-gravity waves of phase speeds ± 25 ms^{-1} is summarised as:

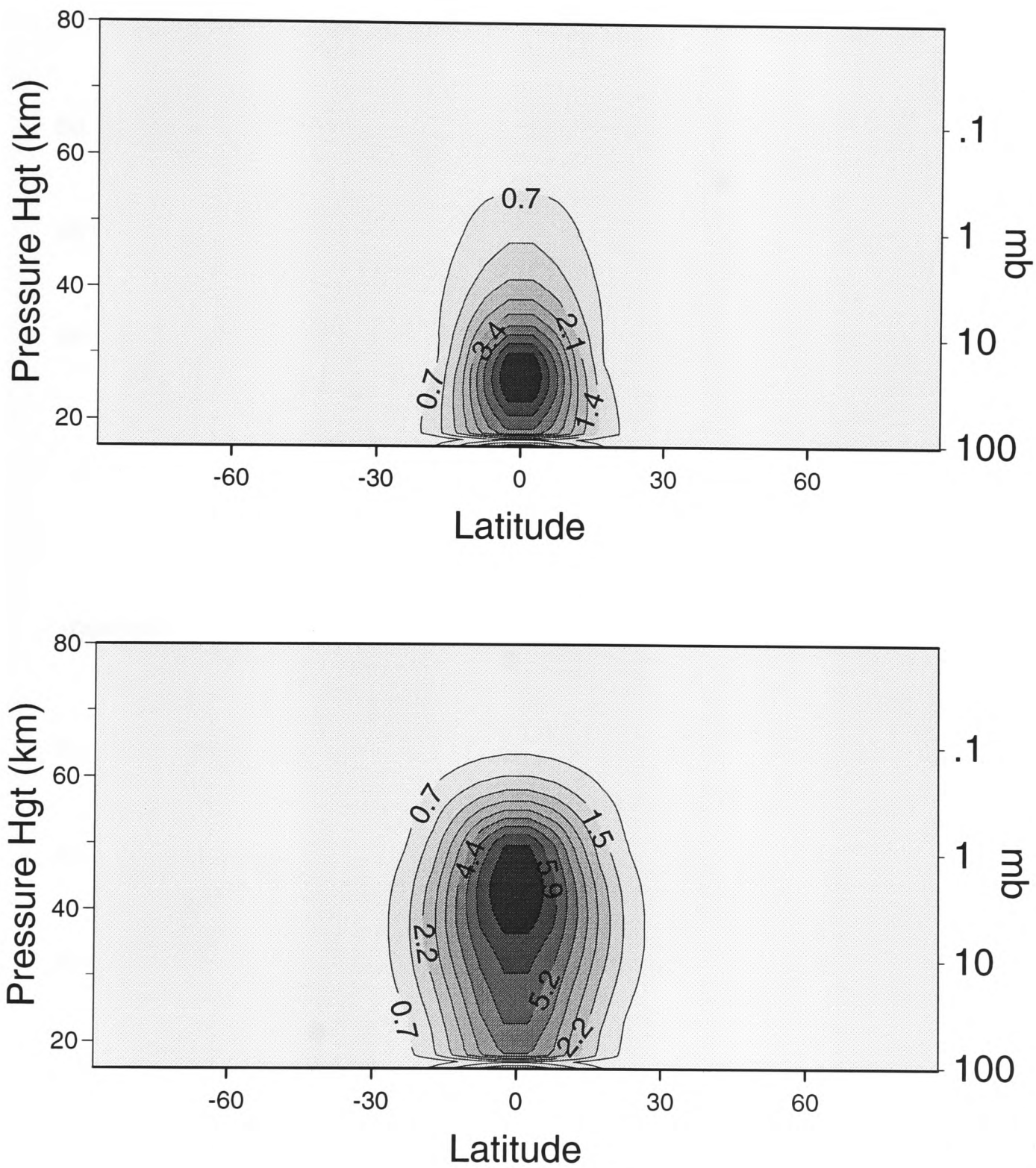

Figure 5.13: Kelvin waves forced into a fixed background flow. The plots show the amplitude of wave number 1 u-wind (in ms^{-1}) for the runs where the background jet forced is westerly (upper) and easterly (lower).

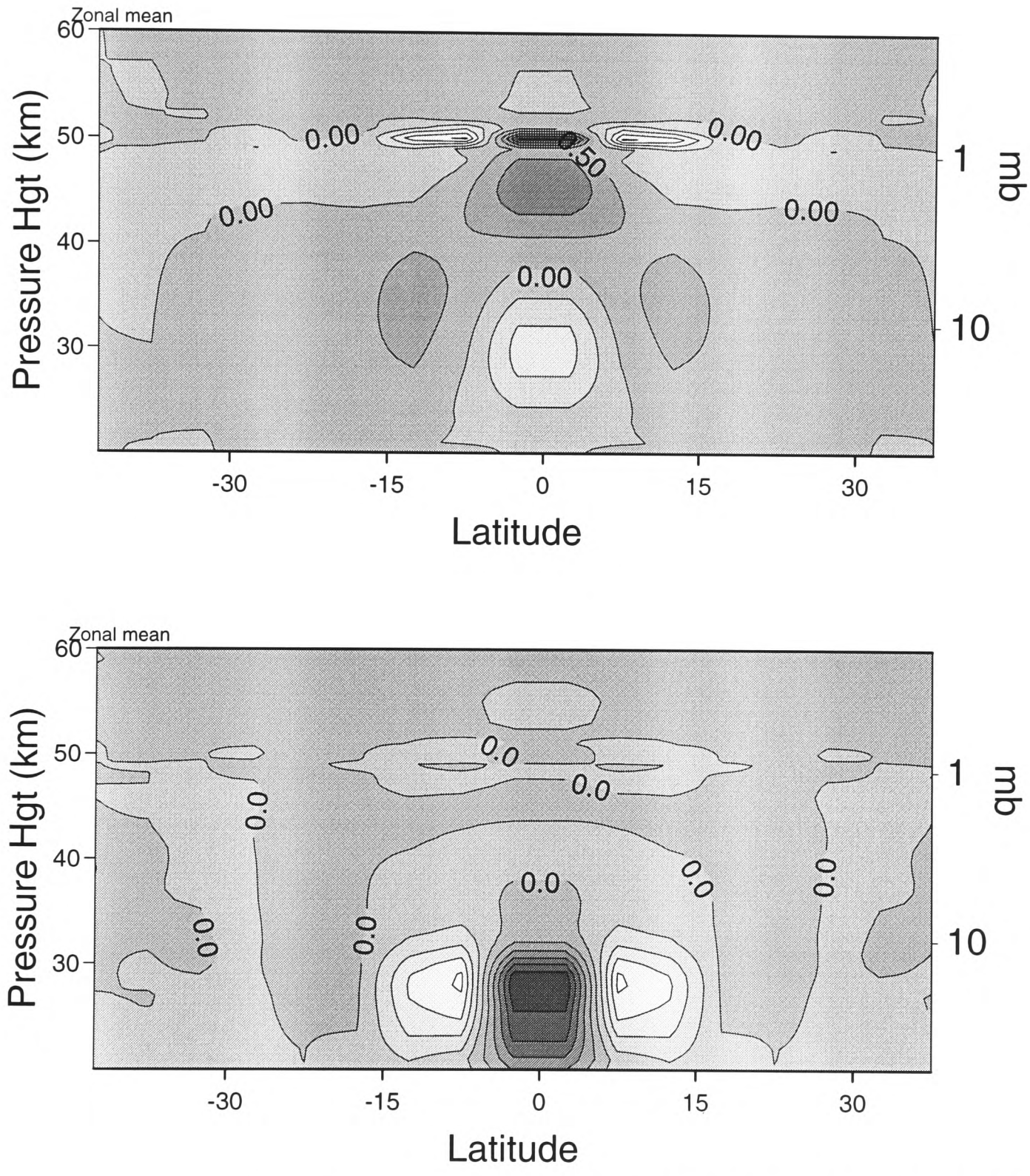

Figure 5.14: EP-flux divergence for Kelvin waves forced into easterly (upper) and westerly (lower) jets. The contour intervals are the same in the two runs. The plots are the average of EP-flux divergence over days 100 to 200 of each model run.

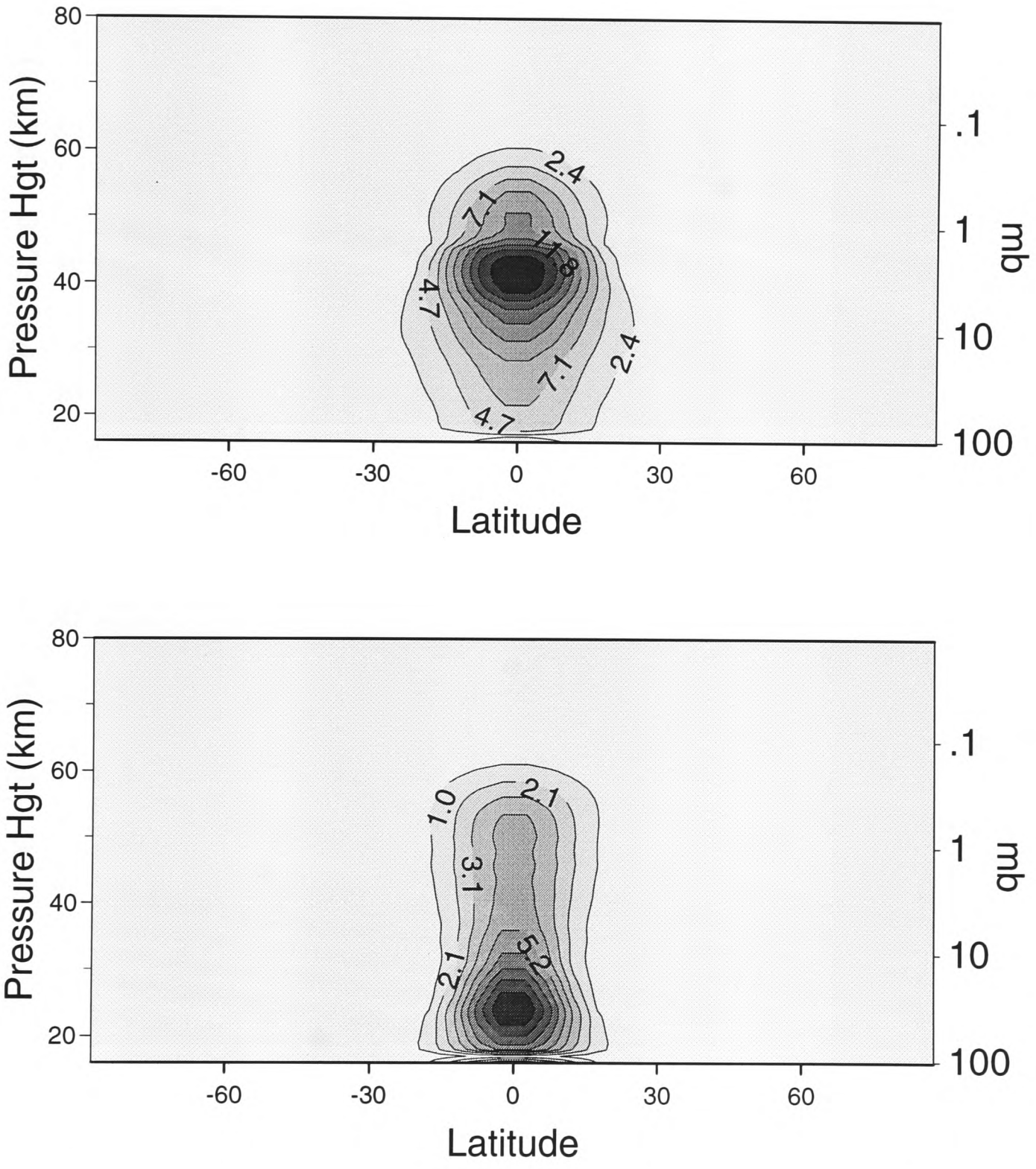

Figure 5.15: As for figure 5.13 but looking at the amplitude of wavenumber 4 (in ms^{-1}) in the v-wind with Rossby-gravity waves forced. Again, waves forced into a westerly jet are shown in the upper panel, and waves forced into an easterly jet are shown in the lower.

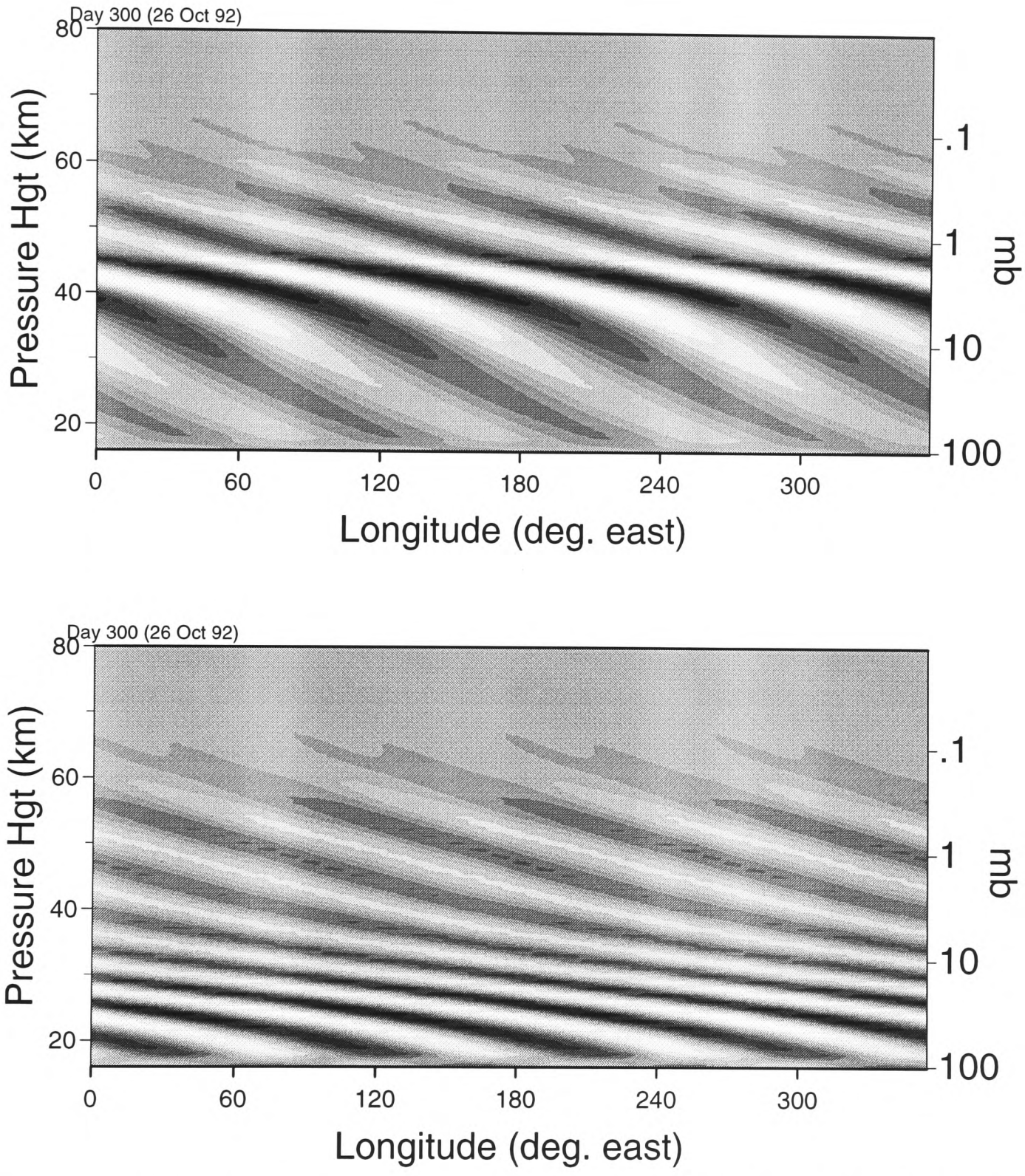

Figure 5.16: A plot showing the variation of wavelength with the background wind. In this figure, the deviations from the zonal mean of the v-winds (in ms^{-1}) are plotted over the equator for a day in the Rossby-gravity wave run. The upper plot shows the Rossby-gravity wave propagating through the westerly jet, and the lower panel shows the propagation through an easterly jet.

Background Flow $U_0(\mathrm{ms}^{-1})$	Kelvin Wave $\lambda_{vertical}$	Rossby-gravity Wave $\lambda_{vertical}$
-20	11.23	0.51
0	7.24	5.58
20	1.55	14.88

These model results are very much in line with the predictions obtained from the linear theory presented in section 2.3. It is important that this variation in the waves' propagation through such jets is sufficiently well modelled if the QBO is to be simulated. The model representation of waves as their wavelength becomes shorter is examined in appendix A and some potential problems are noted. In particular it would appear that as the wavelengths become shorter, the model numerics will artificially slow the group velocity of the waves. In the extreme case, where the waves are particularly short, the group velocity can actually be in the wrong direction. This will act to enhance the dissipation of the waves as they are propagating through regions where their phase velocity is in the same sense as the background winds. The model is however providing a sufficiently good simulation of these waves to generate realistic jets. In section 5.5 it is seen that the generated jet structure is fairly insensitive to vertical resolution.

5.3.3 The Effect of Varying the Newtonian Cooling

Waves are dissipated in the model far away from *critical-levels*. In nature, it may be anticipated that radiative cooling is the principal source of this dissipation. In the model, the time-scale associated with the Rayleigh friction is about 120 days below 50 km. In the lower stratosphere, the Newtonian cooling time-scale is under 20 days. It might be expected that the dissipation of waves in the model is principally due to radiative cooling. It is possible however that the model numerics may contribute to the dissipation of the waves through numerical inaccuracies in the finite difference methods. Such mechanisms are described later in this section. Numerical inaccuracies may further contribute to the dissipation of waves in a more indirect way: as the waves become shorter in wavelength,

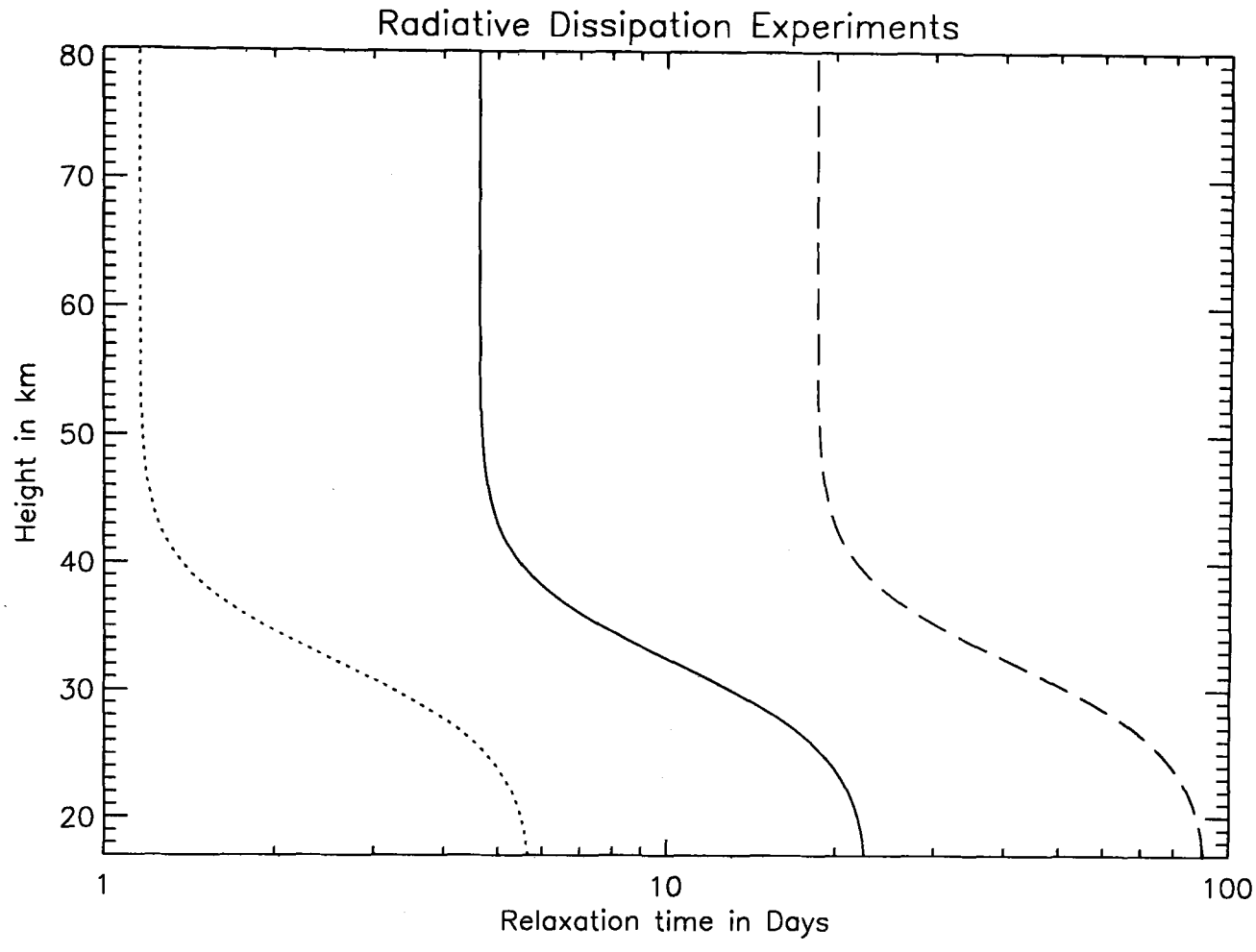

Figure 5.17: The Newtonian relaxation time in days for the dissipation runs. The dotted line shows the Newtonian cooling reduced by a factor of four, and the dashed line the Newtonian cooling increased by a factor of four. The usual dissipation is shown in solid line.

their group velocity can become slowed or even reversed,[2] exaggerating the dissipation of the waves through other processes. It is also quite possible that other processes such as Kelvin-Helmholtz instabilities would contribute to the dissipation of the waves, both in nature and possibly in the model. To establish that the dissipation of waves in the model was principally due to the radiative scheme, a series of runs were performed with both Kelvin and Rossby-gravity waves where the Newtonian cooling time-scale was varied between the runs. (The Newtonian cooling in the model is described in section 4.2.2.) In these runs, the Newtonian cooling is increased and decreased by a factor of four between the different experiments. Figure 5.17 shows the Newtonian relaxation times for these runs.

The series of plots, 5.18–5.21 show wave propagation and resulting mean wind accelerations for this series of runs. It can be seen that the height at which the waves are

[2]See Appendix A.

dissipated, and correspondingly, the u-wind jet accelerated, is strongly dependent on the strength of the Newtonian cooling. In the cases with reduced Newtonian cooling, the waves initially propagate through most of the domain of the model until they reach the *sponge layer* at 50 km. They are then dissipated by a mixture of the Newtonian cooling (which increases with height) and the Rayleigh friction which becomes significant at this level. This strong dependence of the wave dissipation on the Newtonian cooling indicates that, as would be expected, the dissipation of waves in the model is principally due to radiative damping.

With the Rossby-gravity wave being forced, in the weaker Newtonian cooling case, the jet created is very narrow in the vertical. It is likely in this case that the waves are being strongly dissipated as they reach the strong easterly jet, depositing momentum in a narrow region. This is due to the very strong dependence of the vertical wavelength of the Rossby-gravity waves to $(\overline{u} - c)$ (as given in equation (2.54)). As the waves approach the sharp shear at the bottom of this jet, they are in a very narrow region, strongly dissipated. In appendix A, it is also seen that as the wavelength of the waves becomes small, the vertical group velocity of the waves will be further slowed through numeric effects in the model, contributing to the narrowness of this jet. In the increased Newtonian cooling case, the waves are smoothly damped over a large range of altitude and a smooth acceleration is experienced through a large part of the model domain.

As described in section 2.3.1, theory predicts that the dissipation mechanism can have a large influence on the nature of the deposited momentum. This is especially true for Rossby-gravity waves, where it may be expected that in a case where the dissipation is completely radiative (rather than mechanical), the dissipation of the waves will result in acceleration off the equator, with no acceleration at the equator. In the runs forced in this chapter, the Rossby-gravity waves are producing a jet over the equator. Figure 5.22 shows the latitudinal jet structure generated about three months into a model run in which Rossby-gravity waves have been forced. This model run is one in which Rossby-gravity waves are generated in an atmosphere in which the Newtonian cooling rates and the mechanical (Rayleigh) friction are set at the standard levels (see figures 4.1 and 4.4),

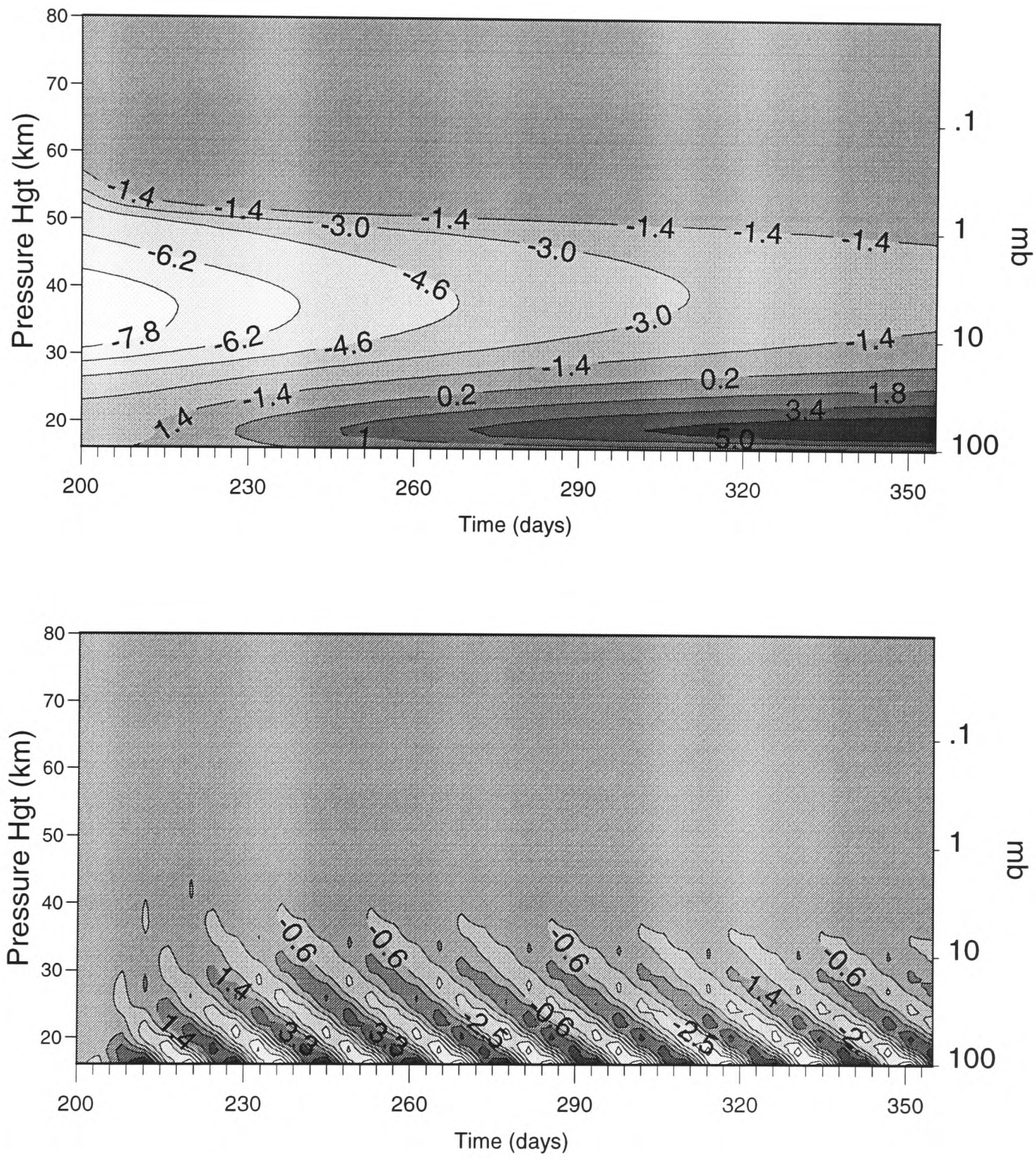

Figure 5.18: Time-plots of the zonal mean (upper) and deviations from zonal mean (lower) u-wind in ms^{-1} for a Kelvin wave run with the increased Newtonian cooling. When compared to figure 5.19, the waves are dissipated quickly, only propagating to a low level.

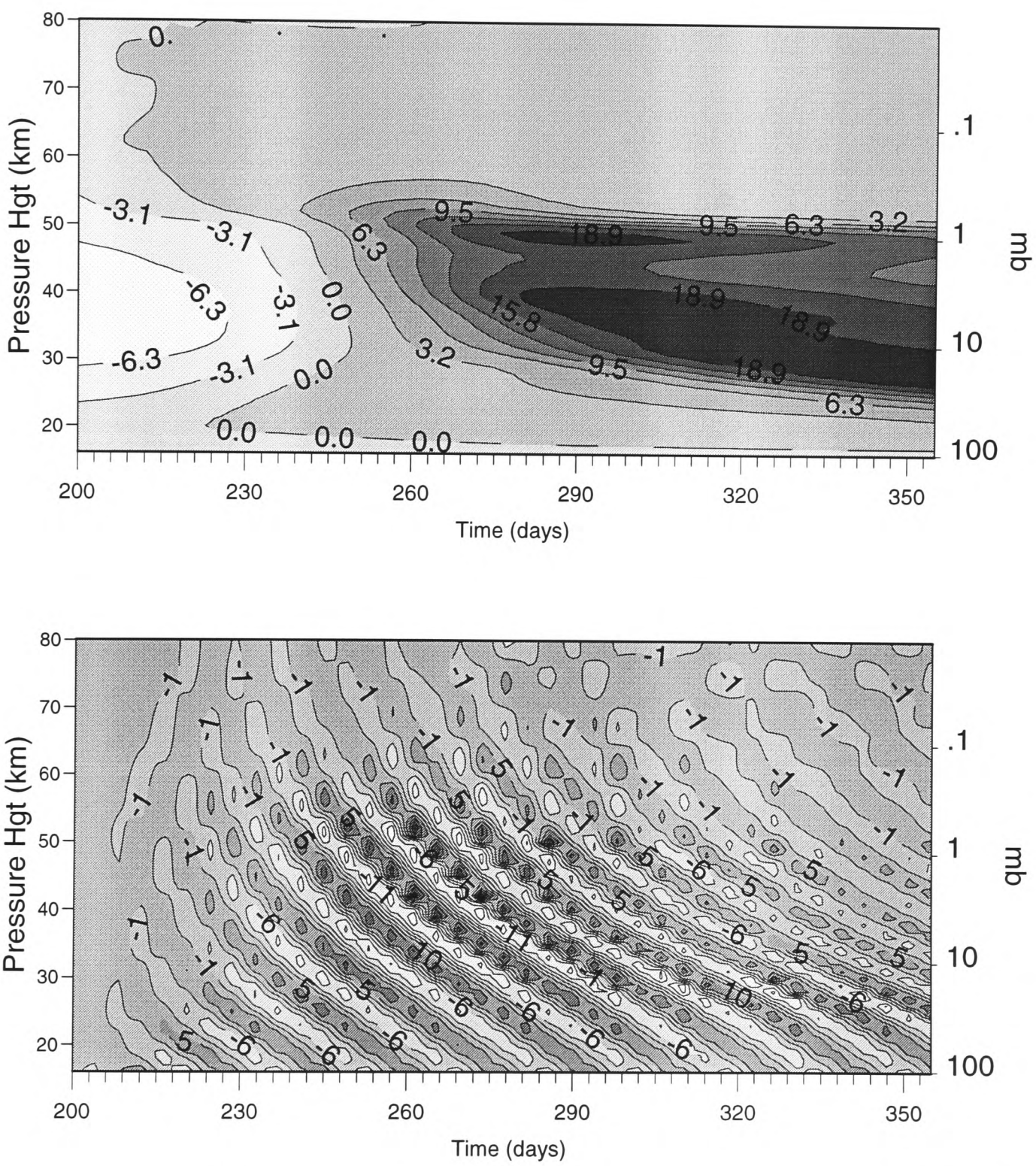

Figure 5.19: Kelvin waves. Plots as figure 5.18 except the Newtonian cooling is reduced to a quarter of the normal model Newtonian cooling rates. In this plot, the waves are able to propagate very much higher, initially reaching the model *sponge layer* before they are dissipated.

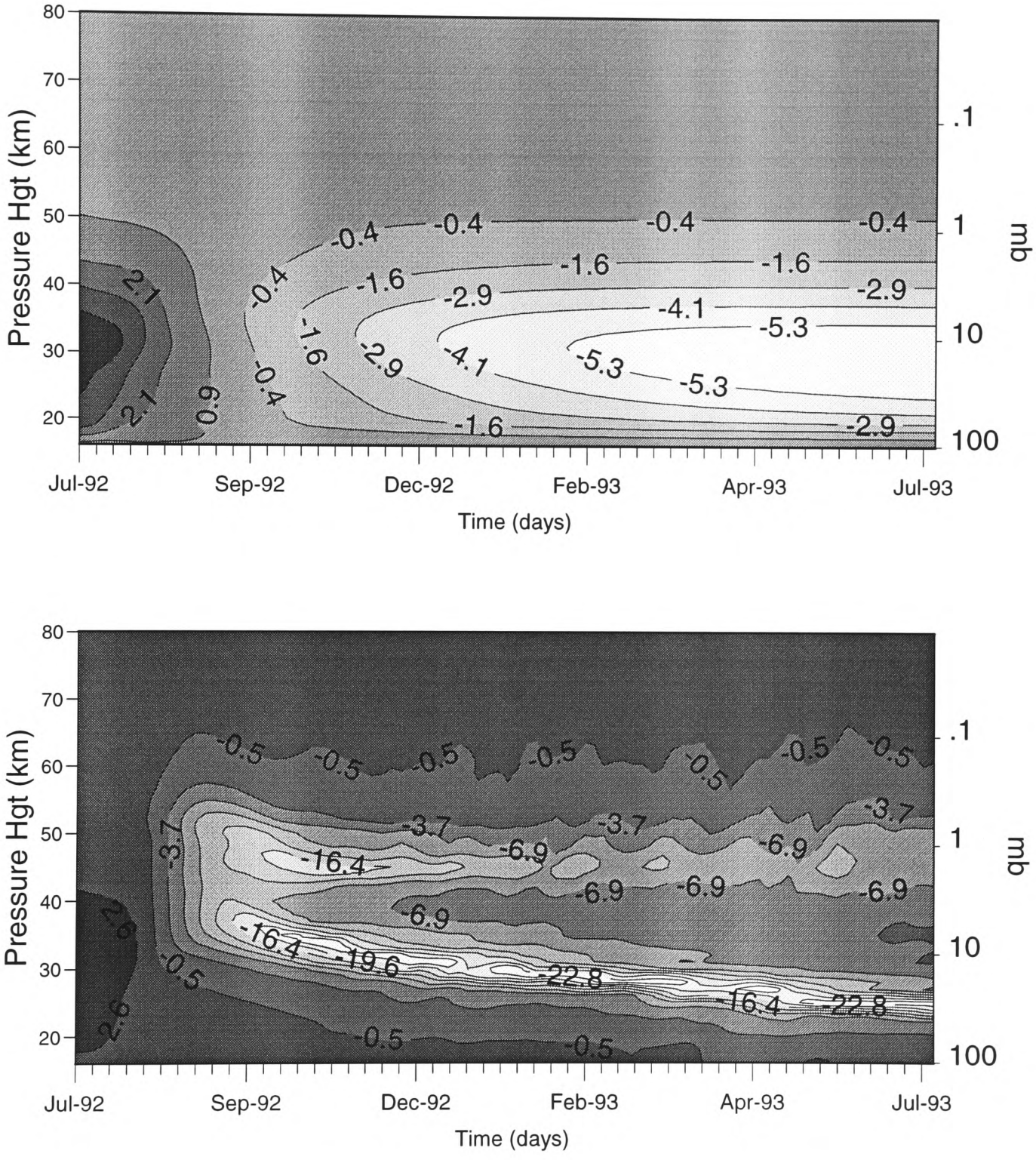

Figure 5.20: The zonal mean u-winds (in ms^{-1}) shown for the Rossby-gravity runs with Newtonian cooling increased (upper plot) and decreased (lower). The shape of these plots is quite different as the waves are able to propagate to the *sponge layer* in the reduced Newtonian cooling case and a region of strong easterlies is formed, which propagates downwards as easterly momentum is dumped on its lower edge.

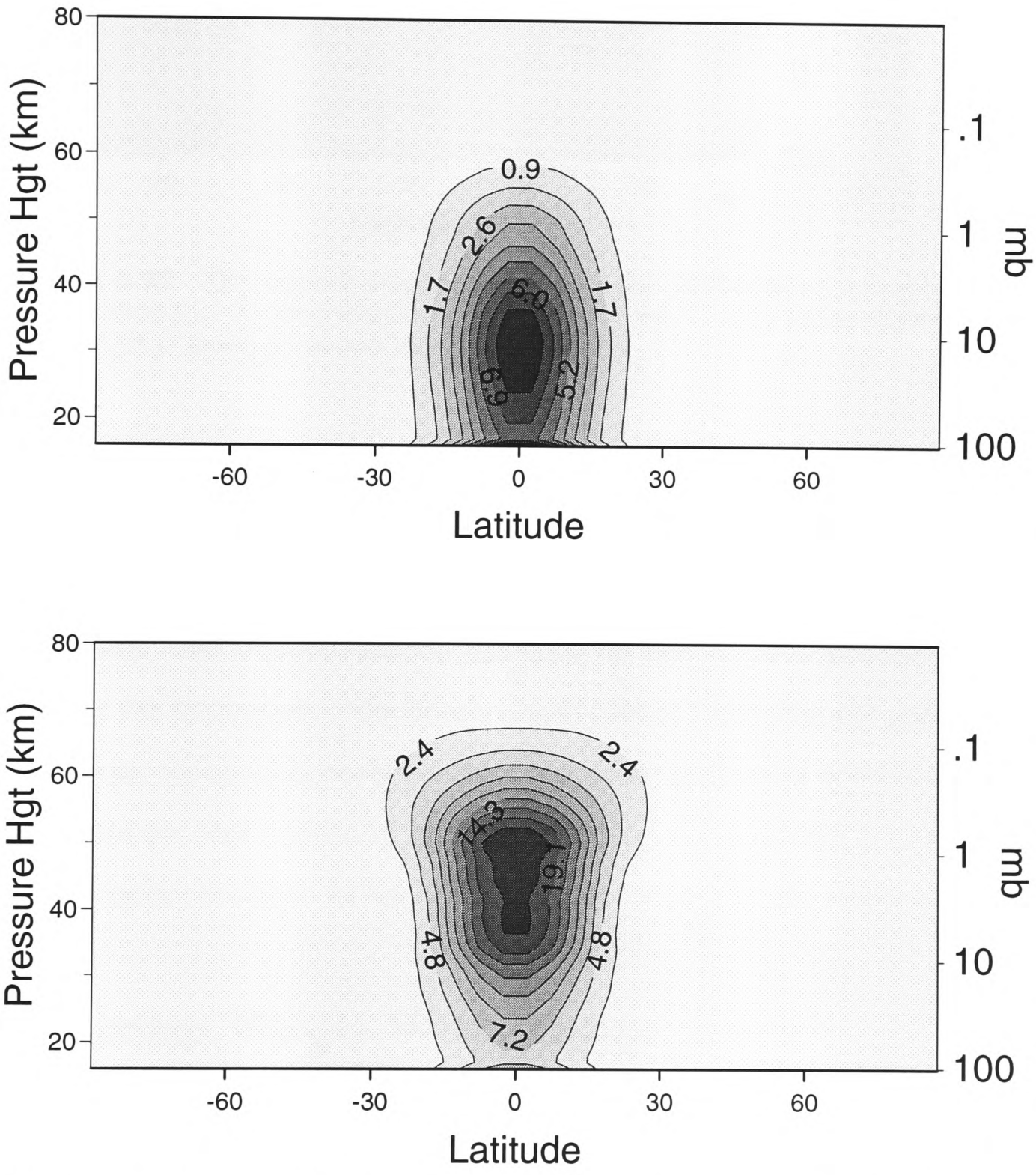

Figure 5.21: The amplitudes of wavenumber 4 in the v-winds for Rossby-gravity runs with increased (upper) and decreased (lower) Newtonian cooling. In the case with the reduced Newtonian cooling, the waves propagate higher than when the Newtonian cooling is increased.

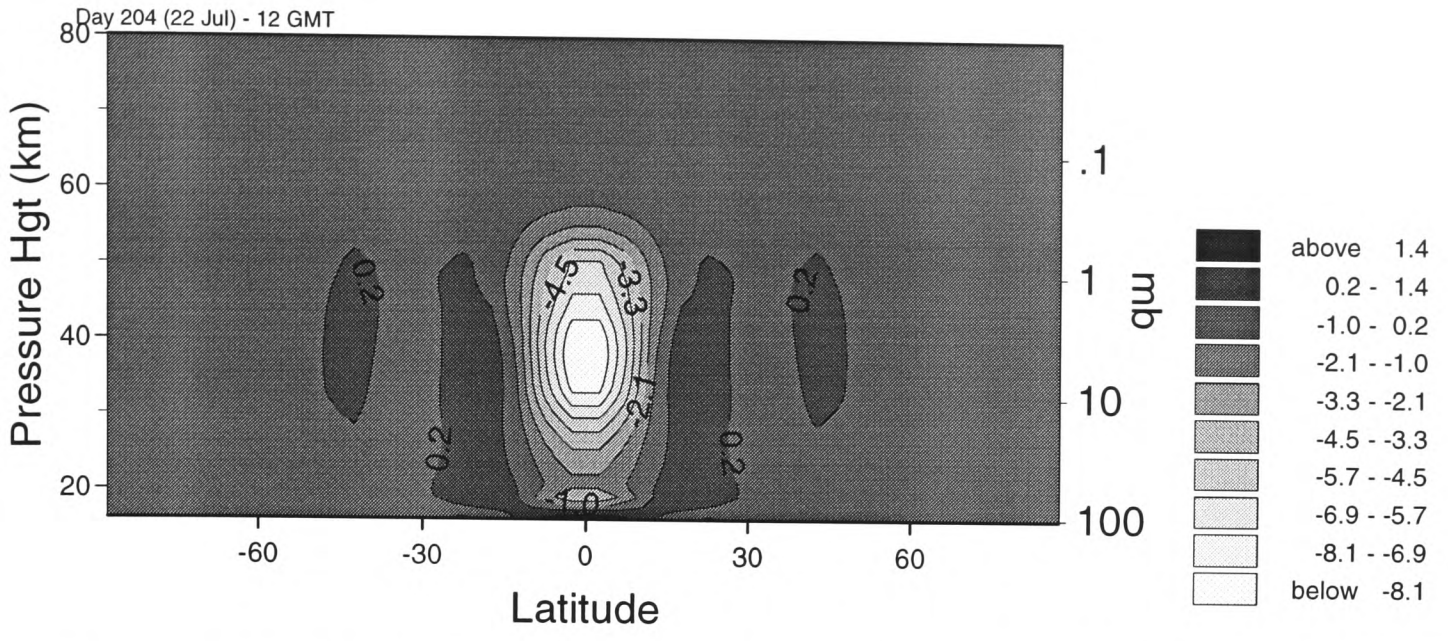

Figure 5.22: The latitude-height structure of the jet forced as a Rossby-gravity wave is forced in the isothermal model. Units are ms^{-1}. This figure shows that the easterly jet is being generated on the equator.

but in all the simulations run in the project, the jet is centred over the equator.

Even with the Rayleigh friction reduced by a factor of 100, it is found that the model produces a jet that is centred over the equator when Rossby-gravity waves are forced at the lower boundary. This is maybe not surprising as the assumptions used in the theoretical description of the dissipation of the Rossby-gravity waves are strong and particularly when the shear in the background winds is strong, the theory will break down [Andrews, 1998]. Certainly in all the runs performed in this project, the jets produced are centred over the equator and similar in shape to the QBO jets observed in the atmosphere.

5.4 Forcing Waves With Temperature

Temperature can be added to the wave forcing of the lower boundary of the model as described in section 5.4.1. Several experiments were performed in the model with both the temperature and geopotential forced. It was found, while investigating problems with the model stability, that the bottom boundary problems could be somewhat suppressed by specifying the temperature in addition to the geopotential on the bottom boundary. This is not surprising when it is noted that the problem in the vertical advection was due to prognostic model variables being obtained by extrapolation through the model bottom boundary. If temperature is being specified on the model bottom boundary, there is one

less prognostic variable being extrapolated and the positive feedback situation may be partially avoided. Once the advection problems were corrected in the model (described in section 4.3), model runs with and without temperature forcing were indistinguishable.

5.4.1 Adding Temperature to GEOPER

The code necessary to force additional bottom boundaries exists in the model. The model can support 1, 2 or 4 boundary fields, representing either geopotential only, geopotential and temperature or geopotential, temperature and wind fields in both the zonal and meridional directions. If temperature is forced, the temperature bottom boundary will then consist of a background field, either from realistic data or an isothermal or otherwise simplified boundary, with a perturbation superimposed on it by the GEOPER routine.

The GEOPER routine must be modified to add this temperature perturbation, T', to the temperature boundary field. T' will generally be a forcing similar to the geopotential forcing but with some phase change. T and geopotential Φ are related according to the expression:

$$T' = H/R\frac{\partial}{\partial z}\Phi'. \tag{5.3}$$

For the Kelvin and Rossby-gravity waves, wave-like solutions of the primitive equations were sought (equation (2.34)) such that

$$\Phi' = \hat{\Phi}(y)e^{\frac{z}{2H}}\sin(kx + mz - \omega t). \tag{5.4}$$

Combining these gives us a statement for T' as a function of time, position and the wave properties m, k and ω as follows:

$$T' = \hat{\Phi}(y)e^{\frac{z}{2H}}\left[\frac{1}{2H}\sin(kx + mz - \omega t) + \frac{mH}{R}\cos(kx + mz - \omega t)\right]. \tag{5.5}$$

This is a sinusoidal oscillation with phase difference to the geopotential oscillation[3].

The model wave forcing specifies the waves in terms of k and ω so that in order to

[3]The trigonometric identity relevant here is: $a\sin\alpha + b\cos\alpha = \sqrt{a^2+b^2}\cos(\alpha - \beta)$, with β given by $\beta = \tan^{-1}(a/b)$.

force the waves, we must eliminate m for the equation. This is achieved by substituting the dispersion relation, which describes the relation between m to k and ω, into equation 5.5. The dispersion relation differs between the different classes of waves to be considered and the expressions for temperature perturbations separate according to wave type as follows:

Kelvin (or gravity Waves) These have the dispersion relation

$$m = -\frac{Nk}{\omega}.$$

Putting this into equation (5.5) we get an expression for the temperature perturbation of:

$$T' = \hat{\Phi}(y)e^{\frac{z}{2H}}\left[\frac{1}{2H}\sin(kx + mz - \omega t) - \frac{NHk}{R\omega}\cos(kx + mz - \omega t)\right]. \quad (5.6)$$

Values of k and ω are specified explicitly for each wave to be forced. N is approximated to a value of 0.0224 s^{-1} which is a typical value for the stratosphere (the value is fairly constant over the extent of the stratosphere).

Rossby-gravity Waves These have a slightly more complicated dispersion relation than Kelvin waves. Here,

$$m = \frac{N}{\omega^2}(\beta + \omega k).$$

This is substituted into equation (5.5) to give an expression of the temperature perturbation of:

$$T' = \hat{\Phi}(y)e^{\frac{z}{2H}}\left[\frac{1}{2H}\sin(kx + mz - \omega t) + \frac{NH}{R\omega^2}(\beta + \omega k)\cos(kx + mz - \omega t)\right]. \quad (5.7)$$

5.4.2 Using Temperature Wave Forcing

These expressions for the temperature perturbation are implemented in the `GEOPER` subroutine, described in section 4.2.1. The model has been run with the temperature forcing

applied and produces realistic waves. When the advection problems of the bottom boundary are avoided through the patch described in section 4.3, temperature forcing on the bottom boundary is found to be unnecessary to maintain stability. Model runs with and without temperature forcing are indistinguishable and temperature forcing was not used in the runs performed in later chapters of this thesis. The code is retained as it may be useful in further work. The model is being forced with geopotential, temperature and horizontal wind boundaries by other researchers and this code would be useful if, for example, the wave forcing used in this thesis was to be combined with gravity wave parameterisation work being performed by Bryan Lawrence.

5.5 A Comparison of Model runs at different Vertical Resolutions

The model has been run with vertical resolutions of 2000, 1000 and 500m in log-pressure height. It is desirable that at the resolution used for the QBO runs, the results are not sensitive to a further increase in model resolution. It has already been seen that for Kelvin waves, the results are similar for the model in the 32 level and 64 level configurations. Rossby-gravity waves are more testing of the model as they have smaller vertical wavelength and importantly, are more sensitive to variations in the background flow [Plumb and Bell, 1982].

A pair of model runs are performed with Rossby-gravity waves forced and resolutions of 1000 and 500 m. Figure 5.23 shows a longitude-height plot of the propagating Rossby-gravity waves. As the waves propagate through the easterly jet that has been formed by Rossby-gravity waves, their vertical wavelength becomes shorter and they approach the limits of the model resolution. In this region, there is some difference evident between the different model resolutions. This difference appears, however, to have little effect on the zonal mean winds. Figure 5.24 shows the zonal-mean u-winds against height and time. The evolution of this wind jet is very similar in the two figures. As there was very little difference between the different resolutions, the 1000 m vertical resolution was chosen as

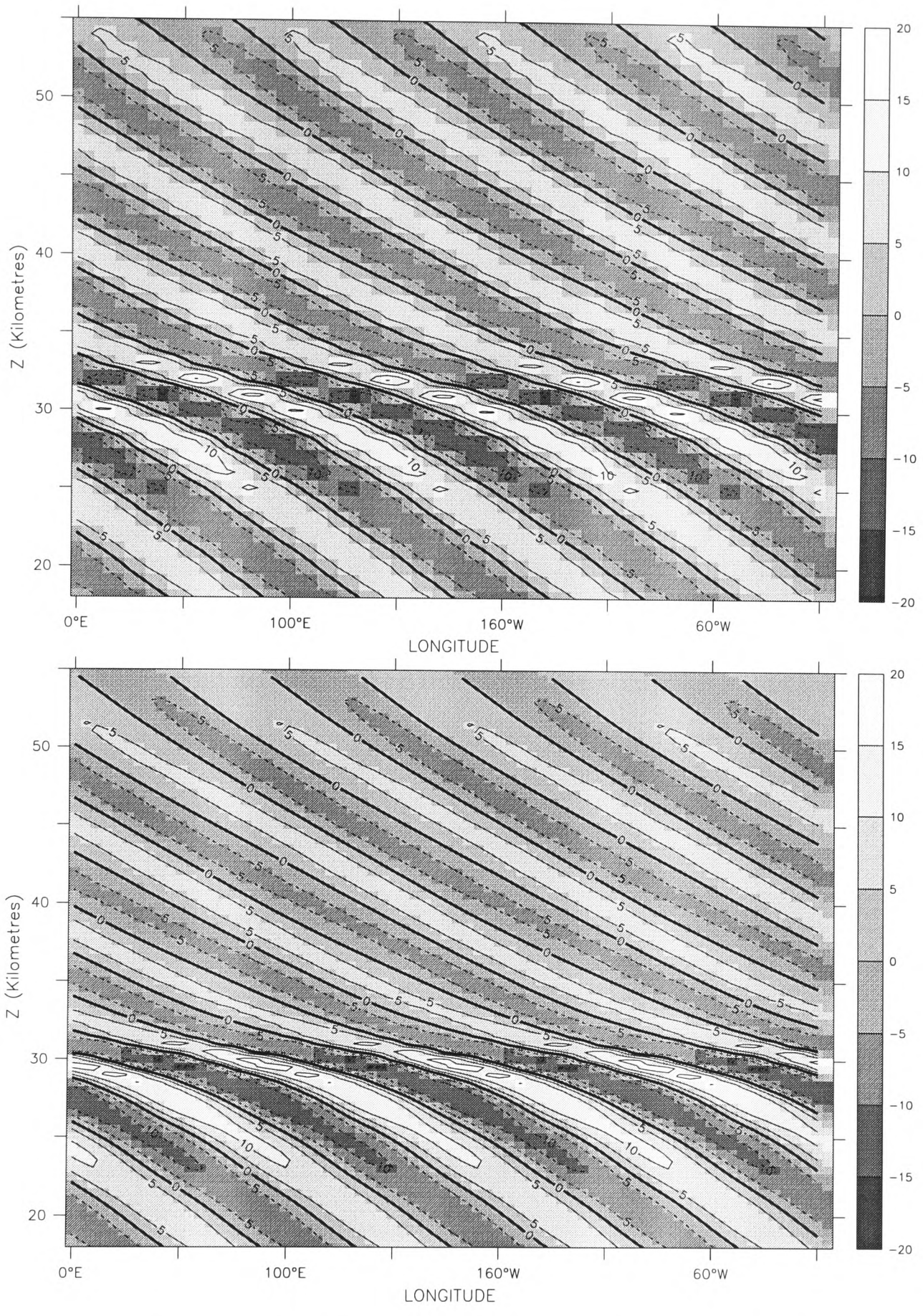

Figure 5.23: Longitude-height plots of v-wind (units are ms^{-1}) in the Rossby-gravity wave runs with varying vertical resolution. The top plot shows a run with vertical resolution of 1000m. The lower plot shows the same waves forced in a model with vertical resolution of 500m. (The filled squares, just visible in the plots, are the actual model grid squares.)

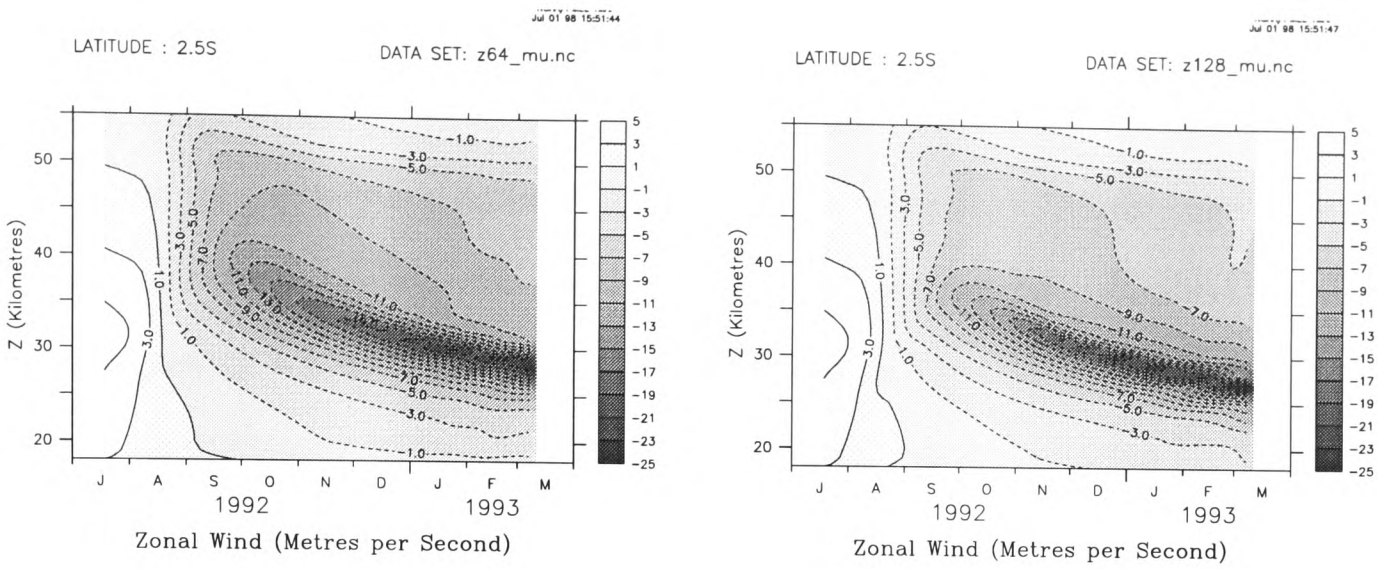

Figure 5.24: Height-time plots of zonal-mean u-wind as Rossby-gravity waves are forced into the model at different vertical resolutions (1000m on the left and 500m on the right). The evolution of the jets is remarkably similar in the two runs, indicating that there is no advantage in going to 500m resolution.

adequate for the experiments to be performed. The higher resolution makes longer model runs prohibitively expensive in terms of computer time needed and storage needed for the results and would offer no advantages in terms of modelling the waves.

5.6 Summary

5.6.1 Forcing and Identifying the Waves

In this chapter, the equatorial waves thought to be largely responsible for the driving of the QBO are generated and analysed in the SMM. The waves forced are Kelvin and Rossby-gravity waves, as cited by Holton and Lindzen [1972] as driving waves of the QBO. To force these waves, the model is run in a state where the Newtonian cooling scheme is acting to relax the model temperatures towards an isothermal state. This provides a very simple model background state on which the waves and their effects will be easily identified.

Kelvin waves prove fairly straightforward to model and appear to be very well resolved at all of the model resolutions used (2,1 and 0.5 km). Accompanying the simulation of Kelvin waves in the model is the formation of a westerly jet in the model middle stratosphere. This jet is formed as the Kelvin waves are dissipated through radiative

processes as they propagate in the model.

Rossby-gravity waves prove to be more troublesome to simulate in the model and are not seen in the model in its standard 2 km vertical resolution. When the model vertical resolution is increased, the Rossby-gravity waves are successfully modelled. In the model with Rossby-gravity waves forced, an easterly jet is generated as the waves are dissipated. There are some questions regarding how well the Rossby-gravity waves are being resolved in the model, even at the higher resolutions. Figures 5.16 and 5.23 show the Rossby-gravity waves with very short vertical wavelengths under certain circumstances. It is, however, reassuring that the waves appear to be fairly insensitive to a change in vertical resolution from 1 km to 500m, which suggests that the vertical resolution of 1 km is doing an adequate job of representing the waves. The model was not run at vertical resolutions finer than 500m (which is 128 levels in the vertical); such runs would be impractical to use for the long runs required to observe the properties of any generated QBO.

The identity of the wave-like disturbances seen in the model is checked by comparing measured properties of the modelled waves with those predicted by linear theory for the equatorial waves. In particular, the Kelvin waves are predicted to have a very small wave amplitude in v-wind as compared to the u-wind and the Rossby-gravity waves are predicted to have a structure where the v-winds are centred on the equator and the u-winds to have maxima to either side of the equator. For both the waves, the properties of the modelled waves are found to agree very well with those predicted by linear theory which allows them to be identified as Kelvin and Rossby-gravity to a high degree of certainty.

5.6.2 Experiments With the Waves

Several sets of experiments are performed with the Kelvin and Rossby-gravity waves.

Wave amplitudes The amplitude of the wave forcing is varied over a large range of values (from very small amplitude to several times that observed in the stratosphere) and the amplitude of the resulting waves is observed in the output model fields. It is found that the wave amplitudes in the model fields scale very linearly with the

forcing amplitudes.

Propagation through a background flow A background jet is established in the model (with either an easterly or westerly wind direction) and both Kelvin and Rossby-gravity waves are forced into this jet. A very dramatic difference is seen in the propagation of the waves as they encounter the jets. The Kelvin waves propagate very easily through an easterly jet but are strongly dissipated in a westerly jet. The Rossby-gravity waves are affected in the opposite sense (as would be expected), propagating very easily through the westerly jet and being strongly dissipated as they pass through an easterly jet.

Several other properties of the waves are shown in this section. In the Rossby-gravity wave runs, particularly striking is the effect of the background wind on the vertical wavelength. This is illustrated in figure 5.16 where the vertical wavelength is seen to be large as the Rossby-gravity wave passes through the westerly jet, and much smaller as it passes through the easterly jet. This is significant because the accuracy of the model simulation of the Rossby-gravity wave is better when the vertical wavelength of the Rossby-gravity wave is large (compared to the vertical resolution of the model). If there are problems in the simulation of Rossby-gravity waves, they might be expected to be more evident when the background flow is easterly.

Varying the Newtonian cooling The Newtonian cooling time-scales are varied in a series of experiments and the effects on the propagating of the waves observed. It is found in this section that the Newtonian cooling coefficient very strongly affects the propagation of the waves. When the Newtonian cooling is weak, the waves propagate easily and reach the model *sponge layer* where the Rayleigh friction is turned on. With stronger Newtonian cooling, the waves are dissipated low in the model domain.

It is interesting to observe the difference between the Rossby-gravity and Kelvin waves in these runs. The jets produced in both the runs with the Kelvin waves are

similar in shape but at different altitudes. The easterly jet formed as the Rossby-gravity wave jet is dissipated is however quite different in the two runs. In the increased Newtonian cooling run, a smooth jet is produced at around 30 km. In the reduced case, a much narrower, sharper jet is produced. This is due to the Rossby-gravity waves reaching a sharp shear, where their wavelengths very quickly become shorter and the mean flow is driven over a very shallow region. Numerical inaccuracies, described in appendix A, will contribute to this very shallow region of forcing as the vertical group velocity of the waves will be further reduced, more than the dynamics would predict, on encountering such a shear zone in the model.

The model's zonal mean response to the wave forcing in all the cases described has been the generation of a jet on the equator. This is potentially in disagreement with results presented in Andrews and McIntyre [1976*a*], which predict that under certain circumstances, specifically when the waves are dissipated soley by the action of radiation, the wave-induced accelerations will be to either side of the equator, with no acceleration on the equator. There are several reasons why this apparent discrepancy occurs. Only a small amount of mechanical damping relative to the radiative damping is necessary to centre the accelerations on the equator. Also Andrews and McIntyre [1976*a*] used an idealised model of the atmosphere, specifically with carefully controlled shears in the wind field. The wind structure seen in the SMM is somewhat outside the conditions asserted in the paper.

5.6.3 Importance of Model Vertical Resolution

Finally, in this chapter, the effects of varying the model vertical resolution were discussed. As already established, the model is unable to model Rossby-gravity waves with a vertical interval of 2 km. Reasonable looking Rossby-gravity waves are seen in the model with a vertical resolution of 1 km. The sensitivity of the forced Rossby-gravity waves to a further increase in vertical resolution (to 500m) was investigated.

It was found that, although there are small differences visible in the fields produced, the modelled waves and the induced mean flow are very similar between the two runs.

This is taken to indicate that the 1 km resolution is adequate to model the Rossby-gravity waves.

Chapter 6

The QBO in the Model

Rossby-gravity and Kelvin waves are being successfully generated and dissipated in the model, which should, according to Holton and Lindzen [1972], be adequate to force a QBO-like oscillation. In the light of more recent developments in QBO modelling (eg. Takahashi and Holton [1991]), it is anticipated that the model will require wave amplitudes that are larger than observed for the Rossby-gravity and (to a lesser extent) Kelvin waves in order to generate the required QBO oscillation. The production of an idealised Holton-Lindzen QBO, however, will be a good test of the model and is a necessary initial step towards modelling a realistic QBO. In section 6.2.1, the model is run in a more realistic configuration, with initial conditions and bottom boundaries derived from the CIRA climate dataset. Further, more sophisticated model runs are described in chapter 7, where the `MIDRAD` radiation scheme is reintroduced into the model, and the interaction between the QBO and extra-tropical disturbances is investigated.

6.1 A Three-Dimensional Holton-Lindzen Model

The simplest model circumstances in which a QBO[1] is forced are where the model is run with the 100 hPa bottom boundary set to a constant geopotential height of 16 km with additional wave perturbations, as supplied by the `GEOPER`, superimposed on this

[1]The term 'QBO' is used often in this chapter to refer to the oscillation generated in the model as a result of the wave forcing. This oscillation is not in fact of a 2-year (or near 2-year) period.

flat pressure surface. In these experiments, radiation effects are handled through the Newtonian cooling scheme (described in section 4.2.2) with the reference temperature profile set at an isothermal 240 K throughout the model domain. The initial conditions for this run are T=240 K and u, v=0 ms^{-1}.

The model is run with these initial conditions and no additional wave forcing (all amplitudes in GEOPER set to zero) for several months. The model fields after this time show no significant deviations from the initial conditions. Any deviations from this stationary state in later runs are due to the additional wave forcing added to the bottom boundary level.

With the model in this isothermal configuration, a long model run is performed with forced wave properties as described below:

Property	Kelvin Waves	Rossby-Gravity Waves
Amplitude	50m	20m
Zonal Wave Number	1	4
Period	14 days	4 days

Some plots from these model runs are shown in figures 6.1 and 6.2. Figure 6.1 shows a time–height plot of the $\overline{u}$-winds of a 66 month run with this forcing. Figure 6.2 shows the latitudinal structure of the oscillation (upper plot) with a latitude-time plot of $\overline{u}$ and the time evolution of the $\overline{u}$-wind (lower plot), averaged between 10° north and south. Both of the panels are at 37 km in altitude. Alternating regions of easterly and westerly winds are evident and a clear oscillation is produced.

Several aspects of this modelled QBO agree very well with properties of the observed QBO. The gross structure of descending alternating easterly and westerly wind zones is very like the observed QBO (compare figure 6.1 to figure 3.1). The shear associated with the descending westerly zone is sharper than that associated with the easterly zone, as observed. The modelled oscillation is equatorially confined as with the real phenomenon.

Other properties such as the period and vertical extent of the modelled 'QBO' however are quite different to the real QBO. The period of the modelled oscillation is around 15 months. The period will be affected by a range of factors. In almost all of the experiments

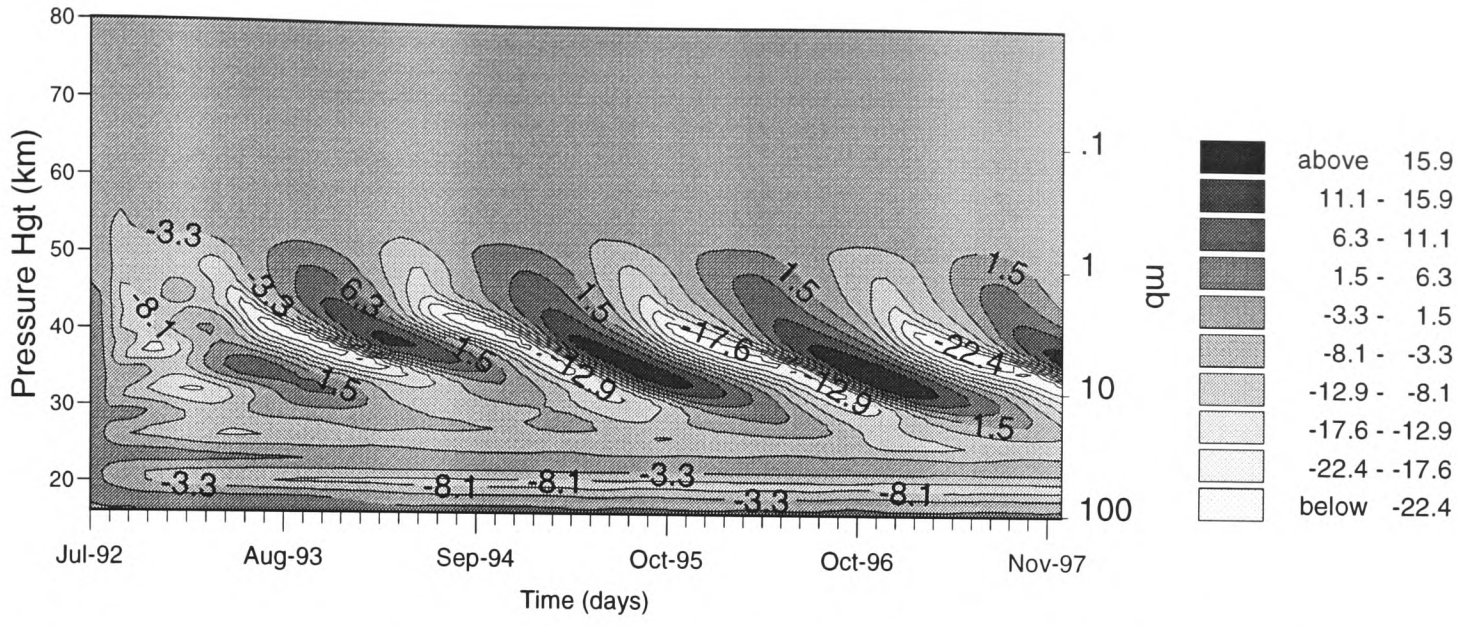

Figure 6.1: A QBO-like oscillation in zonal-mean u-wind forced in a model run. The model has Newtonian cooling relaxing towards an isothermal temperature profile. The bottom boundary of the geopotential height of the 100 hPa level is a uniform 16 km with the wave disturbances forced on top of this. The dates on the x-axis of this plot, and many others in this chapter, are labelled in time. These dates are nominal as there is no time dependent observational data going into the model.

performed in this project, the period of the oscillation generated is found to be significantly shorter than the observed QBO. The period of this generated oscillation appears fairly insensitive to wave parameters[2] and far more sensitive to the dissipation of the waves and especially the background model state (a large variation in forced oscillation period with changes in the reference profile is shown in section 6.3). It may be that the main reason for the shorter QBO period in so many of the runs is that the model is not generating realistic levels of ascent in the tropics. This is a known problem in the model [Lawrence, 1997] and appears to be quite sensitive to the height of the model lid. In observations, this up-welling is typically the same order of magnitude as the speed at which the QBO shear zones descend, and will act to inhibit the descent of the QBO jets [Kinnersley and Pawson, 1996], [McIntyre, 1994]. The period of the forced model oscillation is seen in section 6.2.1 to be strongly dependent on this residual circulation.

It is perhaps not surprising that the altitude of the oscillation produced in this run is unrealistic. The model is being run in an isothermal configuration which results in a model background state that is very different from the real world. In the real atmosphere,

[2]This appears to be true when an oscillation is being generated. Large changes in wave forcing can in fact result in non-oscillatory behaviour. This is observed in section 7.1.1

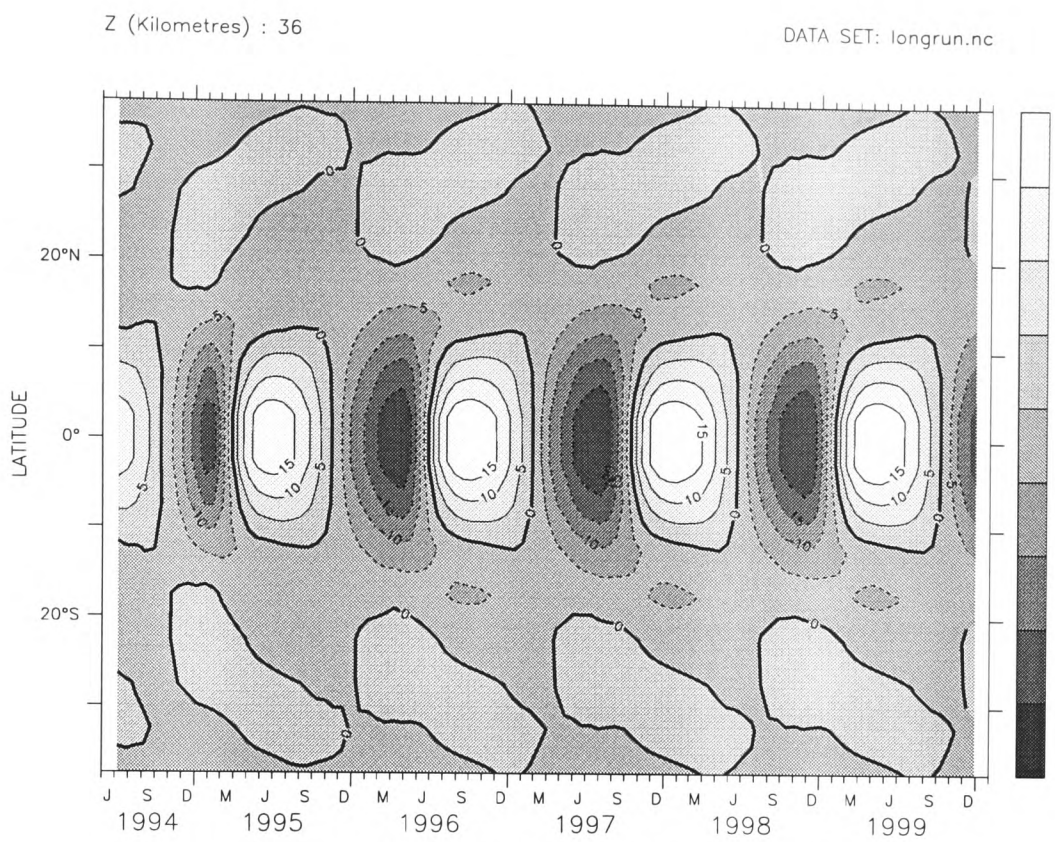

Figure 6.2: The $\overline{u}$-wind in ms^{-1} for the isothermal reference temperature run. The upper panel shows the meridional structure of the $\overline{u}$-wind. The lower panel shows the time evolution of the $\overline{u}$-wind averaged between 10° north and south. Both plots are at 37 km altitude.

the temperature profile varies quite strongly with height, and there is significant structure in the zonal winds. These are not present in this model run. In runs with more realistic vertical profiles of temperature and background winds, the oscillation occurs at a lower level, in very good agreement with observations.

The model QBO is very regular, a feature of all the QBOs forced in this project. The irregularity of the observed QBO is one of its most striking properties and the failure of the model to capture this is one aspect in which the simulation of the QBO fails. The phase propagation of the QBO in nature is influenced by many factors such as variations in the forcing waves, (in turn possibly influenced by sea surface temperatures [Geller, Shen, Zhang and Tan, 1997]), and the annual cycle. These factors are absent in the model runs performed in the project. In addition, it appears that the QBO does not interact non-linearly with itself adequately to create much variability from cycle to cycle. It is possible that the variability in the observed QBO may be recreated if the wave forcing was modulated with time and the annual cycle was included. These experiments were not performed in this project but would be interesting future experiments.

Along with the large oscillation in the model zonal winds, there are associated temperature, vertical wind and meridional wind disturbances. These are described qualitatively in section 3.2.1 and shown in figure 3.4. In the real atmosphere these are difficult to observe in the wind and temperature fields but their effects are evident in the advection of chemical species and tracers. This circulation will be evident as small perturbations in the appropriate model fields but these are largely obscured in the model fields as there are large variations in the T, u and v fields in the region of the QBO as a result of the waves that are forced in the tropics. The circulation can be seen in the residual circulation as the waves and other eddy quantities are filtered. These changes in meridional and vertical circulation are visible in figure 6.3. This plot shows contours of $\overline{v}^*$ (lower panel) and $\overline{w}^*$ (upper panel) plotted over the background zonal mean wind. The region of induced descent is clearly visible below the westerly jet in the $\overline{w}^*$ panel. The lower panel shows the meridional parts of this induced transport.

The disturbance is equatorially confined as would be expected. It is thought that the

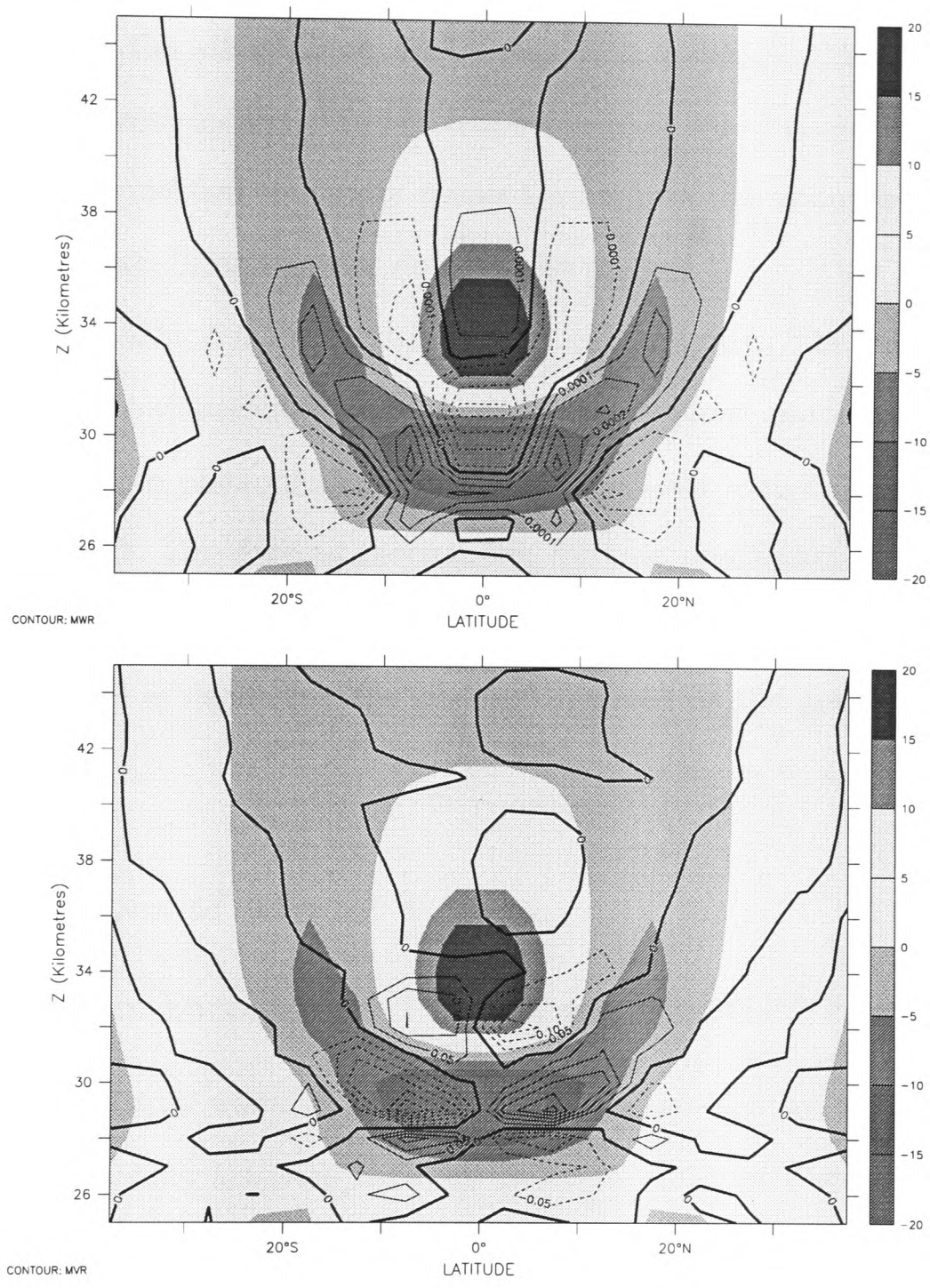

Figure 6.3: Contours of the induced vertical (upper panel) and meridional (lower panel) residual circulations in the model when a westerly jet is over an easterly jet. The $\overline{u}$ winds are shown in the background shading. The contours, and the key to the shading have units of ms^{-1}. A region of descent (negative $\overline{w}^*$) is visible under the descending westerly jet, with a meridional circulation consistent with the induced circulation visible in the $\overline{v}^*$-wind plot.

confinement of the QBO to the tropics is not, in fact, solely a result of the localisation of the forcing, but also due to the differing response of the atmosphere to a zonal forcing at different latitudes [Haynes, 1996]. In the tropics, the response to a forcing is a zonal acceleration whereas in the extra-tropics, the response to the zonal torque is to supply angular momentum to the atmosphere, which results in a meridional acceleration. In this project, the forcing is also localised to the tropics so that we cannot test this hypothesis. (The model could be modified to supply waves throughout the latitude range in order to test whether this is true. This was not done in the project.)

This modelled oscillation is on the whole very encouraging. The model is very much stripped down from the distributed code, and the atmosphere modelled is very different from that on earth. The phenomenon modelled still shows many similarities to the observed terrestrial QBO. The forcing mechanism for this oscillation is greatly simplified from what must occur in nature but is still producing a realistic oscillation. It would appear that the model is capturing the physics involved in the generation of the QBO quite well.

6.1.1 Amplitudes of Model Waves

Comparison Between Forced Model Waves and Observed Waves

The properties of equatorial waves in the middle atmosphere are not very well known from observations. There is only a sparse network of direct observations (i.e. radiosondes) in the tropics and satellite radiances and temperatures are difficult to relate to wind values where the Coriolis parameter is small. As a result of this, there are very great uncertainties in the real values of wave amplitudes (and indeed wavelengths, wavenumbers and periods) in the equatorial middle atmosphere.

A well-accepted reference for wave parameters in the lower stratosphere is Andrews et al. [1987] where the equatorial wave properties are presented in a table (edited) as follows:

Property	Kelvin Wave	Rossby-gravity Wave
Period (from ground)	15 days	4–5 days
Zonal wavenumber	1–2	4–5
Vertical wavelength	6–10km	4–8km
Average phase speed	+25 ms^{-1}	-23 ms^{-1}
Approx. observed amplitudes		
u'	8 ms^{-1}	2–3 ms^{-1}
v'	0	2–3 ms^{-1}
T'	2–3 K	1 K
Approx. inferred Amplitudes		
Φ'/g	30m	4m
w'	1.5×10^{-3} ms^{-1}	1.5×10^{-3} ms^{-1}

As mentioned above, there is considerable uncertainty in the amplitudes of the waves propagating in the lower stratosphere. In particular, there is uncertainty about the uniformity of the waves. The wave parameters in the table above appear to be a good description of the average wave properties. Other studies, for example Randel [1992], suggest that the wave properties vary quite strongly with longitude, and Wilke, Madden and Chen [1997] suggest that the waves may consist of several quite distinct modes, the properties of which, when averaged, give values in line with those presented in the table above. For the purposes of this discussion, in the absence of more conclusive data, the wave properties given in Andrews et al. [1987] will be taken as the observations. It should be remembered though that these figures are subject to a large uncertainty.

It is not useful to compare the wave amplitudes of runs by the amplitude of the geopotential forcing as changes to the vertical advection through the model lower boundary[3] strongly affect the relation between forcing amplitude and the amplitude of the propagating waves. A better measure is to observe the wave properties at one of the levels near the bottom of the model. In this section, the wind perturbations on the 18 km (nominal height, in fact 76.4 hPa) level will be compared to observational data. Figure 6.4 shows

[3]Described in section 4.3

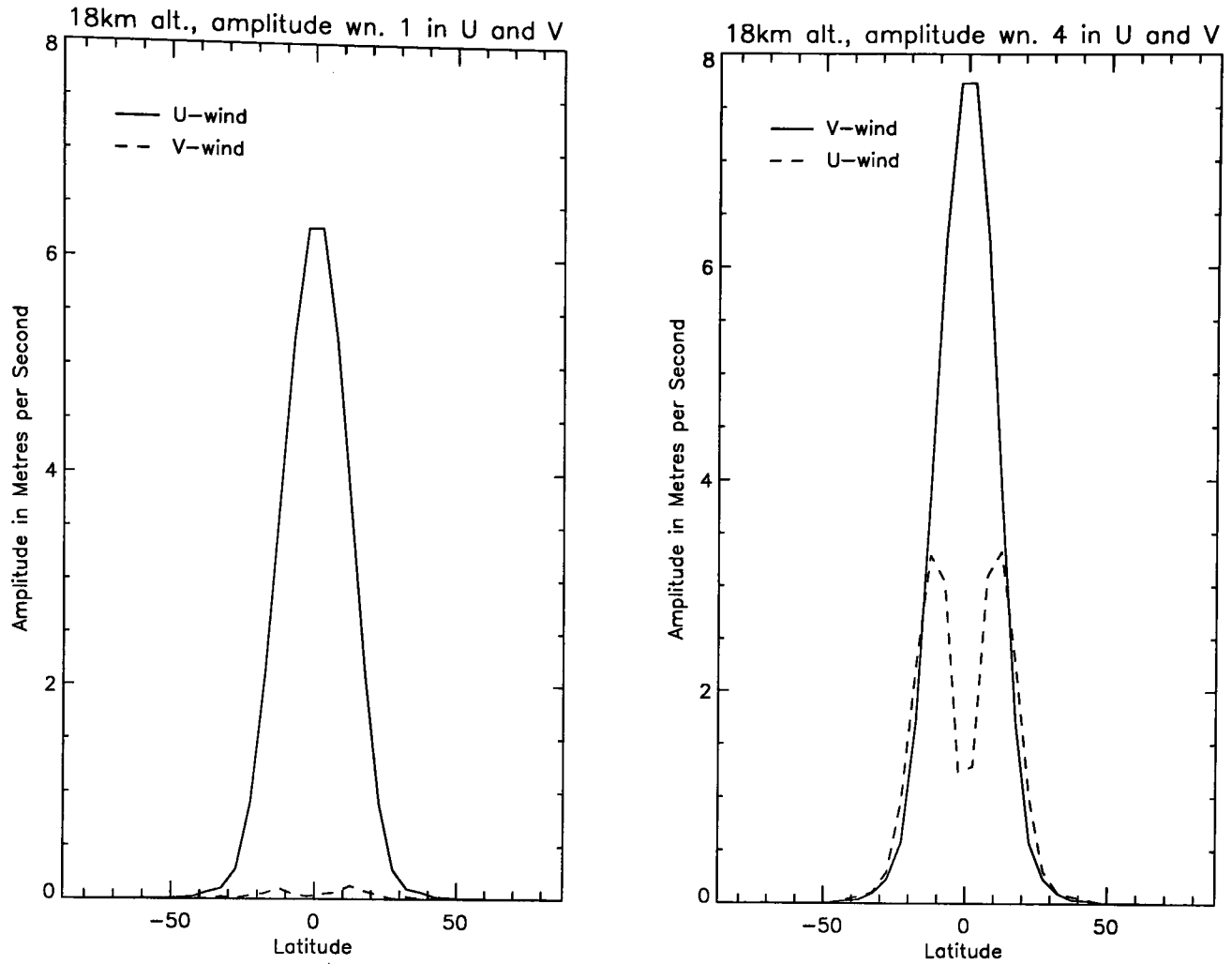

Figure 6.4: Wave amplitudes (ms^{-1}) at 18 km altitude for the Holton-Lindzen QBO. The left panel shows amplitudes of wavenumber 1 in the u and v-winds (ie. Components associated with the Kelvin Wave). The right panel shows the amplitude of wavenumber 4 in the wind fields. These wind components are associated with the Rossby-gravity wave.

a latitudinal profile of the amplitude of Kelvin and Rossby-gravity waves in the u and v winds. The waves can be separated into Kelvin and Rossby-gravity waves by looking at wavenumber 1 and wavenumber 4 disturbances respectively. Both the plots are obtained by averaging the wave properties over 300 days towards the end of this run. Amplitudes are shown in units of ms^{-1}.

This figure shows that the amplitude of the Kelvin wave is very much in accordance with observations. It is certainly well within the error on the 'observations'. The temperature perturbation (not shown) is just under 3 K for the Kelvin waves in the same run, again in line with observations. The Rossby-gravity wave, however, is being forced at approximately double the observed amplitude. Previous studies, for example Takahashi [1996], found that more than observed amplitudes of Rossby-gravity waves were found to be necessary for an oscillation to be forced. It is not obvious from the available ob-

servational data whether the amplitude of Rossby-gravity waves forced in the model is in fact outside the error bars on the observed waves. It is likely that the amplitude of Rossby-gravity waves in the atmosphere is in fact smaller than the amplitude forced here. It certainly appears in later modelling (chapter 7) that the oscillation is absent if the amplitude of (especially) Rossby-gravity waves is too small. This might suggest that a lack of easterly momentum might be important in explaining the lack of a QBO in many general circulation models.

Model Response to Differing forcing Amplitude

When the model is forced with equatorial waves, it does not always respond with an oscillation as described above. In some cases, the model responds by producing layers of easterly and westerly winds which do not propagate downwards with time but instead remain fairly constant. This behaviour has been observed in simpler models of the QBO, for example in a two-dimensional model where momentum fluxes are specified explicitly at the lower level [Gray, 1998]. The model is run with a variety of wave-forcing amplitudes; the response to differing amplitudes of forcing is partially explored in section 7.1. A more complete exploration of this parameter space is prevented by the computer time and the disk space needed to perform many runs of the length required to characterise the model response to the forcing.

6.2 A More Realistic Model

The model is refined from the quasi-isothermal model used in the previous section by adding a background reference temperature profile and geopotential bottom boundary derived from climatological data. The model is still run without an annual cycle, now run in perpetual January mode, and waves are forced in a similar way as before. Several interesting results come out of this modelling, and it is shown eventually that the Newtonian cooling scheme is unsuitable for the runs that will be performed later in the project.[4]

[4]It is not clear what comprises an optimum background temperature profile and changes in this temperature profile create large differences in the modelled QBO.

6.2.1 A Realistic Temperature Profile

In section 6.1 the Newtonian cooling was continuously driving the model towards an isothermal state. The temperatures in the model never strayed more than a few Kelvin from this isothermal reference profile. A more realistic simulation of the earth's atmosphere would include a realistic temperature profile and the corresponding background lower bottom boundary field and initial values of T, u and v.[5] It was decided to take the data from the CIRA climatology. It was decided to use a constant temperature profile corresponding to January from the CIRA dataset. A constant temperature reference profile avoids having an annual cycle in the model which would, at this stage in the project, add noise to the QBO signal that is to be studied. In addition, January is an interesting month as the interannual variability of the stratosphere, thought to be somewhat influenced by the QBO, is very large in the early spring in the northern hemisphere. In later runs (see section 7.2) some investigation is done on the interaction between the QBO and extra-tropical phenomena.

The Background Temperature Profile

The choice of reference temperature profile to be used is not obvious. In principle, the reference temperature should be the radiative equilibrium temperature of the atmosphere. In order to get a model field of the radiative equilibrium temperature, a model is run with the Rayleigh friction set to zero throughout the domain and `MIDRAD` in perpetual January mode. The removal of the gravity wave parameterisation should allow the model to approach radiative equilibrium. Unfortunately, through the long model run, the temperatures in the model do not in fact approach a steady state condition but continue to cool. After two years of model running, the temperatures near the top of the model domain in the winter pole have dropped to below 80 K. The temperature profile closely resembles that of the thermal equilibrium atmosphere (as compared to figure 2.34 in Andrews et al. [1987]) after approximately 80 model days of integration. This temperature profile is

[5] These are based on the same data as the reference temperature, but in order to prevent any radical adjustment at the beginning of the model run, balanced initial and bottom boundary fields are obtained by running the model for several model weeks with constant boundary data. These fields do not vary greatly from the original T, u and v, but prevent any rapid adjustment at the beginning of the run.

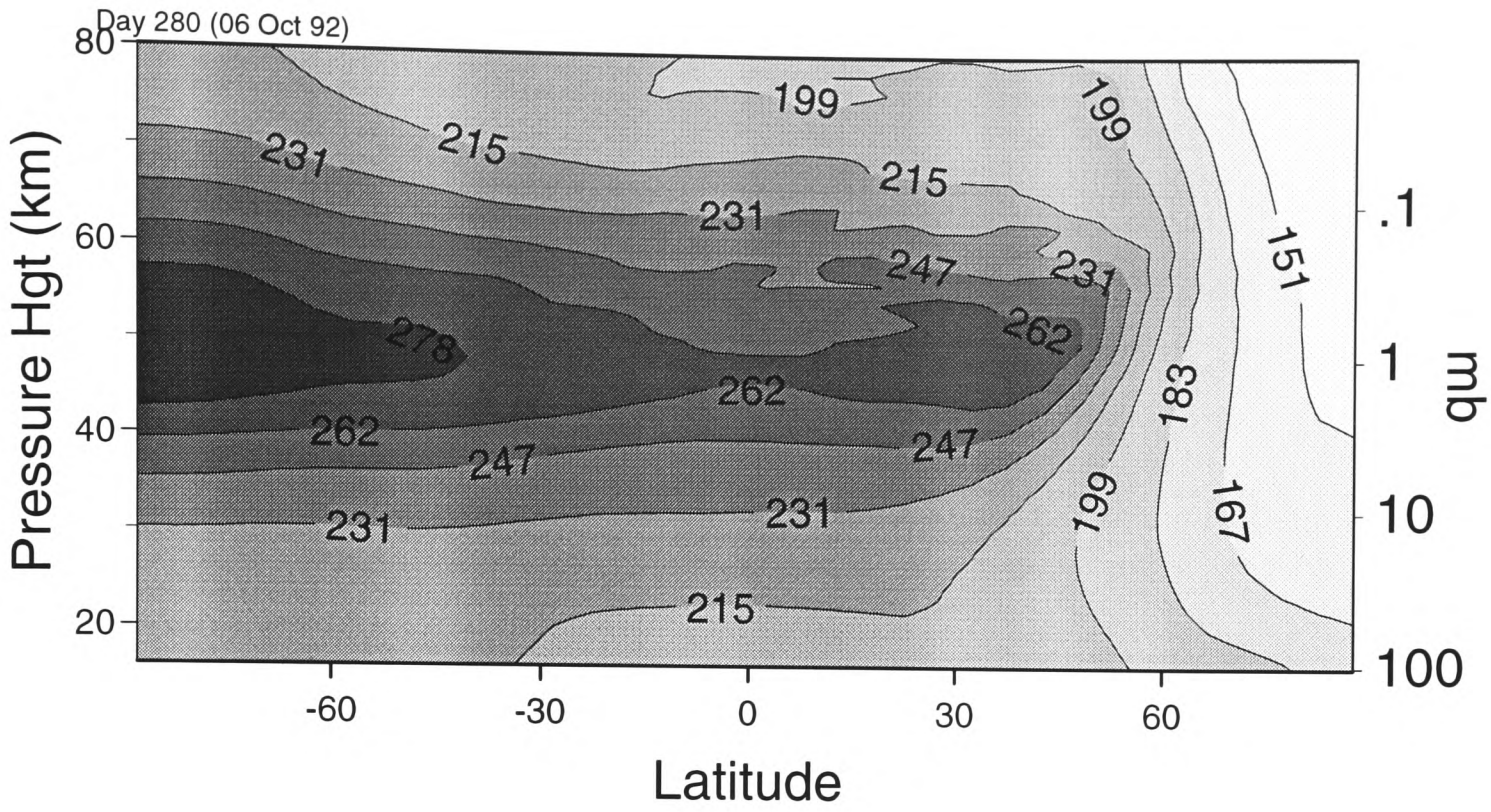

Figure 6.5: Temperature profile 80 days into a run with no Rayleigh friction applied to the model winds. This profile is taken as being close to the radiative equilibrium temperature for the middle atmosphere in January.

shown in figure 6.5. This field is smoothed in order to produce a reference temperature field for the model, which is shown in figure 6.6.

In hindsight, it seems likely that a better way of achieving the temperature equilibrium is to run `MIDRAD` in a normal seasonal cycle with no gravity wave parameterisations in the upper middle atmosphere. The 80 days of model run used to get the reference temperature profile are a similar length of time as the winter pole will be out of sunlight in the winter through to January. In perpetual mode, the northern pole has no radiative heating and continues to cool, certainly for as long as the model was run and probably until the polar jets became too large in magnitude and the CFL criterion was exceeded in the model. As the 'radiative equilibrium' temperature profile is not in fact used for later runs (for reasons described below), the profile was not recalculated with a seasonal cycle added.

Figure 6.7 shows the zonal mean u-wind against height and latitude several months into a run with the derived 'radiative equilibrium' reference temperature profile imposed. Although the waves propagate and generate an oscillation in this run, the structure of the temperature and zonal winds are quite unrealistic. It turns out, as shown in section 6.3, that the cold temperatures over the pole have very little effect on the equatorial wave

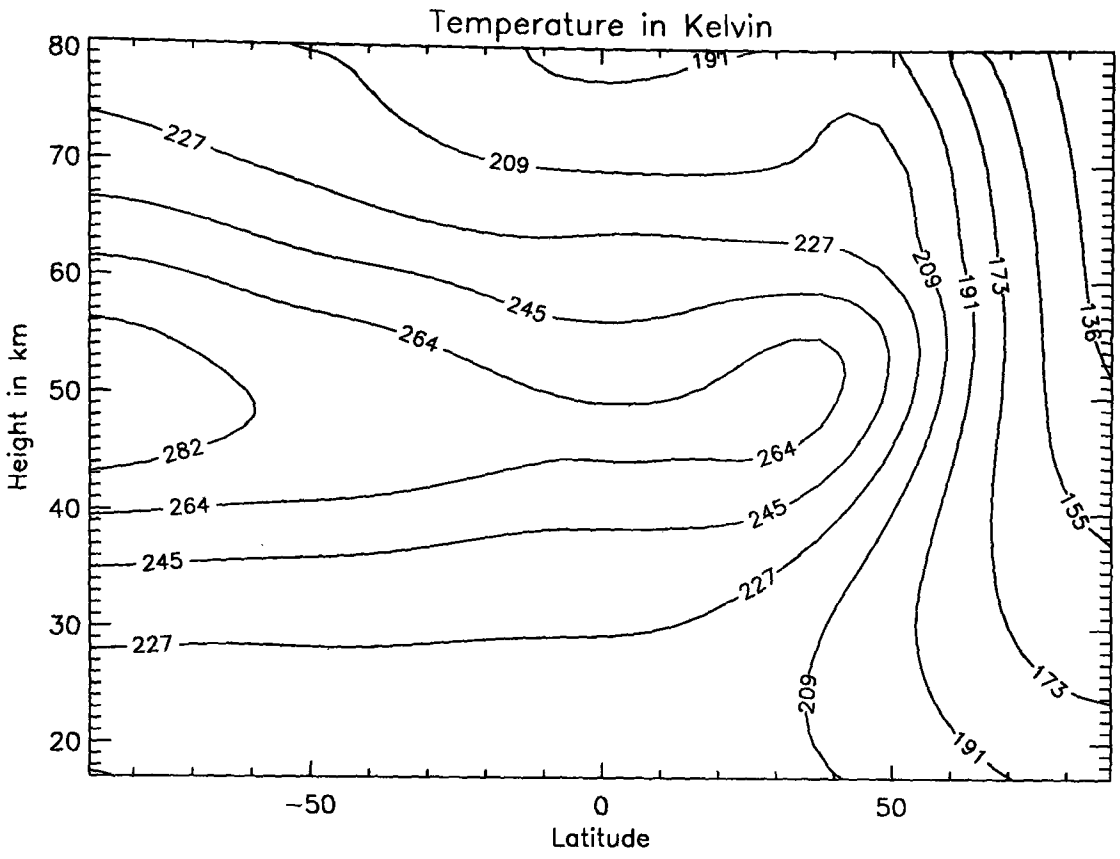

Figure 6.6: The temperature profile used as the 'radiative equilibrium' profile in model runs. This field is obtained by smoothing the field shown in figure 6.5 in both latitude and height.

propagation and resulting QBO-like oscillations. In this section though, the aim is to model the QBO in a more realistic atmospheric state and getting a reasonable winter polar jet is quite important in modelling a realistic January atmospheric state.

An alternative temperature reference profile would appear to be necessary. The options considered are to impose a background temperature that is a model climatology as obtained by running the model with `MIDRAD` in perpetual January, and to merge a radiative equilibrium temperature profile in the lower atmosphere with model climatology in the higher atmosphere where the Newtonian radiative time-scales are very much shorter. It would also be possible to alter the radiative time-scales in the Newtonian cooling subroutine, but as these are the values used in the model before `MIDRAD` was added, they are left unaltered.

A model was run for several hundred days with `MIDRAD` radiation in perpetual January mode and the CIRA bottom boundary with no additional wave forcing. The output temperature fields over the last half of the run were averaged to produce a reference profile. (In perpetual mode as run here, the gravity wave parameterisation (Rayleigh

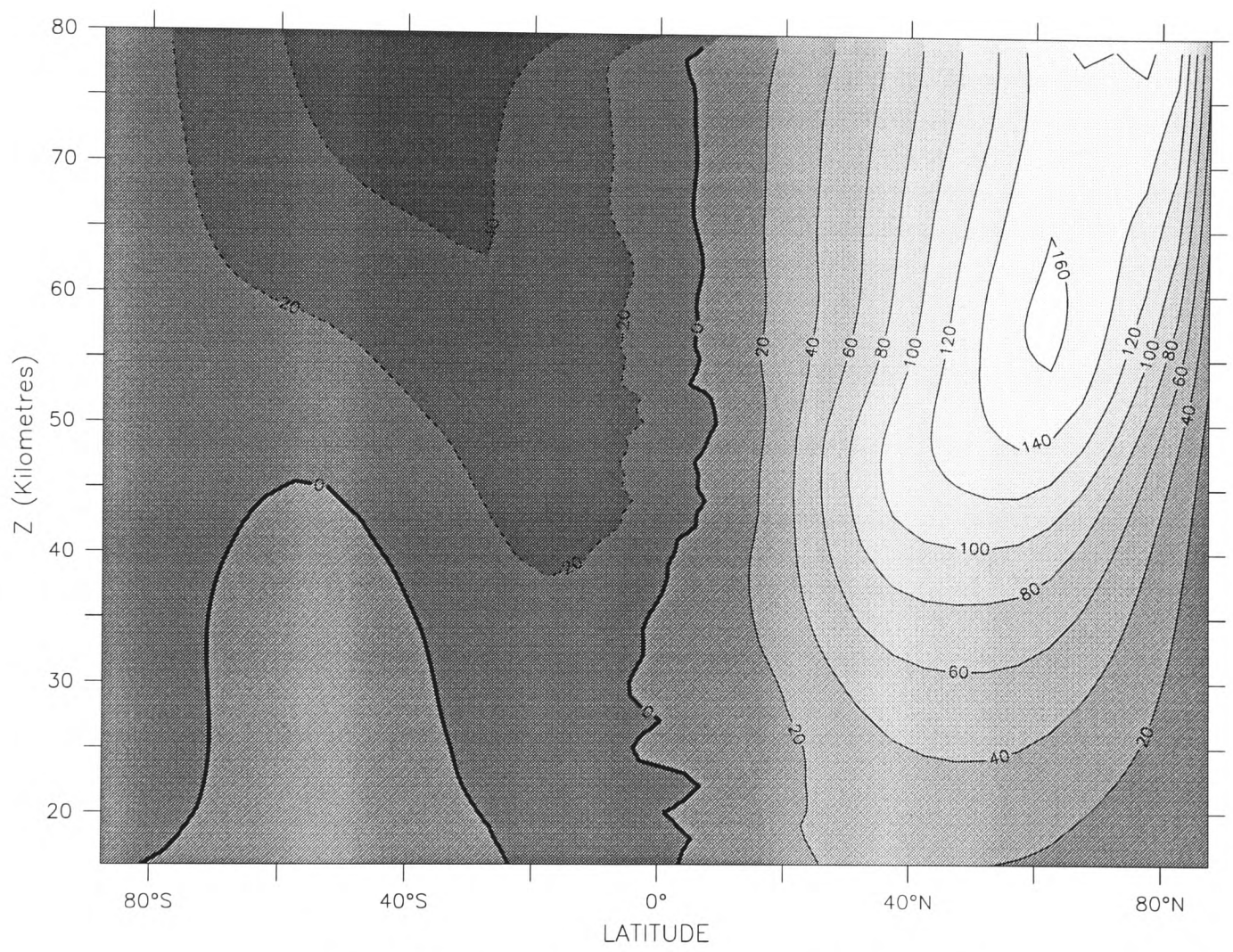

Figure 6.7: The zonal mean u-winds (in ms^{-1}) for the run with the 'radiative equilibrium' temperature reference profile. The jet is very strong and is not closed at the top of the model.

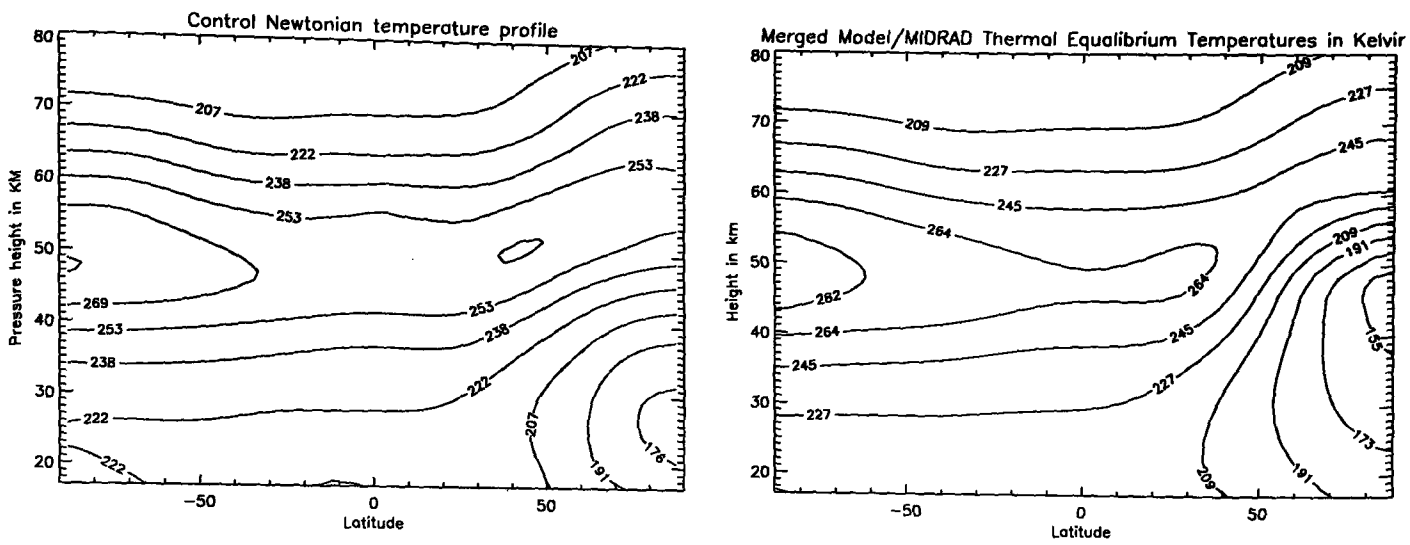

Figure 6.8: The two temperature fields (in Kelvin) used as Newtonian reference profiles for model runs. The left panel shows the 'climatological profile' where the temperature fields from the model in perpetual January are averaged over a month. The right panel shows the 'merged profile' where the temperature is a combination of the 'radiative equilibrium' and 'climatological' fields as described in the text.

friction) prevents the polar jet from growing too large in the upper atmosphere and the temperatures remain realistic throughout the model domain.) This profile is shown in the left-hand plot in figure 6.8. This is a reasonable climatological temperature field. The right-hand plot in figure 6.8 shows the 'merged' temperature field. In the merged field, the `MIDRAD` thermal equilibrium temperature shown in figure 6.6 is used between 16 and 36 km. Above 62 km, the temperatures are taken from the run shown in the left-hand side of figure 6.8. Between 36 and 62 km, the reference temperature is a linear interpolation between the two fields. This produces a rather odd-looking temperature field, but it is described here as some of the results using this temperature field are interesting.

Runs are performed with these reference temperature profiles using a wave forcing of:

Property	Kelvin Waves	Rossby-Gravity Waves
Amplitude	50m	20m
Zonal Wavenumber	1	4
Period	14 days	4 days

as in the Holton-Lindzen model described in section 6.1.

In both these runs, a reasonable January atmosphere is simulated. Figure 6.9 shows the zonal mean u-winds averaged over each run. They both show a strong polar jet in the northern hemisphere as would be expected. The zonal mean structure is quite a

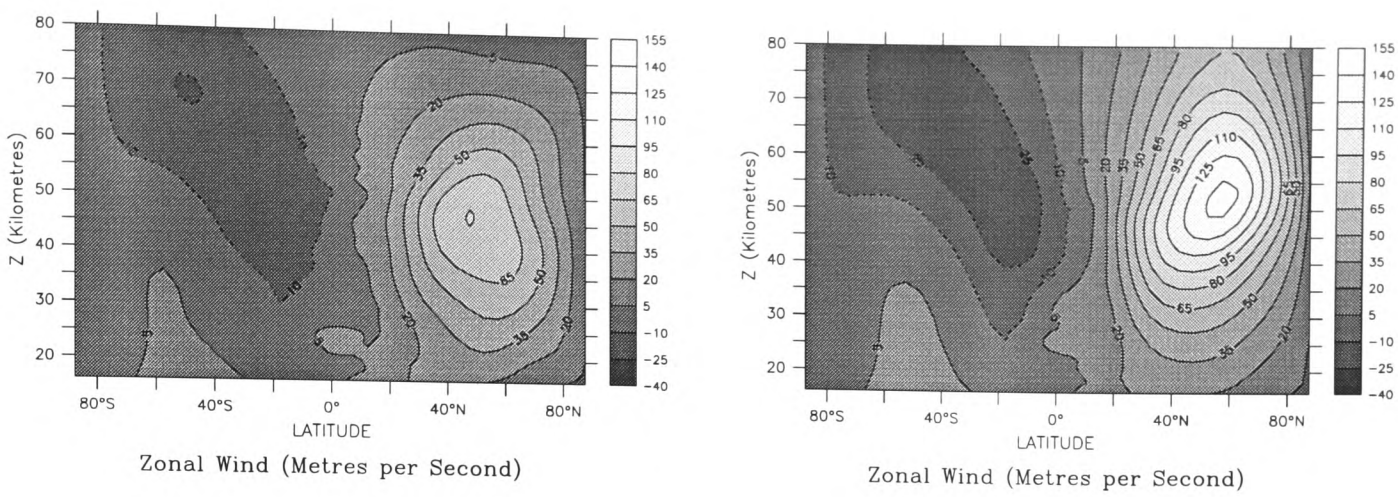

Figure 6.9: The zonal mean u-winds (in ms^{-1}) averaged over the entire run for the climatological (left) and merged (right) runs. Both runs show fairly realistic jet structures except the merged run has a much stronger polar jet, associated with the colder temperatures in the reference profile over the pole.

reasonable approximation to that observed. (This is to be expected as the dynamics are very much influenced by the radiative state of the atmosphere in the middle atmosphere.) The polar jet in the 'merged' run is considerably stronger than that in the 'climatology' run, which is due to the colder polar temperatures in this run.

The time evolution of the equatorial zonal mean u-winds for these two runs are shown in figure 6.10. In both runs, an oscillation is produced and the modelled QBO is in many ways an improvement over the 'isothermal' model described in section 6.1. With the introduction of a more realistic model atmosphere, the oscillation occurs significantly lower in the model domain, with maximum amplitude at around 26 km. This is very similar to the observed QBO which has a maximum at around 24 km. Both oscillations are again equatorially confined and very regular. They both appear to be quite realistic QBO-type oscillations.

There is however a very significant difference in the periods of the two runs. For the 'climatological profile', the period of this oscillation is around 16 months, similar to the isothermal model. In the 'merged' temperature profile case, the period of the oscillation is much larger, around 34 months. The difference in the Newtonian cooling reference profile is having a huge effect on the period of the QBO. In section 6.3, the source of this difference is sought. It is interesting that the period of the modelled oscillation in the two runs spans the range of the period of the real QBO.

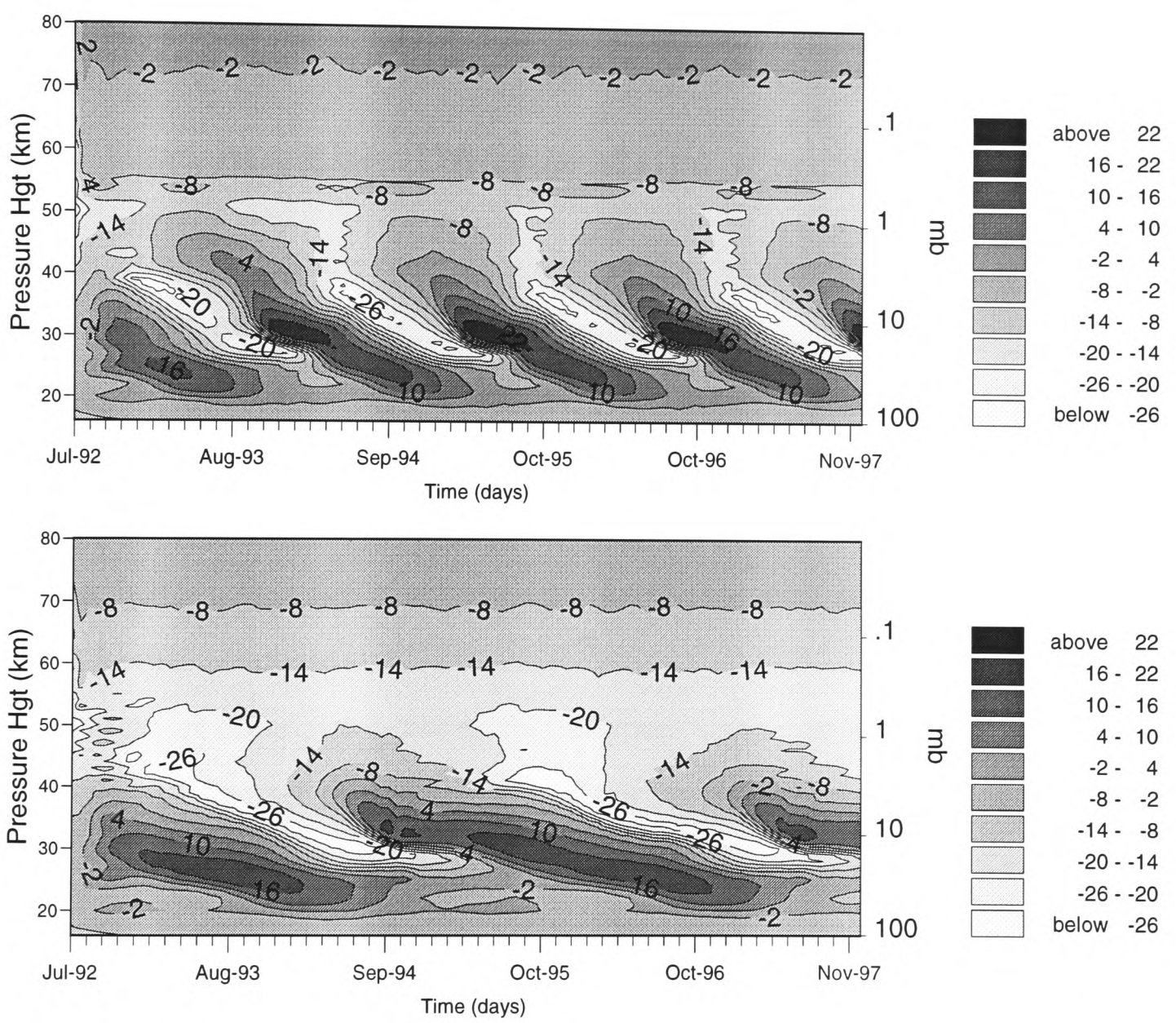

Figure 6.10: Time-height plots showing the evolution of $\overline{u}$ for two runs with identical wave forcing but different Newtonian cooling reference profiles. The upper plot is run with the model climatology temperature field (left panel in figure 6.8). The lower plot is run with the 'merged' temperature field (right-hand plot in figure 6.8). The periods of the two oscillations are markedly different.

In both these runs, the vertical range of the QBO is lower than that seen in section 6.1. This is due to the change in vertical stratification brought about by the imposition of a realistic vertical temperature profile. This increases the buoyancy frequency of the atmosphere and has the effect of reducing the vertical group velocity of the propagating equatorial waves (see equations (2.44) and (2.53)) and causing them to be dissipated lower in the atmosphere.

6.3 Varying the Temperature Profile

It is interesting to examine the dependence of the modelled QBO period on the temperature reference profile. The mechanism responsible for this variation may be important in other models, and indeed the atmosphere, and it is important to discover how the change in the temperature field has affected the QBO. In order to ascertain which aspect of the different reference profiles is responsible for such a radical change in the period of the modelled QBO, a series of model runs are performed with specific modifications applied to the reference temperatures.

The greatest difference between the reference temperature profiles in the runs which give longer and shorter period QBOs is, by a large margin, over the winter pole and at an altitude of ~45 km. This difference is shown in figure 6.11, where the polar difference in temperature dominates the other differences that may occur in the fields. It would not be expected that a temperature anomaly in the polar region should have a great effect on the meridional circulation. The meridional circulation response to a cooling such as this is limited by angular momentum conservation [Haynes, McIntyre and Shepherd, 1991] and cannot adjust *ad hoc* to new radiative conditions.

In order to rule out the polar temperature difference as the cause of the period difference, and to investigate which aspect of the temperature forcing is responsible for it, a series of runs is performed where temperature perturbations are added to the 'climatological' reference profile. The influence of the winter pole temperature is investigated by performing a model run where a temperature anomaly, shown in figure 6.12, is subtracted from the climatological temperature profile to provide a new temperature reference pro-

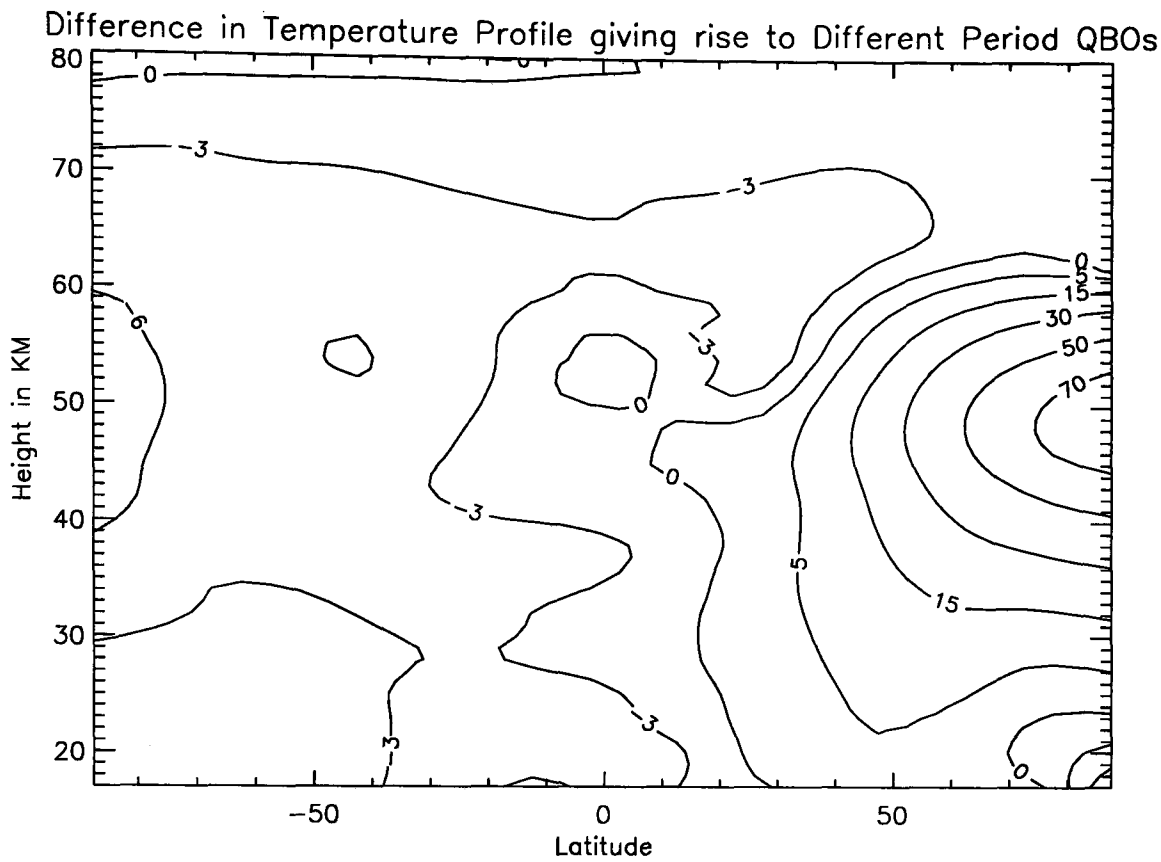

Figure 6.11: The difference between the model climatological reference temperature field and the merged reference temperature field. Contours are in Kelvin. The largest difference is that the merged reference temperature profile is much colder over the winter pole.

file. This creates a temperature reference profile that is the same as the climatological profile apart from the cold pole. The climatological profile is used as the reference profile in the other 'control' run. The two reference profiles used are shown in shown in figure 6.13.

Figure 6.14 shows the equatorial $\overline{u}$ wind against time at 26 km for the control and 'cold pole' runs. It shows that the very large temperature difference over the pole is having almost no effect on the period of the QBO. The residual mean circulation is not greatly changed through the addition of this cold spot. Figure 6.15 shows the residual circulations averaged over each run. There is little difference in the residual circulation between the two runs and consequently, very little change in the QBO period. There is more difference in the residual winds in the polar regions, and some limited change in the circulation above 50 km, where the Rayleigh friction can apply a torque to the winds. Importantly for the QBO simulation, there is little change in the circulation below 40 km in the tropics.

The similarity between the tropical oscillation produced in the two runs, even with

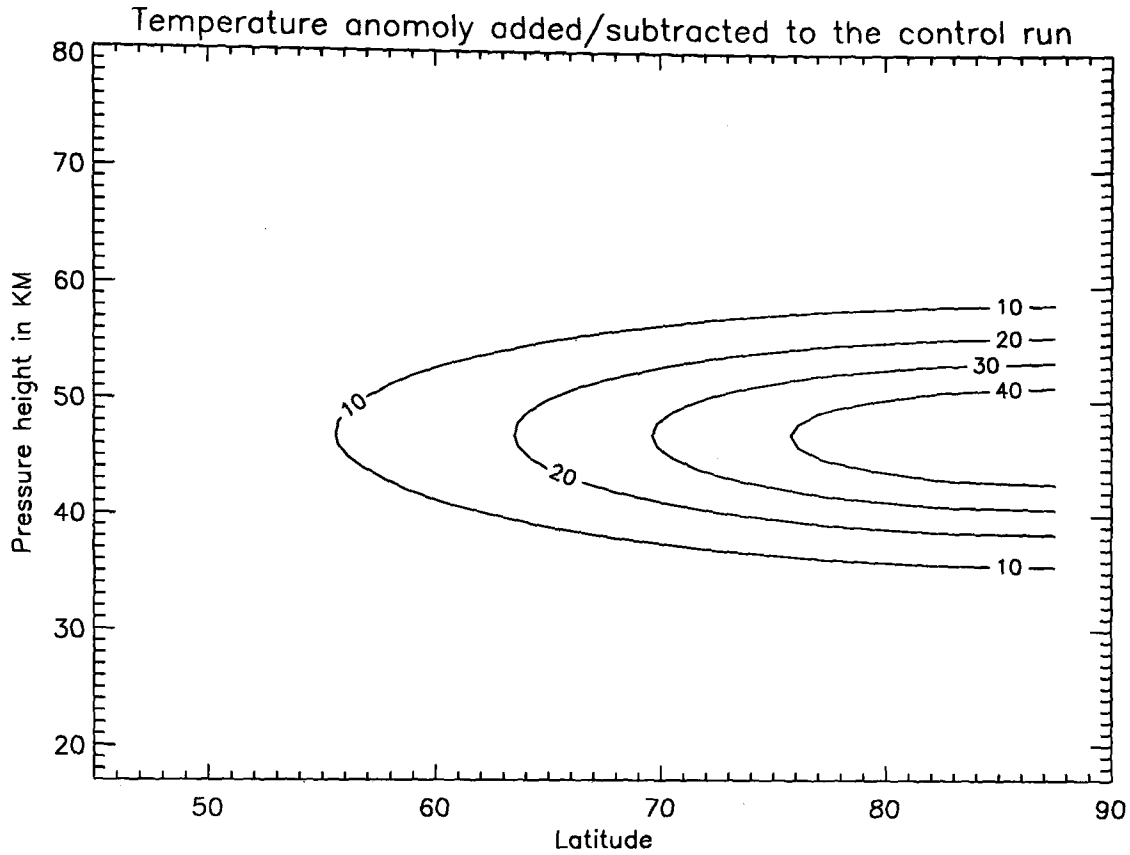

Figure 6.12: The anomaly, in Kelvin, to be subtracted from the control, climatological profile to give the 'cold pole' Newtonian profile.

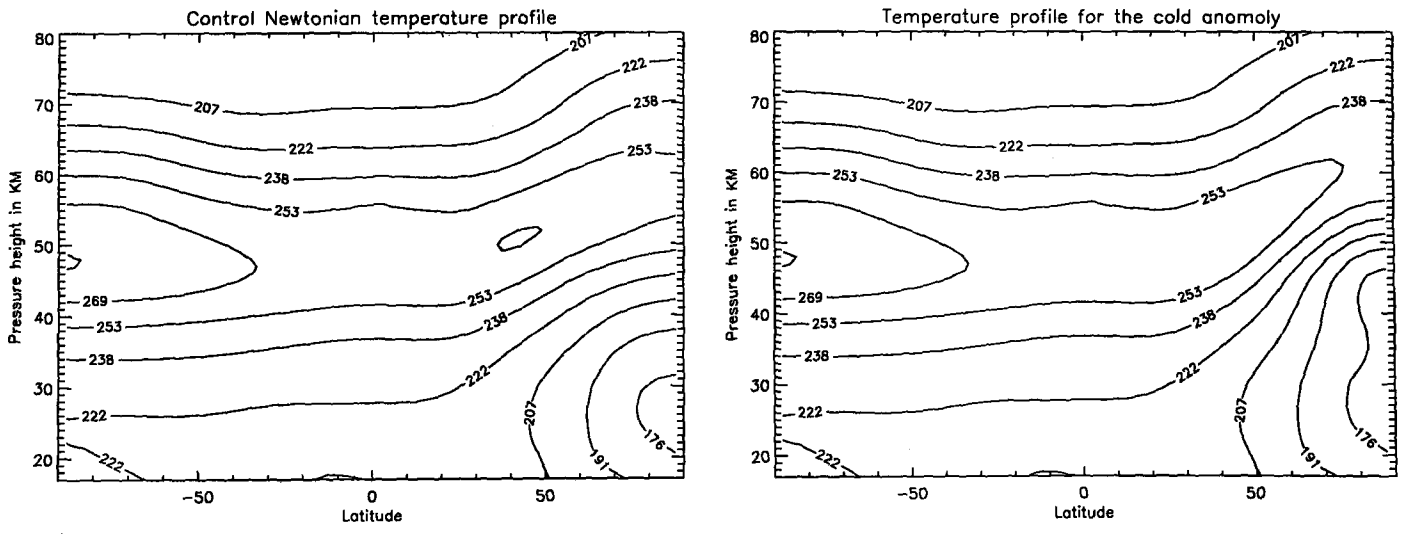

Figure 6.13: The control and cold pole reference temperature profiles, in Kelvin, used to investigate the effect of a cold pole on the period of oscillation of the QBO. The left-hand panel is the climatological reference temperature, used as a control run. The right-hand panel is the 'cold pole' reference temperature profile.

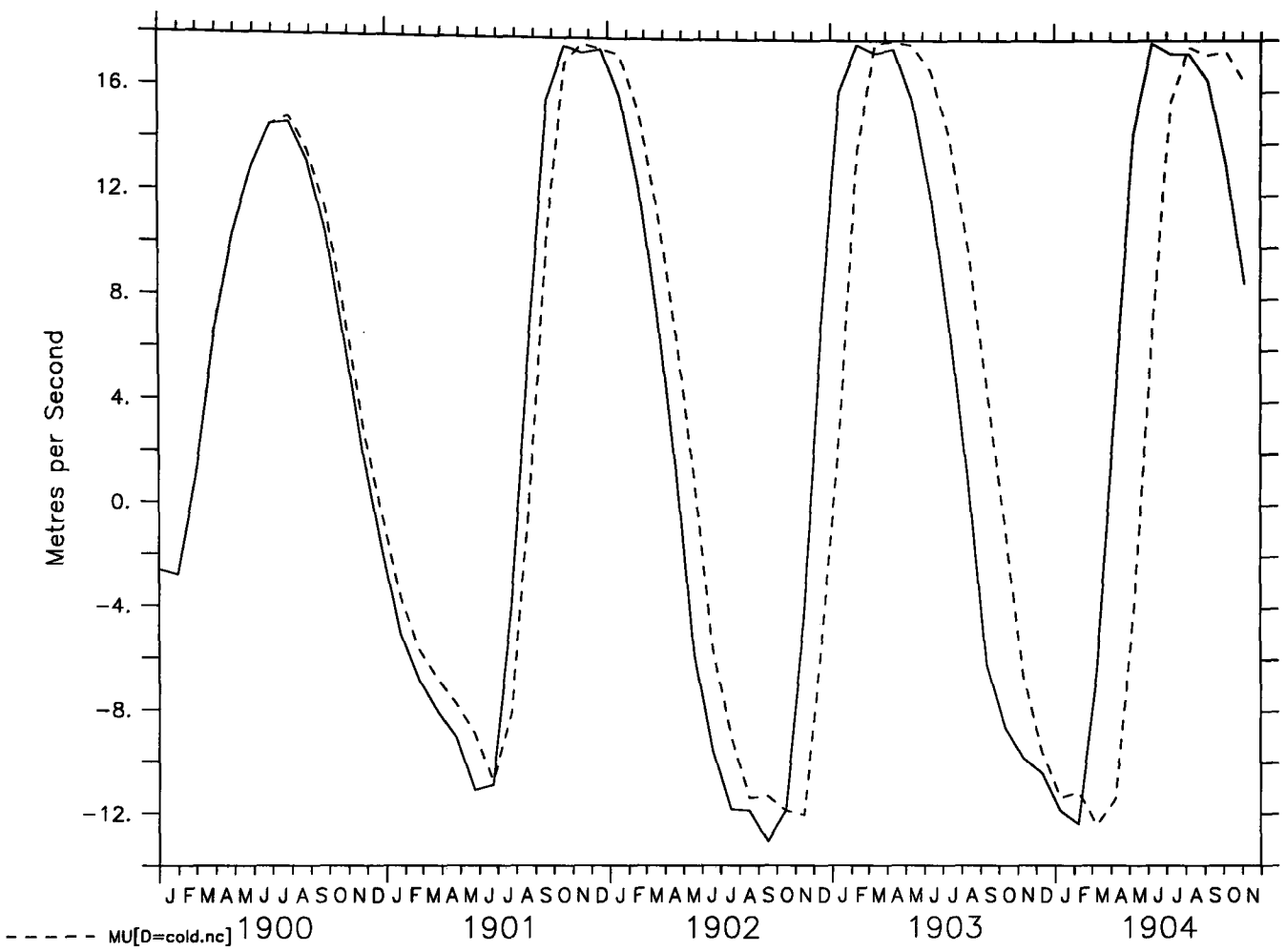

Figure 6.14: The equatorial zonal mean u-wind at 26 km altitude for the control (solid line) and 'cold pole' (dashed line) run with temperature perturbations applied to the winter pole. The periods of these runs are slightly different, but certainly nothing like the difference in periods shown in figure 6.10

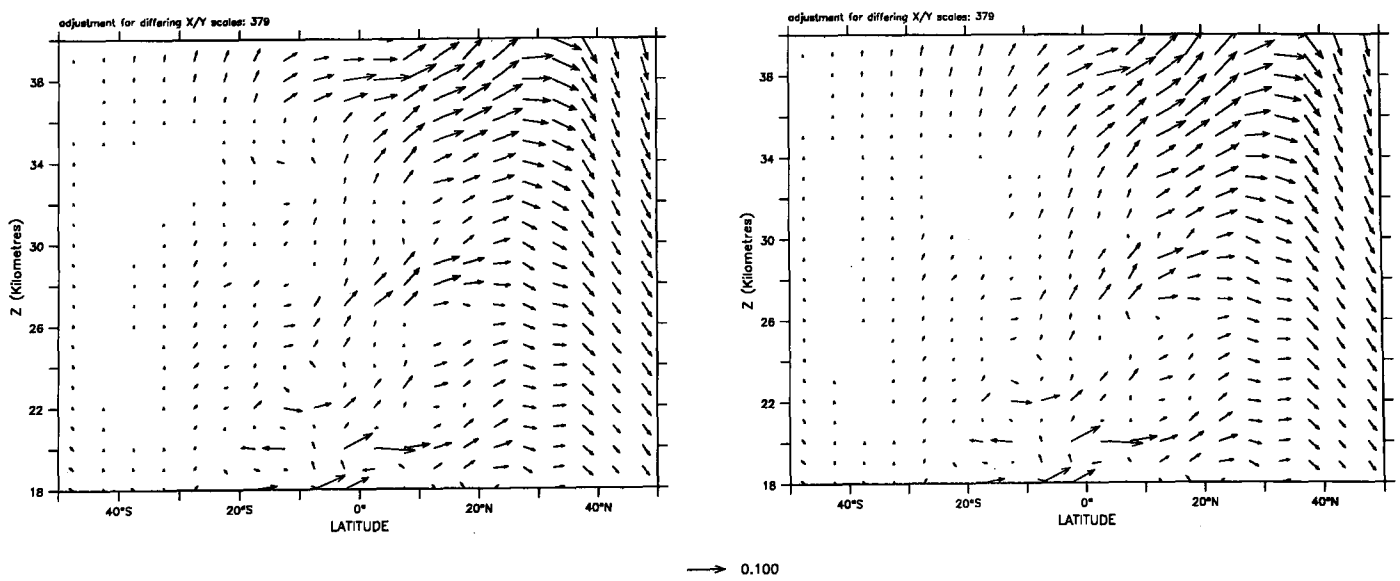

Figure 6.15: The residual mean circulation for the (left) control run and the (right) run with a cold zone added over the winter pole. The sample arrow represents $0.1\,\mathrm{ms}^{-1}$.

this very large temperature difference applied to the polar region implies that the polar temperature difference has little effect on the phase propagation of the QBO. Some other difference between the 'merged' and 'climatological' temperature fields must be responsible for the difference in period between the two runs. Ignoring the difference of several tens of Kelvin present at the pole, a closer look at the smaller differences between the 'climatological' and 'merged' temperature fields yields another important difference in the temperature fields. The summer hemisphere in the 'radiative equilibrium' temperature profile was in constant sunshine in the run described in section 6.2.1 (much as the winter pole was in constant darkness). This results in temperatures warmer than the 'climatological' run over much of the model domain. Figure 6.16 shows that in the merged run, temperatures are warmer throughout a large part of the model domain, everywhere except in the winter hemisphere middle to higher latitudes. This will act to enhance the normal summer hemisphere to winter hemisphere overturning. The differences in the residual mean flows, averaged over each run, are noticeably different.

Figure 6.17 shows the residual circulations in a limited latitude region for the 'control' and 'merged' runs. (This plot is comparable with figure 6.15.) Even by eye, it is evident that the fields are quite different. This difference is clearer in figure 6.18, which shows the residual mean circulation in the 'control' run (left panel in figure 6.17) subtracted from the residual mean circulation in the 'merged' run (right panel). It can be seen that there is generally enhanced summer to winter hemisphere flow in the middle atmosphere, with much enhanced ascent in the tropics. This ascent is better quantified by looking at a contour plot of the difference in residual vertical wind ($\overline{w}^*$) between the two runs. Figure 6.19 shows a latitude-height plot of the difference in the residual mean vertical circulation. It can be seen that the difference in residual velocity consists of increased ascent to the south of the model domain and increased descent in the north, with the changeover from ascent to descent occurring at around 15° north. Looking in the tropical stratosphere, the ascent in the region where the QBO jets are being formed is of order $0.0002\,\mathrm{ms}^{-1}$, or around 15–20 metres per day. This equates to around 500 metres per month. The descending shear zones in the 'control' run are descending at around 1 km per month

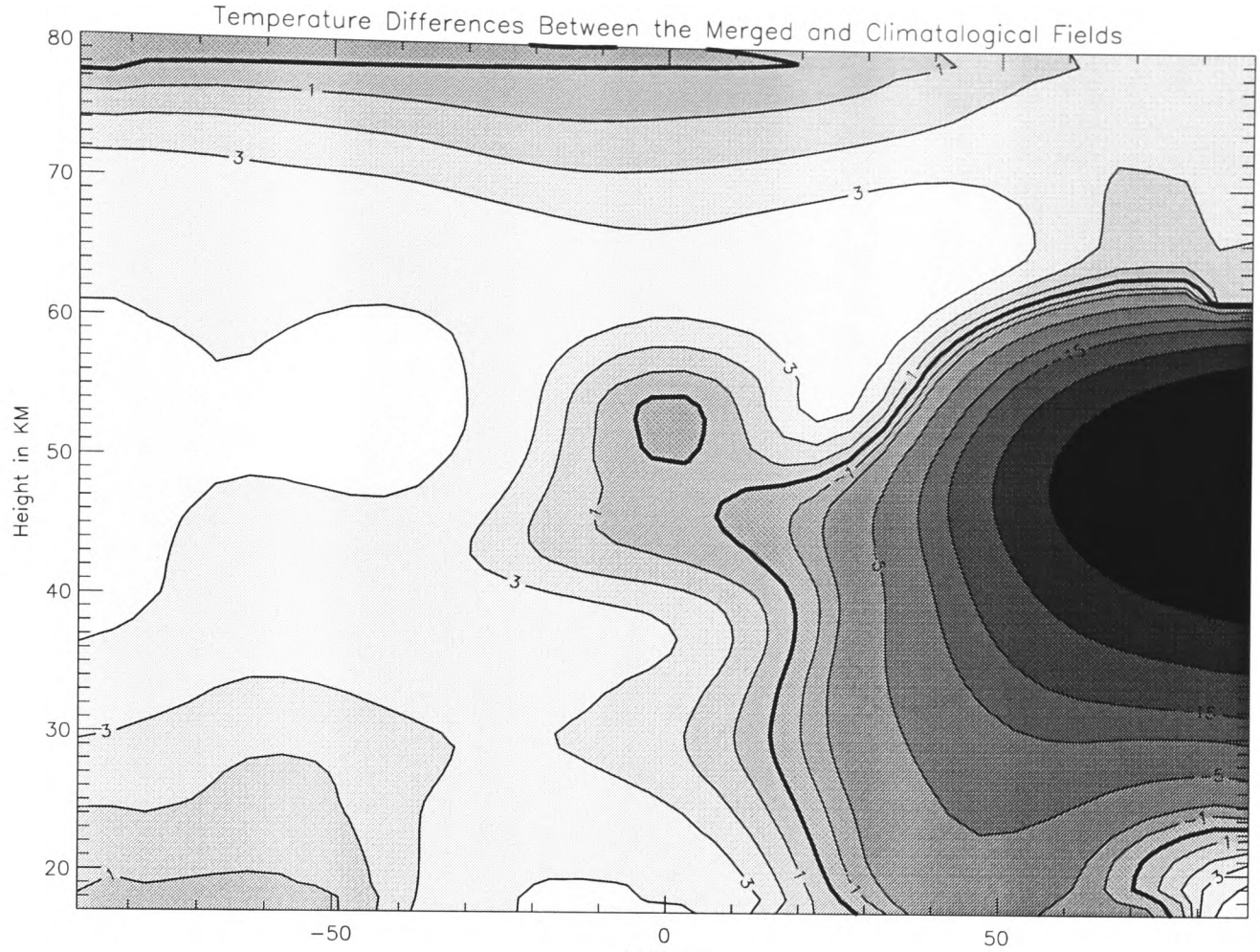

Figure 6.16: A smoothed field of the difference in temperature (in Kelvin) between the merged and climatological temperature fields. (These fields are in fact not the reference fields input into the Newtonian cooling scheme as plotted in figure 6.11 but the difference in temperature between the model runs, averaged over several months of model run.) A large-scale warm temperature bias is seen in the model domain everywhere except in the northern hemisphere.

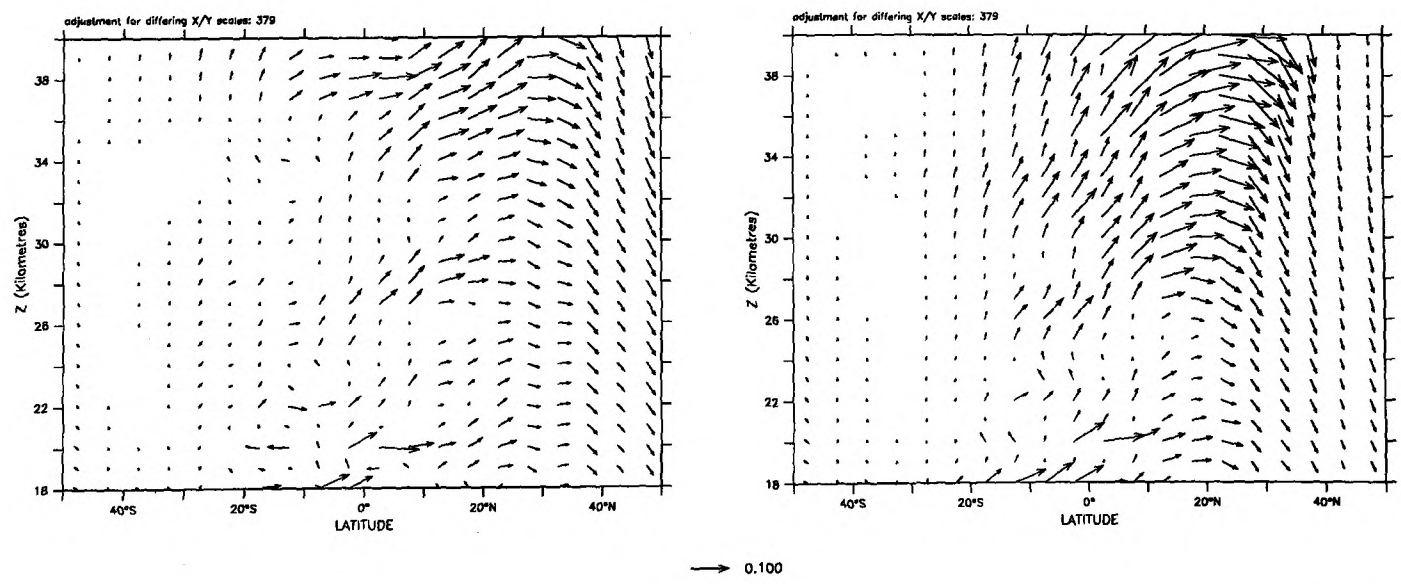

Figure 6.17: The residual mean circulations, averaged over the entire runs, for the (left) control and (right) merged runs. Enhanced ascent is visible in the tropics. The difference between these plots is shown in figure 6.18. The sample arrow represents $0.1\,\mathrm{ms}^{-1}$.

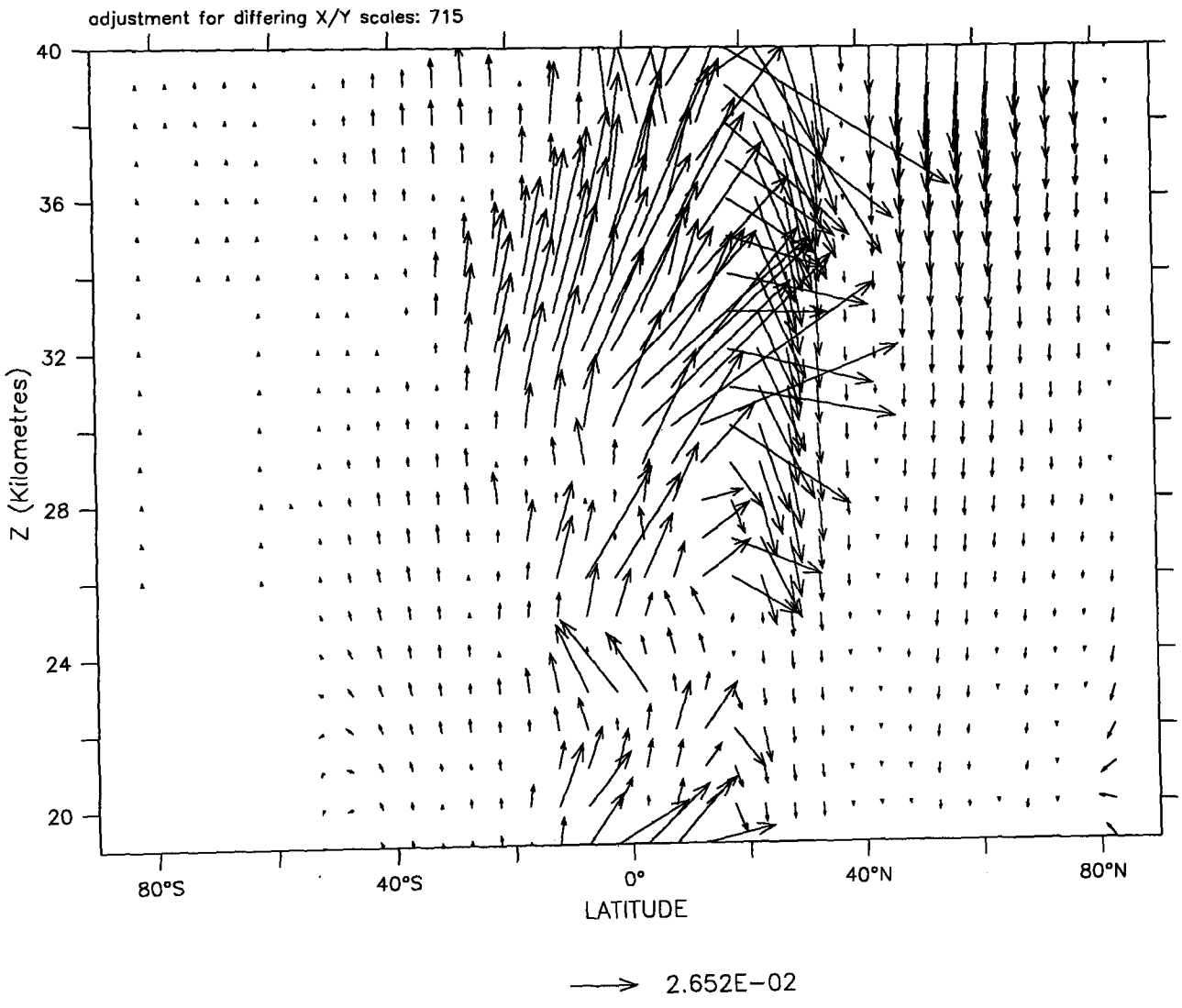

Figure 6.18: The difference between the panels shown in figure 6.17. This plot shows the control run (left-hand plot in figure 6.17) subtracted from the merged temperature profile run (the right-hand panel).

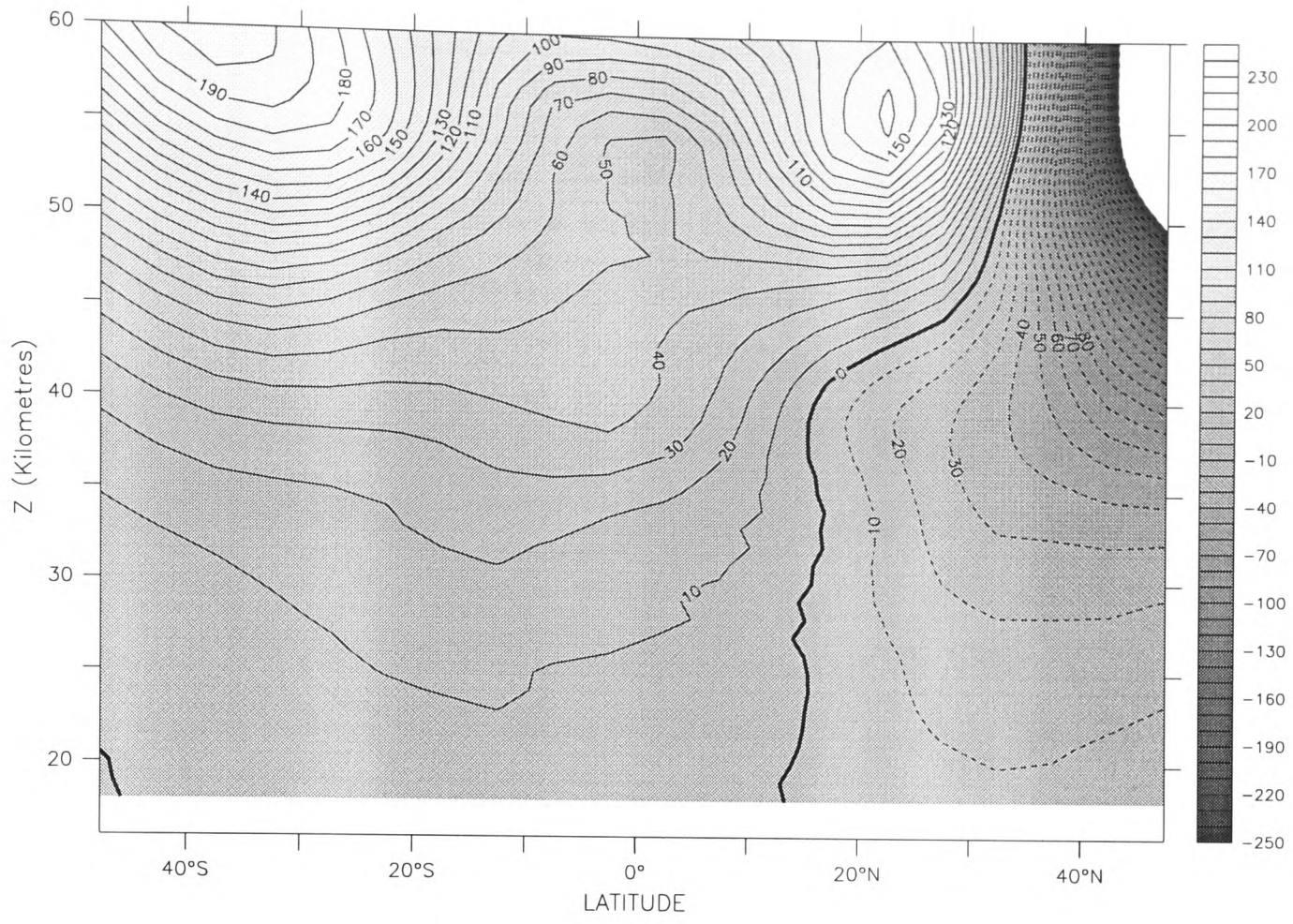

Figure 6.19: The difference in the vertical residual mean wind between the 'merged' and 'control' runs. The units are metres per day. This plot shows a generally enhanced ascent south of 15° north, which acts to retard the descending QBO jets.

so that an ascent of around 500 metres per month would account for the approximate halving of their propagation speed.

This dependence of period on such a large-scale but small magnitude change in temperature is tested by running the model with identical wave forcing and a temperature profile that is taken from the 'control' run profile, with the addition of 3K to all the temperatures south of 17.5° north. This profile is plotted in figure 6.20.

This results in a QBO-like oscillation, with period much longer than the control run, more similar to that shown in the lower panel of figure 6.10. A time plot of the u-wind from this run is plotted against height in figure 6.21.

This sensitive dependence of the modelled oscillation to the temperature profile is interesting in itself. It does show the importance of modelling the atmosphere as a whole in order to satisfactorily model a particular phenomenon. Lawrence [1996] shows that the ascent in the model can be improved through raising the model upper boundary to 96 km. If the QBO is to be accurately modelled, including its period, then this ascent must be

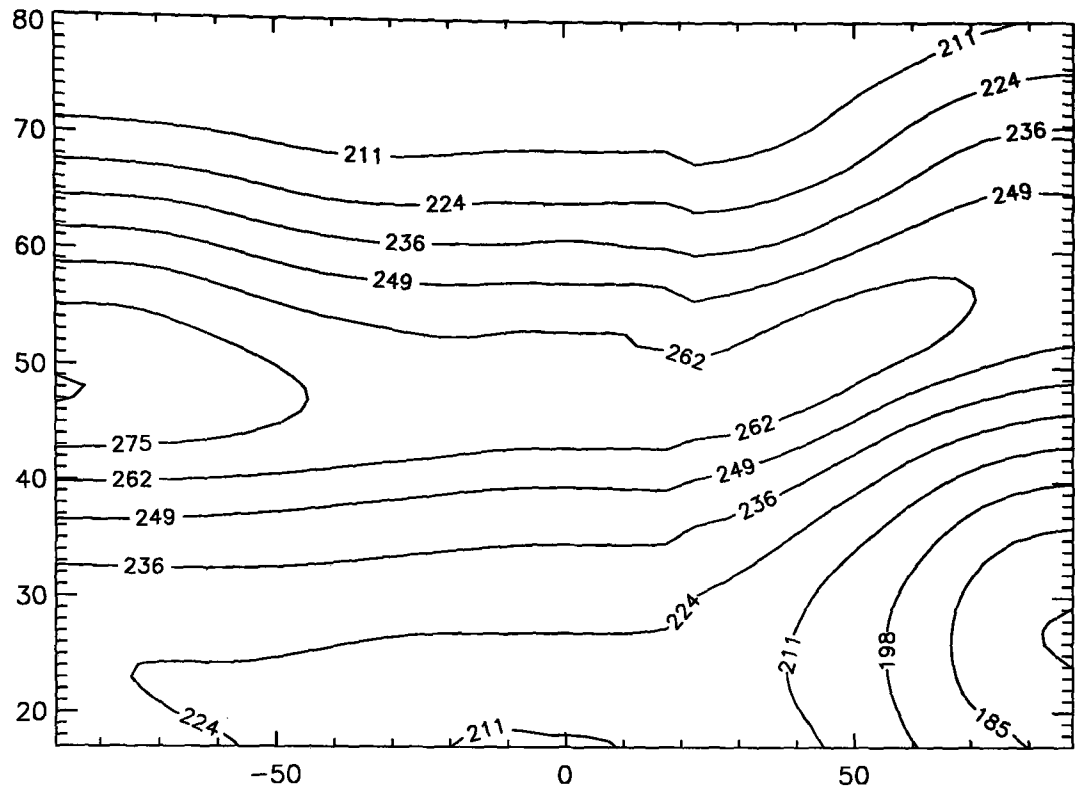

Figure 6.20: The reference temperature profile used in the run where the southern hemisphere and tropics have had 3 K added to the temperature. Contour units are Kelvin.

accurately modelled and it may be that modifications such as those being performed by Lawrence will be necessary.

6.4 Summary

In this chapter, an equatorial oscillation is generated in the model through the simultaneous forcing of both Rossby-gravity and Kelvin waves. Generally speaking, the QBO is fairly well captured in the model. Descending regions of easterly and westerly winds are clearly evident and the associated meridional and vertical circulations are visible. The model oscillation is equatorially confined as with observations and is of approximately the right amplitude. The period of the modelled oscillation is not in good agreement with observations. The modelled oscillation is (in all but a very few runs) considerably shorter than that observed. In experiments performed in this chapter, the modelled QBO period is shown to be most strongly affected by the background circulation in the model.

The QBO is forced in a model with various levels of complexity. In the simplest cases,

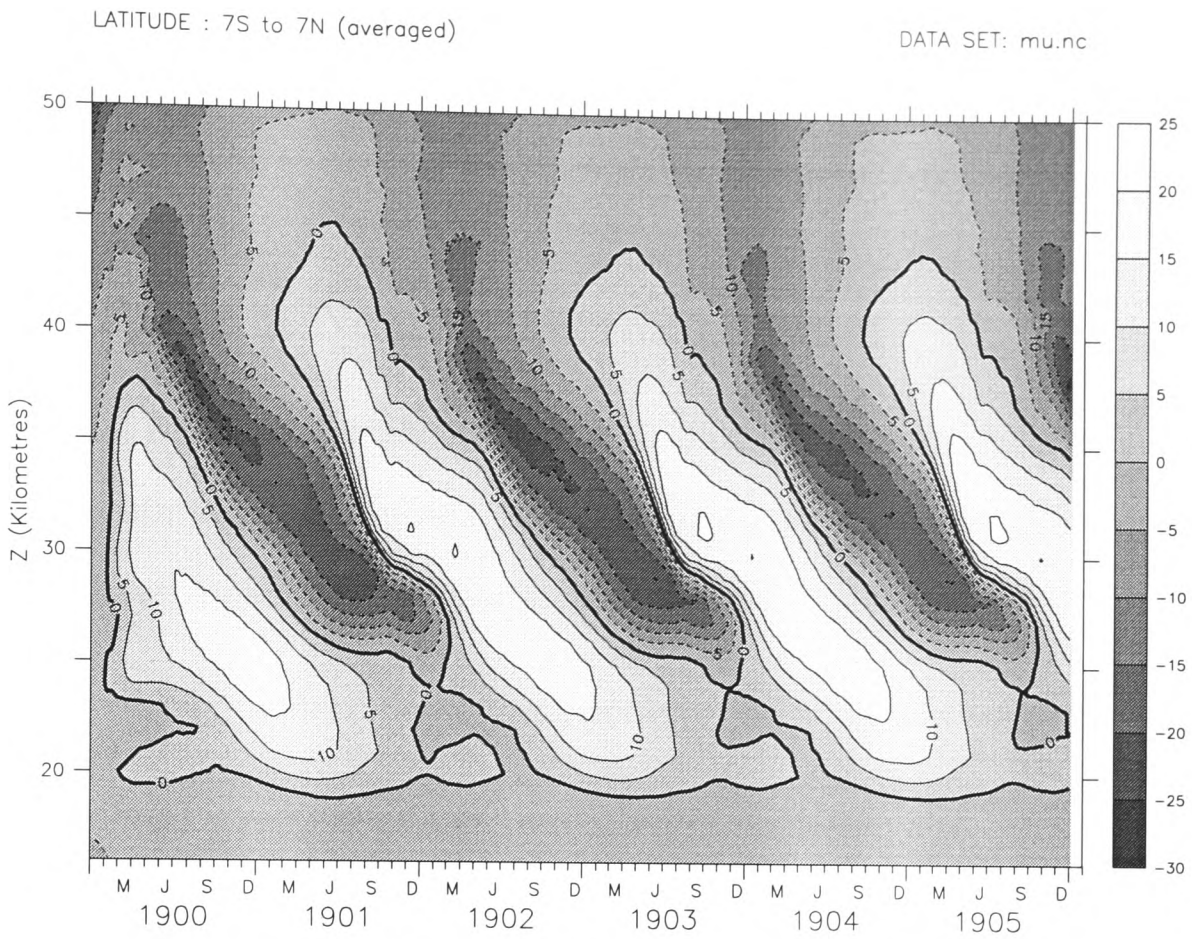

Figure 6.21: Time-plots of equatorial $\overline{u}$-wind against height and time (upper panel) and against time at 28 km altitude for the experiment where 3 K is added to the Newtonian reference temperature in the southern hemisphere and tropics. A QBO is generated with a period of around 23 months.

equatorial waves are forced into a model with Newtonian cooling relaxing the model towards an isothermal state. In later runs, the reference temperature for the Newtonian cooling routine is altered to several more complex temperature profiles.

6.4.1 A QBO in a Near Isothermal Model

In this isothermal reference profile state, Kelvin and Rossby-gravity waves are forced and an equatorial oscillation is produced. This oscillation is remarkably good given the model conditions. Positive aspects of this oscillation include:

- There are clearly evident descending zones of easterly and westerly winds.
- The latitudinal structure of the oscillation is realistic.
- The meridional and vertical structures predicted to accompany the zonal wind QBO are visible.
- The westerly shear is sharper than the easterly.

The oscillation produced is not however completely realistic. It is different from the observed QBO in many ways. Some of them include:

- The period of the oscillation is around 15 months which is too short.
- The oscillation produced has a height range of around 30 to 50 km, which is well above the observed altitude of the QBO.
- The generated oscillation is very regular. The observed QBO has a lot of variation in its period, which is not captured in the model.

These similarities and discrepancies are discussed in section 6.1. Given the near isothermal state of the model and lack of realistic background wind structures, the simulation is actually surprisingly realistic.

The amplitudes of the forcing waves are examined in this section. It is found that the amplitude of forced Kelvin waves is in fairly good agreement with observations. The Rossby-gravity waves are forced with an amplitude somewhat larger than that observed,

although it is not absolutely clear if this amplitude is outside the uncertainties on the observations.

6.4.2 A More Realistic Temperature and Wind Structure

A more realistic simulation of the atmosphere is sought. To this end, the isothermal reference temperature profile used in the Newtonian cooling scheme is to be replaced by one based on the CIRA climatology. Several different reference temperature profiles are used and the different profiles produce quite different results.

In all the runs performed in this section, the vertical range of the modelled QBO is an improvement on that achieved in the model with an isothermal reference temperature. The oscillation now appears to be limited in height to between 19 and 35 km, which is not far from what is observed.

Several different reference temperature profiles are used in the Newtonian cooling scheme. These can be summarised as:

Thermal Equilibrium Profile The model is run with the `MIDRAD` radiation code in place, in a perpetual January mode, with no Rayleigh friction present. The temperature profile is taken about 80 days into this run.

When this temperature profile is used as the background temperature profile, the model simulation of the atmosphere is not very realistic. Temperatures are too cold in the polar night mesosphere and the Rayleigh friction is not strong enough to close the polar jets below the top of the model.

Climatological Profile The temperatures in the model are relaxed towards a temperature profile obtained by averaging the temperatures in a model run with `MIDRAD` in a perpetual January mode and the normal Rayleigh friction terms present. This profile is a fairly typical January zonal mean temperature profile and is shown in the left panel of figure 6.8.

The simulated atmosphere when this temperature profile is used is much more realistic than that obtained when the thermal equilibrium profile is used. The QBO pro-

duced with this temperature profile is compared with that produced in the merged temperature profile (described next) in some detail, and will be summarized below.

Merged Profile As an experiment, a reference temperature profile is produced which is a combination of the climatological and thermal equilibrium profiles described above. The profiles are merged as follows:

Altitude	Temperature Profile Used
16–36 km	The thermal equilibrium temperature profile.
37–61 km	A linear combination of thermal equilibrium and climatological temperature profiles.
62–80 km	The climatological temperature profile.

This profile is shown in the right-hand panel of figure 6.8. A QBO is generated when equatorial forcing is added to a model using this reference temperature profile and is described below.

The climatological and merged temperature profiles are both used in runs with equatorial wave forcing. Figure 6.10 shows the evolution of the equatorial zonal wind for two runs which have identical equatorial wave forcing and different Newtonian reference temperature profiles. In both cases an encouraging QBO is produced. The period of the oscillation is however quite different in the two runs.

The reasons behind the large difference in the periods were sought in section 6.3. The dependence of the modelled oscillation period to the reference temperature profiles is investigated by running the model with reference temperature profiles formed by adding various perturbations to the climatological temperature profile. It is found that the largest difference in the climatological and merged temperature profiles, which is a difference of several tens of Kelvin over the winter pole, is not responsible for the change in period. Instead, it is a smaller change, of only a few Kelvin, in the reference temperature profile over a large area of the model. This difference in temperature profile produces increased ascent in the equatorial stratosphere which causes a decrease in the descent rates of the QBO and an increase in the period modelled.

This result is interesting for several reasons. It illustrates very well that the QBO is not an isolated phenomenon and that it is sensitive to other aspects of the modelled atmosphere. This will be true of any QBO that is to be modelled in GCMs (or indeed other simpler models). In particular, the residual circulation should be examined when diagnosing QBO-like oscillations appearing in any model. It also suggests that some of the variability in the period of the QBO in the real atmosphere may be related to changes in the large scale circulation. Such a relationship may partially explain the seasonal variation in the rate of phase propagation seen in the QBO [Wallace et al., 1993], although other aspects such as variations in the forcing waves are likely to be as important.

Chapter 7

Further Modelling of the QBO

Having successfully generated a QBO-like oscillation in the SMM, it is interesting to proceed and use this oscillation in further modelling studies. In this chapter, the model is modified through the re-introduction of the MIDRAD radiation scheme and the equatorial oscillation reproduced with this scheme in place. Experiments are performed where a variety of extra-tropical waves are generated in the model and their effect on the model atmosphere and interaction with the QBO examined.

7.1 MIDRAD in the model

That the modelled QBO may be manipulated so readily by changes in the Newtonian cooling reference temperature profile is an interesting result but somewhat disturbing for the next stage of the project. In order to get a more consistent, and hopefully more realistic, treatment of the radiation, the MIDRAD radiation scheme is reinstated. MIDRAD is a fairly complex and well-tested radiation code; it will allow more confidence in the results from the experiments that are to be performed. The main disadvantage of reinstating MIDRAD is the additional computing power needed[1] but the ever-increasing performance of the computers available more than offsets this. The next level of model complexity then becomes running the model with MIDRAD in a perpetual January mode, with a bottom

[1]Roughly, memory requirements are doubled and the cpu time per model day increases by around a third.

boundary of zonally-averaged, time-independent, CIRA data (corresponding to the same day as MIDRAD has been set to, ie. 16th of January), with superimposed geopotential perturbations from the GEOPER routine. This model setup is identical to that used in section 6.2.1 with the exception of the changed radiation scheme.

With MIDRAD reinstalled in the model, the QBO is again to be forced. Rossby-gravity and Kelvin waves are successfully generated in isolation, as in chapter 5, and, as before, reasonable jets are generated. When both waves are forced simultaneously, some further aspects of modelling the QBO in the SMM are brought to light and must be addressed in order to get a more realistic QBO. A plot of the equatorial zonal mean u-wind against time for a run with a QBO type bottom boundary forcing in the bottom boundary and MIDRAD radiation is shown in figure 7.1. It appears that jets are not being sufficiently well dissipated as they propagate towards the bottom of the model and the westerly jet is persisting in these lowest levels. This arises due as the model, being a middle atmosphere model, has a lower boundary at 100 hPa. The jet is unable to propagate below the model domain and there exists no mechanism to effectively dissipate the large jet in the lower levels of the model. In the Newtonian cooling case, the radiation scheme was able to dissipate the jet, but MIDRAD appears to be unable to do this. Plumb [1977] describes similar features in a much simpler one-dimensional model and Takahashi [1996] notices similar problems in a three-dimensional model. In the one-dimensional model, Plumb found that diffusion between the model lower boundary and the bottom of the jet would dissipate the jet and allow an oscillation to take place. To effect the dissipation in this model, a Rayleigh friction type relaxation (towards $0\,\mathrm{ms}^{-1}$) was applied to the zonal mean u-winds below 20 km. This relaxation is applied to the zonal mean u-wind field according to the relation

$$\frac{\partial u}{\partial t} + \ldots = -\alpha \overline{u}.$$

This additional relaxation is not attributable as a parameterisation of any particular physical mechanism. The persistent jet in the lower levels of the model is brought about by the unrealistic existence of a bottom boundary at 100 hPa. The additional Rayleigh friction acts in a manner similar to the *sponge layer* at the top of the model (see section

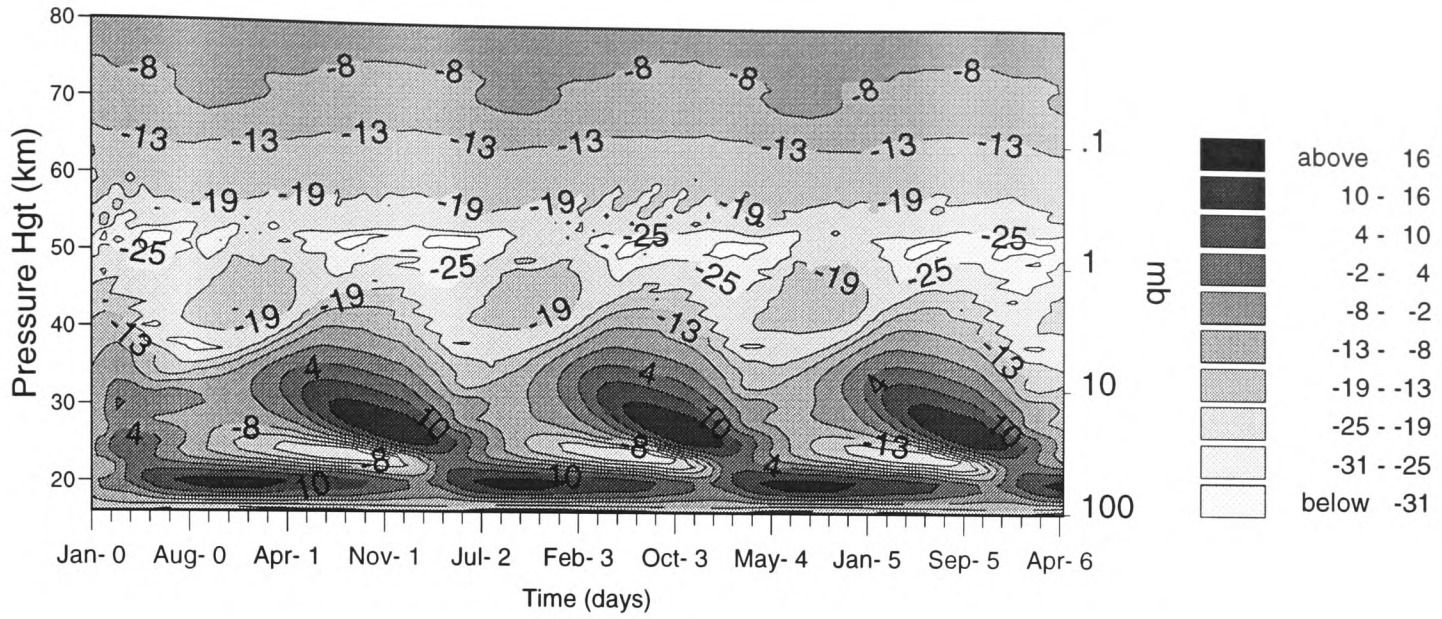

Figure 7.1: A time-height plot of the zonal mean u-wind against time (in ms^{-1}) for a QBO type run with the MIDRAD scheme performing the radiation calculation. An oscillation is produced, but the persistence of the westerly jets at low altitude is not observed in the real QBO.

4.1.2) and removes unwanted effects near a boundary. It is not particularly realistic to impose the additional friction in these lower levels, but in this case, it acts to remove the even more unrealistic persistent westerly jet.

Relaxation time-scales of this extra Rayleigh friction term ($\frac{1}{\alpha}$) vary from 20 days at 17 km to 80 days at 20 km. (These time-scales are comparable with the relaxation time-scales applied to the temperature field in the Newtonian cooling case.) With this zonal mean Rayleigh friction applied to the lowest boundary, the QBO simulation is far more satisfactory. Figure 7.2 shows the equatorial zonal mean u-wind against time and height in a run with this zonal mean Rayleigh friction applied.

Both figures 7.1 and 7.2 show an oscillation produced in the model. The addition of the zonal mean Rayleigh friction to the lower model levels also has the effect of altering the period of the modelled oscillation quite considerably. In the original run, with no zonal mean friction term, the period of the oscillation is approximately 24 months (in fact, in fairly good agreement with observations of the real QBO). After the addition of the zonal mean Rayleigh friction, the period of the oscillation produced is approximately 12 months. The reason for this change in period appears to be the more rapid dissipation of the jets at lower levels allowing waves to propagate easily through the lower stratosphere to be dissipated higher in the stratosphere where new jets are being formed. (The tropical

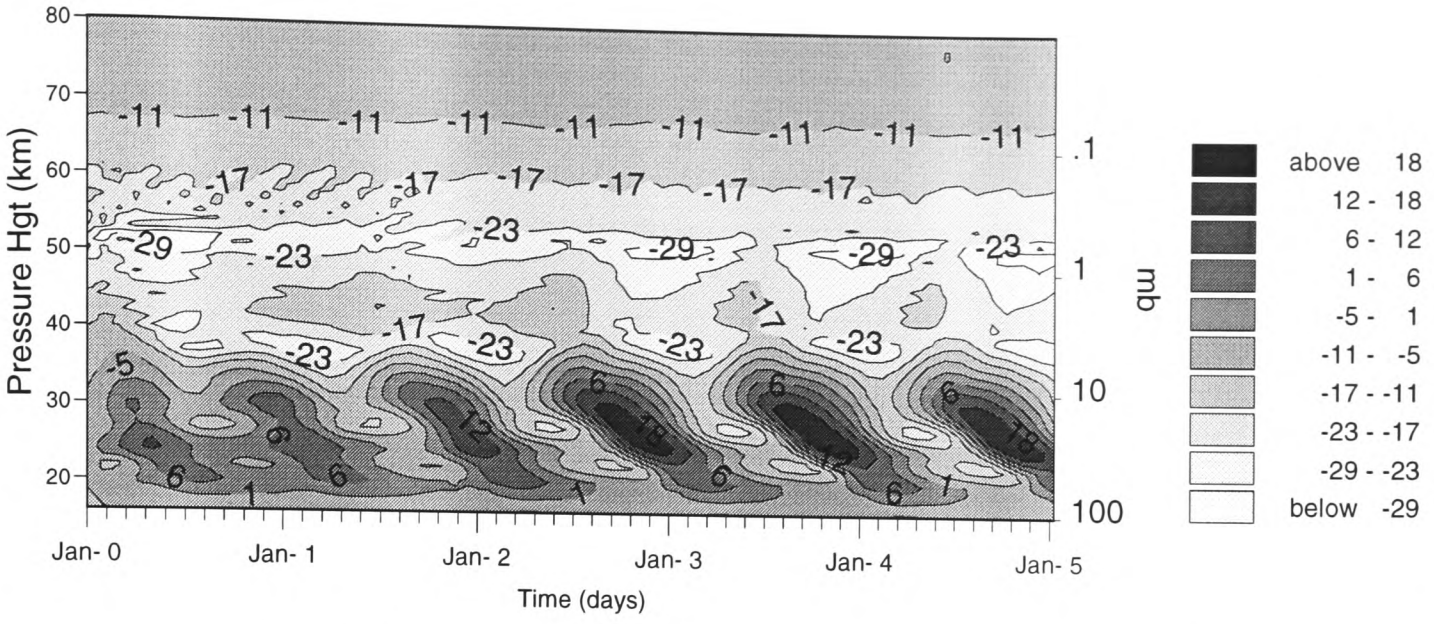

Figure 7.2: A time-height plot of the zonal mean u-wind against time (in ms^{-1}) as in figure 7.1. In this run a frictional term has been added to the zonal wind on the lowest four levels of the model in order to dissipate the persisting westerly jet. The resulting oscillation looks very like the observed QBO.

ascent is not significantly changed between the two runs, indicating that the change in period is not due to changes in the circulation.) It should be remembered that this 12 month oscillation is in no way tied into a seasonal cycle since the model is run in perpetual January mode and there is no seasonal cycle present.

The oscillation is equatorially confined, as shown in figure 7.3, and the maximum of the oscillation is at around 26 km which is in good agreement with the real QBO. The wave amplitudes forced in this run are in fact slightly larger than those forced in the Newtonian cooling model, with peak amplitudes of wavenumber one u-winds and wavenumber four v-winds of over $9\,ms^{-1}$ at 18 km altitude. These wave amplitudes are shown in figure 7.4, which is directly comparable with figure 6.4. The success or otherwise of the simulation of the QBO appears to be quite sensitive to the wave amplitudes, as will be discussed in the next section. It appears that the model is having some trouble generating easterly jets at low altitude. It is likely that this could be overcome if additional sources of easterly momentum were used, for example gravity waves. This was not done in this project.

Despite the differences between the model setups, the modelled equatorial oscillation appears to have translated from the Newtonian cooling version of the model to the `MIDRAD` version with very few problems.

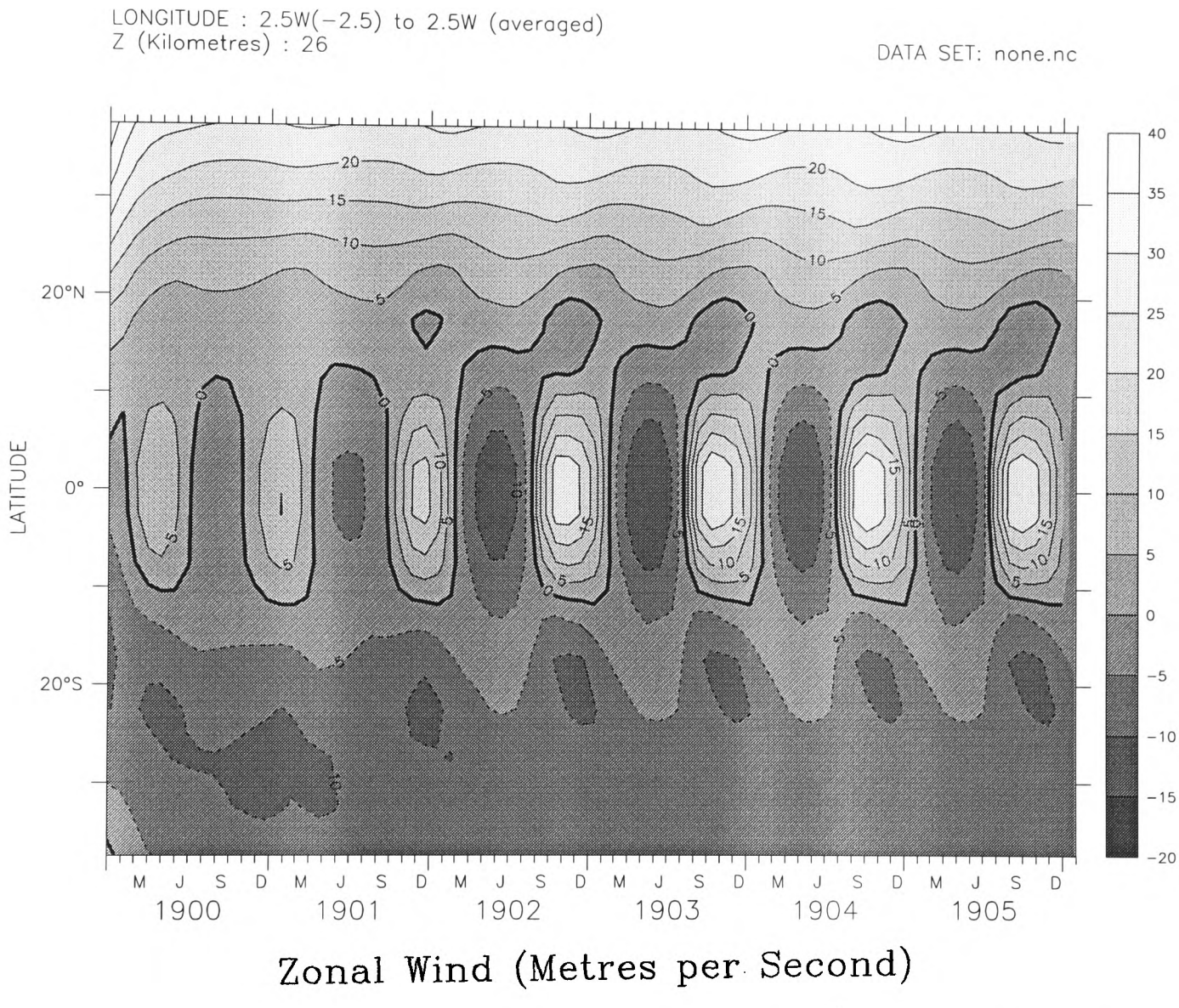

Figure 7.3: A latitude-time plot showing the zonal mean u-wind (in ms^{-1}) at 26 km altitude, for the QBO run with no planetary waves forced.

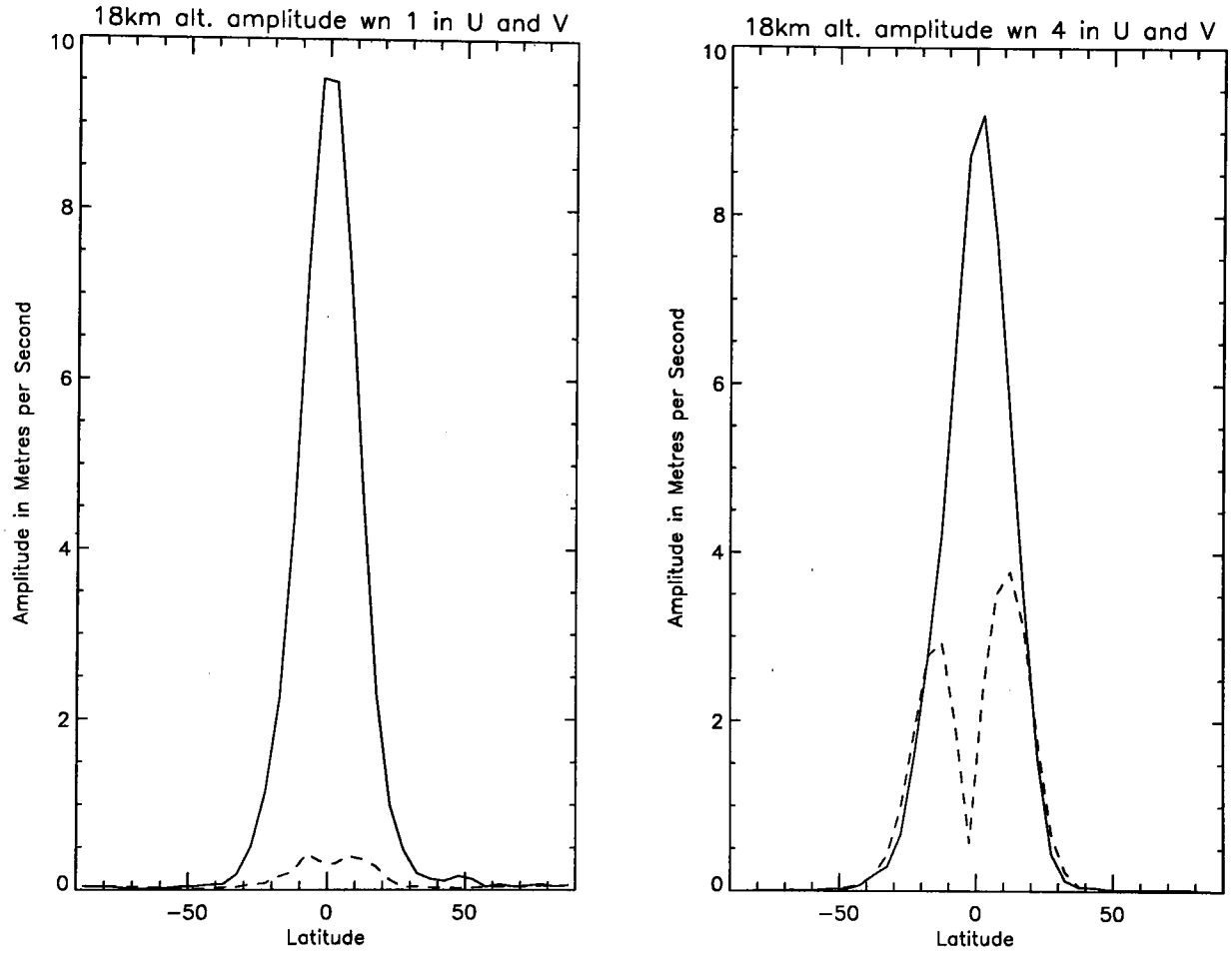

Figure 7.4: Wave amplitudes (ms^{-1}) at 18 km altitude for the run shown in figures 7.2 and 7.3. The left-hand panel shows amplitudes of wavenumber one in the u and v-winds (Kelvin wave components). The right-hand panel shows the amplitude of wavenumber four in the wind fields. These wind components are associated with the Rossby-gravity wave. This figure is directly comparable with figure 6.4.

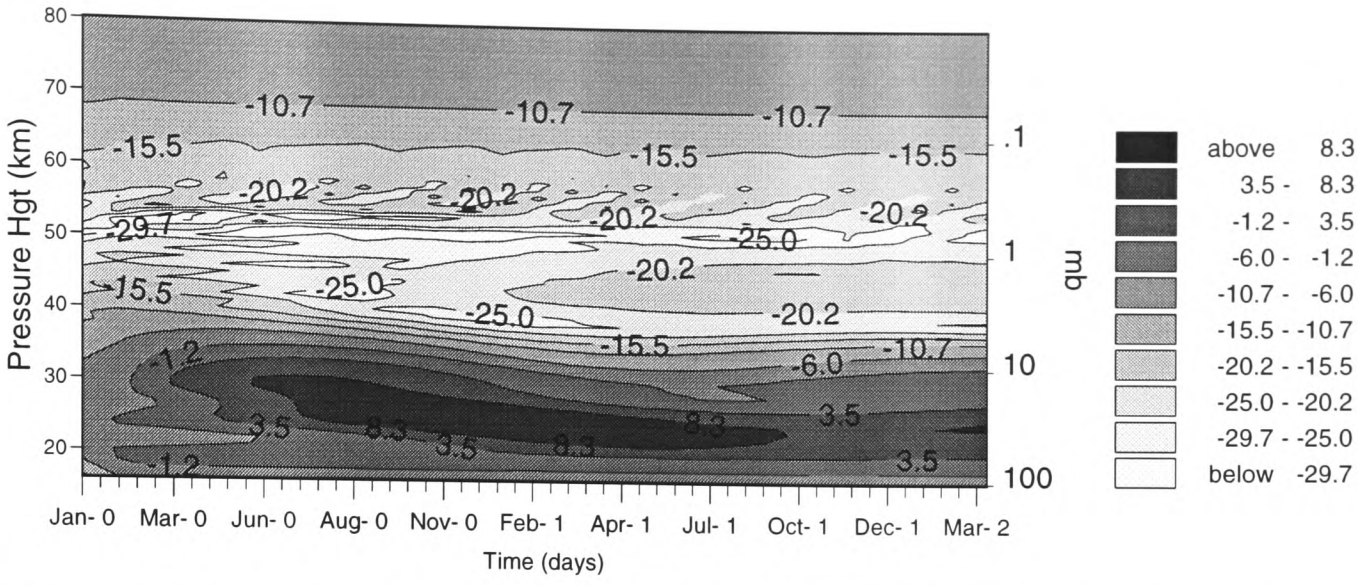

Figure 7.5: An unsuccessful attempt at modelling the QBO. This plot shows the equatorial zonal mean u-wind (in ms^{-1}) for just over two years of model run. An oscillation was successfully forced if the wave amplitudes were increased by approximately one-third.

7.1.1 Varying the forcing waves

As the advection through the bottom boundary was altered in order to prevent the model crashing (as described in section 4.3), it was noticed that the response of the model to the forcing amplitude was changed. With the bottom boundary problems eradicated, the model was found to need slightly larger amplitude wave forcing to achieve the same amplitude of waves in the model domain. During the tuning work performed to refine the amplitude of the wave forcing, several runs were performed which failed to generate a QBO. It appears that while small adjustments to the wave properties, for example to the phase speeds, have little effect, the existence of the oscillation itself is sensitive to larger changes in wave forcing.

Figure 7.5 shows one such run where the amplitudes of Kelvin and Rossby-gravity waves were both smaller than those eventually used to force the oscillation in the `MIDRAD` model. In this model run, no equatorial oscillation was generated. The wave amplitudes can be seen in figure 7.6. The difference between the amplitudes shown here and those in figure 7.4 is not that large, yet the resulting mean flow simulation is very different between the runs.

This sensitivity of the modelled oscillation to the forced model waves is interesting. The QBO in the atmosphere has been observed since the 1960s and appears to be fairly

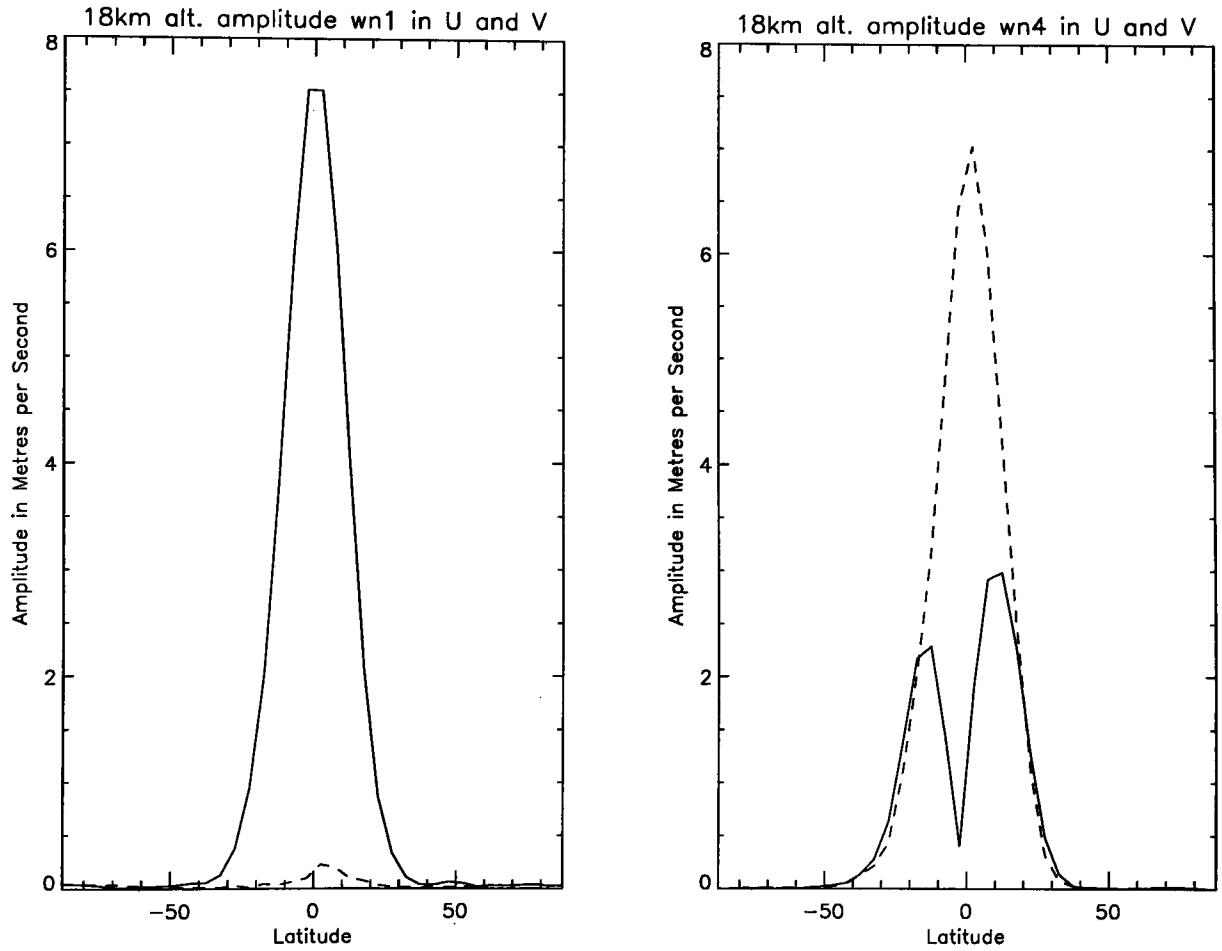

Figure 7.6: The wave amplitudes (in ms^{-1}) for the unsuccessful run shown in figure 7.5. The left hand panel shows the amplitude of Kelvin waves in the u (solid line) and v (dashed line) winds. The right hand panel shows the amplitude of the Rossby-gravity wave in the u (solid) and v (dashed) winds.

robust. No experiments were performed where the amplitude of the wave forcing was varied, either on seasonal or interannual time-scales. Wallace et al. [1993] find that the variation in the rate of phase propagation of the observed QBO varies greatly with the QBO almost completely stalling on occasion. It may be that the unsuccessful modelling attempts such as that shown in figure 7.6 may be similar to conditions when the QBO phase has stalled. It would be interesting to perform a series of experiments where the amplitude of the forcing waves were modulated in time and to investigate the effect on the QBO. Some experiments were performed by Geller et al. [1997] in a one-dimensional model where the wave forcing was modulated in time. They found that the modelled QBO could phase-lock with the variation in the forcing amplitudes, and went on to speculate about the natural variability of the forcing waves of the QBO. They postulate that variations in this wave forcing could be driven by processes outside the annual cycle and put forth sea surface temperatures as a possible candidate.

7.2 Adding Planetary Waves

With the model now producing an oscillation in a manner consistent with Holton and Lindzen [1972], several different experiments may be performed using the forced QBO. Options considered for further experimentation include:

- Attempt to better model the observed QBO. This could be achieved by addition of further and time-varying wave forcing on the bottom boundary and the inclusion of a more realistic gravity wave parameterisation.

- Investigate the properties of the modelled oscillation. The model is producing an oscillation that is in many respects similar to the observed QBO. The model oscillation is forced by vertically propagating waves, very much in the way that the real QBO is thought to be forced. The two-way interaction between planetary waves and the QBO would be an interesting avenue of investigation.

It was decided that the second of these options would be followed. The equatorial wave forcing will be applied to the bottom boundary (as before), producing a QBO-

like oscillation. A source of planetary waves will be added to the model through the addition of a stationary perturbation in the geopotential bottom boundary at a latitude of 60° north. The interaction of the QBO and these planetary waves will be an interesting experiment. The literature contains several examples of three-dimensional models being used to investigate the effect of the QBO on planetary waves (for example, see O'Sullivan [1997*a*]). This model is unusual in that the QBO is forced by a realistic process of dissipating equatorial waves; the effect of planetary waves on the QBO jets will be a particularly interesting experiment.

There is presently considerable interest in the interaction of planetary waves and the QBO. Planetary waves are largely observed in the winter hemisphere, in this case the northern hemisphere, and propagate upwards and generally equator-ward. In the winter, the stratospheric zonal wind is predominantly westerly, allowing the waves, according to equation (2.57), to propagate relatively freely. The presence of these large-scale waves contributes greatly to the interannual variability of the polar vortex and is implicated in stratospheric sudden warmings [Rosier, 1996]. During the summer months, the zonal wind is predominantly easterly and these planetary waves are not observed in the stratosphere. A plot of a summertime meteorological field (for example, geopotential height or temperature) in the stratosphere will typically be very close to zonally symmetrical. Planetary waves transfer great amounts of momentum between remote regions of the atmosphere and an understanding of their propagation and dissipation is essential in the accurate modelling of the atmosphere.

There is thought to be an intricate relationship between the QBO and these waves. The QBO is known to have a modulating effect on the propagating Rossby waves [Dunkerton and Baldwin, 1991], with easterly QBO winds preventing the Rossby waves from crossing the equator and acting to trap them in the winter hemisphere. Westerly winds have the opposite effect, allowing more Rossby waves to cross the equator, resulting in less EP-flux divergence near the polar vortex. This is the mechanism suggested by Holton and Tan [1980] for the apparent QBO signature on the frequency of sudden warmings in the winter polar stratosphere (further investigated by Labitzke [1982]). Further investigation into

this area suggests that the situation is more complex than that proposed by Holton and Tan [1980] but the QBO is still thought to play a large part in the interannual variability of the stratosphere. The interaction of the equatorial jets produced in this model and the propagating planetary waves can be investigated in the model. Some evidence will be found of a QBO modulation of the cross-equatorial EP-flux by the QBO.

Despite this modulating effect of the QBO on the Rossby waves, it is not clear that the planetary waves should have any great influence on the QBO itself. That the QBO is being so well modelled in the previous sections of this thesis, with no planetary wave forcing present, would suggest that planetary waves are not important in the forcing of the QBO. Certainly, given the sensitivity that the model has shown to the amplitudes of the forced waves, if the QBO simulation is relatively unaffected by the addition of the planetary waves, it would be good evidence to suggest that they are having little influence in the lower stratosphere.

If planetary waves were to have an influence on the QBO, an aspect of the simulation that might be particularly sensitive is the westerly jets. These might be expected to be rapidly dissipated if planetary waves were to deposit momentum in the equatorial region. In previous work, three-dimensional model has been initialised with such a jet present and planetary waves forced [O'Sullivan, 1997*a*]. It is found that, so long as the horizontal resolution is adequate, the jet is relatively unaffected by propagating planetary waves. It is also found that one effect of the planetary waves is to narrow the QBO zones. The experiments performed in this section are more sophisticated than those performed in O'Sullivan [1997*a*] in that rather than initialising a model with a particular wind structure and observing its evolution with time (it will naturally decay, even in the absence of any wave–mean-flow interactions, through radiative processes), planetary waves are forced into an evolving QBO jet structure and the effects observed.

It is hoped that in forcing planetary waves in the extra-tropics of this model, several interesting results may be obtained. Questions that can be asked, and hopefully to some extent answered, include:

- What effect will planetary waves have on the stratospheric state modelled in this perpetual January state?
- Will a QBO still be successfully generated in the model with planetary waves present?
  - If so:
    * What effect will the planetary waves have on the modelled QBO?
    * What effect will the QBO have on the propagating planetary waves?
  - If not:
    * Can the forcing be tuned to once again generate a QBO?
    * Is the effect of the planetary waves realistic in the model?

7.2.1 Control Runs

Several runs are examined in this section. Waves were forced by means of a perturbation added to the geopotential height field. This additional perturbation is of the form:

$$\Phi' = \Phi'_0 e^{-r^2/r_0}.$$

Here r is the distance from the centre of the planetary wave source and r_0 is the 'radius of influence' defining the horizontal extent of the perturbation. In these model runs, r_0 is set at 3350 km. (In the model subroutine, it is actually specified in terms of an angle, which is set at 30°.) The shape of the geopotential height perturbation is shown in figure 7.7. The amplitude of the planetary wave source, Φ_0, is set to various values. In the runs described in this chapter, forcing amplitudes of 150, 250 and 400 metres are used.

Figure 7.8 shows the amplitudes of wavenumbers one and two seen in the UKMO assimilated data for the winter 1991–1992. This data is taken at 72.5° north which is the latitude at which the maximum wave amplitude was seen in this year. It shows that the amplitudes of the various waves vary greatly with time. The maximum amplitude for wavenumber one is about 470m on this plot but the average is somewhere around

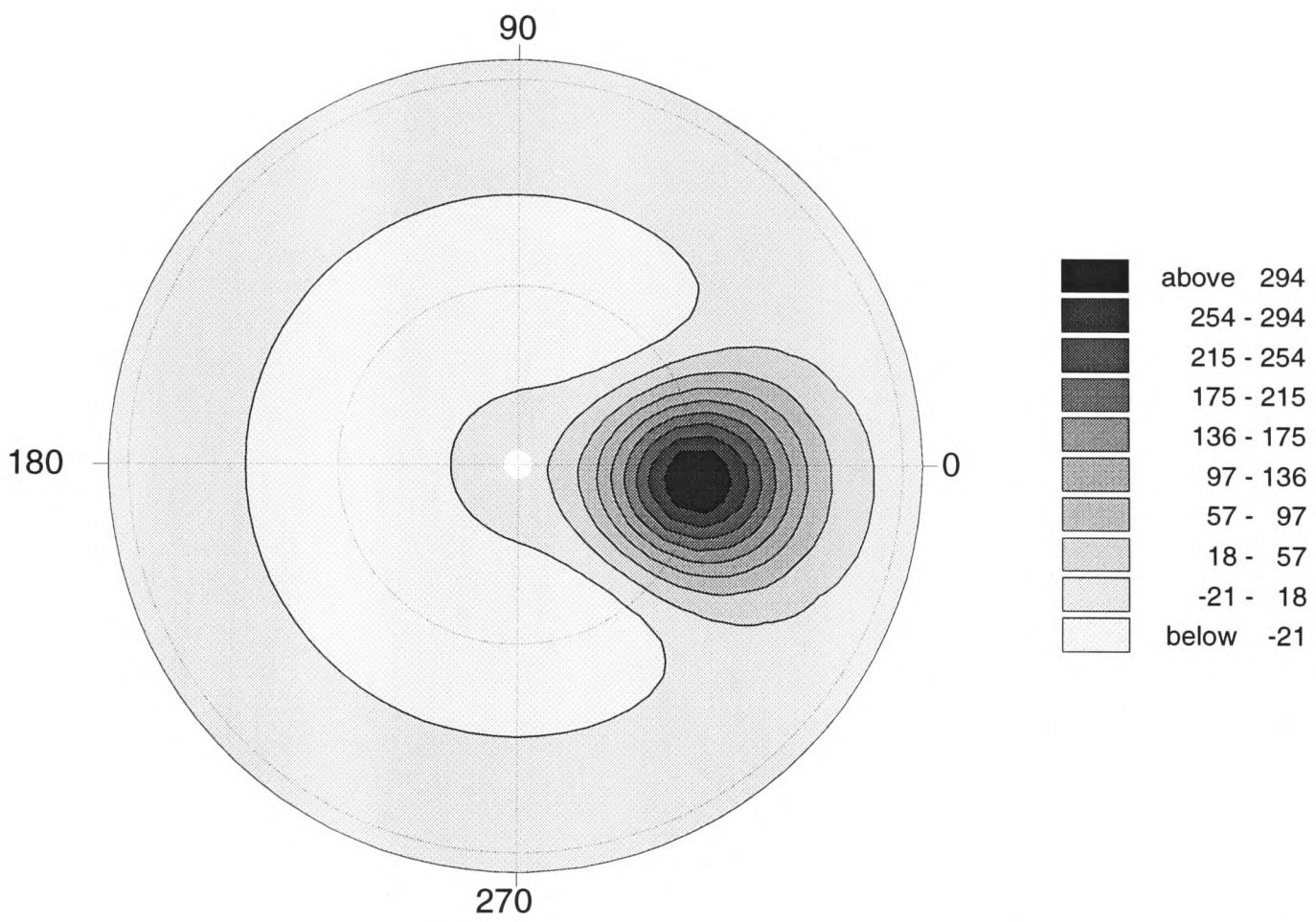

Figure 7.7: Geopotential perturbation in the bottom boundary (units are metres) added to generate planetary waves. The field shown is actually the deviation from the zonal mean geopotential of the bottom boundary, hence the small negative values of geopotential height forcing shown away from the forcing region.

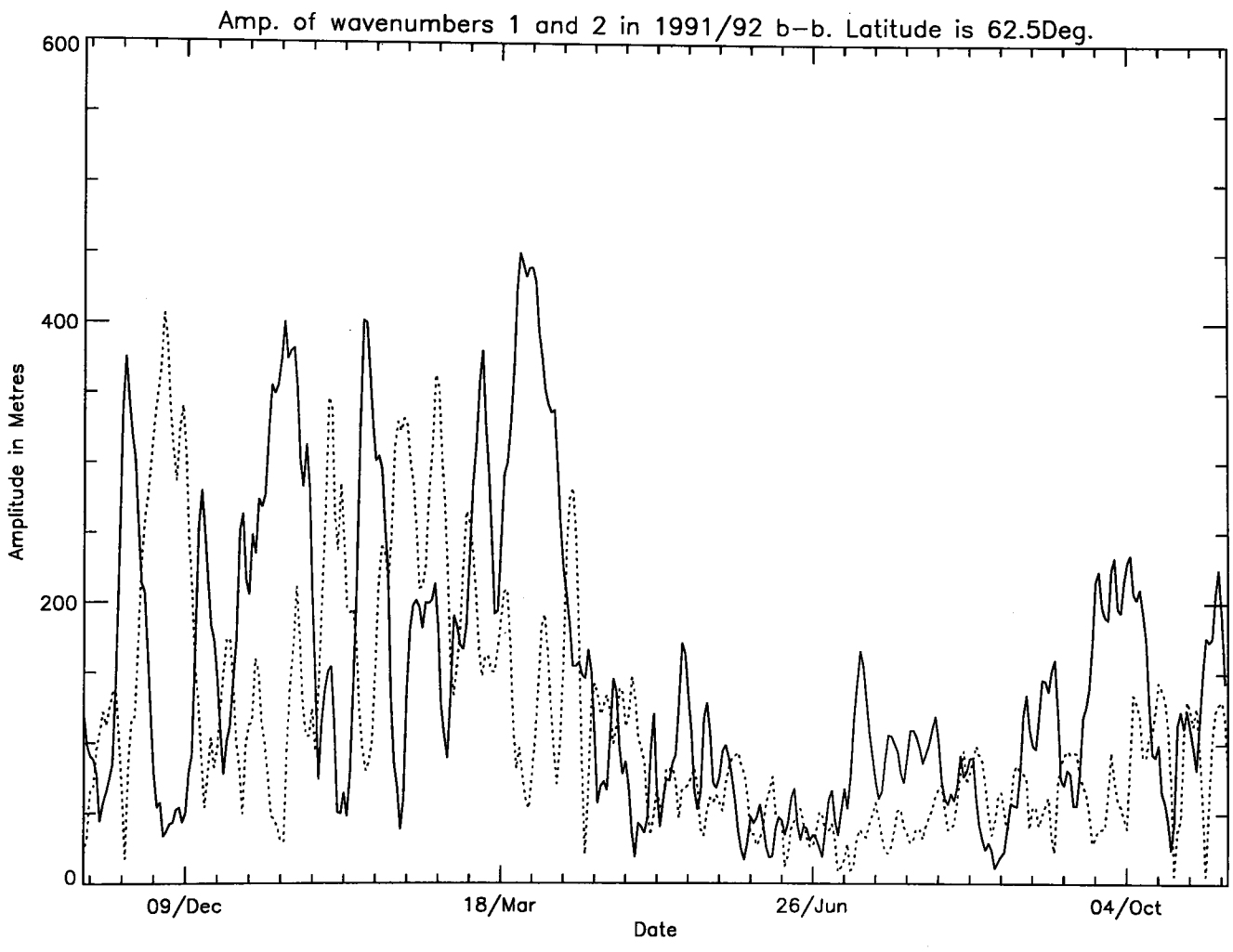

Figure 7.8: The amplitudes of wavenumbers one and two in geopotential height (units are metres) seen in the UKMO assimilated dataset for the 1991–1992 winter. The solid line shows the amplitude of wavenumber one, the dotted wavenumber two.

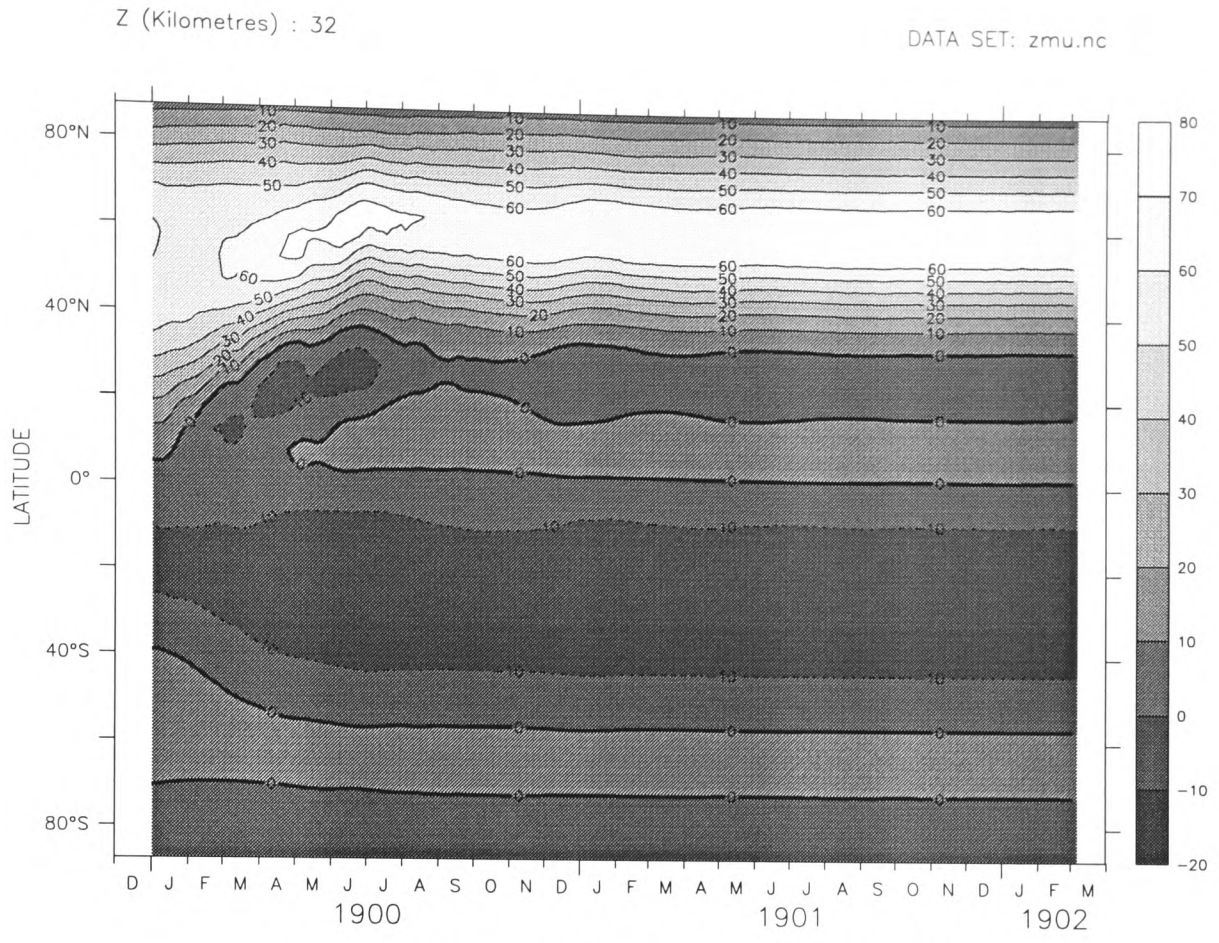

Zonal Wind (Metres per Second)

Figure 7.9: The zonal mean u-winds against time (in ms^{-1}) at 32 km altitude for a model run in which a 400m planetary wave source has been added to the model bottom boundary. The model can be seen to settle down to a fairly undisturbed state after the first few months of integration.

200m during the winter. The smaller amplitude forcings are within the range of observed amplitudes of planetary waves. At 400m amplitude, the largest amplitude source of planetary waves is somewhat larger than the observed average planetary wave amplitude, although less than the maximum amplitude seen. No attempt was made in this project to force a time-varying planetary wave, although this would be more realistic, as this would add noise to the effects to be investigated.

After the addition to the planetary waves, the model state adjusts within a few months to the imposed forcing and reaches a steady state. A plot of the zonal mean u-wind at 32 km altitude against time is shown in figure 7.9 for the control run with a planetary wave of 400 m amplitude forced. The differences between the state reached after the addition of planetary waves to that before planetary waves are added are shown later in this section. As might be expected, the addition of planetary waves provides a strong source of EP-flux that propagates into the model domain. Figure 7.10 shows a vector plot of this EP-flux

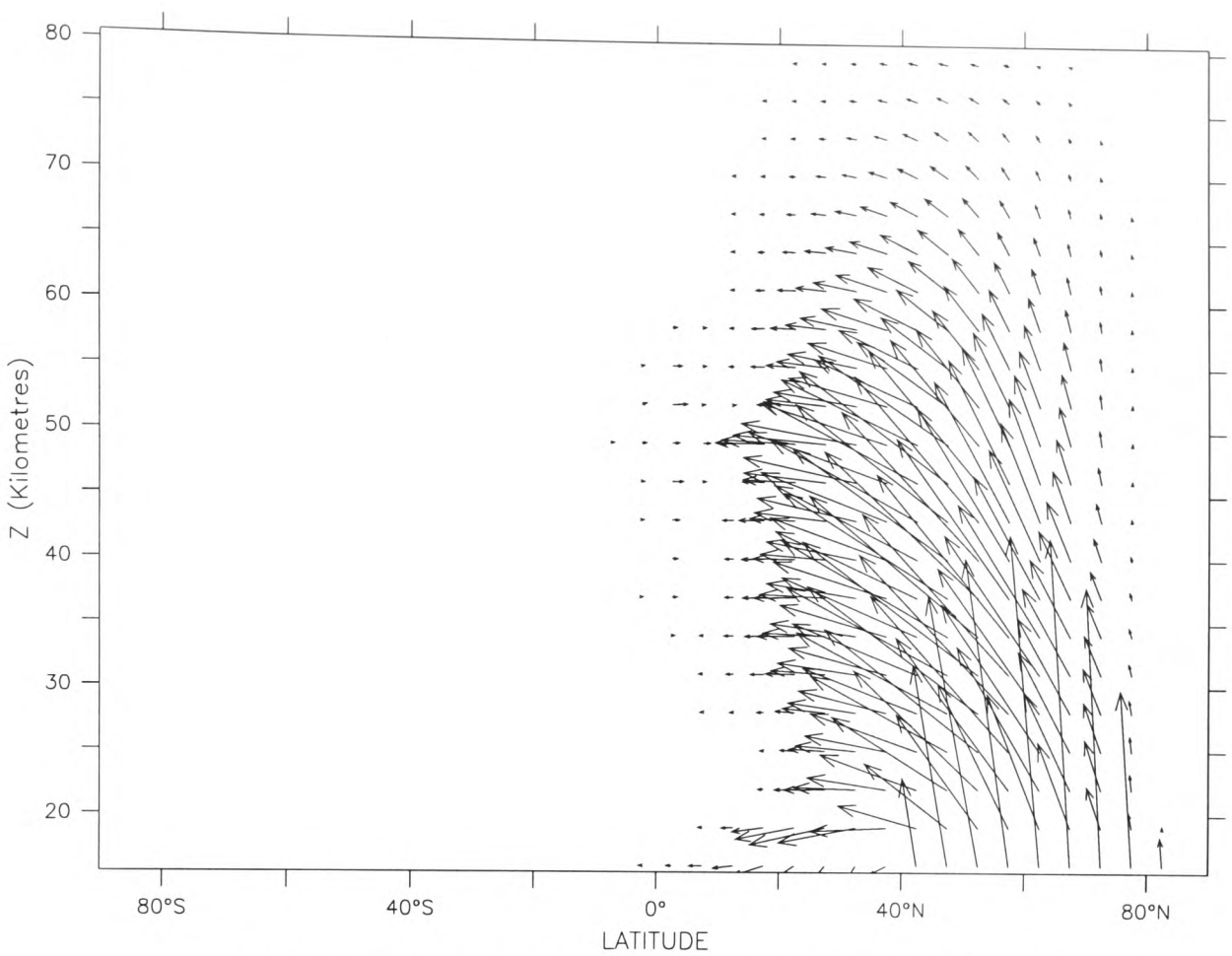

Figure 7.10: The EP-flux resulting from the addition of the 400m planetary wave source to the bottom boundary. A sample arrow is shown. Units are m^2s^{-2}.

when the 400 m planetary waves are added. The EP-flux vectors show that the wave activity is propagating upwards and equator-ward from the forcing region at 60° north.

This perturbation is Gaussian in shape, not a pure sine-wave, and contains components of many wavenumbers. The largest amplitudes in this shape are the components of wavenumbers one and two. It is interesting to look at the amplitudes of wavenumbers one and two in, for example, the u-winds, produced as a result of the forcing of these waves. Figure 7.11 shows the amplitudes of wavenumber one forced for each of the amplitudes of wave forcing. Figure 7.12 shows the amplitudes of wavenumber two for the same range of wave forcing experiments. The first thing obvious from the plot is that the structure is very similar for both the 150 and 250m forcing cases. The structure for the 400m case seems rather different with a relatively much larger amplitude of wavenumber two present and quite different spatial distributions of the wave components.

The amplitudes of the 150 and 250m waves vary proportionally to the forcing ampli-

tudes in both the wavenumber one and two to a very large degree. The waves appear to be propagating fairly linearly. This is not true for the 400m forcing where the patterns of wave amplitudes are quite different. The maximum amplitude of wavenumber two in the 400m wave forcing case is around $18\,\mathrm{ms}^{-1}$ whereas the maximum amplitude of wavenumber two in the 250m wave forcing case is around $4\,\mathrm{ms}^{-1}$.

In these control runs, the effect of the planetary waves on the mean flow in the absence of any equatorial wave forcing can be observed. Figures 7.13 and 7.14 show a zonal wind latitude-height section for the run with no planetary wave forced and then the difference between the various planetary wave forcings and this 'no planetary wave' case. In all the runs, the structure of the changes in zonal wind are quite similar. There is a strong deceleration of the mean flow in a region between around 20° to 40° north, over most of the vertical domain of the model. This is the 'surf zone' where the majority of the planetary waves are being dissipated. In the real atmosphere, this is a region of extensive mixing of the air [McIntyre and Palmer, 1983]. This deceleration does not appear to be restricted to the northern hemisphere and in all the planetary wave runs, there is a region of deceleration in the southern hemisphere where waves have propagated over the equator. As well as this deceleration, there is an acceleration in the polar jet in all the runs which occurs as the global circulation adjusts to the new state.

The changes in the mean flow are very similar in all the control runs performed. They differ mainly in the magnitude of the change seen in the zonal wind. There is very little difference in the extent and shape of the changes produced.

Polar Warmings

In figure 7.9, the model can be seen to settle down to a very undisturbed state. This is perhaps surprising as there are several modelling studies that suggest that the imposition of planetary waves such as these should act to trigger stratospheric warmings [Iwi, 1997]. Such warmings are not observed in this model with the Gaussian-shaped planetary wave forcing, even when the amplitudes of the waves are relatively large. It appears that the nature of the wave forcing is critical to the effect of the planetary waves on the polar

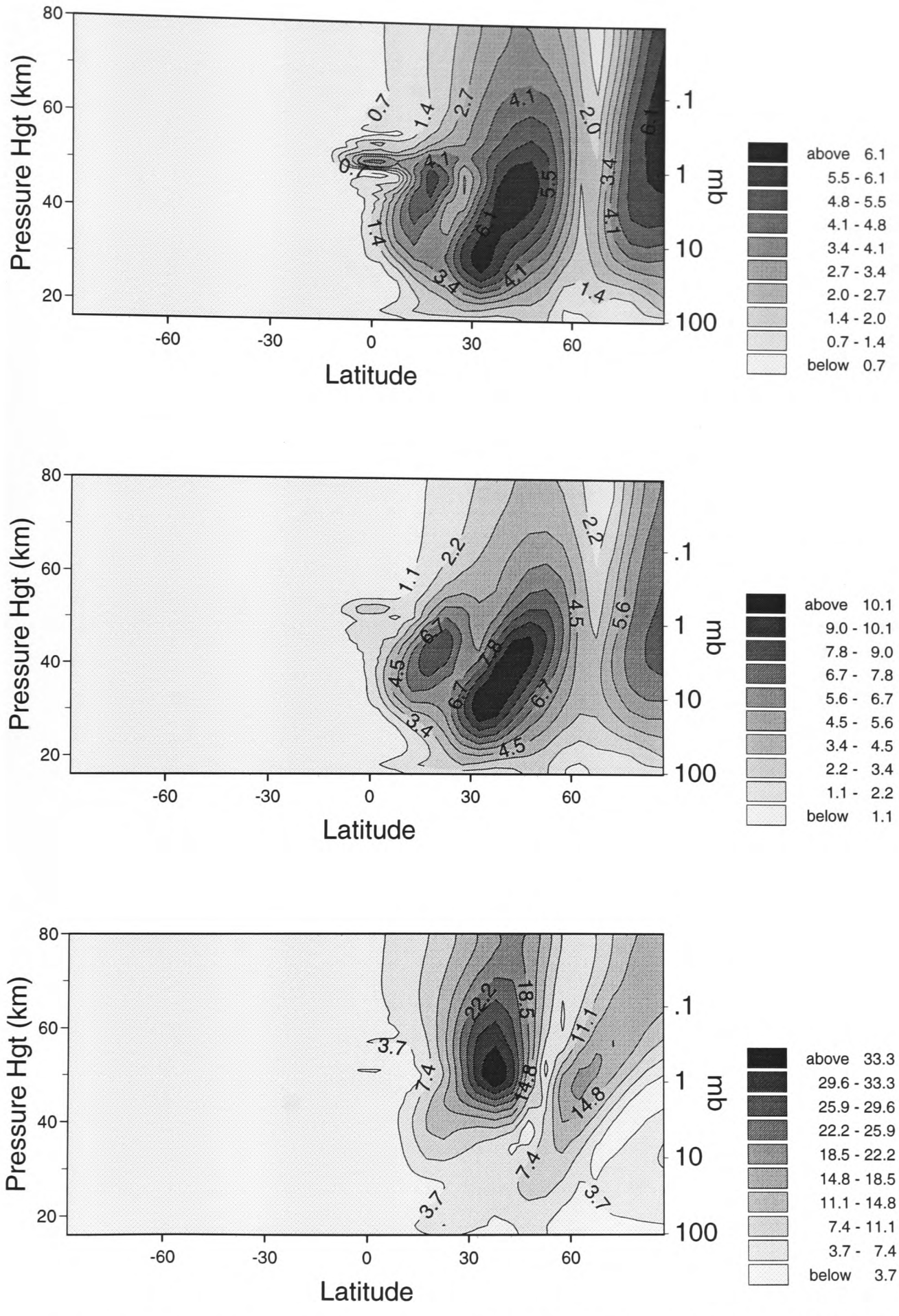

Figure 7.11: Amplitudes of wavenumber one in the model u-winds (in ms $^{-1}$) as a result of adding planetary wave forcing to the bottom boundary of the model. The forcing amplitudes are 150m (top), 250m (middle) and 400m (bottom). The structure of the 150 and 250m amplitude forcing runs are similar but the 400m case is quite different.

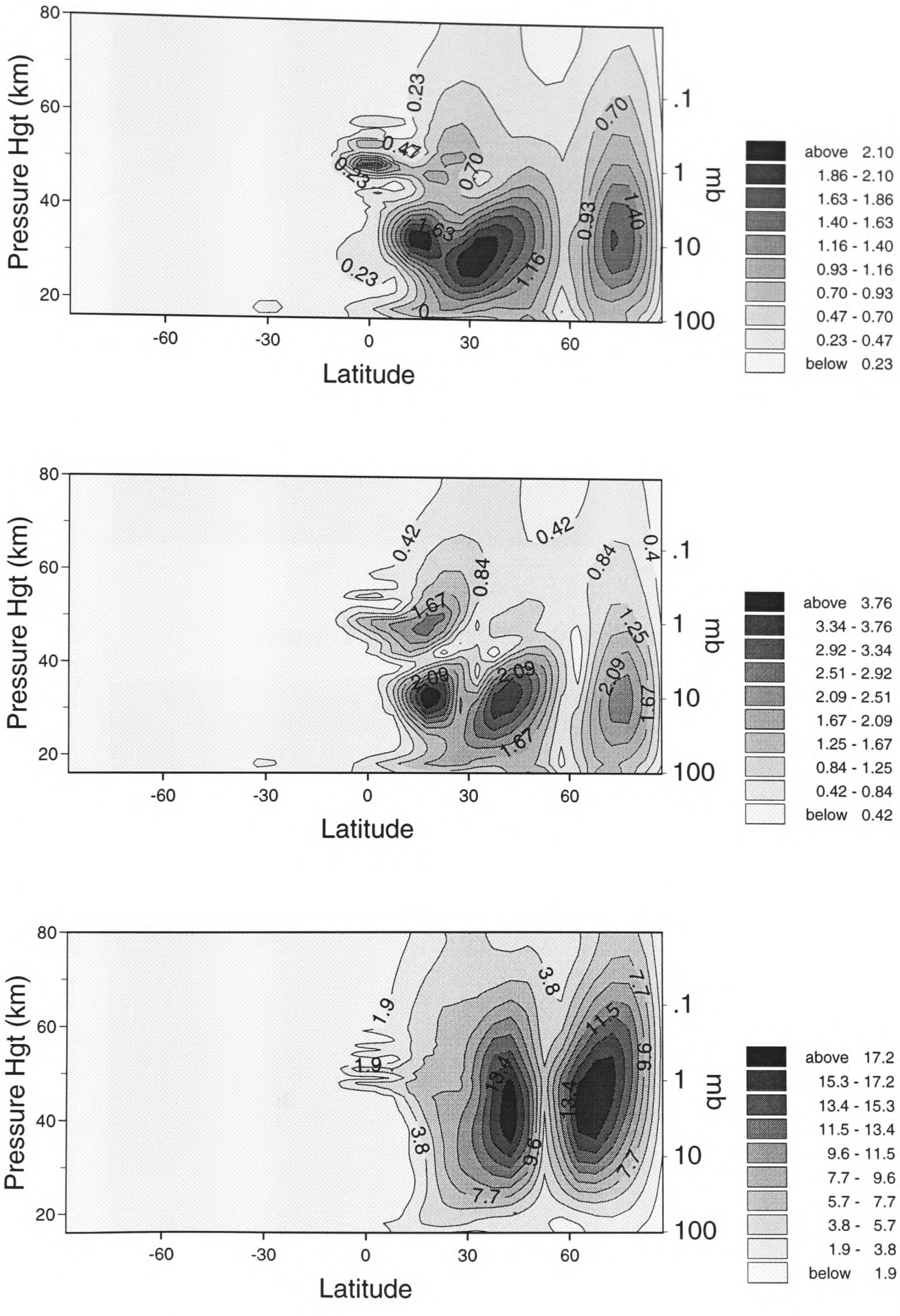

Figure 7.12: Amplitudes of wavenumber two in the model u-winds (in ms^{-1}) as a result of forcing planetary waves in the model. The forcing amplitudes are 150m (top), 250m (middle) and 400m (bottom). Again, the structure of the 150 and 250m amplitude forcing runs are similar but the 400m case is quite different, with larger amplitudes of wavenumber two generated.

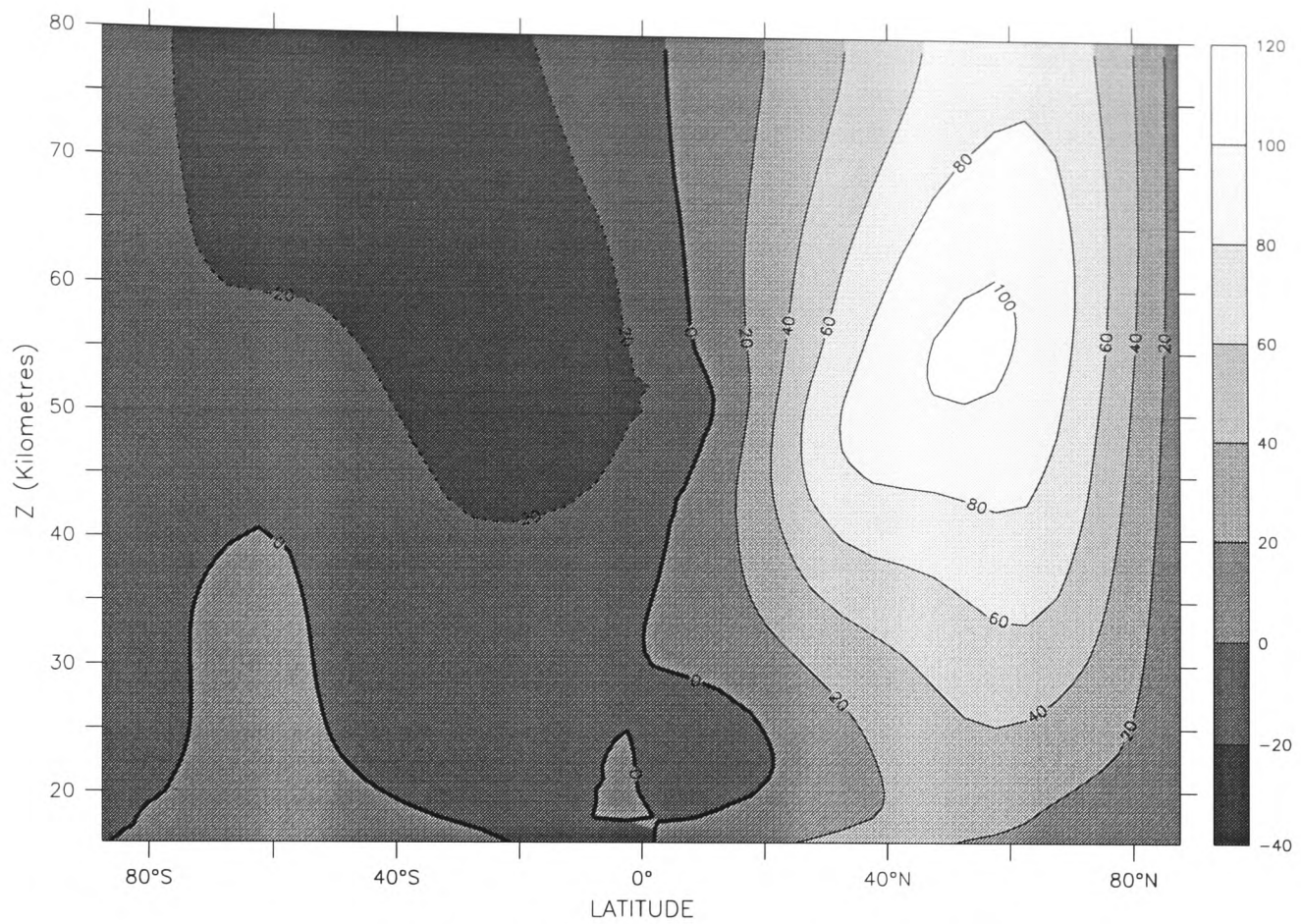

Figure 7.13: The time-averaged (after the model has reached a constant state) zonal mean u-wind (in ms^{-1}) for the model run with no additional waves (either tropical or extra-tropical) is shown in the upper plot. The lower plot shows the difference between the steady state solution achieved in the run with 150m planetary waves and the wind profile shown in the upper plot (contours and shading again in units of ms^{-1}).

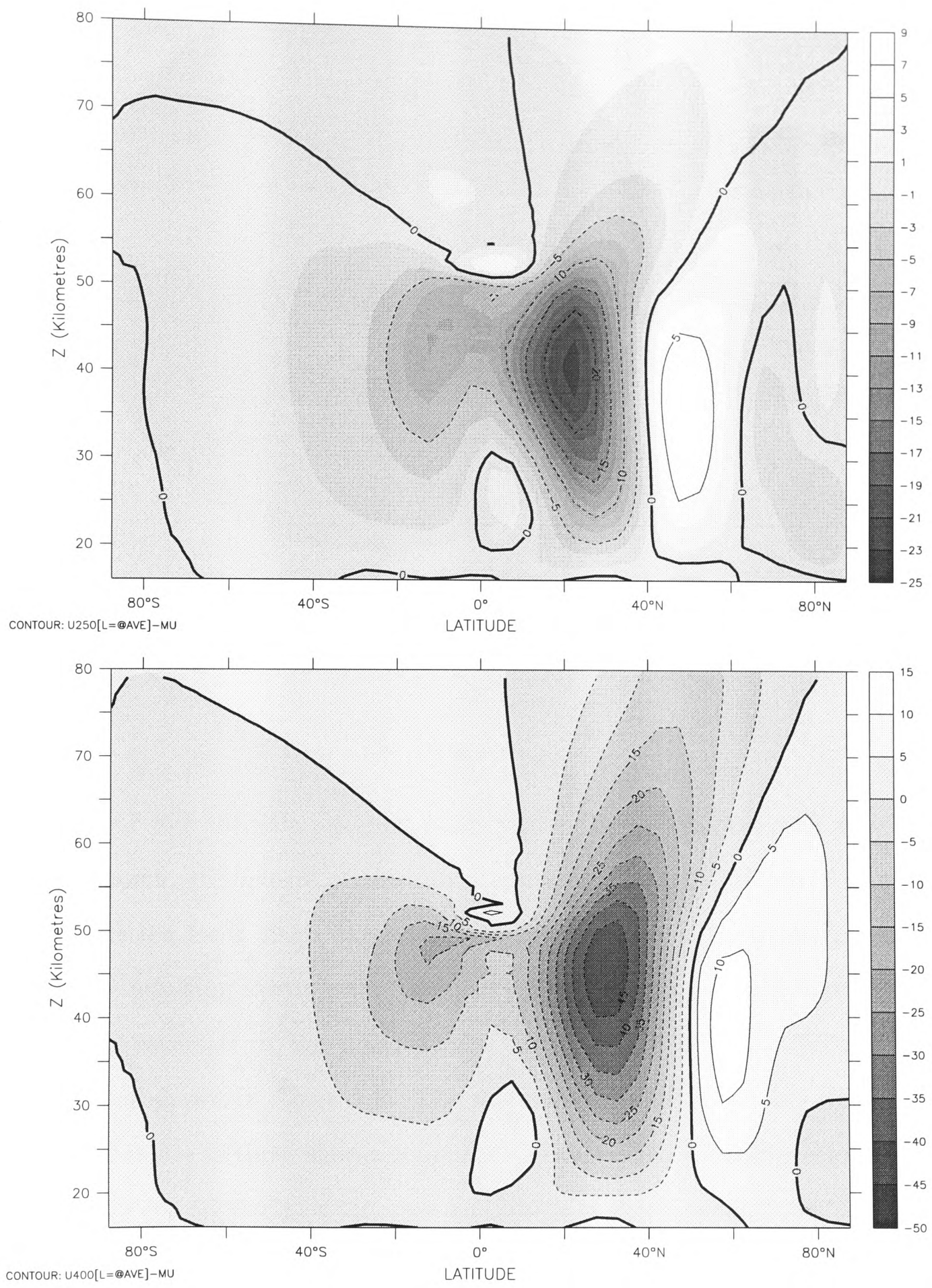

Figure 7.14: Differences between the upper plot in figure 7.13 and the steady state wind profiles achieved in runs with (upper) 250m and (lower) 400m planetary wave forcing added. Units are again in ms^{-1}. The shading intervals vary between the plots, but contour intervals are the same in the lower panel of figure 7.13 and both the panels in this figure.

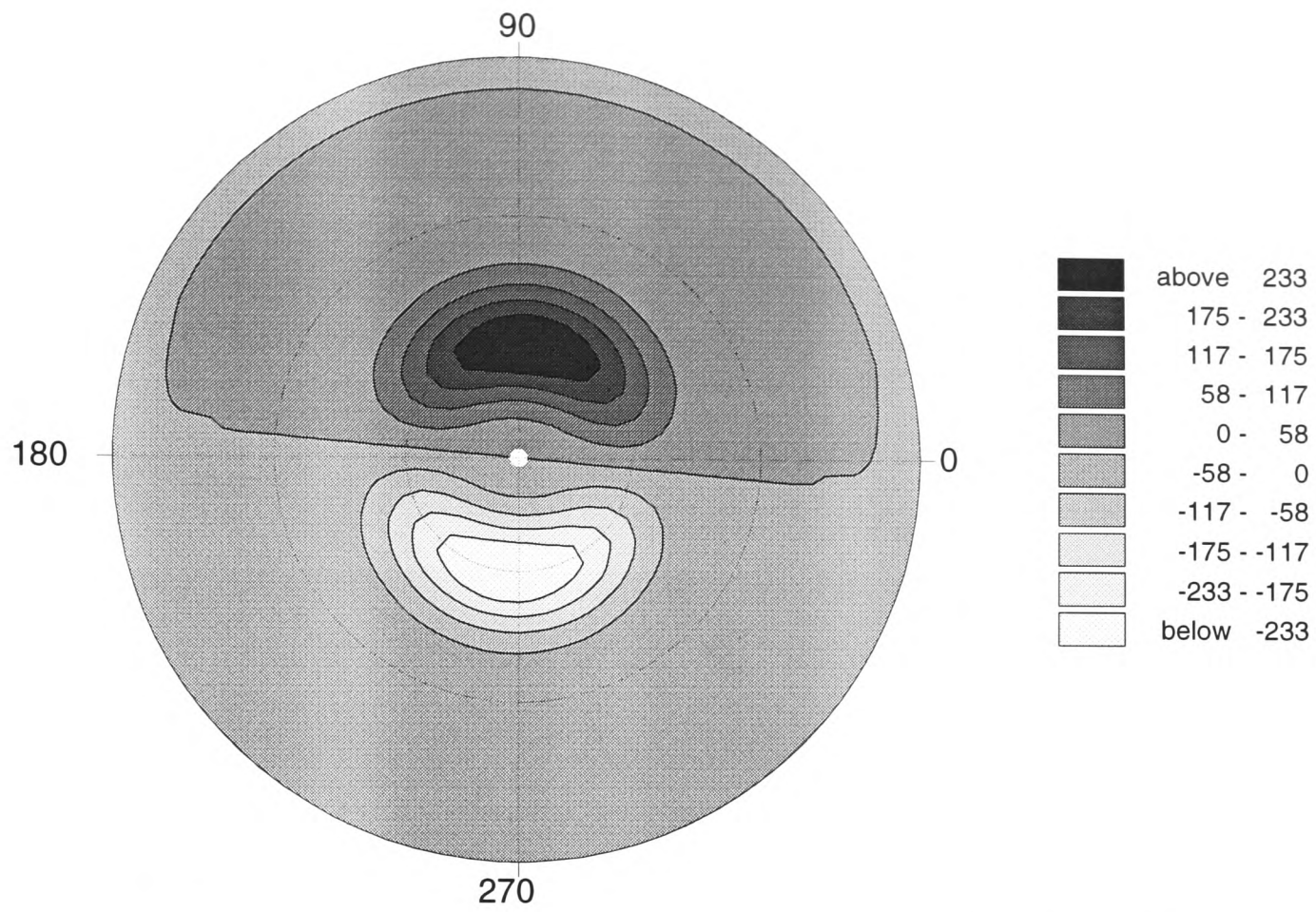

Figure 7.15: The geopotential height signature (in metres) added to the bottom boundary for the run with a wavenumber one perturbation on the bottom boundary.

vortex.

If, instead of this Gaussian-shaped perturbation, a wavenumber one disturbance is added at 60° north, the nature of the run changes significantly. Figure 7.15 shows the geopotential forcing for a 300m amplitude wavenumber one in the geopotential. Figure 7.16 shows the resulting latitude-time field at 32 km. It can be seen that this run has frequent strong reversals in the polar winds. This is very much in contrast with the undisturbed plot shown in figure 7.9. The wave amplitudes forced are shown in figure 7.17 are of similar size to those shown in figures 7.11 and 7.12. Warmings still occur, albeit not so frequently (or regularly) if the wave amplitude of the wavenumber one geopotential perturbation is reduced as far as 150m.

It was found that if the amplitude of the planetary wave forcing was raised to a very high value (the value used was 550m) then warmings are observed with the Gaussian-shaped forcing. A study of this dependence of the model polar response to the details of the supplied planetary waves would be an interesting investigation in another project. Another extension of the work performed in this thesis would be to force a wavenumber

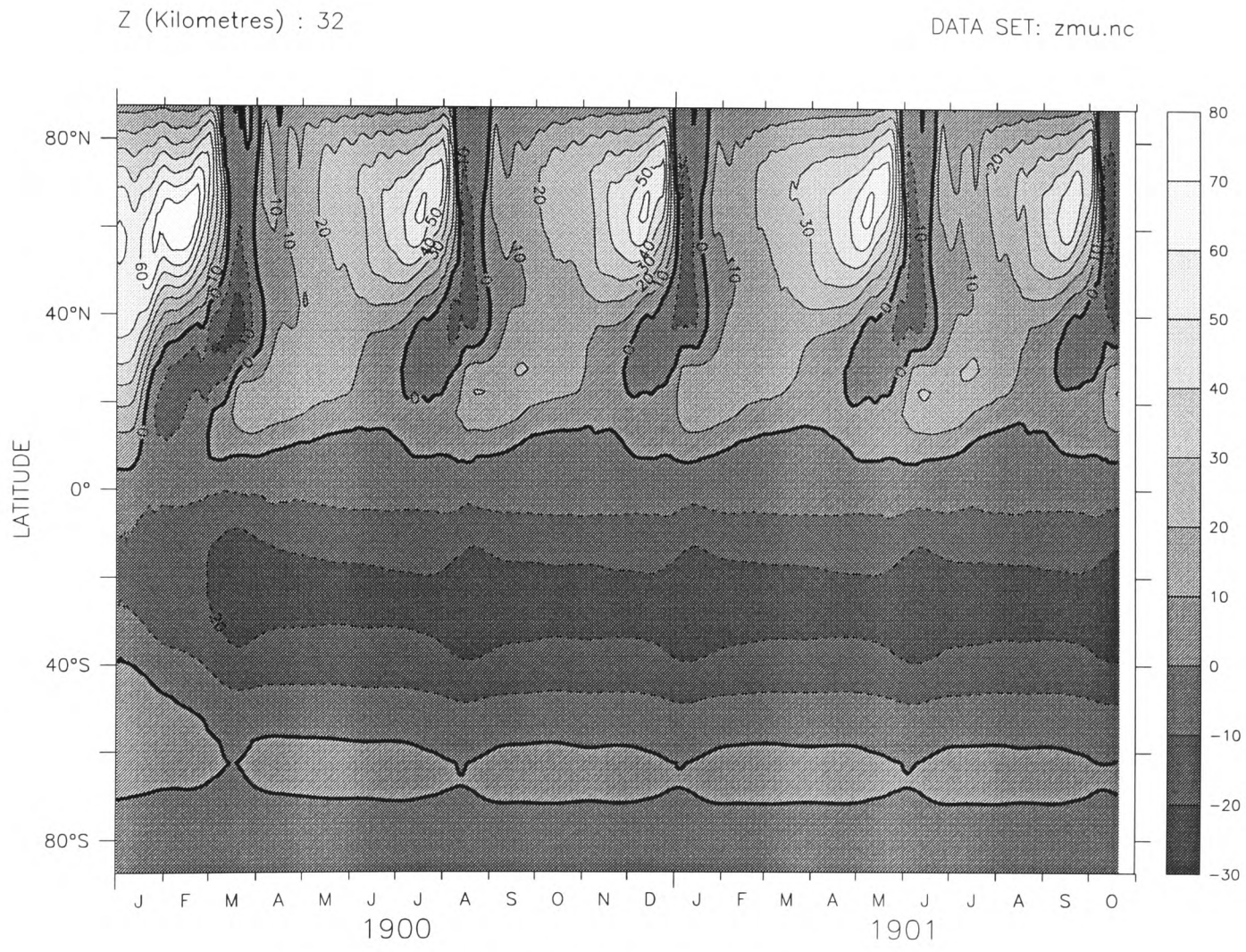

Figure 7.16: A latitude–time plot of the zonal mean u-wind (in ms^{-1}) at 32 km altitude ($\sim$10 hPa) for a model run in which a 300m wavenumber one disturbance has been added to the bottom boundary of the model at 60° north. The modelled polar vortex undergoes regular reversals in zonal mean u-wind.

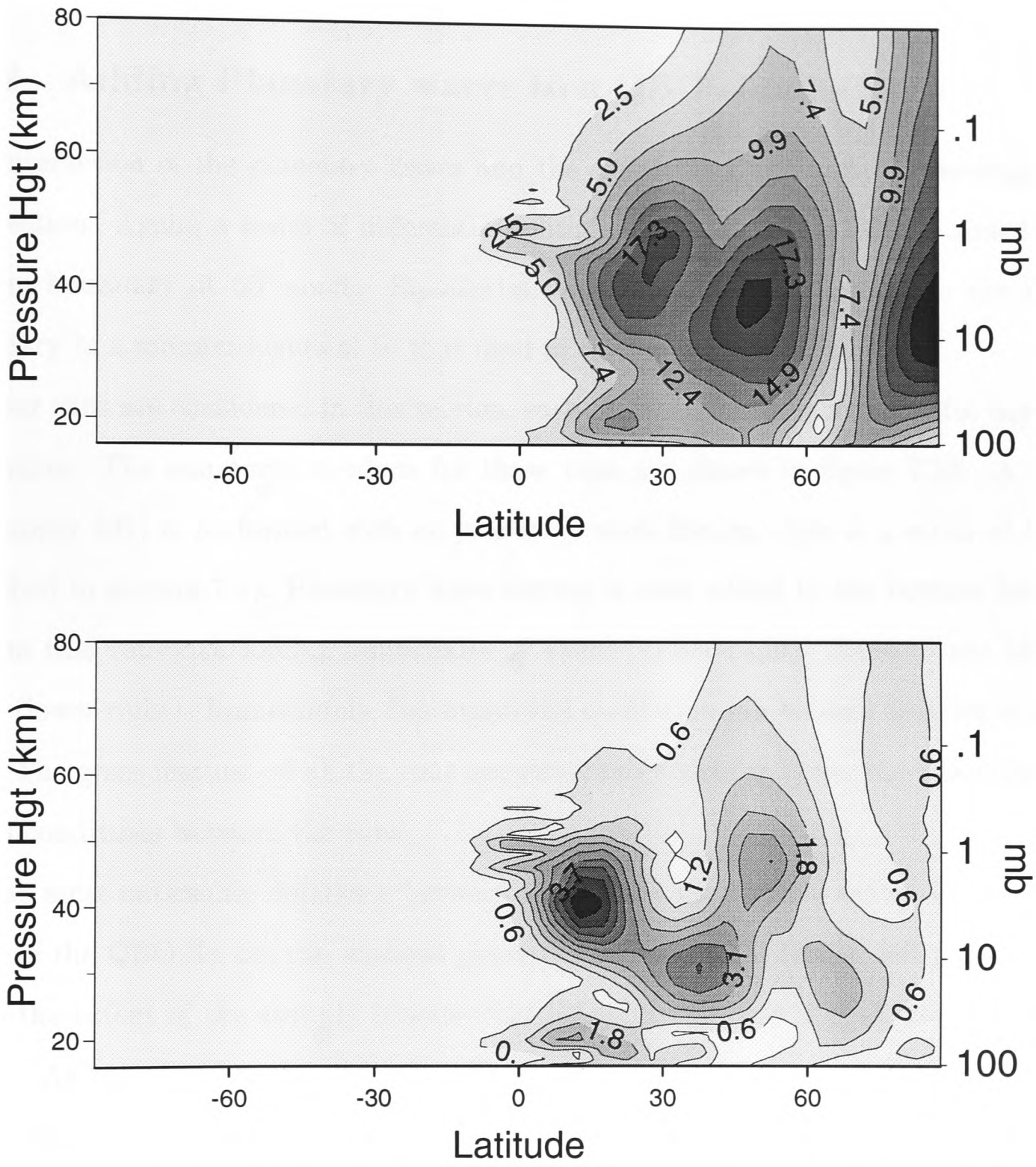

Figure 7.17: Amplitudes of wavenumber one (above) and wavenumber two (below) in the u-wind for the control run with a wavenumber one extra-tropical wave added to the bottom boundary.

one planetary wave, along with the QBO oscillation and look for a QBO modulation in the frequency of the stratospheric warmings produced. It might be expected that there would be some relation between the QBO phase and the frequency and/or severity of the polar warmings.

7.2.2 Adding Planetary waves to a QBO simulation

The interaction of the planetary waves and the simulated QBO is to be investigated in this section. Again, a series of different amplitude planetary waves will be added to the bottom boundary at 60° north. Equatorial forcing will also be applied to the bottom boundary in a manner identical to that used in section 7.1.

Four runs are considered in this section, each of which features a successful equatorial oscillation. The equatorial $\overline{u}$-winds for these runs are shown in figure 7.18. A control run (upper left) is performed with no planetary wave forcing (this is a rerun of the run described in section 7.1). Planetary wave forcing is then added to the bottom boundary used in this run with forcing amplitudes of 150m (upper right), 250m (lower left) and 400m (lower right). Immediately, the equatorial oscillation can be seen to exist in all four runs. The gross features of all the runs are remarkably similar, given the variation in the model conditions between the runs.

The most noticeable difference between the runs is the vertical extent of the easterly phase of the QBO. In the run without planetary waves forced, (upper left panel in figure 7.18), the extent of the easterly is somewhat limited, with only a weak oscillation below 26 km. As the planetary wave amplitude is increased from zero, to 150m and then to 250m, the amplitude of the easterly oscillation below 26 km is significantly increased. Interestingly, with 400m amplitude planetary wave forcing, this effect is not observed and the extent of the easterly wind zone appears to be smaller than in the smaller planetary wave amplitude runs.

Figure 7.19 shows the zonal mean u-wind against time and latitude at an altitude of 26 km for the four runs. The arrangement of the runs is the same as in figure 7.18, with planetary wave amplitudes of 0m (upper left), 150m (upper right), 250m (lower left) and

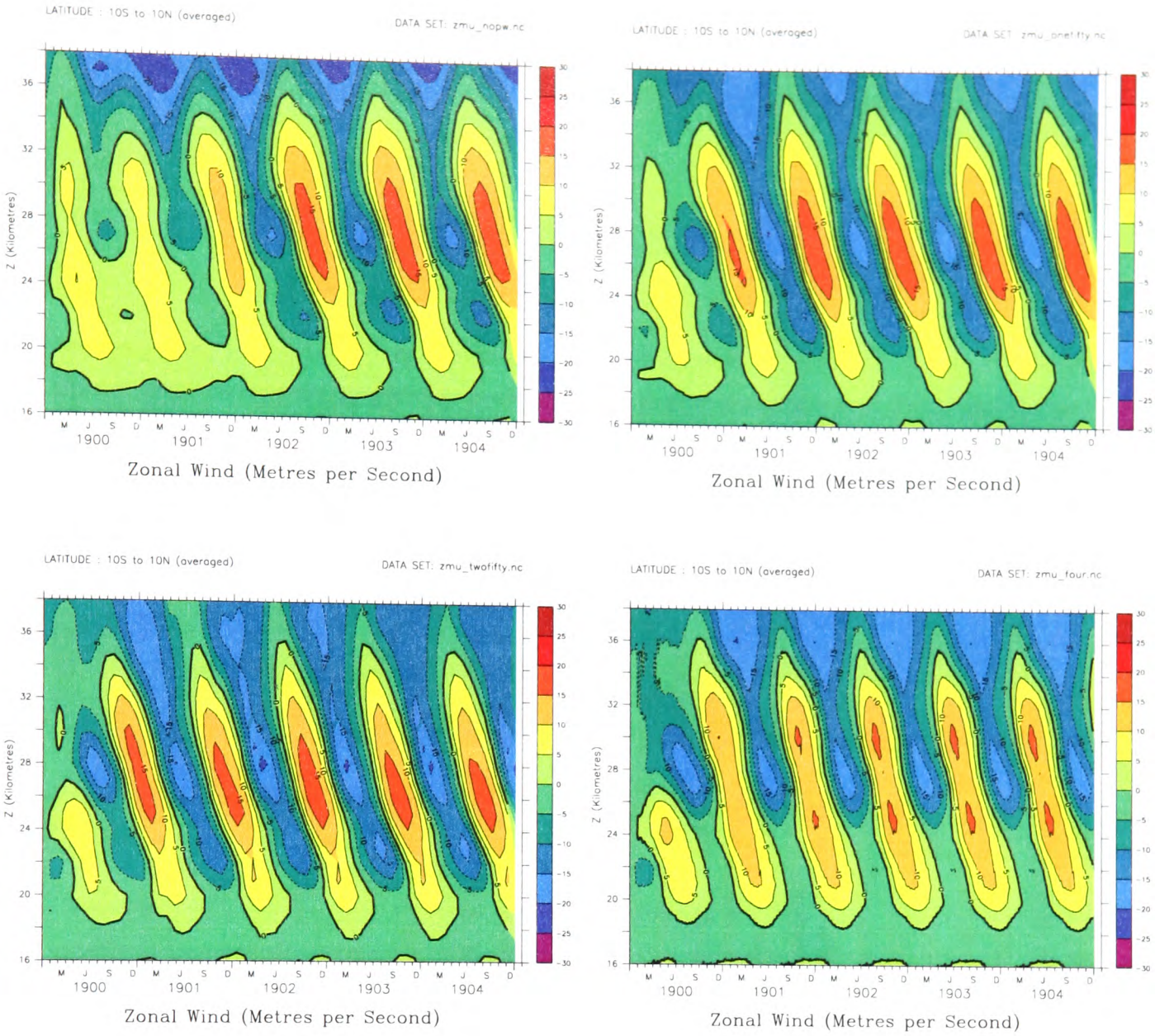

Figure 7.18: Zonal mean equatorial u-wind (in ms^{-1}) for the four different amplitude planetary wave runs. The amplitude of the planetary wave forcing for each run is: control run, 0m, (upper left), 150m (upper right), 250m (lower left) and 400m (lower right). The $\overline{u}$-wind is averaged between 10° north and south. The contour intervals and shading are the same in the four plots.

400m (lower right). The difference in the zonal wind, as observed in the control runs shown in figures 7.13 and 7.14, can be clearly seen in the model extra-tropics. It is quite striking that despite these changes away from the QBO jets, there appears to be very little variation in the QBO jets between the plots.

As the experiments were being planned, it was not known how the modelled QBO would be affected by the addition of the planetary waves. It was considered a strong possibility that the equatorial oscillation would not be generated as the planetary wave amplitudes were increased. This is obviously not the case. This is maybe not that surprising given that the changes in the zonal-mean u-winds seen in the control runs (shown in figures 7.13 and 7.14) were very small in the equatorial lower stratosphere.

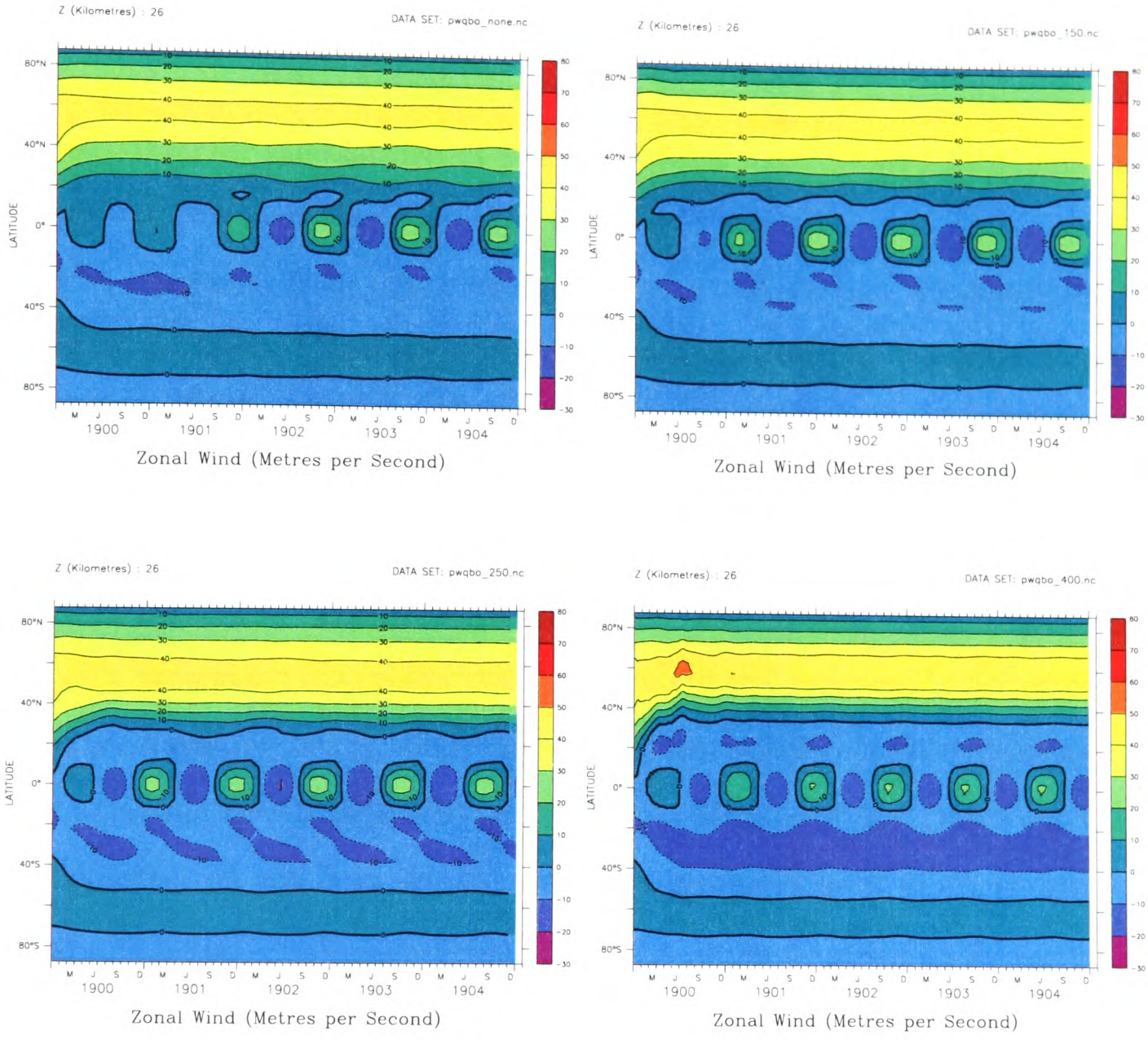

Figure 7.19: The zonal mean u-wind (in ms^{-1}) against latitude and time at an altitude of 26 km for the four runs performed. As in figure 7.18, the panels are arranged as follows: control run, no planetary waves, (upper left), 150m planetary waves (upper right), 250m planetary waves (lower left) and 400m planetary waves (lower right). The changes in the zonal wind in the sub-tropics and mid-latitudes is evident, but the QBO jets are very much unaffected by the planetary waves.

O'Sullivan [1997*a*] suggests that a possible consequence to the addition of planetary waves might be a reduction in the width of the QBO jets. There is no discernible change in the width of the QBO jets seen in the model. O'Sullivan [1997*a*] also observes that the response of a tropical jet to planetary wave forcing is sensitive to the horizontal resolution of the model. His results suggest that in the case where the planetary waves are being well resolved, the planetary waves will have little influence on the tropical jet. No experiments were performed with different horizontal resolution so such a sensitivity could not be investigated. Overall, the addition of planetary waves has had very little effect on the modelled QBO. This is of course an interesting result in itself.

It can be concluded from this work that planetary waves play no significant role in the forcing of the QBO. Planetary waves have been suggested as one possible source of the additional easterly momentum that appears necessary generate a QBO with realistic amplitudes of equatorial waves [Dunkerton, 1983], although later work [Takahashi and Holton, 1991] suggests that Rossby waves are not effective at generating a QBO-like oscillation. In the control runs (presented in section 7.2.1), the addition of planetary waves produces only very small changes in the zonal wind in the lower equatorial stratosphere. The planetary waves are largely dissipated outside the tropical region or propagate above the levels at which the QBO oscillation is present. It appears the planetary waves are having little effect on winds in the tropical lower stratosphere with or without a QBO present.

7.2.3 The Effect of the QBO and the Planetary Waves

As well as the effect, or lack of effect, that the planetary waves are having on the QBO, it is interesting to look at the effect of the QBO on the planetary waves. It might be expected that there would be some modulation of the waves propagating into the tropics as a result of the QBO in the zonal winds.

This is found to be the case, although the effect is somewhat difficult to isolate. In order to look at the effects of the QBO on the propagating planetary waves, a limited period of the 250m planetary wave run is selected to be analysed in more detail. The

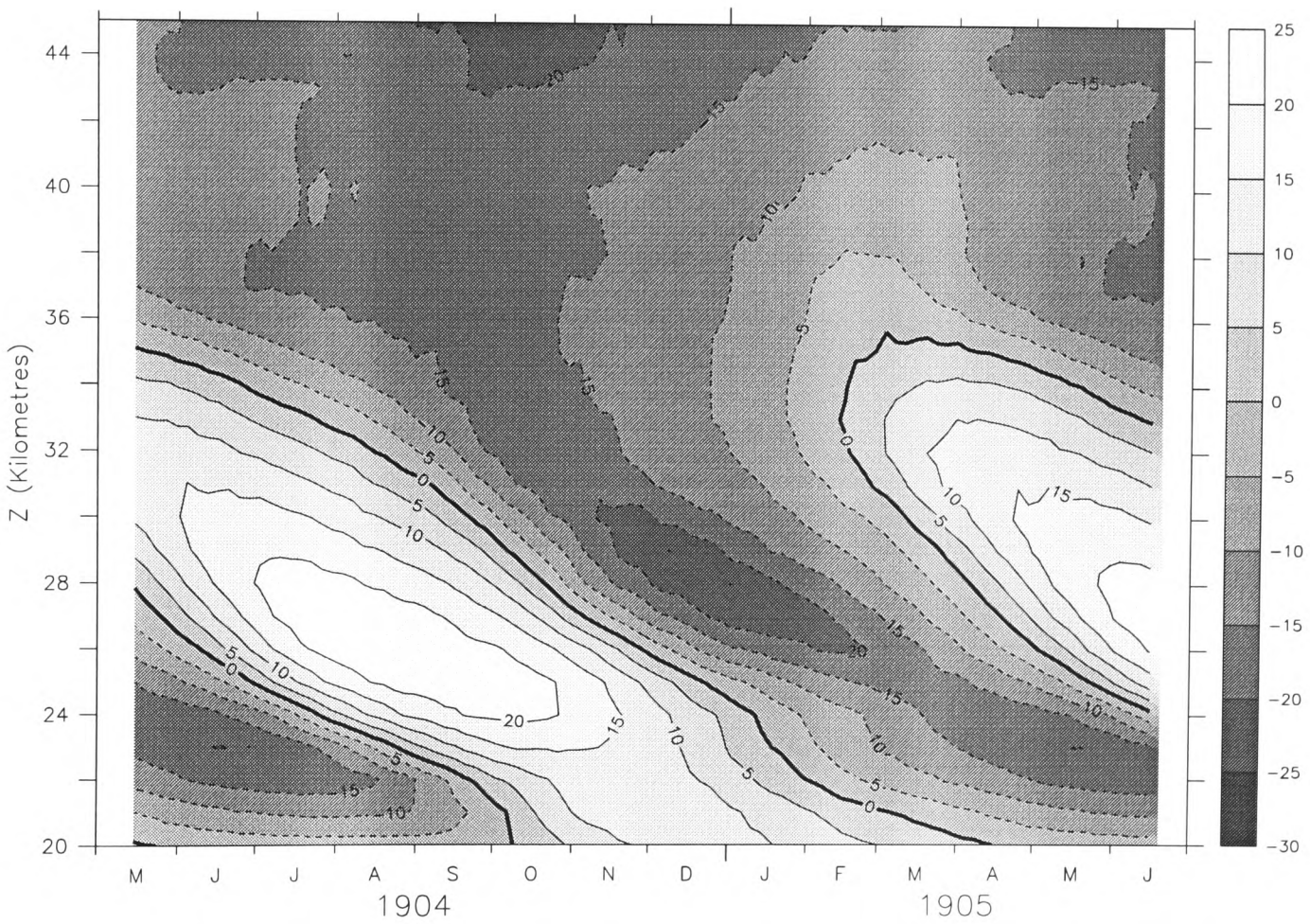

Figure 7.20: The zonal mean u-winds for the period selected for further analysis into the effect of the QBO on planetary wave propagation. The date used for the westerly jet case is 23/8/04 and 19/2/05 is used as the easterly jet case. The zonal wind profiles on these days are shown below in figure 7.23.

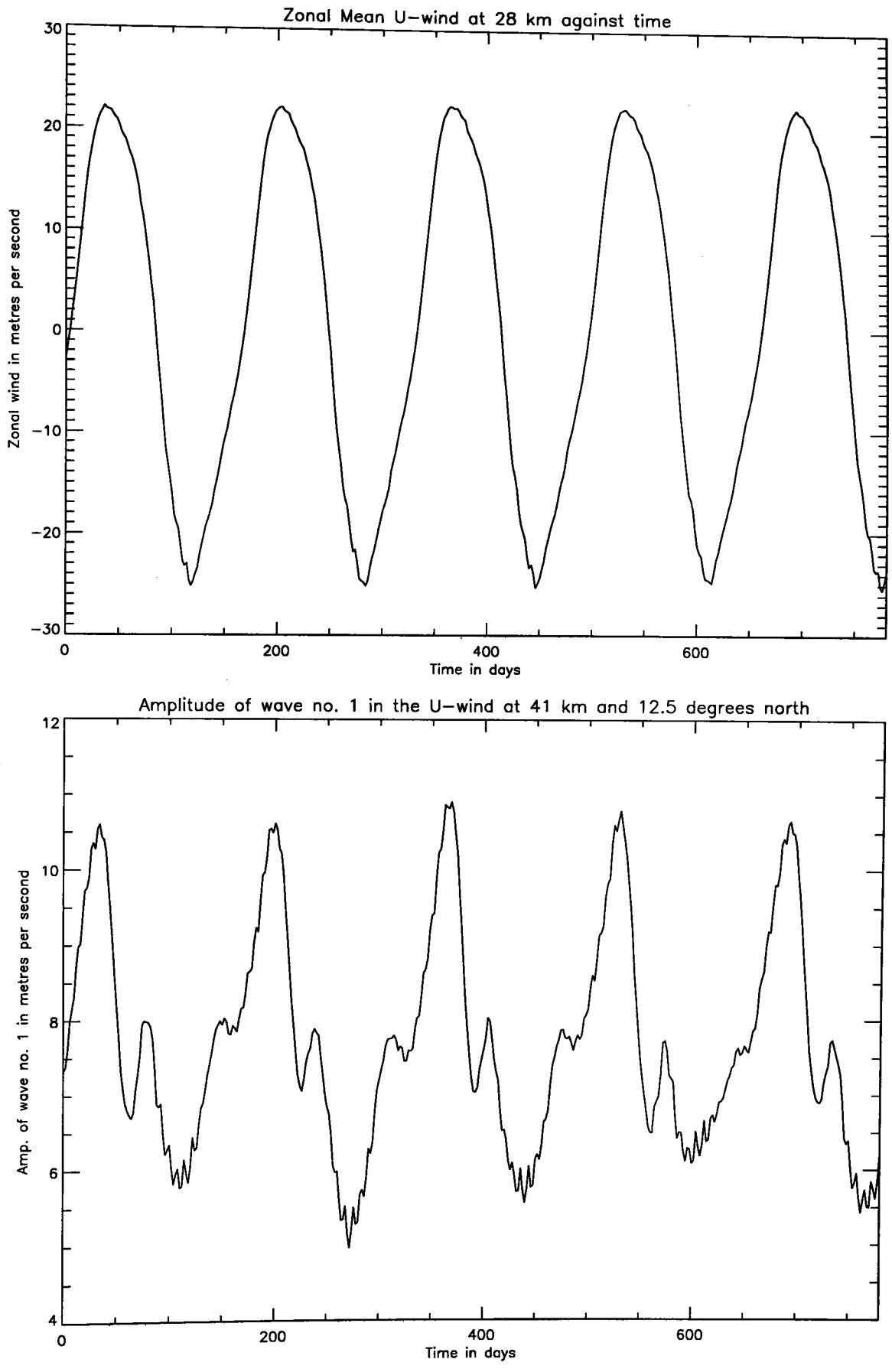

Figure 7.21: The upper panel shows the variation in the equatorial zonal mean u-wind (in ms^{-1}) against time at 28 km altitude. The bottom shows the amplitude of the wavenumber one (again in ms^{-1}) against time at 41 km altitude and 12.5° north.

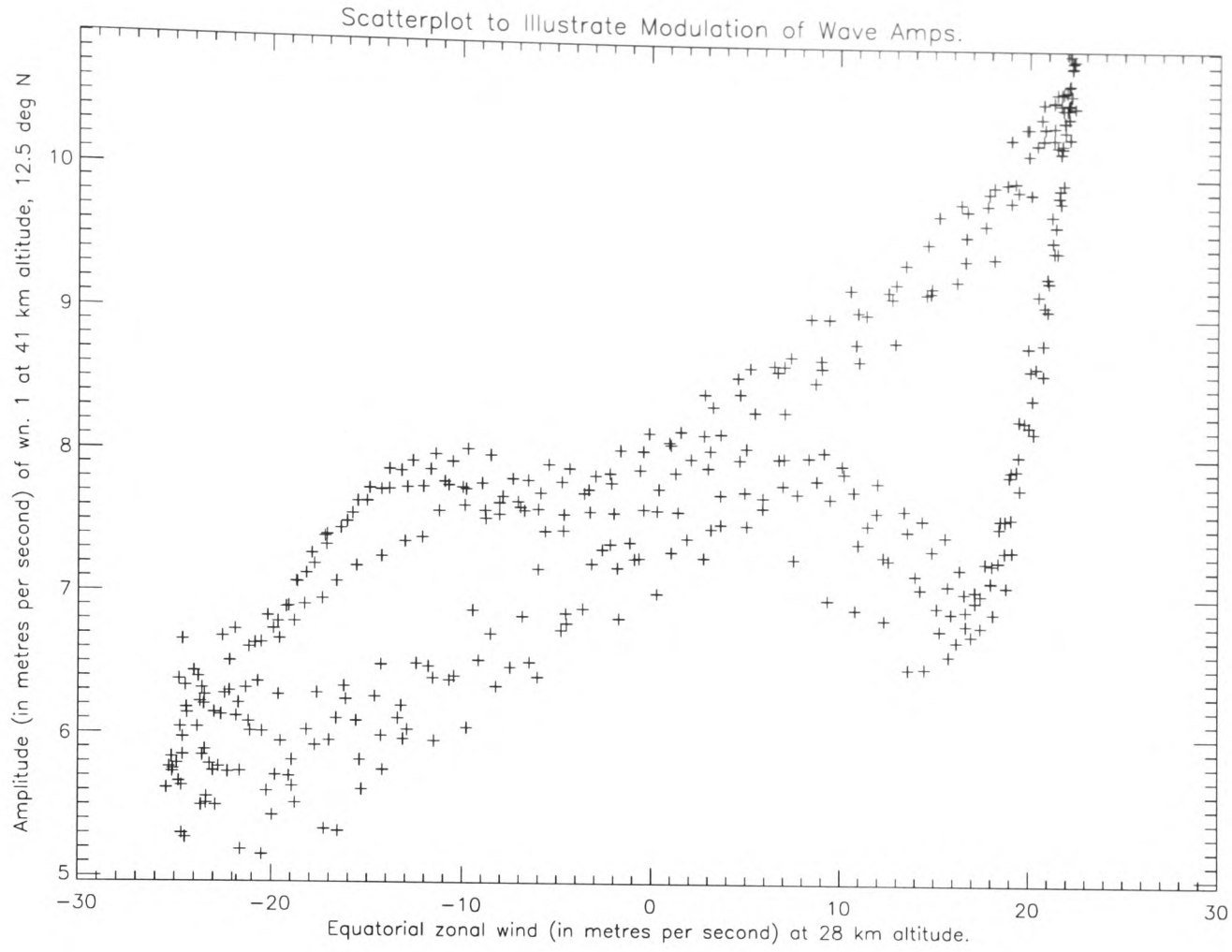

Figure 7.22: A scatter plot showing the amplitude of zonal wavenumber one planetary waves against the equatorial zonal wind. Both axes are in units of metres per second. There is a clear signal of the QBO on the wave amplitude. The points do not lie on a single line due to the slightly different shapes of the oscillation in the u-wind and the amplitude of the planetary waves as shown in figure 7.21.

equatorial zonal mean winds over this period are shown in figure 7.20. Where individual days have been taken to represent opposite phases of the QBO, the dates of these days are the 23rd of August 1904 for the westerly phase and the 19th of February 1905 for the easterly case. These dates are of course relative to the model start date of the 1st of January 1900 and not representative of the atmospheric state in these actual dates.

Perhaps the clearest indicator of the variation in the planetary wave propagation can be seen in the amplitude of the wavenumber one u-wind observed at around 12° north and 40 km in altitude. This variation can be seen in figure 7.21 where the modulation in the amplitude of wavenumber one by the QBO is shown. The upper panel shows the equatorial zonal mean u-wind at an altitude of 28 km. This trace shows the familiar QBO signal seen in the model. The lower panel shows the amplitude of wavenumber one observed in the u-winds at an altitude of 41 km and a latitude of 12.5° north. A clear

QBO signal is seen in the plot. It is worth checking that this signal is not an artifact caused by equatorial waves propagating to this height. If the same region is observed in the run with no planetary wave forcing then the amplitude of the wavenumber one in the u-winds is only around $3\,\mathrm{ms}^{-1}$. This modulation of the planetary wave amplitudes is illustrated in another way in figure 7.22, where the two traces in figure 7.21 are plotted against each other.

Two single days from this period are chosen to be examined in more detail. The zonal u-winds are plotted against longitude and height for these two days in figure 7.23. These days are taken to represent the easterly and westerly phases of the QBO. The EP-fluxes for these days are shown in figure 7.24 and the difference between these two days is shown in figure 7.25.

It can be seen that apart from the difference in QBO jets, there is not much difference between the zonal mean winds shown in figure 7.23. The EP-fluxes shown in figure 7.24 are however quite different. There is some noise in the lower tropical stratosphere due to the equatorial waves, but outside this region, it can be seen that there is a much enhanced upwards and equator-wards EP-flux.

7.3 Summary

7.3.1 Adding MIDRAD to the model

Largely due to the variation in the QBO period observed as the Newtonian cooling reference temperature profile was adjusted in section 6.3, the MIDRAD radiation scheme was reintroduced into the model. The modelling performed with MIDRAD reinstated is described in section 7.1. In order to generate a realistic QBO, it was found to be necessary to introduce a Rayleigh friction term acting on the zonal mean flow to dissipate persistent westerlies in the lower few levels of the model. With this modification made, the QBO is seen to be fairly well modelled in, for example, figure 7.2. With MIDRAD successfully reintroduced to the model, and the model producing an equatorial, QBO-like oscillation, the system is ready to be used for further studies of the modelled QBO.

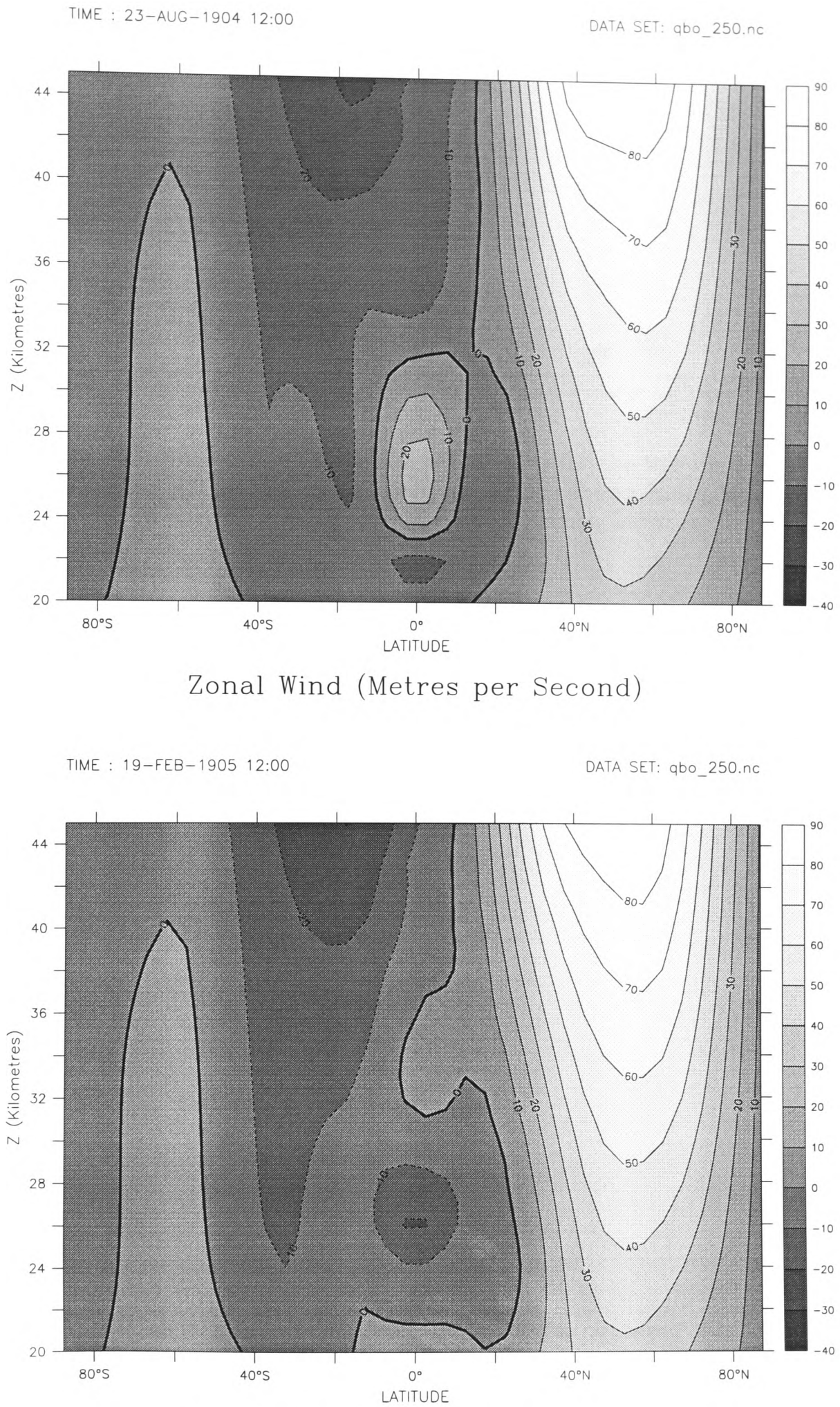

Figure 7.23: The zonal mean structure of the u-winds (in ms^{-1}) for the days selected as the westerly (above) and easterly (below) QBO jets.

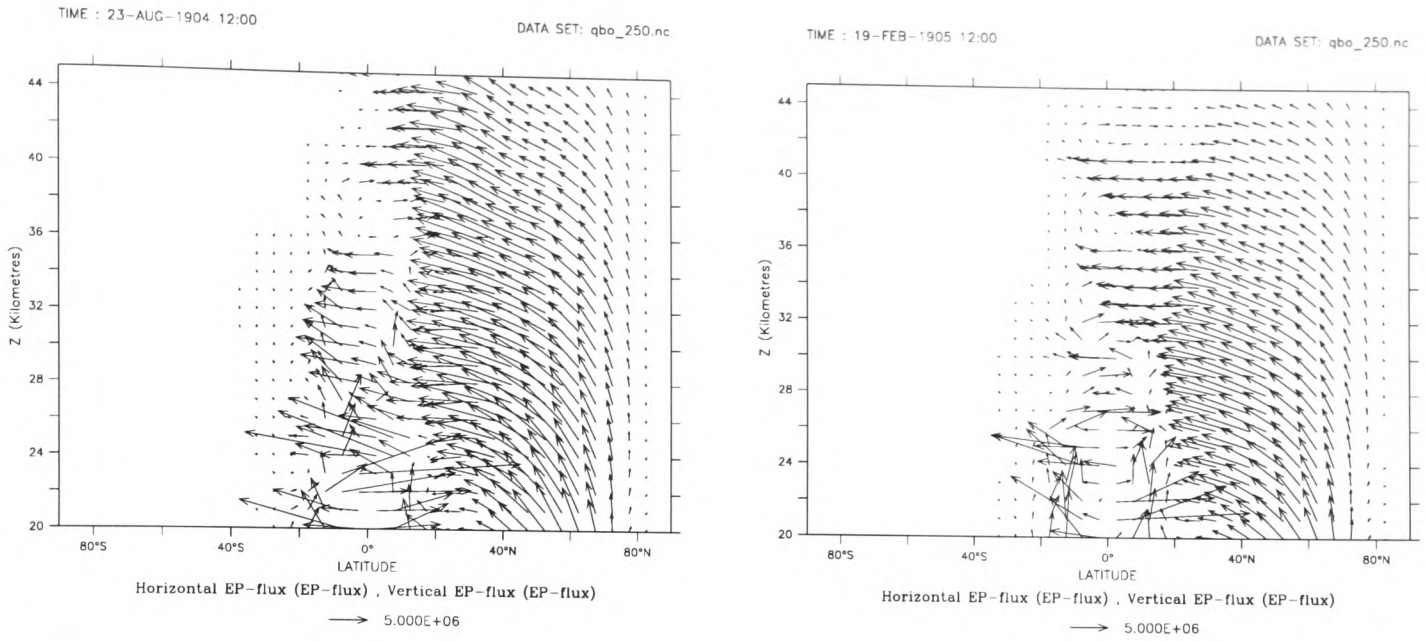

Figure 7.24: EP-flux vectors (the units are m^2s^{-2}) for the two model days shown in figure 7.23. The EP-flux for the westerly jet case is shown in the left-hand panel, the easterly jet in the right-hand panel. The difference between the EP-fluxes is shown in figure 7.25.

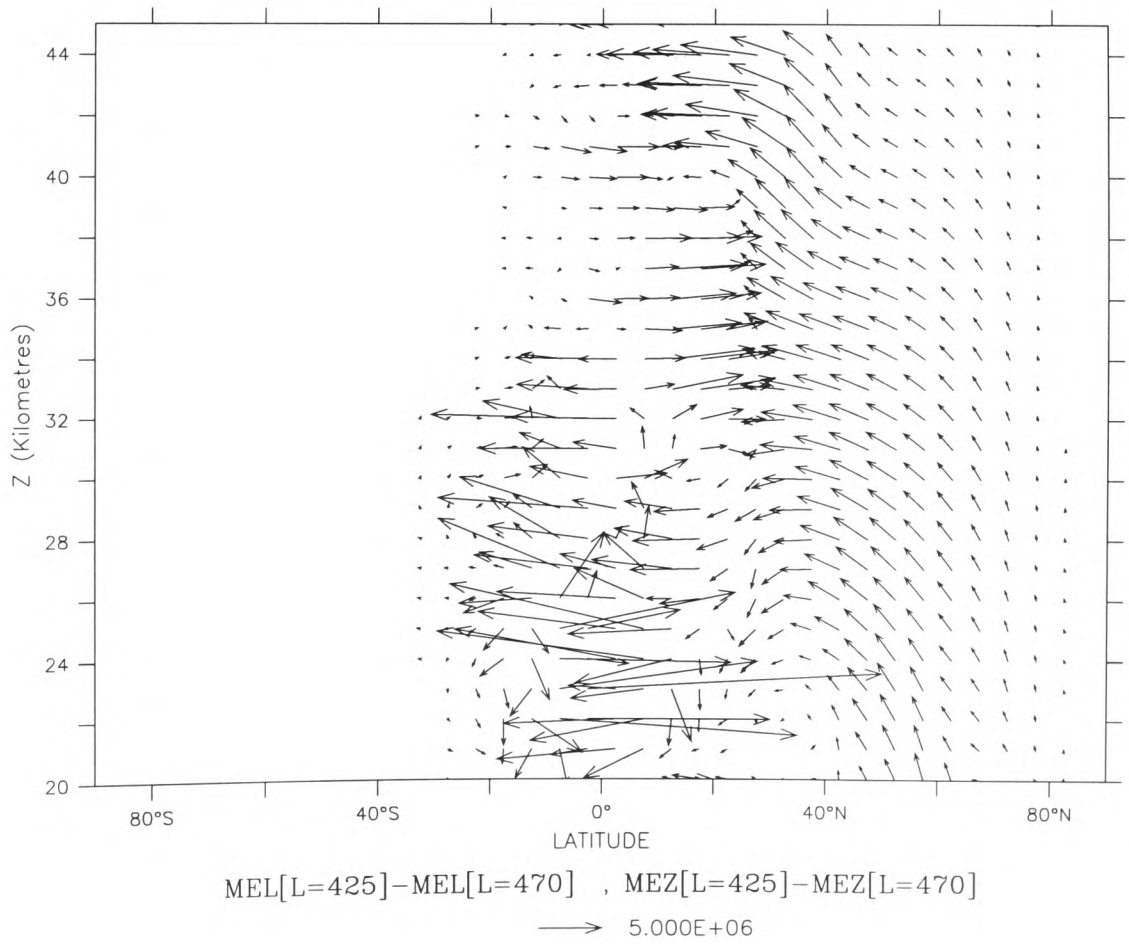

Figure 7.25: The differences in EP-flux between the westerly and easterly phase of the QBO. The vectors show the right-hand panel subtracted from the left-hand panel of figure 7.24. It can be seen that there is considerably more wave activity propagating upwards and equator-wards in during the westerly phase of the QBO.

7.3.2 Modelling Planetary Waves and the QBO

Planetary waves are added to the model simulations in section 7.2. This is done under several different model conditions. Initially, runs are performed with no equatorial forcing applied and the effect of the planetary waves on the zonal mean u-wind is observed. Following this, a series of runs are performed where varying amplitudes of planetary waves are added to the model with equatorial forcing applied.

Figure 7.9 shows the time evolution of the zonal mean u-winds at 32 km following the introduction of 400m planetary waves. It is interesting to note that the model settles down to a very undisturbed state after several months of this run. This is perhaps slightly surprising as other studies suggest that polar warmings might be expected when planetary waves of these amplitudes are added to the model extra-tropics. These warmings are however observed in the model when much larger amplitude planetary waves are forced or the shape of the planetary wave forcing is changed. A series of plots, shown in figures 7.13 and 7.14, show the effects of planetary waves of amplitudes 150, 250 and 400m on the mean flow. The strongest signal in these plots is a deceleration of the zonal wind in the northern hemisphere low latitudes, which is associated with the dissipation of these planetary waves. There is very little change in the zonal winds in the equatorial lower stratosphere.

Planetary waves of various amplitudes are then added to the model while equatorial waves of the type used to generate a QBO are being forced. This allows an investigation of the interaction of planetary waves and the QBO under very controlled circumstances. It is found that a QBO is generated in all of these runs. There is very little difference between runs with large variations in planetary wave forcing. The investigation of the effect of the planetary waves on the QBO leads to the conclusion that the planetary waves have very little effect on the QBO. This would indicate the planetary waves are not an important contributor to the forcing of the QBO in the real atmosphere. From a modelling point of view, it means that when attempting to model the QBO in a model (and possible attempting to diagnose the failure of a model to generate a QBO), an investigation of the planetary waves present in the model is unlikely to be useful.

In section 7.2.3, the QBO is seen to have significant effects on the propagation of the planetary waves. This is seen most strongly (as shown in figures 7.21 and 7.22) in the modulation of wavenumber one in the upper stratosphere in the northern hemisphere low latitudes. The effect is seen throughout the northern hemisphere in, for example, vectors of EP-flux as shown in figures 7.24 and 7.25. This result is a confirmation that the QBO can modulate the planetary waves in the northern hemisphere without being radically altered itself. Such a modulation implies that it is possible that the QBO could influence the circulation in the northern hemisphere (such as stratospheric sudden warmings) through changes in the planetary wave propagation. The modelling studies do not provide any evidence that such the Holton-Tan mechanism is responsible for the QBO signal seen in the stratospheric sudden warmings but shows that it is possible.

Chapter 8

Conclusions and Future Work

In this thesis, the UKMO stratosphere-mesosphere model is modified in several ways to allow a QBO to be modelled. Having developed the model to a stage where a robust QBO is observed, further experiments are performed to investigate the properties of the modelled QBO. The results from these runs can be used to address the questions posed in chapter 1.

8.1 Conclusions

Modelling Equatorial Waves Equatorial waves are successfully modelled in the SMM. The chief modification to the model which allows them (especially the shorter vertical wavelength Rossby-gravity waves) to be modelled is an increase in the model's vertical resolution. This is a result which has implications for other models in which equatorial waves and the QBO are to be simulated.

Results in chapter 5 indicate that a vertical resolution of 1 km is adequate to resolve the equatorial waves thought to play a role in the forcing of the QBO. An increase in vertical resolution to 500m is not found to change the simulation of these waves significantly, suggesting that there is little to be gained in increasing the model resolution beyond the 1 km resolution used in the majority of the runs described in this thesis.

As the equatorial waves are dissipated, they produce accelerations in the zonal flow. The jets produced are in the direction of the wave's phase velocity, in agreement with expectations. These jets will in later experiments become the jets that make up the QBO oscillation.

Experiments are performed to investigate the propagation of the waves under different conditions. The waves are launched into regions of background zonal wind, and the vertical propagation of the waves is found to be strongly inhibited when the background wind is in the same sense as the wave's phase velocity. This is in good agreement with theory. The radiative damping rate is altered in the model, and this is seen to have a very strong influence on the propagation of waves, indicating that the dissipation of the waves is predominantly through radiative processes rather than mechanical damping or wave breaking.

In conclusion, equatorial waves are well modelled in the SMM provided that a vertical resolution of 1 km or better is used. As they are dissipated, equatorial jets are produced in the model. This result and the behaviour of equatorial waves propagating through background zonal winds, suggest that a combination of equatorial waves forced in the model are likely to be able to generate a QBO.

Initial Modelling of the QBO A combination of Rossby-gravity and Kelvin waves are forced in the model, which is relaxed towards an isothermal background temperature. In this run, the model does a fairly good job at producing a realistic QBO. Descending zones of easterly and westerly wind are clearly seen over the equator. The modelled QBO has a good latitudinal structure and captures meridional and vertical winds associated with the QBO. The modelled QBO is however not entirely realistic for several reasons: the period is too short (15 months) and the height range over which it is produced is too high (30–50 km as opposed to 17–32 km in the real atmosphere). The height range in particular is found later to be a consequence of the simplified temperature structure of the model atmosphere.

Equatorial wave amplitudes used in this run are compared to the amplitudes observed and it is found that Kelvin waves are being forced at approximately realistic

amplitudes. The Rossby-gravity waves are being forced at approximately double the observed amplitude (although the observations are subject to a very large uncertainty), suggesting that gravity waves or some alternative source of momentum must play a significant role in generating the easterly phase of the QBO.

In conclusion, the oscillation simulated in this run suggests that equatorial waves may well be able to generate a realistic QBO. The amplitude of the Rossby-gravity waves needed would suggest that equatorial waves are not the sole driving force for the QBO in the real atmosphere. The model state in these runs is not particularly realistic (model temperatures are being relaxed towards an isothermal reference temperature profile) which means that more detailed comparisons between the modelled QBO and the real QBO were not performed.

Vertical Temperature Structure Having produced a QBO-like oscillation in the model with temperatures relaxed towards an isothermal reference profile (set at 140 K), more realistic reference temperature profiles are used in the Newtonian cooling scheme. The addition of a realistic temperature profile has the effect of lowering the altitude of the QBO from 30–50 km to around 18–40 km. This change in altitude is due to the altered vertical temperature gradient, specifically the associated increase in buoyancy frequency, N, and the subsequent reduction in the vertical group velocity of the equatorial waves.

Experiments With Different Temperature Profiles In the experiments performed to add a realistic temperature profile to to the Newtonian cooling scheme, it was noticed that the period of the modelled QBO was sensitive to different temperature profiles. The crucial difference between the two profiles, one of which produced an oscillation of period 16 months and the other an oscillation of period 32 months, was a difference in temperature of around 4 K throughout the tropics and the summer hemisphere. Experiments show that the important change between the two simulations is in the tropical vertical residual circulation. The run with a warmer summer hemisphere has increased ascent in the tropics which acts to retard the descent of the QBO jets and hence increase the period of the QBO.

These experiments are somewhat unrealistic as the temperature profiles are created through adding artificial perturbations to an existing, fairly realistic temperature profile. The experiments do however show the sensitivity of the modelled QBO to the background circulation. Ascent in the tropics is known to be deficient in the standard version of the SMM and has been shown to be sensitive to changes in the model configuration such as gravity wave parameterisation and model lid height [Lawrence, 1997]. It is notable that in almost all the experiments performed in this project, the QBO period obtained has been significantly shorter than two years. These results show that the amount of ascent in the tropics is likely to be responsible for this. As well as demonstrating the direct effect of tropical ascent on the QBO, the results emphasise the importance of considering the circulation of the atmosphere as a whole even when considering a single phenomenon.

Reinstating `MIDRAD` into the Model `MIDRAD` was reintroduced to the model and the QBO was again forced. It was found necessary to introduce an extra friction term to the zonal wind in the lowest three levels of the model in order to prevent persistent westerlies from existing. Having done this, the QBO was successfully generated in the model with `MIDRAD` in place.

Planetary Waves Planetary waves are generated in the model through the addition of a stationary, Gaussian-shaped perturbation to the model's lower boundary. This forcing is applied at a variety of amplitudes, initially without equatorial waves forced. Planetary waves are observed in the model, and their influence is clearly observed in the middle atmosphere circulation.

With the QBO forced through the addition equatorial wave forcing, it is seen that the planetary waves have little effect on the propagation of the QBO. This is strong evidence that planetary waves play no significant role in the forcing of the QBO.

A significant QBO signature is seen in the propagating planetary waves. This is interesting as it confirms that a QBO modulation of the planetary waves is possible, as required by the Holton-Tan [Holton and Tan, 1980] mechanism to explain the

apparent connection between QBO phase and stratospheric sudden warmings. The results described in this thesis do not, however, provide any direct evidence that is it the Holton-Tan mechanism by which the QBO signal is being transported to the polar stratosphere.

In summary, equatorial waves and the tropical stratospheric QBO have been fairly well modelled in a three dimensional primitive equation model. Planetary waves have then been forced into the model and the interaction between planetary waves and the QBO is observed. Several key conclusions are drawn:

- Vertical resolution must be 1 km or finer to support the equatorial waves thought to force the QBO. At this resolution, the waves are well modelled and have properties that match the theoretical predictions very well.

- Equatorial waves can force a realistic QBO, but the amplitude of Rossby-gravity waves required is larger than that observed. Planetary waves are shown to have little effect on the QBO, making it more likely that gravity waves will provide the additional forcing required.

- The QBO simulation is sensitive to other aspects of the model simulation. In these studies, a sensitivity is found to both the temperature stratification and the background circulation. Such factors must be considered as well as the equatorial waves when analysing a QBO simulation in a model.

- Planetary waves have little direct effect on the equatorial QBO. They are unlikely to be important in the forcing of the QBO and seasonal variations of the planetary wave amplitudes are unlikely to contribute directly to the QBO variability.

- The QBO has a significant modulating effect on the planetary waves, consistent with the Holton-Tan mechanism [Holton and Tan, 1980] for propagating the tropical QBO signal to the extra-tropics.

8.2 Future Work

The model, with the modifications applied in the course of this project, is one of the most valuable outcomes of the work described here. The QBO is generated in this model through processes that are very similar to those that force the real QBO. This makes the model particularly useful as it may be used to investigate two-way interactions involving the QBO. An example of such an investigation would be to examine the feedback effects of the ozone QBO.

The model would be useful in many areas of future research. These include:

Gravity Waves Gravity waves are thought to play a significant role in the forcing of the QBO. Gravity wave schemes are being developed in this model. It would be interesting to combine the explicit forcing of a equatorial waves such as performed in this project with a gravity wave scheme and try to improve the modelling of the QBO. In particular it might be expected that the easterly jet of the QBO might be better modelled.

Interactive Ozone The addition of an interactive ozone scheme to the model is planned. Runs where the QBO was forced through equatorial wave forcing in the presence of an interactive ozone scheme would be interesting. Ozone feedback effects are thought to have an effect on both the equatorial waves and the QBO itself [Cordero and Nathan, 1998],[Echols and Nathan, 1996].

Varying Wave Amplitudes and a Seasonal Cycle Several interesting experiments may be performed with the model as it is without any serious modifications. A simple experiment would be to force the model with a equatorial waves with a time-varying amplitude. Another experiment would be to run the model with an annual cycle present. Both of these experiments could well force the model to exhibit some inter-cycle variation.

Appendix A

Model Numerics

In order to solve the differential equations that describe the evolution of the atmosphere, these equations must be written in a form that can be numerically manipulated. In this model, the primitive equations are represented on a regular grid in space, and integrated with a constant time-step. The finite difference scheme uses centred differences in both the vertical and time directions. (The horizontal differencing is performed using a fourth order accurate scheme which is not examined in this appendix. Many of the results obtained here are extensible to the fourth order case and this is noted where relevant.) Several aspects of the model's numerical scheme are examined in this appendix, including its stability and accuracy. The vertical differencing is particularly important in this project as a limiting factor in some of the runs has been the vertical resolution of the model. Even in higher vertical resolution runs, the waves modelled are often near the limits of resolution and the effects described in this appendix will be relevant in understanding their representation in the model. The subject of the numerical representation of finite equations is given in more detail in many texts, for example see Haltiner and Williams [1980].

The evolution of a variable Φ can be written in a 'leapfrog' or centred difference scheme as:

$$\Phi(t+1) = \Phi(t-1) + 2\Delta t \times f(\Phi(t)),$$

where the future state (at time $t+1$) of the quantity, Φ, is given by its value at a past

time $(t-1)$ plus an increment which is a function of the present state of Φ (multiplied by $2\Delta t$, where Δt is the increment in time). This numerical scheme has several useful properties that make it suitable for use in a model such as this. It is numerically fairly inexpensive compared, for example, to an implicit scheme. In principle, a model using this scheme must know the model state at three intervals, $t-1$, t and $t+1$. The need to store three levels of model variables can be neatly avoided by overwriting the values of the model state at $t-1$ with the amended $t+1$ values. This means that the model must store variables only at two points in time, which allows the scheme to make efficient use of memory. Compared to other integration schemes available, this scheme has some disadvantages. There are quite strict conditions that must be met if the solutions to the model equations are not to grow exponentially with time. These are described in section A.1. These conditions put tight constraints on the length of the time-step that may be used in the model. The solutions produced are, as with all numerical calculations, approximations to the analytical or real solutions. These are for the most part good approximations but under certain circumstances the errors associated with the scheme are very large.

To illustrate the properties of the leapfrog time-scheme, the partial differential equation

$$\frac{\partial \Phi}{\partial t} + c\frac{\partial \Phi}{\partial z} = 0 \tag{A.1}$$

will be solved both analytically and numerically and the results compared. This equation is known as the 'advection equation'. The general solution of equation (A.1) is well known to be:

$$\Phi = F(z - ct), \tag{A.2}$$

Where F is an arbitrary differentiable function. If a wave-like initial condition is taken such that

$$\Phi(z, 0) = Ae^{ikz}, \tag{A.3}$$

then the solution (A.2) becomes:

$$\Phi(z,t) = Ae^{ik(z-ct)}. \tag{A.4}$$

This equation can now be solved through finite difference methods. The time axis is discretised so that the time variable, t, is replaced by $t = n\Delta t,\ n = 0, 1, 2, 3, \ldots$. Similarly, on the spatial axis, z becomes $z = m\Delta z,\ m = 0, 1, 2, 3, \ldots$. The notation Φ_m^n will be used to represent the variable $\Phi(z,t)$ at time $t = n\Delta t$ and position $z = m\Delta z$. Centred differences in this notation for the quantities $\frac{\partial \Phi}{\partial t}$ and $\frac{\partial \Phi}{\partial z}$ give:

$$\left(\frac{\partial \Phi}{\partial t}\right)_m^n = \frac{\Phi_m^{n+1} - \Phi_m^{n-1}}{2\Delta t} + O(\Delta t^2) \quad \text{and} \quad \left(\frac{\partial \Phi}{\partial z}\right)_m^n = \frac{\Phi_{m+1}^n - \Phi_{m-1}^n}{2\Delta z} + O(\Delta z^2).$$

Substitution into equation (A.1) produces:

$$\frac{\Phi_m^{n+1} - \Phi_m^{n-1}}{\Delta t} = -c \times \frac{\Phi_{m+1}^n - \Phi_{m-1}^n}{\Delta z} \tag{A.5}$$

A solution will be sought to this equation of the form:

$$\Phi_m^n = B^{n\Delta t} e^{ikm\Delta z}. \tag{A.6}$$

Substitution into equation (A.5) and some manipulation gives:

$$B^{2\Delta t} + 2i\sigma B^{\Delta t} - 1 = 0, \tag{A.7}$$

where

$$\sigma = \frac{c\Delta t}{\Delta x} \sin k\Delta x.$$

$B^{\Delta t}$ can be solved from this quadratic expression to give

$$B^{\Delta t} = -i\sigma \pm \sqrt{1 - \sigma^2}. \tag{A.8}$$

A.1 Stability

If $|\sigma| \leq 1$ then $|B^{\Delta t}| = 1$ and there is no exponential growth of the solution. This condition can be assured if

$$\frac{c\Delta t}{\Delta x} \leq 1. \tag{A.9}$$

This condition is known as the Courant-Friedrichs-Levy (CFL) condition and the quantity $\frac{c\Delta t}{\Delta x}$ is known as the Courant number. The CFL criterion sets a limit on the size of time-step that can be used in a model using this numerical scheme. The relation between time-step and resolution means that if the model resolution is increased, the time-step must in turn be decreased, which can result in a model becoming very expensive to run at higher resolutions. Other numerical schemes, especially those which include some influence of the model's future state on the evolution of Φ, can be run stably when the Courant number is greater than one. These schemes are known as implicit schemes and are more expensive to calculate as the equations must be solved simultaneously. There are still problems associated with accuracy in implicit schemes which become very large at high Courant numbers and limit the time-step that may be practically used. It turns out that, compared to explicit schemes, the added complexity and the longer time-steps possible in the implicit schemes approximately cancel and models employing either scheme run at around the same rate.

A.2 Phase Velocity

Equation (A.8) produces two solutions to the equation being solved. These solutions can be written in complex polar form as:

$$B^{\Delta t} = e^{-i\alpha}, e^{i(\alpha+\pi)} \quad \text{where } \alpha = \sin^{-1}\sigma. \tag{A.10}$$

The finite difference solution to equation (A.1) now becomes:

$$\Phi_m^n = \left[Me^{-i\alpha n} + Ee^{i(\alpha+\pi)n}\right] e^{ikm\Delta z} \tag{A.11}$$

or

$$\Phi_m^n = Me^{ik(m\Delta z - \alpha n/k)} + (-1)^n Ee^{ik(m\Delta z + \alpha n/k)}. \tag{A.12}$$

A and E are constants that are to be found from the boundary conditions specified. The two solutions are easily identifiable in equation (A.12). The first solution is referred to as the 'physical mode' and corresponds to the analytical solution, equation (A.4). The second solution is the 'computational mode'. The computational mode reverses sign every time-step and propagates in the opposite direction to the physical mode. This mode is filtered in the model and will not be examined in detail. The properties of the physical mode are of interest as this is the solution that is the model description of the system being simulated. There are some interesting differences between the true (analytical) solution and the finite difference solution. Comparing terms between the physical mode solution,

$$\Phi_m^n = Me^{ik(m\Delta z - \alpha n/k)},$$

and equation (A.4), it can be seen that the finite difference solution produces a phase speed, c_F, that can be written:

$$c_F t = \frac{\alpha n}{k}. \tag{A.13}$$

Remembering that $t = n\Delta t$, and substituting for α, a finite difference phase velocity may be written:

$$c_F = \frac{\sin^{-1}\left\{\frac{c\Delta t}{\Delta z}\sin k\Delta z\right\}}{k\Delta t} \tag{A.14}$$

The relation between the finite difference phase speed and the analytical phase velocity is shown in figure A.1. This figure shows the ratio between the finite difference phase velocity and the analytical phase velocity (which is just c) for waves varying in wavelength from $2\Delta z$ up to $12\Delta z$. Two lines are plotted, at different values of the Courant number. It can be seen that waves of wavelength $2\Delta z$ are stationary in the finite difference solution with longer waves approaching the analytical phase speed. This variation is known as computational dispersion. Interestingly, the phase speed is better represented when the Courant number is higher and in the case where it is equal to 1, the phase speed is exactly correct.

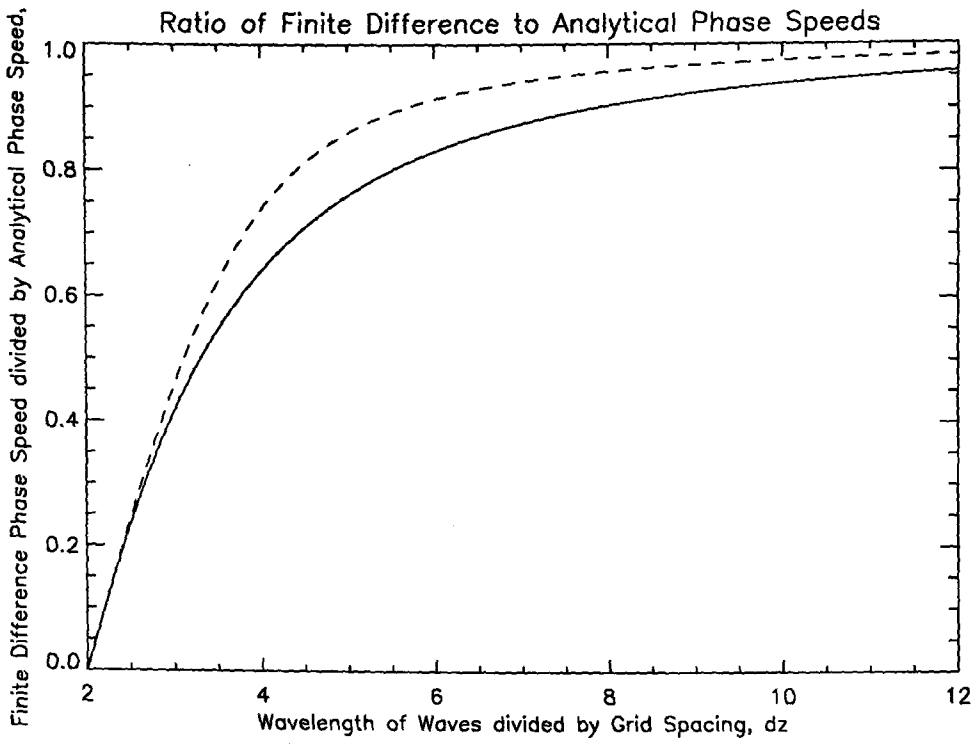

Figure A.1: The ratio between phase speeds calculated in the finite difference approximation, c_F and the analytical solution, c. The solid line is for a Courant number of 0.2 and the dashed line a Courant number of 0.8

A.3 Group Velocity

Having found the phase velocity, it is useful to examine the group velocity, which is the velocity at which energy and information are transferred by these waves. The group velocity arose in section 2.3 in connection with quantifying the dissipation of the waves as they propagate. Numerical effects on the propagation of these waves may be important in understanding the dissipation of waves in the model. The group velocity can be written as

$$c_F^g = \frac{\partial \omega}{\partial k}$$

or using $\omega = kc$,

$$c_F^g = \frac{\partial (k c_F)}{\partial k}. \tag{A.15}$$

Differentiation of equation (A.14) as appropriate gives

$$c_F^g = c \frac{\cos k\Delta z}{\left[1 - (\frac{c\Delta t}{\Delta z} \sin k\Delta z)^2\right]^{\frac{1}{2}}}. \tag{A.16}$$

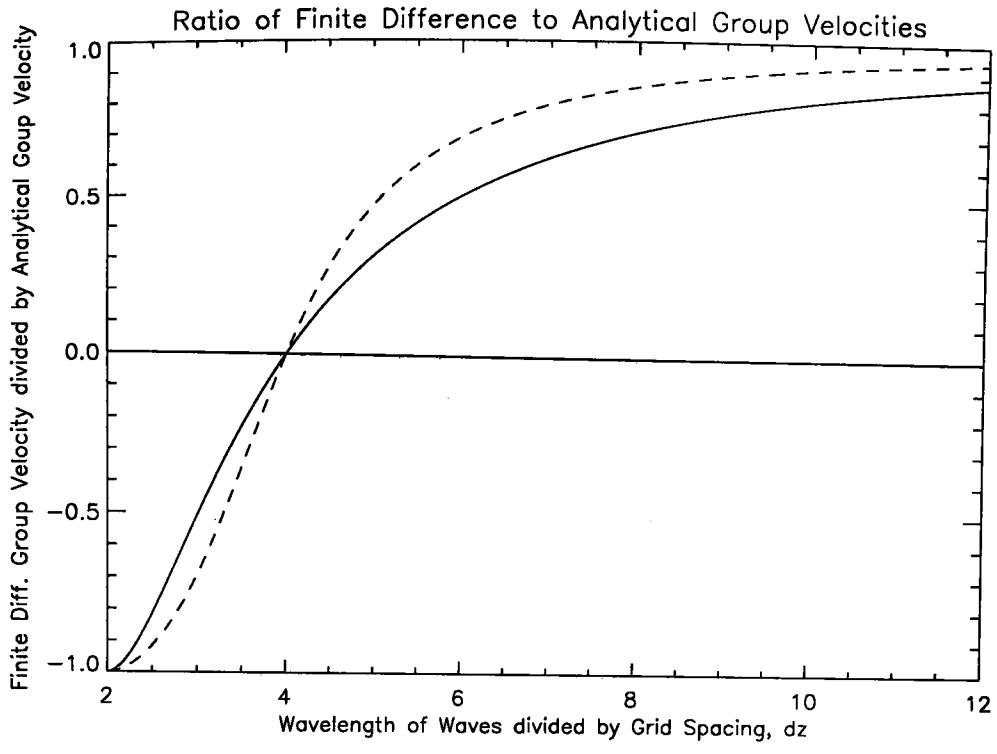

Figure A.2: The ratio between the group velocities calculated in the finite difference calculation and the analytical solution. As in figure A.1, the solid line is for a Courant number of 0.2 and the dashed line a Courant number of 0.8.

The relation between the group velocity and the wavelength of the modelled waves is shown in figure A.2 for two different values of the Courant number. In this figure, the ratio of the finite difference group velocity to the analytical group velocity (which is simply c as the real system is non-dispersive) is shown. As in the phase velocity calculation, longer wavelength waves are well represented with good agreement between the finite difference and the analytical solutions. There are however some serious errors in the representation of smaller waves. For a wave of wavelength $4\Delta z$, the group velocity is zero. For even shorter waves, the group velocity takes the opposite sign to the analytical value. As with the phase velocity, there is a special case when the Courant number is 1 and the finite difference group velocity is exactly that obtained through analytical means.

In this project, the vertical wavelengths of modelled waves are in some cases small (see for example figure 5.23) and are likely to be affected by the inaccuracies in the numerical scheme. This is especially the case for the Rossby-gravity waves that are forced. It seems likely that as Rossby-gravity waves propagate into a region where their vertical wavelength becomes small, they will have their group velocity slowed both through physical processes and the numerical effects shown in figure A.2. This will cause them to be very effectively dissipated in a thin layer and encourage the development of thin shear zones as seen in

section 5.3.2.

A.4 The Amplitude of the Waves

When the CFL condition is satisfied and the solutions are stable, the amplitude of the propagating waves is constant as $|B^{\Delta t}| = 1$. It is interesting to look at the amplitude of the finite difference solution, in particular the physical mode, of the equations as compared to the analytical solution.

When the initial condition (equation (A.3)) is applied to the finite difference solution, equation (A.11), the condition

$$A = M + E$$

is obtained and one of M or E may be eliminated from equation (A.11). This produces the equation:

$$\Phi_m^n = (A - E)e^{ik(m\Delta z - \alpha n/k)} + E(-1)^n e^{ik(m\Delta z + \alpha n/k)}. \tag{A.17}$$

More information is required to obtain $A - E$ and get the amplitude of the physical mode. A leapfrog time-step is unsuitable for use in the initial time-step of a model as model variables will be known on only one time level. It is normal practice to perform a forward time-step for the first time-step and then continue with leapfrog time-steps after this.[1] It is this forward time-step that will define the amplitude of the physical and numerical modes. This forward time-step can be written:

$$\Phi_m^1 = \Phi_m^0 - \frac{c\Delta t}{2\Delta x}(\Phi_{m+1}^0 - \Phi_{m-1}^0), \tag{A.18}$$

which, using the relation $\Phi_m^0 = Ae^{ikm\Delta z}$ becomes:

$$\Phi_m^1 = A(1 - i\sin\alpha)e^{ikm\Delta z}. \tag{A.19}$$

This can be substituted into equation (A.17) to produce an equation giving the amplitudes

[1] The SMM also performs forward time-steps after every dump to file as described in section 4.1.

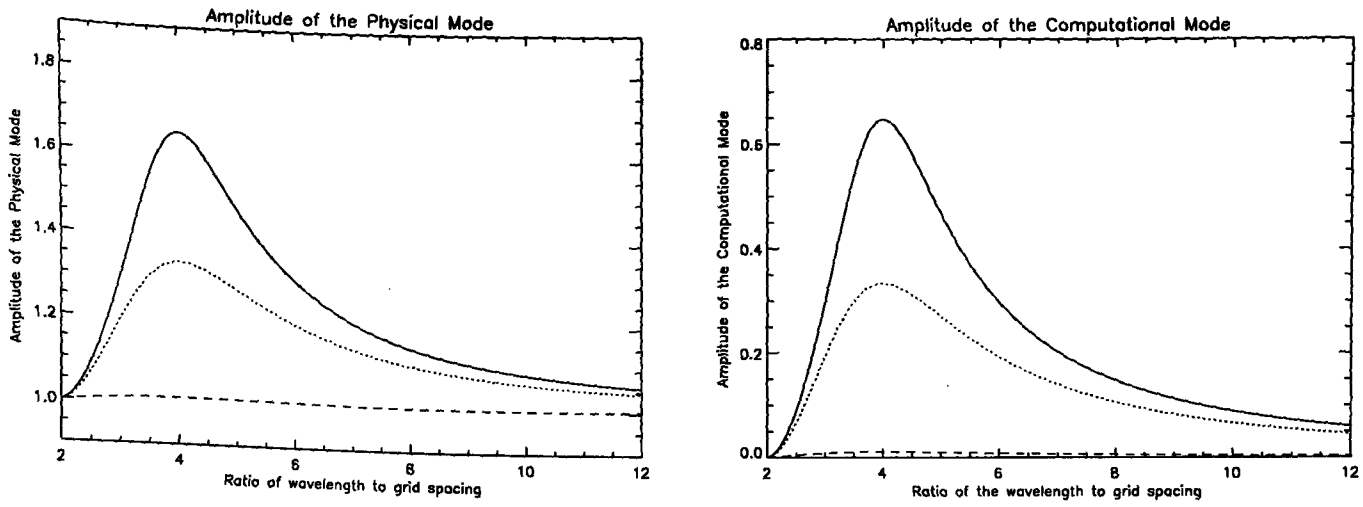

Figure A.3: Amplitudes of the physical (left panel) and computational (right panel) modes in the finite difference solution against the ratio of wavelength to grid spacing. (The values are normalised so that an amplitude of 1 represents the true solution.) Three lines are plotted on each diagram, the solid line is for Courant number 0.9, the dotted line, Courant number 0.8 and the dashed line Courant number 0.2.

of the two modes. The amplitude of the physical mode is given by:

$$A - E = A\left\{\frac{\cos\alpha + 1}{2\cos\alpha}\right\}, \tag{A.20}$$

and the amplitude of the computational mode is given by:

$$E = A\left\{\frac{1 - \cos\alpha}{2\cos\alpha}\right\}. \tag{A.21}$$

The variation of these amplitudes with the wavelength of the modelled waves is shown in figure A.3. It can be seen, as before, that the physical mode is accurately modelling the analytical solution when the waves are much longer than the grid length. There are, as might be expected, errors when the wavelength becomes smaller (although the error seems largest at $\lambda = 4\Delta z$ and reduce at smaller λ). The errors are very small for waves that are significantly longer than $4\Delta z$. These errors could be reduced further by using a more sophisticated numerical method for the first time-step. The errors introduced at the forward time-steps are not particularly large (as long as the number of forward time-steps is kept small) and simple forward time-steps are used where necessary in the model.

Appendix B

Some Model Code

B.1 The GEOPER Subroutine

The GEOPER subroutine is described in section 4.2.1 and is central to the project. The code is included in full in this section. This is the full code after preprocessing. Several model common parameter statements have been removed to shorten the code.

```
      SUBROUTINE GEOPER (IFLAG,ZNOW,ISEC,IDAY,IMON,IYEAR)
C
c Version:
c
c V01 BNL 23/08/94 13/12/94
c V02 EFD 21/04/97
c
c Description:
c
c This subroutine adds a perturbation to the bottom boundary field durin
c the run. It takes over the interpolation of the data between dates!
c
c The waves are turned on over the first GTURN days
c
c A number of optional perturbations are allowed:
c 1) Localised                                                    (GOPT=0)
c      Parameters are
c               height (m)                                       (GHGT)
c               radius of influence: distance on sphere (km)     (GRAD)
c               period of oscillation (hours)                    (GPER)
c               latitude and longitude of maximum                (GLAT,GL
c
c 2) Wavelike                                                     (GOPT=1)
c      Parameters are
c               waveamp (m)                                      (GHGT)
c
```

```
c                waveno k                                              (GWN)
c                latitude of maximum (degrees)                         (GLAT)
c                radius of influence: distance on sphere (km)          (GRAD)
c                period of oscillation (hours)                         (GPER)
c
c All options support multiple waves (GWAV > 1)
c hence, all the above variables are dimensioned GWAV
c
c 3) Added EFD 10/96 Rossby-Gravity like. See notepad.
c       Parameters as 2) but GOPT=2
c
c
c V02 Added 21/04/97. Want to add Temperature peturbations to the lower
c  as well. Code added to do this. Code from update deck incorporated to
c  RG waves and co. to reduce size of update deck.
c
c GEOPER NOT STANDARD ANYMORE
c
c
c
c arguments
c
        INTEGER          IFLAG
        REAL             ZNOW(MERIDS+2,LATS,nbot)
        INTEGER          ISEC,IDAY,IMON,IYEAR
c
c local variables that are saved between calls
c
        REAL             Z1(MERIDS+2,LATS,nbot)
        REAL             Z2(MERIDS+2,LATS,nbot)
        REAL             DELTA(MERIDS+2,LATS,nbot)
        COMMON  /ZWAVES/Z1,Z2,DELTA
c
c local variables that define the waves
c

        REAL             GTURN
        INTEGER          GWAV
        PARAMETER        (GWAV=2)          !number of additional waves

c
        REAL GOPT(GWAV),GHGT(GWAV),GRAD(GWAV),GPER(GWAV),GWN(GWAV)
        REAL GLAT(GWAV),GLON(GWAV)

c
c and the rest of the local variables
c
        INTEGER          ISTART  !start of model integration in seconds
        INTEGER          Z1TIME  !time of the first boundary field
```

```
      INTEGER          Z2TIME  !time of the second boundary field
      INTEGER          INOW    !current time in seconds
      REAL             EARG    !scale factor for slowing onset of pertu
      REAL             RLAT    !latitude of perturbation centre in radi
      REAL             RLON    !longitude of perturbation centre in rad
      REAL             RGAUSS  !scaling factor to use to limit size of
      REAL             TSCALE  !scaling factor for time oscillation
      REAL             PHI     !current latitude
      REAL             LAMBDA  !longitude like variable
      REAL             DIST
      REAL             SCALE, TARG
      REAL             ARG
      REAL             PERT(NBOT)
      REAL             ALPHA
      REAL             DEGRAD,PI,TWOPI
      LOGICAL FIRST /.TRUE./
      LOGICAL STARTING /.TRUE./
      INTEGER          I,J,K,n
c
c external functions
c
      INTEGER          IDTSEC
      REAL             DSTSPH
      EXTERNAL         IDTSEC,DSTSPH
c
c Data statements defining the wave perturbations:
c the following is a wave 1 perturbation, centred on 60N with 30 lat ran
c
      DATA GTURN /10.0/
      DATA GOPT /2,1/
      DATA GLAT /0., 0./
      Data GLON /0., 0./
      DATA GHGT /30.,70./
      Data grad /30.,30./
      DATA GPER /96.,336./
      DATA GWN /4.,1./
c
c EXECUTABLE CODE FOLLOWS
c


c
c iflag=-2 means load znow into the old field (ie first model step)
c iflag=-1 means load znow into the new field (ready for first time step
c iflag=1 means load znow into the new field (and load z2 into z1)
c iflag=0 means get on and do some interpolation
c
      If (IFLAG.eq.-2) then
```

```
      Do i=1,lats
         Do j=1,merids+2
           do n=1,nbot
            z1(j,i,n)=znow(j,i,n)
           enddo
         Enddo
      Enddo
      z1time=idtsec(isec,iday,imon,iyear)
      Print *,'GEOPER: Start time ',z1time
      Return
   Else if (iflag.eq.-1) then
      Do i=1,lats
         Do j=1,merids+2
            do n=1,nbot
              z2(j,i,n)=znow(j,i,n)
            enddo
         Enddo
      Enddo
      z2time=idtsec(isec,iday,imon,iyear)
      Print *,'GEOPER: Next time ',z2time
      Return
   Else if (iflag.eq.1) then
      Do i=1,lats
         Do j=1,merids+2
           do n=1,nbot
             z1(j,i,n)=z2(j,i,n)
             z2(j,i,n)=znow(j,i,n)
             delta(j,i,n)=z2(j,i,n)-z1(j,i,n)
            enddo
         Enddo
      Enddo
      z1time=z2time
      z2time=idtsec(isec,iday,imon,iyear)
      Print *,'GEOPER: Boundary times ',z1time,z2time
      Return
   Endif
c
c On first invocation where we want to do something sensible, we have
c to initialise a few things
c
      IF (FIRST) THEN

         FIRST=.FALSE.
         GTURN=GTURN*86400 !turn the turnon time straight into seconds
         PI=4.*ATAN(1.0)
         TWOPI=2.*PI
         DEGRAD=PI/180.0
```

```
            ISTART=IDTSEC(ISEC,IDAY,IMON,IYEAR)
            Print *,'Subroutine GEOPER NOT VALIDATED (BNL 16/12/94)'
         ENDIF
c
c get current time
c
         INOW=IDTSEC(ISEC,IDAY,IMON,IYEAR)
c
c Now calculate a factor to turn on the waves over the turnon period
c after model initialisation.
c
         EARG=1.0
         IF (STARTING) THEN
            EARG=FLOAT(INOW-ISTART)/GTURN
            IF (1.0-EARG.LE.0) STARTING=.FALSE.
            EARG=0.5*EARG**2
            EARG=1.-EXP(-EARG*10.)
         ENDIF
c
c First do the standard linear interpolation between boundary fields
c
         alpha=float(inow-z1time)/(z2time-z1time)
         Do i=1,lats
            Do j=1,merids+2
               do n=1,nbot
                 znow(j,i,n)=z1(j,i,n)+alpha*delta(j,i,n)
               enddo
            Enddo
         Enddo
c
c Now cycle through the various additional waves and add them
c
         DO I=1,GWAV
            RLAT=DEGRAD*GLAT(I)
            RGAUSS=(0.5*GRAD(I)*DEGRAD)**2
            ARG=0.0
            IF (GPER(I).GT.0) ARG=TWOPI*(INOW-ISTART)/(GPER(I)*3600)
            TSCALE=COS(ARG)
            TARG=ARG !targ is omega*t
            DO J=1,LATS
               PHI=PI*(.5+(.5-J)/LATS)
               IF (GOPT(I).EQ.0) THEN
                  RLON=DEGRAD*GLON(I)
                  DO K=1,MERIDS
                     LAMBDA=twopi*FLOAT(K)/FLOAT(MERIDS)
                     DIST=DSTSPH(PHI,LAMBDA,RLAT,RLON)
                     SCALE=EXP(-DIST**2/RGAUSS)
```

```
                PERT(1)=EARG*SCALE*GHGT(I)*TSCALE
                if (nbot.eq.2) then
                 Pert(2)=0
                endif
                do n=1,nbot
                  ZNOW(K+1,J,n)=ZNOW(K+1,J,n)+PERT(n)
                enddo
              ENDDO
            ELSE IF (GOPT(I).EQ.1) THEN
              DIST=DSTSPH(PHI,0.,RLAT,0.)
              SCALE=EXP(-DIST**2/RGAUSS)
              DO K=1,MERIDS
                ARG=TWOPI*K*GWN(I)/MERIDS
                PERT(1)=EARG*SCALE*GHGT(I)*SIN(ARG-TARG)
                if (nbot.eq.2) then
                pert(2)=earg*scale*ghgt(i)*(0.017*sin(arg-targ)-
& GPER(I)*GWN(I)*(4.24e-4)*cos(arg-TARG))
                endif
                do n=1,nbot
                  ZNOW(K+1,J,n)=ZNOW(K+1,J,n)+PERT(n)
                enddo
              ENDDO
            ELSE IF (GOPT(I).EQ.2) THEN
              DIST=DSTSPH(PHI,0.,RLAT,0.)
              SCALE=8.*PHI/(ABS(PHI))*DIST*EXP(-DIST**2/RGAUSS) ! y-d
              DO K=1,MERIDS
                ARG=TWOPI*K*GWN(I)/MERIDS    ! ARG is kx
                PERT(1)=EARG*SCALE*GHGT(I)*SIN(TARG+ARG)
                if (nbot.eq.2) then
                pert(2)=earg*scale*ghgt(i)*(0.0174*sin(arg+targ)-
& GPER(i)*GPER(i)*(4.24e-5+(gwn(i)/gper(i)*4.25e-4))*
& cos(arg+targ))
                endif
                do n=1,nbot
                  ZNOW(K+1,J,n)=ZNOW(K+1,J,n)+PERT(n)
                enddo
              ENDDO
            ENDIF
            do n=1,nbot
              ZNOW(1,J,n)=ZNOW(MERIDS+1,J,n)
              ZNOW(MERIDS+2,J,n)=ZNOW(2,J,n)
            enddo
          ENDDO
        ENDDO

        RETURN
        END
```

Appendix C

Notation and Symbols Used

C.1 Symbols Used

x, y	Position coordinates in the north-south and east-wast direction respectively.
z	Vertical coordinate in log-pressure co-ordinates. (z^* is the geometric height).
ϕ	Latitude.
λ	Longitude.
a	Radius of the Earth.
u, v, w	Wind component in the zonal, meridional and vertical directions respectively.
T	Temperature.
p	Pressure. p_0 is a constant reference pressure, often taken as 1000 hPa.
Φ	Geopotential.
θ	Potential Temperature.
Ω	The rotation vector of the earth.
f	The Coriolis Parameter.
β	The derivative of f with respect to latitude.
κ	Ratio of the molar gas constant, R, to c_p.
N	The buoyancy frequency.
ρ	The density. $\rho_o(z)$ is the background, hydrostatic density function.
s	Model vertical coordinate, defined as $s = \ln\left(\frac{p}{p_0}\right)$.

C.2 Model Equations

In the model equations, given in section 4.1.2, several operators are used which must be defined.

The differential and averaging operators are defined as:

$$\delta_{nx}X = \frac{1}{n\Delta x}\left[X\left(x+n\frac{\Delta x}{2},...\right)-\left(X-n\frac{\Delta x}{2},...\right)\right] \tag{C.1}$$

and

$$\overline{X}^{nx} = \frac{1}{2}\left[X\left(x+n\frac{\Delta x}{2},...\right)+\left(X-n\frac{\Delta x}{2},...\right)\right]. \tag{C.2}$$

The advection term $(\mathbf{u}.\nabla)$ is given by:

$$\begin{aligned} D(x) \;=\; & \frac{1}{a\cos\phi}\left\{\frac{4}{3}\left[\delta_\lambda\left(\overline{u}^\lambda\overline{X}^\lambda\right)+\delta_\phi\left(\overline{v}^\phi\overline{X}^\phi\cos\phi\right)\right]\right. \\ & \left.-\frac{1}{3}\left[\delta_{2\lambda}\left(\overline{u}^{2\lambda}\overline{X}^{2\lambda}\right)+2\delta_{2\phi}\left(\overline{v}^{2\phi}\overline{X}^{2\phi}\cos\phi\right)\right]\right\} \\ & +\frac{1}{p}\delta_s\left(p\dot{s}\overline{X}^s\right). \end{aligned} \tag{C.3}$$

Bibliography

Andrews, D. [1998], Personal Communication.

Andrews, D., Holton, J. and Leovy, C. [1987], *Middle Atmosphere Dynamics*, Academic Press.

Andrews, D. and McIntyre, M. [1976*a*], 'Planetary waves in horizontal and vertical shear: The generalized Eliassen-Palm relation and the mean zonal acceleration', *Journal of the Atmospheric Sciences* **33**(11), 2031–2048.

Andrews, D. and McIntyre, M. [1976*b*], 'Planetary waves in horizontal and vertical shear: The generalized Eliassen-Palm relation and the mean zonal acceleration', *Journal of the Atmospheric Sciences* **33**(11), 2049–2053.

Baldwin, M. P. and Dunkerton, T. J. [1998], 'Quasi-biennial modulation of the southern hemisphere stratospheric polar vortex', *Geophysical Research Letters* **25**(17), 3343–3346.

Boville, B. A. and Randel, W. J. [1992], 'Equatorial waves in a stratospheric GCM: Effects of vertical resolution', *Journal of the Atmospheric Sciences* **49**(9), 785–801.

Collimore, C. C., Hitchman, M. H. and Martin, D. W. [1998], 'Is there a quasi-biennial oscillation in tropical deep convection?', *Geophysical Research Letters* **25**(3), 333–336.

Cordero, E. and Nathan, T. R. [1998], 'An analytical study of ozone feedbacks on Kelvin and Rossby-gravity waves: Effects on the QBO', *Journal of the Atmospheric Sciences* **55**, 1051–1062.

Dunkerton, T. J. [1983], 'Laterally propagating Rossby waves in the easterly acceleration phase of the quasi-biennial oscillation', *Atmosphere-Ocean* **21**(1), 55–68.

Dunkerton, T. J. [1996], 'The role of gravity waves in the quasi-biennial oscillation', *Journal of Geographical Research* .

Dunkerton, T. J. and Baldwin, M. P. [1991], 'Quasi-biennial modulation of planetary-wave fluxes in the northern hemisphere winter', *Journal of the Atmospheric Sciences* **48**(8), 1043–1061.

Echols, R. S. and Nathan, T. R. [1996], 'Effects of ozone heating on forced equatorial Kelvin waves', *Journal of the Atmospheric Sciences* **53**(2), 263–275.

Fisher, M. [1987], The met. O. 20 stratosphere–mesosphere model DOTN 52, Technical report, UK Meteorological Office.

Geller, M. A., Shen, W., Zhang, M. and Tan, W.-W. [1997], 'Calculations of the stratospheric quasi-biennial oscillation for time-varying wave forcing', *Journal of the Atmospheric Sciences* **54**, 883–894.

Goswami, B. [1995], 'A multiscale interaction model for the origin of the tropospheric QBO', *Journal of Climate* **8**, 524–534.

Gray, L. J. [1998], Personal Communication.

Gray, L. J. and Dunkerton, T. J. [1990], 'The role of the seasonal cycle in the quasi-biennial oscillation of ozone', *Journal of the Atmospheric Sciences* **47**(20), 2429–2451.

Gray, L. J. and Ruth, S. [1993], 'The modeled latitudinal distribution of the ozone quasi-biennial oscillation using observed equatorial winds.', *Journal of the Atmospheric Sciences* **50**(8), 1033–1046.

Gray, L. and Pyle, J. [1989], 'A two-dimensional model of the quasi-biennial oscillation of ozone', *Journal of the Atmospheric Sciences* **46**(2), 203–220.

Hack, J. J., Boville, B. A. et al. [1993], Description of the NCAR Community Climate Model (CCM2), Technical Report NCAR/TN-382+STR, National Center for Atmospheric Research.

Haltiner, G. J. and Williams, R. T. [1980], *Numerical Prediction and Dynamic Meteorology*, John Whiley and Sons.

Hamilton, K. [1998], 'Effects of an imposed quasi-biennial oscillation in a comprehensive troposhpere-stratosphere-mesosphere general circulation model', *Journal of the Atmospheric Sciences* **55**, 2393–2418.

Hasebe, F. [1994], 'Quasi-biennial oscillations of the ozone and diabatic circulation in the equatorial stratosphere', *Journal of the Atmospheric Sciences* **51**(5), 729–745.

Haynes, P. [1996], 'The latitudinal structure of the quasi-biennial oscillation', *Submitted to the Journal of Geophysical Research* .

Haynes, P., McIntyre, M. and Shepherd, T. [1991], 'On the downward control of extratropical diabatic circulations by eddy induced mean zonal forces', *Journal of the Atmospheric Sciences* **48**, 651–678.

Hines, C. [1996], 'Doppler-spread parameterisation of gravity-wave momentum deposition in the middle atmosphere, part 1', Laboratory for Atmospheres, NASA Goddard Space Flight Center.

Holton, J. and Lindzen, R. [1972], 'An updated theory for the quasi-biennial oscillation', *Journal of the Atmospheric Sciences* .

Holton, J. and Tan, H. [1980], 'The influences of the equatorial quasi-biennial oscillation on the global circulation at 50 mb', *Journal of the Atmospheric Sciences* **37**, 2200–2208.

Iwi, A. [1997], Personal Communication.

Kennaugh, R., Ruth, S. and Gray, L. J. [1997], 'Modelling the quasi-biennial variability in the semiannual double peak', *Journal of Geophysical Research* **102**(D13), 16169–16187.

Kinnersley, J. S. and Pawson, S. [1996], 'The descent rates of the shear zones of the equatorial QBO', *Journal of the Atmospheric Sciences* **53**(14), 1937–1949.

Labitzke, K. [1982], 'On the interannual variability of the middle stratosphere during northern winters', *Journal of the Meteorological Society of Japan* **60**(1), 124–139.

Labitzke, K. [1987], 'Sunspots, the QBO, and the stratospheric temperature in the north polar region', *Geophysical Research Letters* **14**(5), 535–537.

Lawrence, B. [1996], The effect of parameterized gravity wave drag on simulations of the middle atmosphere during northern winter 1991/1992-general evolution. Unpublished.

Lawrence, B. and Allinson, R. [1992], Middle Atmosphere Dynamics Package at Oxford. Available from: Atmospheric, Oceanic and Planetary Physics, Clarendon Laboratory, Parks Road, Oxford, OX1 3PU.

Lawrence, B. N. [1997], 'Some aspects of the sensitivity of stratospheric climate simulation to model lid height', *Journal of Geophysical Research* **102**(D20), 23805–23811.

Lindzen, R. and Holton, J. [1968], 'A theory of the quasi-biennial oscillation', *Journal of the Atmospheric Sciences* .

McIntyre, M. [1994], The quasi-biennial oscillation: Some points about the terrestial QBO and the possibility of related phenomena in the solar interior, *in* E. Nesme-Ribes, ed., 'The Solar Engine and its influence on the Terrestial atmosphere and Climate', Vol. 25 of *NATO ASI Subseries I,Global Environmental Change*, Springer-Verlag, pp. 293–320.

McIntyre, M. and Palmer, T. [1983], 'Breaking planetary waves in the stratosphere', *Nature* **305**, 593–599.

Nagashima, T. and Takahashi, M. [1998], 'The first simulation of an ozone QBO in a general circulation model', *Geophysical Research Letters* **25**(16), 3131–3134.

Naito, Y. and Hirota, I. [1997], 'Interannual variability of the northern winter stratospheric circulation related to the QBO and the solar cycle', *Journal of the Meteorological Society of Japan* **75**(4), 925–937.

O'Sullivan, D. [1997*a*], 'Cross equatorially radiating stratospheric Rossby waves', *Geophysical Research Letters* **24**(12), 1483–1486.

O'Sullivan, D. [1997*b*], 'Interaction of extratropical Rossby waves with westerlt quasbiennial oscillation winds', *Journal of Geophysical Research* **102**(D16), 19461–19470.

Plumb, R. [1977], 'The interaction of two internal waves with the mean flow: Implications for the theory of the quasi-biennial oscillation', *Journal of the Atmospheric Sciences* **34**(12), 1847–1858.

Plumb, R. A. and Bell, R. C. [1982], 'Equatorial waves in steady shear flow', *Quarterly Journal of the Royal Meteorological Society* **108**, 313–334.

Plumb, R. and McEwan, A. [1978], 'The instability of a forced standing wave in a viscous stratified fluid: A laboratory analogue of the quasi-biennial oscillation', *Journal of the Atmospheric Sciences* .

Rae, A. [1992], *Quantum Mechanics*, 3rd edn, Institute of Physics.

Randel, W. J. [1992], 'Upper tropospheric equatorial waves in ECMWF analysis', *Quarterly Journal of the Royal Meteorological Society* **118**, 365–394.

Rosier, S. [1996], Dynamical Evolution of the Northern Stratosphere in Early Winter, 1991/92: Observational and Modelling Studies, PhD thesis, Oxford University.

Shine, K. [1987], 'The middle atmosphere in the absence of dynamical heat fluxes', *Quarterly Journal of the Royal Meteorological Society* **113**, 603–633.

Takahashi, M. [1996], 'Simulation of the stratospheric quasi-biennial oscillation using a general circulation model', *Geophysical Research Letters* **23**(6), 661–664.

Takahashi, M. and Holton, J. R. [1991], 'The mean flow response to Rossby wave and gravity wave forcing in the equatorial lower stratosphere: Relationship to the QBO', *Journal of the Atmospheric Sciences* **49**(18), 2078–2087.

Thuburn, J. [1993], 'Use of a flux-limited scheme for vertical advection in a GCM', *Quarterly Journal of the Royal Meteorological Society* **119**, 469–487.

Wallace, J. M., Panetta, R. L. and Estberg, J. [1993], 'Representation of the equatorial quasi-biennial oscillation in EOF phase space', *Journal of the Atmospheric Sciences* **50**(12), 1751–1762.

Wilke, C. K., Madden, R. A. and Chen, T.-C. [1997], 'Seasonal variation of upper tropospheric and lower stratospheric equatorial waves over the tropical pacific', *Journal of the Atmospheric Sciences* **54**, 1895–1909.